QUANTUM OPTO-MECHANICAL SYSTEMS FOR QUANTUM TECHNOLOGIES

Dissertation
zur Erlangung des Grades
des Doktors der Naturwissenschaften
der Naturwissenschaftlich-Technischen Fakultät
der Universität des Saarlandes

von
LUIGI GIANNELLI

Saarbrücken
2020

Tag des Kolloquiums:	04.06.2020
Dekan:	Prof. Dr. Guido Kickelbick
Berichterstatter/in:	Prof. Dr. Giovanna Morigi
	Prof. Dr. Christiane Koch
	Assoc. Prof. Dr. Peter Rabl
Vorsitz:	Prof. Dr. Rolf Pelster
Akad. Mitarbeiter:	Dr. Stephan Kucera

ABSTRACT

In this thesis we theoretically explore the perspectives of control of the quantum dynamics of experimentally relevant systems for quantum technological applications.

In Part II we analyze a quantum memory for single photons consisting of a single atom confined in an optical cavity and driven by a laser. We optimize the absorption of the single photon into an atomic excitation by suitably tailoring the laser pulse.

In Part III we analyze a monolithic diamond structure which embeds a nitrogen-vacancy center. We identify the parameters regime and the processes that lead to radiative cooling of a mechanical mode of the diamond structure by laser-driving the NV-center.

In Part IV we investigate spontaneous spin-spatial pattern formation in an ensemble of laser driven thermal atoms confined in an optical cavity and explore the perspectives of using this system as quantum simulator of quantum magnetism.

ZUSAMMENFASSUNG

In dieser Arbeit erforschen wir theoretisch die Perspektiven die Dynamik von Quantensystemen zu kontrollieren. Systeme, die relevant für quanten-technologische Anwendungen sind, liegen dabei im Fokus dieser Arbeit.

In Abschnitt II untersuchen wir Quantenspeicher für einzelne Photonen, bestehend aus einem einzelnen Atom, welches sich in einem optischen Resonator befindet und durch einen Laser angetrieben wird. Wir optimieren die Absorption des einzelnen Photons in eine atomare Anregung durch geeignetes Manipulieren der Form des Laserpulses.

In Abschnitt III untersuchen wir eine monolithische Diamantstruktur, welche ein Stickstoff-Fehlstellen-Zentrum einbettet. Wir identifizieren das Parameterregime und die Prozesse, die durch das Laser angetriebene Stickstoff-Fehlstellen-Zentrum zu einer Kühlung der mechanischen Mode der Diamantstruktur führen.

In Abschnitt IV untersuchen wir die spontane Entstehung von spinräumlichen Mustern in einem Ensemble, bestehend aus thermischen Atomen, welche sich in einem optischen Resonator befinden und durch einen Laser angetrieben werden. Wir erforschen die Perspektiven zur Nutzung dieses Systems als Quantensimulator im Bereich des Quantenmagnetismus.

PUBLICATIONS

[1] L. Giannelli, R. Betzholz, L. Kreiner, M. Bienert, and G. Morigi. "Laser and cavity cooling of a mechanical resonator with a nitrogen-vacancy center in diamond." In: *Physical Review A* 94 (2016), p. 053835.

[2] L. Giannelli, T. Schmit, T. Calarco, C. P. Koch, S. Ritter, and G. Morigi. "Optimal storage of a single photon by a single intracavity atom." In: *New Journal of Physics* 20 (2018), p. 105009.

[3] L. Giannelli, T. Schmit, and G. Morigi. "Weak coherent pulses for single-photon quantum memories." In: *Physica Scripta* 94 (2019), p. 014012.

[4] F. Petiziol, E. Arimondo, L. Giannelli, F. Mintert, and S. Wimberger. "Optimized three-level quantum transfers based on frequency-modulated optical excitations." Forthcoming in *Scientific Reports*.

Publication [4] is not discussed in this thesis.

ACKNOWLEDGMENTS

The PhD's years have been difficult and fun, and I would like to thank all the people who influenced me and this work.

First of all, I would like to thank my supervisor Prof. Giovanna Morigi. Giovanna has been essential for all the projects I worked in, for her new fascinating ideas and for the guidance she gave me. I am deeply grateful for everything Giovanna taught me. I want also to thank Marc Bienert for having supervised me for the first year of this PhD and for having introduced me to the beauty of master equations and opto-mechanics. Then I want to thank my other collaborators who published an article with me: Ralf Betzholz, Laura Kreiner, Tom Schmit, Tommaso Calarco, Christiane P. Koch and Stephan Ritter. A special thank goes to Stephan for his continuous support and for his inspiring passion.

During these years I had the opportunity to meet many wonderful people in the group of Giovanna, so I thank my colleagues/friends: Ralf, Tom, Tristan Tentrup, Stefan Schütz, Katharina Rojan, Mossy (Thomás Fogarty), Susanne Blum, Timo Holz, Oxana Mishina, Florian Cartarius, Andreas Buchheit, Sascha Wald, Rebecca Kraus, Lukas Himbert, Tim Keller, Simon Jäger, Francesco Rosati, Frederic Folz, Aleksei Konovalov, Peter-Maximilian Ney, Nahuel Freitas and Shraddha Sharma.

I also thank Prof. Jürgen Eschner, Prof. Ennio Arimondo, Prof. Anders S. Sørensen, Prof. Malte Henkel, Prof. Christoph Becher and Mathias Körber for the nice discussions about various physics topics. I also thank the secretaries who performed much of the bureaucratic work: Monika Francois, Ingeborg Michel and Susanna Trampert.

I thank Prof. Gerhard Rempe for the kind hospitality at the MPI for Quantum Optics in Garching.

A very important part of my life in Saarbrücken are my friends outside the university: Marie-Christin Lindecke, Kapil Faliya, Ettore Bernardi, Masha Pavlovic, Anika Bratzel, Alessandra Griffo and Fabio Lolicato.

Now it's the turn of my family: grazie mamma e papà! Thanks Francesca Pascale and Gennaro Giannelli, you are my strong roots that make the tree (myself) safe. Thanks Michele Giannelli for your physical (I mean gym-physical) support.

Among all my sud-Italian friends, which I cannot name all, I specially thank Emanuele Cutrone e Raffaele Letizia.

Finally I thank my girlfriend Eugenia Loiudice for supporting me in any imaginable way.

CONTENTS

ACRONYMS

AMO	atomic, molecular, and optical
NV	nitrogen-vacancy
OCT	optimal control theory
QKD	quantum key distribution
RWA	rotating wave approximation

INTRODUCTION

Quantum mechanics is the theory that describes in the most effective and precise way the physical processes at the elementary particle level [1]. Experiments in different physical setups have confirmed the predictions of quantum mechanics, and its validity is in general not questioned. Currently, intensive effort is made to control the quantum dynamics of the interaction between light and matter for practical applications, for instance to develop *quantum based technologies* [2, 3].

A primary goal of quantum based technologies is the realization of *quantum networks* [4]. A quantum network exploits the superposition principle and entanglement in order to enable secure communications between distant nodes in space [2] and in principle warrants secure communications [2] (for instance via quantum key distribution (QKD) [5, 6]), allows clock synchronization [7] and could improve astronomical observations by combining light from different telescopes [8]. The simplest idealization of a quantum network consists of *quantum nodes* connected via *quantum channels*: quantum nodes generate, store and process information via quantum mechanical dynamics, while quantum channels transmit the quantum information between the nodes.

Another primary goal is the realization of a *quantum computer* [9, 10]. A quantum computer is a device that, by means of quantum effects such as superposition and entanglement, can perform certain computational tasks that a classical computer practically cannot. A prominent example is integer factorization: the *Shor's algorithm* [11] (if run on a quantum computer) can factorize an integer in a time which grows polynomially with the input size, differing from classical algorithms known so far. In fact the best known classical algorithm, the *general number field sieve* [12], is sub-exponential in time, i. e. its running time grows with the input size faster than any polynomial. The concept of quantum computers being able to perform tasks which are impossible for classical computers is referred to as *quantum supremacy* [13]. Recently Google published a paper claiming to have experimentally proven quantum supremacy [14, 15] by sampling the output of a random quantum circuit [16]. Furthermore, a quantum computer can be embedded in a quantum node of a quantum network in order to process information.

Developments in applied quantum physics can also lead to the realization of a *quantum simulator* [17, 18], i. e. a device that tailors the quantum dynamics of a system in order to simulate another, less experimentally controllable, quantum system. A quantum simulator could address the solution of outstanding problems in physics such as high-temperature (high-T_c) superconductors [19–21] and the dynamics of spin glasses [22,

23], and improve understanding of quantum processes with applications in fields such as chemistry [24] and biology [25, 26].

Another promising goal is the development of tools for *quantum metrology and sensing* [27–29]. Research in this area aims to develop approaches and devices that allow measurements with a precision beyond what is possible with classical physics [29]. This has implications ranging from measurement of physics' fundamental constants [30] to imaging in biological systems [31].

The progress in each of these research areas draws from the control of the quantum dynamics of many different physical systems, such as for instance single photons [32], trapped ions [33], quantum gases [34], single atoms [35], impurities in solids [36] and superconducting circuits [37]. According to the present knowledge each physical system, having its own advantages and drawbacks, is best suited for a particular task. For instance, single photons seem best suited to transmit information and to distribute entanglement between distant nodes, while atoms and atomic ensembles seem best suited to store and process information [4].

In this thesis we theoretically explore the perspectives of control of the quantum dynamics of physical systems relevant for quantum technological applications. These are (i) a single atom trapped in an optical cavity for the purpose of realizing a quantum memory, (ii) a solid-state system consisting of a nitrogen-vacancy (NV) center embedded in a diamond structure with the aim of identifying promising features it may offer for quantum communications and quantum sensing, and (iii) an ensemble of spins confined in an optical cavity with the goal of assessing its potential as quantum simulator of quantum magnetism and opto-magnonic systems.

The common theoretical grounds for the description of these systems are quantum optics, cavity quantum electrodynamics and the theory of open quantum systems. We use the methods developed in these fields in order to analyze and identify the control tools of light-matter interactions in these setups.

This thesis is divided in four parts. In Part I we introduce the basic theoretical tools: Chapter 1 reviews the basic concepts of *light-matter interactions* in the quantum regime, and in Chapter 2 we review the *Born-Markov* master equation formalism and two methods that can be used to solve it, namely, the *spectral decomposition of the Liouville operator* and the *Wigner transformation*.

In Part II we present the analysis of a *quantum memory* composed by a single atom trapped inside an optical cavity. In Chapter 3 we consider a single photon impinging on one mirror of the cavity. The photonic excitation is stored in an atomic excitation by means of an external driving laser. We derive the optimal shape of the laser field in order to store the single photon with highest efficiency in presence of cavity losses. We analyze both the adiabatic regime in which analytical results are derived, and the non-adiabatic regime where we use optimal control

theory (OCT) to explore the storage of photons which are short in time with respect to the time scale of the atom-cavity system. In Chapter 4 we investigate theoretically how weak coherent pulses can be used to probe the efficiency of single-photon quantum memories.

In Part III, we present the characterization a *hybrid quantum system* composed of a NV-center in a monolithic diamond structure which is both an optical and a mechanical resonator. We analyze the cooling dynamics of the mechanical resonator harnessing an optical pump of the NV-center. We show that the optical resonator has little impact on the cooling rate and final temperature of the mechanical oscillator, while pure dephasing of the electronic energetic levels of the NV-center leads to a more robust cooling. We also examine the spectrum of resonance fluorescence in order to identify the cooling processes. Cooling mechanical degrees of freedom of hybrid devices is important for quantum information processing [38–41], and for ultrasensitive detection applications [42–46] because of the reduced effect of thermal fluctuation.

Part IV is composed of the single Chapter 6. Here we investigate a system composed by an ensemble of atoms confined in an optical cavity. The atoms are driven by two external lasers and scatter light into the cavity mode, which, in turn, dissipate lights. The parameters can be tailored such that the system reaches an out-of-equilibrium steady state. The atoms in this steady state exhibit a controllable antiferromagnetic ordering. This setup can be used to simulate quantum magnetism [47] and opto-magnonic systems [48, 49].

Part I

PRELIMINARIES

We review some of the basic concepts on which the rest of the thesis draws. In the first chapter we summarize some important models of atom-photon interactions in quantum optics. We introduce the Hamiltonian of a two-level atom interacting with an electromagnetic field, both in free space and in an optical cavity. We also shortly discuss cavity opto-mechanics. In the second chapter we review the Born-Markov master equation and sketch its derivation. We discuss the general solution of the master equation by means of the damping basis. We finally introduce the Wigner function and describe its application within the master equation formalism.

1

LIGHT-MATTER INTERACTIONS

Electromagnetic interactions govern the dynamics of charged particles, such as electrons, protons and ions. The understanding of the interactions between matter and light played and plays a central role in modern and contemporary physics. The characterization of black-body radiation [50] and of the photoelectric effect [51], for instance, were fundamental steps in the development of our current understanding of quantum mechanics. The properties of light emitted and absorbed by atoms and molecules allows us to gain information about their structure and their dynamics. In atomic, molecular, and optical (AMO) physics, light-matter interactions are nowadays well understood and used for applications such as high-precision spectroscopy, optical trapping, cooling, manipulation of atomic internal states, and quantum based technologies.

In this chapter we provide some basic concepts of light-matter interactions. In Sec. 1.1 we summarize the formalism used to describe the interactions of an elecromagnetic field with an atom. In Sec. 1.2 we focus on the description of an optical cavity and its interactions with an atom. Finally, in Sec. 1.3 we briefly sketch the concepts at the basis of *cavity-optomechanics*.

The presentation in this chapter follows broadly Refs. [52–56].

1.1 THE INTERACTIONS BETWEEN LIGHT AND ATOMS

Consider an atom of mass m which moves freely in space. The system energy is the sum of the atom kinetic and internal energies, the electromagnetic field energy and the atom-field interaction. The corresponding Hamiltonian is conveniently cast into the sum of three terms

$$\hat{H} = \hat{H}_{\mathrm{at}} + \hat{H}_{\mathrm{em}} + \hat{H}_{\mathrm{int}}, \tag{1.1}$$

where $\hat{H}_{\mathrm{at}}$ is the Hamiltonian of the free atom, $\hat{H}_{\mathrm{em}}$ is the Hamiltonian of the electromagnetic field, and $\hat{H}_{\mathrm{int}}$ describes their interaction.

In quantum optics one typically assumes non-relativistic particles. The fields are assumed to be monochromatic and sufficiently weak such that the electronic levels can be reduced to the ones which resonantly couple to the external driving field. In the following we assume a two-level transition at frequency ω_{a}.

The Hamiltonian $\hat{H}_{\mathrm{at}}$ of the internal and external degrees of freedom of the atom in free space is

$$\hat{H}_{\mathrm{at}} = \frac{\hat{\boldsymbol{p}}^2}{2m} + \hbar\omega_{\mathrm{a}}|e\rangle\langle e|, \tag{1.2}$$

where $\hat{\boldsymbol{p}}$ is the momentum operator of the atom center of mass and $\hbar\omega_a$ is the energy splitting between the ground state $|g\rangle$ and the excited state $|e\rangle$ of the two level transition.

The Hamiltonian $\hat{H}_{em}$ of the electromagnetic field in second quantization reads

$$\hat{H}_{em} = \sum_i \hbar\omega_i \left(\hat{a}_i^\dagger \hat{a}_i + \frac{1}{2}\right), \tag{1.3}$$

where $\hat{a}_i$ and $\hat{a}_i^\dagger$ annihilate and create, respectively, a photon in the i-th mode of the electromagnetic field. They fulfill the commutation relation $[\hat{a}_i, \hat{a}_j^\dagger] = \delta_{ij}$. We assume that the field is quantized over the volume V with periodic boundary conditions. Each mode is indexed by $i = (\boldsymbol{k}_i, \boldsymbol{\epsilon}_i)$ that consists of the wavevector $\boldsymbol{k}_i$ and the polarization $\boldsymbol{\epsilon}_i$, which satisfies $\boldsymbol{\epsilon}_i \perp \boldsymbol{k}_i$. The frequency of the i-th mode is $\omega_i = |\boldsymbol{k}_i|c$ where c is the speed of light in vacuum. The Hamiltonian (1.3) has eigenvalues $\sum_i \hbar\omega_i(n_i + 1/2)$. The integers $n_i = 0, 1, 2, \ldots$ represent the number of photons in the mode i and are the eigenvalues of the operator $\hat{a}_i^\dagger \hat{a}_i$. The corresponding eigenstates are denoted $|n_i\rangle$. The ground state $|\text{vac}\rangle$ fulfills the relation

$$\hat{a}_i|\text{vac}\rangle = 0, \quad \forall i, \tag{1.4}$$

and is called *vacuum state*.

dipole approximation

The interaction Hamiltonian in electric dipole approximation[1] is

$$\hat{H}_{int} = -\hat{\boldsymbol{d}} \cdot \hat{\boldsymbol{E}}(\hat{\boldsymbol{r}}), \tag{1.5}$$

where $\hat{\boldsymbol{d}} = \boldsymbol{d}_{eg}|e\rangle\langle g| + \boldsymbol{d}_{ge}|g\rangle\langle e|$ is the dipole operator and $\boldsymbol{d}_{eg} = \boldsymbol{d}_{ge}^*$ are the transition matrix elements between the two states. The electric field operator $\hat{\boldsymbol{E}}(\hat{\boldsymbol{r}})$ is quantized and taken at the center of mass position $\hat{\boldsymbol{r}}$ of the atom

$$\hat{\boldsymbol{E}}(\hat{\boldsymbol{r}}) = \sum_i \sqrt{\frac{\hbar\omega_i}{2\epsilon_0 V}} \boldsymbol{\epsilon}_i u_i(\hat{\boldsymbol{r}}) \hat{a}_i + \text{H.c.} \tag{1.6}$$

The sum in Eq. (1.6) runs over the modes of the electromagnetic field, ϵ_0 is the electric permittivity and $u_i(\boldsymbol{r})$ is the mode function of the mode i. The mode functions $\{u_i(\boldsymbol{r})\}$ satisfy the orthogonal condition

$$\int_V \mathrm{d}^3\boldsymbol{r}\, u_i(\boldsymbol{r}) u_j(\boldsymbol{r}) = V\delta_{ij}. \tag{1.7}$$

1 The electric dipole approximation is valid if the electromagnetic field does not change considerably over the size of the electronic wavepacket. It assumes that the field is constant over the electronic wavepacket. This is a good approximation if the size of the bound state of the electron is small compared to the wavelength of the electromagnetic field. For an atom the typical size of a bound state is $l \approx 10^{-10}\, m$. For optical transitions, where the wavelength is $\lambda \approx 10^{-7}\, m$, this approximation is valid.

Using Eq. (1.6), the interaction Hamiltonian Eq. (1.5) takes the form[2]

$$\hat{H}_{\text{int}} = \sum_i \hbar\big(|g\rangle\langle e| + |e\rangle\langle g|\big)\big(g_i(\hat{\boldsymbol{r}})\hat{a}_i + g_i(\hat{\boldsymbol{r}})^*\hat{a}_i^\dagger\big), \tag{1.8}$$

where we have introduced the coupling strength

$$g_i(\hat{\boldsymbol{r}}) = \sqrt{\frac{\omega_i}{2\hbar\epsilon_0 V}}u_i(\hat{\boldsymbol{r}})\big(\boldsymbol{d}_{\text{eg}}\cdot\boldsymbol{\epsilon}_i\big). \tag{1.9}$$

We now perform the rotating wave approximation[3] (RWA) and obtain

rotating wave approximation

$$\hat{H}_{\text{int}} = \sum_i \hbar\Big(g_i(\hat{\boldsymbol{r}})|e\rangle\langle g|\hat{a}_i + g_i(\hat{\boldsymbol{r}})^*\hat{a}_i^\dagger|g\rangle\langle e|\Big). \tag{1.10}$$

Hamiltonian (1.10) describe processes in which a photon of the i-th mode of the electromagnetic field is absorbed by the atom which undergoes a transition from the ground $|g\rangle$ to the excited state $|e\rangle$, as well as processes where the atom undergoes a transition from the excited $|e\rangle$ to the ground state $|g\rangle$ emitting a photon in the mode i. The strength of the process is position dependent, therefore $\hat{H}_{\text{int}}$ does not commute with the atom's kinetic energy and thus photon absorption or emission affects the atomic center-of-mass dynamics.

1.1.1 *Atom-laser interaction*

In this thesis we will discuss the dynamics of systems driven by lasers. The interaction of an atom with a laser can be described by assuming that the light emitted by a continuous-wave laser corresponds to the state of the electromagnetic field in which each mode is in a coherent state [57] of a harmonic oscillator. More precisely, each mode of the electromagnetic field, labeled by the subscript i, is in the coherent state $|\alpha_i\rangle$, with $\hat{a}_i|\alpha_i\rangle = \alpha_i|\alpha_i\rangle$. The coherent state $|\alpha_i\rangle$ can be, in particular, the vacuum state $|0_i\rangle$ with $\hat{a}_i|0_i\rangle = 0$. The total state of the electromagnetic field is then

$$|\psi_{\text{em}}\rangle = \bigotimes_i |\alpha_i\rangle \equiv |\ldots, \alpha_{i-1}, \alpha_i, \alpha_{i+1}, \ldots\rangle, \tag{1.11}$$

where the tensor product runs over the modes of the electromagnetic field.

By applying a unitary transformation [52] to Hamiltonian $\hat{H}$, Eq. (1.1), in dipole and rotating wave approximation (i. e. with the interaction

2 We have considered the dipole moment to be real. This is possible by adding a phase to the definition of the states $|g\rangle$ and $|e\rangle$ [53].

3 In order to understand the rotating wave approximation (RWA), one can see in interaction picture with respect to $\hat{H}_0 = \hat{H}_{\text{at}} + \hat{H}_{\text{em}}$ that the terms $\hat{a}_i|g\rangle\langle e|$ and $\hat{a}_i^\dagger|e\rangle\langle g|$ in Eq. (1.8) rotate at a frequency $|\omega_{\text{a}} + \omega_i|$, while the terms $\hat{a}_i|e\rangle\langle g|$ and $\hat{a}_i^\dagger|g\rangle\langle e|$ rotate at $|\omega_{\text{a}} - \omega_i|$. If ω_{a} and ω_i are optical frequencies, then[4] $|\omega_{\text{a}} + \omega_i| \gg |\omega_{\text{a}} - \omega_i|$. At the time scales we are interested in, if the coupling strengths $g_i \ll |\omega_{\text{a}} + \omega_i|$, the fast rotating terms average out and the dominating contribution comes from the slowly varying part which rotates at $|\omega_{\text{a}} - \omega_i|$ [53]. The RWA consists in neglecting the fast rotating terms.

Hamiltonian $\hat{H}_{\text{int}}$ given by Eq. (1.10)), in the new representation the atom is coupled to a classical external field and the modes of the electromagnetic field are in the vacuum state $|\psi'_{\text{em}}\rangle = |\text{vac}\rangle$, see Eq. (1.4). The coupling of the atom with the laser is then described by the Hamiltonian

$$\hat{H}_{\text{L}} = \hbar\Omega(\hat{\boldsymbol{r}}, t)|e\rangle\langle g| + \text{H.c.}, \tag{1.12}$$

where

$$\Omega(\hat{\boldsymbol{r}}, t) = \sum_i g_i(\hat{\boldsymbol{r}})\alpha_i e^{-i\omega_i t} \tag{1.13}$$

is the time-dependent coupling strength.

For the case of a monochromatic laser with wavevector $\boldsymbol{k}_{\text{L}}$ and polarization $\boldsymbol{\epsilon}_{\text{L}}$ only one mode of the electromagnetic field (which we denote by the label L) is occupied, and all the other modes are in the vacuum state. The coherent state is given by Eq. (1.11) with $\alpha_i = \delta_{i,\text{L}}\alpha_{\text{L}}$, i. e.

$$|\psi_{\text{em}}\rangle = |\dots, 0_{\text{L}-1}, \alpha_{\text{L}}, 0_{\text{L}+1}, \dots\rangle. \tag{1.14}$$

In this case $\Omega(\hat{\boldsymbol{r}}, t)$ is given by $\Omega(\hat{\boldsymbol{r}}, t) = g_{\text{L}}(\hat{\boldsymbol{r}})\alpha_L e^{-i\omega_{\text{L}}t}$ [52], where $\omega_{\text{L}} = |\boldsymbol{k}_{\text{L}}|c$ is the laser frequency. For a standing wave laser field it takes the form $\Omega(\hat{\boldsymbol{r}}, t) = \Omega\cos(\boldsymbol{k}_{\text{L}} \cdot \hat{\boldsymbol{r}})e^{-i\omega_{\text{L}}t}$, while for a running-wave laser field $\Omega(\hat{\boldsymbol{r}}, t) = \Omega e^{-i\boldsymbol{k}_{\text{L}}\cdot\hat{\boldsymbol{r}}}e^{-i\omega_{\text{L}}t}$. In this representation, the complex number Ω is the so-called *Rabi frequency*[5].

1.2 OPTICAL CAVITY

The setups discussed in this thesis also include optical cavities. Optical cavities (or *resonators*) can be realized experimentally in a multitude of forms [56]. A Fabry-Pérot cavity consists of two highly reflective mirrors facing each other and allows the electromagnetic field to populate quantized modes[6] [58]. If the mirrors are separated by a distance L, the i-th quantized mode has frequency $\omega_{\text{c},i} = i \cdot (c/2L)$. The separation in frequency between two adjacent resonances is denoted *free spectral range* and is $\Delta\omega_{\text{FSR}} = c/2L$. If the cavity length L is sufficiently small[7], one cavity mode can be tuned quasi-resonantly to an atomic dipole transition while all other modes are off-resonant: In this case only the quasi-resonant mode with frequency ω_{c} can be kept in the description of the cavity. The Hamiltonian of the cavity then reads

$$\hat{H}_{\text{c}} = \hbar\omega_{\text{c}}\left(\hat{a}^\dagger\hat{a} + \frac{1}{2}\right), \tag{1.15}$$

5 In order to avoid carrying extra factors of 2 around, Ω is defined as half of the traditional definition of the Rabi frequency [52], so that a π-pulse takes time $\pi/2\Omega$.

6 The electromagnetic field inside optical cavities is quantized using fixed boundary conditions [53].

7 For a cavity length $L \sim 500\,\mu m$ [59] the free spectral range is $\Delta\omega_{\text{FSR}} \sim 300\,GHz$, for a cavity length $L \sim 1\,cm$ [60, 61] it is $\Delta\omega_{\text{FSR}} \sim 15\,GHz$.

where the operators $\hat{a}^\dagger$ and $\hat{a}$ create and annihilate, respectively, a cavity photon of the resonant mode at frequency ω_c, and fulfill the commutation relation $[\hat{a}, \hat{a}^\dagger] = 1$.

1.2.1 *Atom-cavity coupling*

The Hamiltonian describing the interaction of a two-level atom with a cavity mode, in electric dipole and rotating wave approximations, reads [53, 55]

$$\hat{H}_{\mathrm{JC}} = \hbar\big(g(\hat{\boldsymbol{r}})|e\rangle\langle g|\hat{a} + g(\hat{\boldsymbol{r}})^*\hat{a}^\dagger|g\rangle\langle e|\big). \tag{1.16}$$

Here $g(\hat{\boldsymbol{r}})$ is the coupling strength between cavity mode and the atomic transition. For a standing wave mode along the x-axis it takes the form $g(\hat{\boldsymbol{r}}) = g\cos(k_c\hat{x})$, where k_c is the wavevector of the mode and g is the vacuum Rabi frequency [53]. If the atom position is fixed, i. e. if $g(\hat{\boldsymbol{r}}) = g'$ is constant, Eq. (1.16) becomes the celebrated *Jaynes-Cummings model* [62], whose dynamics can be solved exactly.

In Parts III and II we will consider the atom tightly confined inside a cavity, such that it is localized at a cavity field intensity maximum. In this limit the coupling $g(\hat{\boldsymbol{r}})$ can be treated as a constant, i. e. the fluctuations in the coupling strength due to the motion can be neglected. In Part IV instead we will consider that the atoms can move along the cavity axis and thus the coupling $g(\hat{\boldsymbol{r}})$ varies with time.

1.2.2 *Cavity losses*

The finite transmittivity of the cavity mirrors can be described in terms of a coupling between the cavity mode and the external electromagnetic field. For optical cavities this interaction is typically described by the Hamiltonian [55]

$$\hat{H}_{\mathrm{c-em}} = \hbar\sum_i\big(\lambda_i\hat{a}^\dagger\hat{a}_i + \lambda_i^*\hat{a}_i^\dagger\hat{a}\big), \tag{1.17}$$

which is here given in the rotating wave approximation. Here λ_i are the coupling strengths between the cavity mode and the i-th mode of the free field and depend on the characteristics of the mirrors. This interaction gives rise to cavity losses, i. e. to photons escaping the cavity via the mirror finite transmittivity. A description of the losses by means of a Born-Markov master equation is given in Sec. 2.1.

1.3 CAVITY OPTO-MECHANICS

Light exchanges linear momentum with matter giving rise to *mechanical forces*. In this section we briefly mention some effects of mechanical forces of light, namely Doppler cooling of atoms and some sub-Doppler

cooling mechanisms, and then we review some theoretical concepts necessary to describe the system of Chapter 5, thus focusing on the radiation pressure force.

Several methods have been developed to cool particles' motion [63] by means of mechanical effects of light. Doppler cooling, which was first discussed in Refs. [64, 65] and experimentally realized for the first time in Ref. [66], is the first proposed method for cooling atoms with light and is nowadays commonly realized in laboratories. In Doppler cooling the atoms are cooled with counter-propagating lasers whose frequency is tuned below (red detuned) the frequency of an atomic transition. If this transition is closed[8], i. e. if the excited state of the transition decays to the lower state of the transition with rate γ, then, with an appropriate choice of the laser frequency, the atoms are cooled down to temperature of the order of $\hbar\gamma/k_B$, where k_B is the Boltzmann constant. This temperature is referenced to as *Doppler limit* [63]. Laser cooling mechanisms that can reach temperatures below the Doppler limit are denoted by *sub-Doppler cooling* [69–71]. One of the most prominent approaches for sub-Doppler cooling is *polarization gradient cooling* [72] which realizes temperatures close to the recoil limit[9] [73]. In an optical cavity, the particles can be cooled with a mechanism called *cavity cooling* [74]. This method relies on coherent scattering of photons by the particles and has been proposed for cooling particles which do not have a closed transition such as molecules [75, 76]. The steady state temperature of the cooled particles is limited by the cavity loss rate [63]. Cavity cooling has been realized for a single atom [77], for a cloud of atoms [78] and for nanoparticles [79, 80].

In Chapter 5 we analyze the dynamics of a NV-center embedded in a diamond structure. The latter can vibrate and confine light, thus behaving as resonator for both photons and phonons. This can be modeled by an optical cavity with a movable mirror. The interaction between phonons and photons, in this case, is due to the *radiation pressure force*[10] that light exerts on the surface of the movable mirror.

The radiation pressure force exerted by a single photon is exceedingly small. As an example consider a single photon with wavenumber k impinging on a mirror. The photon transfer to the mirror the momentum $\Delta p = 2\hbar k$. For a continuous light beam of power P, the photon rate is $P/\hbar kc$, leading to a force $F = 2P/c$, where c is the speed of light. A kilowatt light beam thus exerts on the mirror a force of about $10^{-5}\,N$. A

8 If the transition is not closed, Doppler cooling can still be effective with the use of a repumping laser [67, 68] which re-excite the population back into a state of the transition used for cooling.

9 The recoil limit corresponds to kinetic energy of the particle of the order of the recoil energy $\hbar\omega_r = \hbar^2k^2/2m$, where k is the wavenumber of the laser field and m the mass of the particle.

10 Radiation pressure force, the force that light exerts on a surface, was already speculated in the 17th century by Kepler [81], described theoretically by Maxwell [82] in 1873, and was experimentally observed [83, 84] at the beginning of the 20th century.

possible way to increase the force a single photon exerts on the mirror is to confine the light into a resonator. In a simplified picture the photon will bounce many times off the mirror instead of only once as in free space, increasing thus the momentum transferred. Inside a cavity the radiation-pressure force is

$$\langle \hat{F} \rangle = \frac{2\hbar k \bar{n}}{\tau_c} = \frac{\hbar \omega_c \bar{n}}{L}, \tag{1.18}$$

where $\tau_c = 2L/c$ is the cavity round-trip time, L is the length of the cavity, $\bar{n}$ is the mean photon number of the cavity and ω_c is the cavity resonance frequency.

In the following we introduce a Hamiltonian description of the interaction between a cavity light field and a movable cavity mirror.

1.3.1 *Opto-mechanical Hamiltonian*

We consider the simplest model in cavity opto-mechanics, which has been useful to describe most of the experiments up to date [56]. It consists in a Fabry-Pérot cavity setup with one fixed mirror and one movable mirror of mass M. For small displacements $x \ll L$ respect to the length L of the cavity, the motion of the movable mirror can be considered harmonic with frequency[11] ω_{mec}. The model thus consists of two harmonic oscillators: One describing the cavity mode with frequency ω_c and annihilation and creation operators $\hat{a}$ and $\hat{a}^\dagger$, with $\left[\hat{a}, \hat{a}^\dagger\right] = 1$; and the other describing the motion of one mirror of the cavity with frequency ω_{mec} and annihilation and creation operators $\hat{b}$ and $\hat{b}^\dagger$, with $\left[\hat{b}, \hat{b}^\dagger\right] = 1$ and $\left[\hat{a}, \hat{b}\right] = \left[\hat{a}, \hat{b}^\dagger\right] = 0$.

The coupling between the optical and the mechanical mode is parametric, i. e. the optical resonance frequency $\omega_c(x)$ depends parametrically on the mirror displacement $\hat{x}$. The motion of the movable mirror, in fact, changes the cavity length, thus changing the cavity resonance frequency. If the mirror displacement is small compared to the average cavity length L, then the Hamiltonian to leading order in x/L reads

$$\begin{aligned} \hat{H} &= \hbar\omega_c(\hat{x})\left(\hat{a}^\dagger\hat{a} + \frac{1}{2}\right) + \hbar\omega_{mec}\left(\hat{b}^\dagger\hat{b} + \frac{1}{2}\right) \approx \\ &\approx \hbar(\omega_c - G\hat{x})\left(\hat{a}^\dagger\hat{a} + \frac{1}{2}\right) + \hbar\omega_{mec}\left(\hat{b}^\dagger\hat{b} + \frac{1}{2}\right), \end{aligned} \tag{1.19}$$

where $\hat{x} = \sqrt{\hbar/2M\omega_{mec}}\left(\hat{b} + \hat{b}^\dagger\right)$ is the mirror position operator and $G = -\partial\omega_c(x)/\partial x|_{x=0}$. Substituting in Eq. (1.19) we arrive at the standard optomechanical Hamiltonian [56]

$$\hat{H}_{om} = \hbar\omega_c\hat{a}^\dagger\hat{a} + \hbar\omega_{mec}\hat{b}^\dagger\hat{b} - \hbar\chi\hat{a}^\dagger\hat{a}\left(\hat{b} + \hat{b}^\dagger\right), \tag{1.20}$$

11 In actual experimental systems the mechanical oscillator has many vibrational modes [85]. However, for the purpose of our work, we focus on a single mode of vibration with frequency ω_{mec}, assuming that the mode spectrum is sufficiently sparse such that there is no spetral overlap with other mechanical modes [56].

where we neglect the terms due to the vacuum energies [86, 87] of both harmonic oscillators[12]. Here we have defined the vacuum optomechanical coupling strength $\chi = G\sqrt{\hbar/2M\omega_{\mathrm{mec}}}$, it quantifies the interaction between a single phonon and a single photon. The last term in Eq. (1.20) captures the basic features of the optomechanical interaction: The radiation pressure of the cavity light results in an intensity-dependent displacement of the cavity mirror, while the displacement of the cavity mirror results in a change of the cavity resonance frequency.

A detailed derivation of Hamiltonian (1.20) can be found in Ref. [88].

12 Notice that the vacuum energy of the cavity field also gives rise to the additional term $-\hbar\chi(\hat{b} + \hat{b}^\dagger)/2$ in Hamiltonian (1.19). This term is a constant force on the cavity mirror and leads to a change of the mirror rest position but does not alter its dynamics. By moving in the reference frame defined by the displacement operator $D^\dagger(\beta) = \exp\left(-\beta\hat{b}^\dagger + \beta^*\hat{b}\right)$, with $\beta = \chi/2\omega_{\mathrm{mec}}$, and by neglecting a constant energy offset, one recovers Eq. (1.19).

2

BORN-MARKOV MASTER EQUATIONS

The quantum dynamics of a non-relativistic quantum system is determined by the Schrödinger equation. The Schrödinger equation generates a unitary transformation of the Hilbert space's vector describing the system state. In quantum optics the quantum system of interest consists only of few degrees of freedom, such as for instance a harmonic oscillator or a single electron in a potential. However no system is isolated from the rest of the universe and thus every system interacts with its surroundings, its environment. Although the Schrödinger equation formalism can be applied to systems of any size and thus could include the environment as part of the system itself, its usage becomes more and more challenging with increasing system size. To overcome this problem an effective description of the environment with use of only few parameters has been developed. This is called *system plus reservoir approach* [89]: the few degrees of freedom of the system of interest are fully considered, while the environment is treated as a reservoir characterized only by a few number of parameters such as its temperature. The system interacts with the reservoir by exchanging energy and/or particles. For this reason the expression *open quantum system* is used. Starting from the dynamics of the full (system and reservoir) density operator, this formalism leads to an equation for the reduced density operator of the system, which is called *master equation*. Such equation does not generate a unitary evolution, but generally introduces damping of energy and loss of quantum-mechanical coherence into the quantum system dynamics.

For certain systems some simplifying assumptions on the interaction with its environment and on the timescales of their evolution can be made. More specifically, if the interaction between the system and the reservoir is weak and the time scale of the reservoir dynamics is order of magnitudes shorter than the one of the system, then the so called *Born-Markov master equation* holds. A peculiar property of this master equation is that the reservoir has no memory of the system at an earlier time. Born-Markov master equations are quite common in quantum optics problems.

In Section 2.1 we present a brief derivation of the Born-Markov master equation mostly following [52], and in Sec. 2.2 of the *quantum regression theorem*. We then introduce in Sec. 2.3 a method for solving the master equation denoted by *damping basis* [90–94]. In Section 2.4 we present another method for solving the master equation based on the *Wigner function*, which is a phase-space representation of a quantum state.

2.1 DERIVATION OF THE BORN-MARKOV MASTER EQUATION

Consider a system S coupled to a reservoir R and denote by $\mathcal{H}_\mathrm{S}$ and $\mathcal{H}_\mathrm{R}$ their respective Hilbert space. Be $\hat{H}_\mathrm{S}$ and $\hat{H}_\mathrm{R}$ the Hamiltonians of the system and reservoir, respectively, and be $\hat{V}$ the operator describing their mutual interaction. The Hamiltonian $\hat{H}$ of the full system, which consists of system S and reservoir R, acts on the Hilbert space $\mathcal{H} = \mathcal{H}_\mathrm{S} \otimes \mathcal{H}_\mathrm{R}$ and reads

$$\hat{H} = \hat{H}_\mathrm{S} \otimes \mathbb{1}_\mathrm{R} + \mathbb{1}_\mathrm{S} \otimes \hat{H}_\mathrm{R} + \hat{V}. \tag{2.1}$$

von Neumann equation

Let $\hat{\chi}(t)$ be the density operator of the full system. The dynamics of system and reservoir is governed by the *von Neumann* equation for the density operator $\hat{\chi}(t)$

$$\frac{\partial}{\partial t}\hat{\chi}(t) = \frac{1}{\mathrm{i}\hbar}\big[\hat{H}, \hat{\chi}(t)\big], \tag{2.2}$$

with $\hat{H}$ given in Eq. (2.1).

reduced density operator and partial trace

We are interested in the evolution of the system S, that is, we are looking for an equation of motion for the reduced density operator $\hat{\rho}(t)$ of the system S defined over $\mathcal{H}_\mathrm{S}$ by

$$\hat{\rho}(t) = \operatorname*{Tr}_\mathrm{R}[\hat{\chi}(t)], \tag{2.3}$$

where Tr_R denotes the partial trace[1] over the reservoir degrees of freedom.

interaction picture

In order to determine the equation of motion of $\hat{\rho}(t)$ from Eq. (2.2), we use perturbation theory in $\hat{V}$. We first transform Eq. (2.2) into the interaction picture with respect to $\hat{H}_0 = \hat{H}_\mathrm{S} + \hat{H}_\mathrm{R}$ and obtain

$$\frac{\partial}{\partial t}\tilde{\chi}(t) = \frac{1}{\mathrm{i}\hbar}\big[\tilde{V}(t), \tilde{\chi}(t)\big], \tag{2.4}$$

where

$$\tilde{O}(t) = \mathrm{e}^{\mathrm{i}\hat{H}_0 t/\hbar}\hat{O}(t)\mathrm{e}^{-\mathrm{i}\hat{H}_0 t/\hbar}, \quad \hat{O} = \hat{\chi}, \hat{V}. \tag{2.5}$$

A formal integration of Eq. (2.4) in the interval $[t, t+\Delta t]$ yields

$$\tilde{\chi}(t+\Delta t) = \tilde{\chi}(t) + \frac{1}{\mathrm{i}\hbar}\int_t^{t+\Delta t} \mathrm{d}t_1 \big[\tilde{V}(t_1), \tilde{\chi}(t_1)\big]. \tag{2.6}$$

Iterating Eq. (2.6) we obtain

$$\begin{aligned}\Delta\tilde{\chi}(t) = \frac{1}{\mathrm{i}\hbar}\int_t^{t+\Delta t} \mathrm{d}t_1 \big[\tilde{V}(t_1), \tilde{\chi}(t)\big] + \\ - \frac{1}{\hbar^2}\int_t^{t+\Delta t} \mathrm{d}t_1 \int_t^{t_1} \mathrm{d}t_2 \big[\tilde{V}(t_1), \big[\tilde{V}(t_2), \tilde{\chi}(t_2)\big]\big],\end{aligned} \tag{2.7}$$

1 The partial trace of an operator O over the reservoir degrees of freedom is defined as $\mathrm{Tr}_\mathrm{R}[O] = \sum_r \langle r|O|r\rangle$, where $\{|r\rangle\}_r$ is a basis of $\mathcal{H}_\mathrm{R}$.

where we have set $\Delta\tilde{\chi}(t) = \tilde{\chi}(t+\Delta t) - \tilde{\chi}(t)$.

Since we are interested in the evolution of the system S, described in interaction picture by the density operator[2] $\tilde{\rho}(t)$, we trace Eq. (2.7) over the reservoir degrees of freedom and obtain

$$\begin{aligned}\Delta\tilde{\rho}(t) = \frac{1}{\mathrm{i}\hbar}\int_t^{t+\Delta t} \mathrm{d}t_1 \operatorname*{Tr}_{\mathrm{R}}\Big\{\big[\tilde{V}(t_1), \tilde{\chi}(t)\big]\Big\} + \\ - \frac{1}{\hbar^2}\int_t^{t+\Delta t}\mathrm{d}t_1 \int_t^{t_1}\mathrm{d}t_2 \operatorname*{Tr}_{\mathrm{R}}\Big\{\big[\tilde{V}(t_1), \big[\tilde{V}(t_2), \tilde{\chi}(t_2)\big]\big]\Big\},\end{aligned} \tag{2.8}$$

where $\Delta\tilde{\rho}(t) = \tilde{\rho}(t+\Delta t) - \tilde{\rho}(t)$. Notice that Eq. (2.8) is still exact.

Now we assume the existence of two very different time scales: the typical time τ_{S} in which the system S changes appreciably is larger than the time τ_{R} in which reservoir correlations disappear, and we choose Δt such that

$$\tau_{\mathrm{R}} \ll \Delta t \ll \tau_{\mathrm{S}}. \tag{2.9}$$

We also assume that the reservoir R is large compared to the system S, and that the interaction $\hat{V}$ is small compared to the Hamiltonians $\hat{H}_{\mathrm{S}}$ and $\hat{H}_{\mathrm{R}}$. The reduced density matrix of the reservoir $\tilde{R}(t) = \mathrm{Tr}_{\mathrm{S}}\{\tilde{\chi}(t)\}$ may thus be considered constant $\tilde{R}(t) = \tilde{R}(0) = R_0$. Moreover we assume that the reservoir is in a stationary state, that is $\big[R_0, \hat{H}_{\mathrm{R}}\big] = 0$. We also assume that $\mathrm{Tr}_{\mathrm{R}}\big\{\hat{V}R_0\big\} = 0$, if that is not the case, it is sufficient to include an additional term in the system Hamiltonian $\hat{H}_{\mathrm{S}} \to \hat{H}_{\mathrm{S}} + \mathrm{Tr}_{\mathrm{R}}\big\{\hat{V}R_0\big\}$ and in the interaction Hamiltonian $\hat{V} \to \hat{V} - \mathrm{Tr}_{\mathrm{R}}\big\{\hat{V}R_0\big\}$.

Based on these assumptions we can now perform several approximations. Using the assumptions that $\hat{V}$ is small compared to $\hat{H}_{\mathrm{S}}$ and $\hat{H}_{\mathrm{R}}$, and that $\Delta t \ll \tau_{\mathrm{S}}$, we neglect the evolution of $\tilde{\chi}$ between t and t_2 in the last term of Eq. (2.8) and replace[3] $\tilde{\chi}(t_2)$ by $\tilde{\chi}(t)$. After such approximation the right and side of Eq. (2.8) contains only $\tilde{\chi}(t)$ which can be written as

$$\tilde{\chi}(t) = \tilde{\rho}(t) \otimes \tilde{R}(t) + \Delta\chi(t). \tag{2.10}$$

Based on the assumption that $\tau_{\mathrm{R}} \ll \Delta t$ and that we keep only terms up to second order in $\hat{V}$, we neglect the contribution $\Delta\chi$. Such approximation is equivalent to write $\tilde{\chi}(t) = \tilde{\rho}(t) \otimes R_0$, where we have also used $\tilde{R}(t) = R_0$.

Now we divide Eq. (2.8) by Δt and, using the approximations above, we obtain[4]

$$\frac{\partial\tilde{\rho}(t)}{\partial t} \simeq -\frac{1}{\hbar^2}\frac{1}{\Delta t}\int_t^{t+\Delta t}\mathrm{d}t_1 \int_t^{t_1}\mathrm{d}t_2 \operatorname*{Tr}_{\mathrm{R}}\Big\{\Big[\tilde{V}(t_1), \big[\tilde{V}(t_2), \tilde{\rho}(t)\otimes R_0\big]\Big]\Big\}, \tag{2.11}$$

where, since $\Delta t \ll \tau_{\mathrm{S}}$, we approximated the derivative $\partial\tilde{\rho}(t)/\partial t$ with the rate of variation $\Delta\tilde{\rho}(t)/\Delta t$. This approximation means that we look

2 $\mathrm{Tr}_{\mathrm{R}}\big[\tilde{\chi}(t)\big] = \mathrm{e}^{\mathrm{i}\hat{H}_{\mathrm{S}}t/\hbar}\hat{\rho}(t)\mathrm{e}^{-\mathrm{i}\hat{H}_{\mathrm{S}}t/\hbar} = \tilde{\rho}(t)$, where $\hat{\rho}(t)$ is defined in Eq. (2.3).

3 Such approximation is equivalent to an iteration of Eq. (2.6) in which only terms up to second order in $\hat{V}$ are retained.

4 The first term of Eq. (2.8) is zero in fact: $\mathrm{Tr}_{\mathrm{R}}\big\{\big[\tilde{V}(t_1), \tilde{\chi}(t)\big]\big\} \simeq \mathrm{Tr}_{\mathrm{R}}\big\{\big[\tilde{V}(t_1), \tilde{\rho}(t)\otimes R_0\big]\big\} = \big[\mathrm{Tr}_{\mathrm{R}}\big\{\tilde{V}(t_1)R_0\big\}, \tilde{\rho}(t)\big] = 0$ because we assumed that $\mathrm{Tr}_{\mathrm{R}}\big\{\hat{V}R_0\big\} = 0$.

at the evolution of $\tilde{\rho}(t)$ with a time resolution which is of the order of Δt. Effects which happen on a shorter time scale are averaged out. By changing variables of integration in Eq. (2.11) to $t_1 = t_1$ and $\tau = t_1 - t_2$ we obtain

$$\frac{\partial\tilde{\rho}}{\partial t}(t) = -\frac{1}{\hbar^2}\frac{1}{\Delta t}\int_t^{t+\Delta t} \mathrm{d}t_1 \int_0^{t_1-t} \mathrm{d}\tau \operatorname*{Tr}_{\mathrm{R}}\Big\{\Big[\tilde{V}(t_1),\big[\tilde{V}(t_1-\tau),\tilde{\rho}(t)\otimes R_0\big]\Big]\Big\}. \tag{2.12}$$

If the interaction Hamiltonian $\hat{V}$ is a sum of products of operators $\hat{s}_i$ on the system S and $\hat{r}_i$ on the reservoir, $\hat{V} = \sum_i \hat{s}_i\hat{r}_i$, then the integrand of Eq. (2.12) scales with $\mathrm{e}^{-\tau/\tau_{\mathrm{R}}}$. Using the assumption on the time scales $\tau_{\mathrm{R}} \ll \Delta t \ll \tau_{\mathrm{S}}$, we can approximate the upper limit of the integral in τ with $+\infty$, and then take the limit for $\Delta t \to 0$. Going back to the Schrödinger picture we then have

$$\frac{\partial}{\partial t}\hat{\rho}(t) = \frac{1}{\mathrm{i}\hbar}[\hat{H}_{\mathrm{S}},\hat{\rho}(t)] - \int_0^{\infty}\frac{\mathrm{d}\tau}{\hbar^2}\operatorname*{Tr}_{\mathrm{R}}\Big\{\big[V,\mathrm{e}^{-\mathrm{i}\hat{H}_0\tau/\hbar}[V,\hat{\rho}(t)\otimes R_0]\mathrm{e}^{\mathrm{i}\hat{H}_0\tau/\hbar}\big]\Big\}. \tag{2.13}$$

Equation (2.13) is called *Born-Markov master equation* or *master equation in Born-Markov approximation*. At this point, knowing the explicit form of $\hat{V}$ and $\hat{H}_0$, it is possible to carry out the τ-integration in Eq. (2.13) and arrive at the differential equation

$$\frac{\partial}{\partial t}\hat{\rho}(t) = \mathcal{L}\hat{\rho}(t). \tag{2.14}$$

Here $\mathcal{L}$ is a superoperator which is time independent and acts on the space of the system operators, and it is often referred to as *Liouville operator* or *Liouvillian*. Equation (2.14) is the type of master equation we will use through the rest of the thesis.

master equation in the Lindblad form

The master equation (2.14) is still physically admissible if it preserves the properties of density operators[5]. It can be shown that a sufficient condition is that it can be written in the *Lindblad form* [95, 96]

$$\mathcal{L}\hat{\rho}(t) = \frac{1}{\mathrm{i}\hbar}[\hat{H}_{\mathrm{S}},\hat{\rho}(t)] + \sum_k \gamma_k \mathcal{D}[\hat{o}_k]\hat{\rho}(t). \tag{2.15}$$

Here $\hat{o}_k$ are bounded system operators[6], $\gamma_k > 0$ are real positive scalars and

$$\mathcal{D}[\hat{o}]\hat{\rho} = 2\hat{o}\hat{\rho}\hat{o}^\dagger - \hat{o}^\dagger\hat{o}\hat{\rho} - \hat{\rho}\hat{o}^\dagger\hat{o}. \tag{2.16}$$

The formal solution of Eq. (2.14) is

$$\hat{\rho}(t) = \mathrm{e}^{\mathcal{L}t}\hat{\rho}(0), \tag{2.17}$$

5 The properties of any density operator $\hat{\rho}(t)$ are that $\mathrm{Tr}[\hat{\rho}(t)] = 1$, that it is Hermitian $\hat{\rho}^\dagger(t) = \hat{\rho}(t)$ and positive semi-definite.

6 They are commonly called jump or Lindblad operators.

where $\hat{\rho}(0)$ is the initial state of the system.

In this thesis we will use the Born-Markov master equation to describe the decay of the cavity field due to the finite transmittivity of the mirrors (see Sec. 1.2.2) and the spontaneous decay of an atomic excitation.

The dynamics of the cavity field due to the finite mirror transmittivity can be cast in terms of the master equation for a damped harmonic oscillator, where S is the cavity mode and R is the electromagnetic field outside the cavity. In this case the Hamiltonian $\hat{H}_{\mathrm{S}}$ is given by Eq. (1.15), $\hat{H}_{\mathrm{R}}$ by Eq. (1.3) and $\hat{V}$ by Eq. (1.17). The master equation in Born-Markov approximation is then[7]

$$\frac{\partial}{\partial t}\hat{\rho}(t) = -\mathrm{i}\omega_{\mathrm{c}}\left[\hat{a}^{\dagger}\hat{a}, \hat{\rho}(t)\right] + \left(\bar{n}_{\omega_{\mathrm{c}}} + 1\right)\kappa\mathcal{D}[\hat{a}]\hat{\rho}(t) + \bar{n}_{\omega_{\mathrm{c}}}\kappa\mathcal{D}[\hat{a}^{\dagger}]\hat{\rho}(t), \quad (2.18)$$

where $\left[\hat{a}, \hat{a}^{\dagger}\right] = 1$, 2κ is the damping rate, and

$$\bar{n}_{\omega} = \frac{\mathrm{e}^{-\hbar\omega/k_{\mathrm{B}}T}}{\left(1 - \mathrm{e}^{-\hbar\omega/k_{\mathrm{B}}T}\right)} \quad (2.19)$$

is the mean occupation number for an oscillator with frequency ω in thermal equilibrium at temperature T.

In a similar way, spontaneous emission is described in terms of a master equation where S is a two-level system and R is the electromagnetic field in space. The Hamiltonian $\hat{H}_{\mathrm{S}}$ is given by Eq. (1.2), $\hat{H}_{\mathrm{R}}$ by Eq. (1.3) and the interaction $\hat{V}$ by Eq. (1.10). The resulting master equation reads[8]

$$\frac{\partial}{\partial t}\hat{\rho}(t) = -\mathrm{i}\omega_{\mathrm{a}}[|e\rangle\langle e|, \hat{\rho}(t)] + \left(\bar{n}_{\omega_{\mathrm{a}}} + 1\right)\gamma\mathcal{D}[|g\rangle\langle e|]\hat{\rho}(t) + \bar{n}_{\omega_{\mathrm{a}}}\gamma\mathcal{D}[|e\rangle\langle g|]\hat{\rho}(t), \quad (2.20)$$

where $|g\rangle$ and $|e\rangle$ are the ground and excited states with energy splitting[9] $\hbar\omega_{\mathrm{a}}$, 2γ is the damping rate[10] and $\bar{n}_{\omega_{\mathrm{a}}}$ is defined in Eq. (2.19). The last terms in Eqs. (2.18) and (2.20) describe the process of absorption of a thermal photon. For optical frequencies $\omega \sim 10^{15}\,Hz$ and room temperatures $T = 300\,K$ one has $\hbar\omega \sim 25 k_{\mathrm{B}}T$ and $\bar{n}_{\omega} \sim 10^{-11}$; in this case the contributions proportional to $\bar{n}_{\omega}$ in (2.18) and (2.20) can be safely neglected.

2.2 QUANTUM REGRESSION THEOREM

The formalism of Sec. 2.1 allows us, at least in principle, to calculate the time evolution of the reduced density operator $\hat{\rho}(t)$ of the system S in

7 Here we neglected the frequency shift due to the interaction with the bath. In the case of the two-level atom this is the *Lamb shift*.

8 Here we consider an atom fixed at the position $\boldsymbol{r}$. This can be achieved for example with an optical trap.

9 See note 7.

10 It is the *Einstein A coefficient* and can be calculated from the Wigner-Weisskopf theory of natural linewidth [97].

Born-Markov approximation. From this density operator one can obtain time-dependent expectation values for any operator $\hat{o}$ acting on $\mathcal{H}_{\mathrm{S}}$ with the formula $\langle \hat{o}(t) \rangle = \mathrm{Tr}[\hat{\rho}(t)\hat{o}]$. However, it does not directly provide a recipe to calculate the expectation values of products of system operators evaluated at two different times, that is, *two-time correlation functions*

$$\langle \hat{o}_1(t)\hat{o}_2(t+\tau) \rangle, \quad \tau > 0, \quad \hat{o}_1, \hat{o}_2 \text{ operators on } \mathcal{H}_s. \tag{2.21}$$

The result of such expectation value was derived in Refs. [98, 99] and it is called *quantum regression theorem* or *quantum regression formula* [89]. Here we present a short derivation.

In order to evaluate the correlation function given in Eq. (2.21) we need to go back to the idea of system plus reservoir. In that case the two-time correlation function is straightforwardly defined in Heisenberg picture

$$\langle \hat{o}_1(t)\hat{o}_2(t+\tau) \rangle = \operatorname*{Tr}_{S\otimes R}[\hat{\chi}(0)\hat{o}_1(t)\hat{o}_2(t+\tau)], \tag{2.22}$$

where $\hat{\chi}(0)$ is the density operator of system and reservoir at the initial time $t = 0$, and the system operators $\hat{o}_i(t)$ in Heisenberg picture satisfy the Heisenberg equations of motion

$$\frac{\mathrm{d}}{\mathrm{d}t}\hat{o}_i(t) = \frac{1}{\mathrm{i}\hbar}[\hat{o}_i(t), \hat{H}], \tag{2.23}$$

whose formal solution is

$$\hat{o}_i(t) = \mathrm{e}^{\mathrm{i}\hat{H}t/\hbar}\hat{o}_i(0)\mathrm{e}^{-\mathrm{i}\hat{H}t/\hbar}. \tag{2.24}$$

Here $\hat{H}$ is the total Hamiltonian given in Eq. (2.1). Furthermore, the formal solution of the von Neumann equation (2.2) is

$$\hat{\chi}(0) = \mathrm{e}^{\mathrm{i}\hat{H}t/\hbar}\hat{\chi}(t)\mathrm{e}^{-\mathrm{i}\hat{H}t/\hbar}. \tag{2.25}$$

Substituting Eqs. (2.24) and (2.25) in Eq. (2.22) and using the cyclic property of the trace one obtains

$$\begin{aligned} \langle \hat{o}_1(t)\hat{o}_2(t+\tau) \rangle &= \operatorname*{Tr}_{S\otimes R}\left[\hat{o}_2(0)\mathrm{e}^{-\mathrm{i}\hat{H}\tau/\hbar}\hat{\chi}(t)\hat{o}_1(0)\mathrm{e}^{\mathrm{i}\hat{H}\tau/\hbar}\right] = \\ &= \operatorname*{Tr}_{S}\left\{\hat{o}_2(0)\operatorname*{Tr}_{R}\left[\mathrm{e}^{-\mathrm{i}\hat{H}\tau/\hbar}\hat{\chi}(t)\hat{o}_1(0)\mathrm{e}^{\mathrm{i}\hat{H}\tau/\hbar}\right]\right\}, \end{aligned} \tag{2.26}$$

where in the last step we have used that the operator $\hat{o}_2(0)$ acts on $\mathcal{H}_{\mathrm{S}}$. We now define the operator

$$\hat{X}(\tau) = \mathrm{e}^{-\mathrm{i}\hat{H}\tau/\hbar}\hat{\chi}(t)\hat{o}_1(0)\mathrm{e}^{\mathrm{i}\hat{H}\tau/\hbar} \tag{2.27}$$

which acts on the system plus reservoir Hilbert space $\mathcal{H}_{\mathrm{S}} \otimes \mathcal{H}_{\mathrm{R}}$. It clearly satisfies the differential equation in the time-variable τ

$$\frac{\partial}{\partial\tau}\hat{X}(\tau) = \frac{1}{\mathrm{i}\hbar}[\hat{H}, \hat{X}(\tau)] \tag{2.28}$$

with initial condition $\hat{X}(0) = \hat{\chi}(t)\hat{o}_1(0)$. Equation (2.28) is the von Neumann equation for the operator $\hat{X}(\tau)$. In order to remove the reference

to the reservoir in Eq. (2.26) we need to calculate the trace over R of $\hat{X}(\tau)$, Eq. (2.27), i. e. we need

$$\hat{x}(\tau) = \operatorname*{Tr}_{\mathrm{R}}\big[\hat{X}(\tau)\big]. \tag{2.29}$$

We are now in the same situation as in Sec. 2.1: we have the von Neumann equation for an operator acting on $\mathcal{H}_{\mathrm{S}} \otimes \mathcal{H}_{\mathrm{R}}$ and we want to calculate an equation for the reduced operator acting only on $\mathcal{H}_{\mathrm{S}}$ by taking the trace over the reservoir degrees of freedom. We can then use the same arguments used in Sec. 2.1 to derive the Born-Markov master equation (2.14), and write

$$\frac{\partial}{\partial\tau}\hat{x}(\tau) = \mathcal{L}\hat{x}(\tau) \tag{2.30}$$

with the formal solution

$$\hat{x}(\tau) = \mathrm{e}^{\mathcal{L}\tau}\hat{x}(0) = \mathrm{e}^{\mathcal{L}\tau}\operatorname*{Tr}_{\mathrm{R}}[\hat{\chi}(t)\hat{o}_1(0)] = \mathrm{e}^{\mathcal{L}\tau}[\hat{\rho}(t)\hat{o}_1(0)], \tag{2.31}$$

where $\hat{\rho}(t) = \mathrm{Tr}_{\mathrm{R}}[\hat{\chi}(t)]$ is the reduced density operator of the system S. Substituting Eq. (2.31) in Eq. (2.26) one obtains

$$\langle\hat{o}_1(t)\hat{o}_2(t+\tau)\rangle = \operatorname*{Tr}_{S}\big\{\hat{o}_2(0)\mathrm{e}^{\mathcal{L}\tau}[\hat{\rho}(t)\hat{o}_1(0)]\big\}; \tag{2.32a}$$

and analogously

$$\langle\hat{o}_1(t+\tau)\hat{o}_2(t)\rangle = \operatorname*{Tr}_{S}\big\{\hat{o}_1(0)\mathrm{e}^{\mathcal{L}\tau}[\hat{o}_2(0)\hat{\rho}(t)]\big\}. \tag{2.32b}$$

Equations (2.32) constitute the result of the *quantum regression theorem*.

2.3 SPECTRAL DECOMPOSITION OF THE LIOUVILLIAN

Consider the space $L(\mathcal{H}_{\mathrm{S}})$ of the linear operators acting on the Hilbert space $\mathcal{H}_s$. The density operators form a convex subset of $L(\mathcal{H}_{\mathrm{S}})$. We can define an inner product in $L(\mathcal{H}_{\mathrm{S}})$ as

$$(A, B) = \mathrm{Tr}\,(A^\dagger B), \tag{2.33a}$$

and an outer product as

$$[A \otimes B]C = A(B, C) = \mathrm{Tr}\,(B^\dagger C)A, \tag{2.33b}$$

$$C^\dagger[A \otimes B] = (C, A)B^\dagger = \mathrm{Tr}\,(C^\dagger A)B^\dagger. \tag{2.33c}$$

Definitions (2.33) are problematic since $(A, B) < \infty$ is not guaranteed for arbitrary operators $A, B \in L(\mathcal{H}_{\mathrm{S}})$. We ignore this problem and assume that $(A, B) < \infty$ holds for all operators A and B we use, for a discussion see [92].

Master equation (2.14) is a linear differential equation for the density operator $\hat{\rho}(t)$. The Liouvillian $\mathcal{L}$ is a linear operator that acts on the space $L(\mathcal{H}_{\mathrm{S}})$, for this reason it is often referred to as *superoperator*. It is in general

not Hermitian and its Hermitian conjugate is defined by means of the scalar product introduced in Eq. (2.33a)

$$(\hat{\rho}, \mathcal{L}\hat{\rho}') = (\mathcal{L}^\dagger\hat{\rho}, \hat{\rho}'), \quad \forall\hat{\rho}, \hat{\rho}' \text{ density operators}, \tag{2.34}$$

as well as its action to the left

$$(\hat{\rho}, \mathcal{L}\hat{\rho}') = (\hat{\rho}\mathcal{L}, \hat{\rho}'), \quad \forall\hat{\rho}, \hat{\rho}' \text{ density operators}. \tag{2.35}$$

Sometimes it is useful to work in the set where the Liouvillian operator is diagonal, if it exists. This set is called the damping basis in [91].

damping basis

The eigenvalues equations for $\mathcal{L}$ are

$$\mathcal{L}\hat{\rho}_\lambda = \lambda\hat{\rho}_\lambda, \quad \check{\rho}_\lambda^\dagger\mathcal{L} = \lambda\check{\rho}_\lambda^\dagger \tag{2.36}$$

where λ are the eigenvalues, $\hat{\rho}_\lambda$ the relative right eigenvectors and $\check{\rho}_\lambda$ the relative left eigenvectors. If the eigenvalues are not degenerate then we can normalize the right and left eigenvectors such that the *orthogonality relation* holds

$$(\check{\rho}_\lambda, \hat{\rho}_{\lambda'}) = \mathrm{Tr}\,(\check{\rho}_\lambda^\dagger\hat{\rho}_{\lambda'}) = \delta_{\lambda\lambda'}. \tag{2.37}$$

For a non-Hermitian operator it is in general not a priori clear if the sets $\{\check{\rho}_\lambda\}$ and $\{\hat{\rho}_\lambda\}$ form complete bases, for this reason the *completeness relation*

$$\sum_\lambda \hat{\rho}_\lambda \otimes \check{\rho}_\lambda = \sum_\lambda P_\lambda = \mathbb{1} \tag{2.38}$$

has to be checked case by case. It has been proved that the damping basis of a damped harmonic oscillator [92, 93] and of a driven and dumped two-level system [94] are complete.

Assuming that the completeness relation (2.38) holds, the damping basis can be used to expand the formal solution Eq. (2.17) of master equation (2.14). If the Liouvillian $\mathcal{L}$ is time-independent and the completeness relation Eq. (2.38) holds, then

$$\hat{\rho}(t) = \mathrm{e}^{\mathcal{L}t}\sum_\lambda[\hat{\rho}_\lambda \otimes \check{\rho}_\lambda]\hat{\rho}(0) = \sum_\lambda c_\lambda \mathrm{e}^{\lambda t}\hat{\rho}_\lambda, \tag{2.39}$$

with the coefficients $c_\lambda = (\check{\rho}_\lambda, \hat{\rho}(0)) = \mathrm{Tr}\big[\check{\rho}_\lambda^\dagger\hat{\rho}(0)\big]$.

2.3.1 *Some properties of the damping basis*

Any physical density operator $\hat{\rho}$ has the properties that $\mathrm{Tr}[\hat{\rho}] = 1$, that is Hermitian $\hat{\rho} = \hat{\rho}^\dagger$ and that all its eigenvalues are non-negative. The Liouvillian $\mathcal{L}$ generates the time evolution of the density operator which must conserve these properties at all times. This consideration puts some constraints on $\mathcal{L}$. Liouville operators which fulfill these constraints are said to be of *Lindblad form* [95], Eqs. (2.15) and (2.16). In the following we summarize some properties of the damping basis arising from those

constraints. For simplicity we assume a non-degenerate Liouvillian and the existence of a unique steady state.

First, the condition $\mathrm{Tr}[\hat{\rho}] = 1$ implies that the identity operator $\mathbb{1}$ is a left eigenvector with eigenvalue zero, $\mathbb{1}\mathcal{L} = 0$. In fact:

$$0 = \frac{\mathrm{d}}{\mathrm{d}t}\mathrm{Tr}(\hat{\rho}) = \mathrm{Tr}\left(\frac{\partial}{\partial t}\hat{\rho}\right) = \mathrm{Tr}(\mathcal{L}\hat{\rho}) = \mathrm{Tr}(\mathbb{1}\mathcal{L}\hat{\rho}) = 0, \tag{2.40}$$

this implies that $\mathbb{1}\mathcal{L} = 0$, i. e., $\check{\rho}_0^\dagger = \mathbb{1}$. Furthermore, the right eigenvector $\hat{\rho}_0$with respect to the eigenvalue $\lambda = 0$ is the steady state. In fact, by definition

$$0 = \frac{\partial}{\partial t}\hat{\rho}_0 = \mathcal{L}\hat{\rho}_0. \tag{2.41}$$

The steady state $\hat{\rho}_0$ is the only right eigenvector which is a density operator. In fact, since $\mathrm{Tr}(\mathcal{L}\hat{\rho}) = 0$, then

$$\mathrm{Tr}(\mathcal{L}\hat{\rho}_\lambda) = \lambda\,\mathrm{Tr}(\hat{\rho}_\lambda) = 0, \tag{2.42}$$

hence $\mathrm{Tr}(\hat{\rho}_\lambda) = 0, \forall\lambda \neq 0$, i. e., all the right eigenvectors $\hat{\rho}_\lambda$ except the steady state $\hat{\rho}_0$ are traceless. Finally, from the Lindblad theorem introduced in Sec. 2.1 follows that $\Re(\lambda) \leq 0$.

2.4 THE WIGNER FUNCTION

In the preceding sections we have described the quantum state of a system by means of its density operator $\hat{\rho}$. However there are equivalent representations which live in phase space and that allows us to express the state in terms of a c-number function, often called *quasi-probability distribution*. The reason for the name is that the quasi-probability distributions allow for the calculation of expectation values of quantum operators using the methods of classical statistical physics. Nonetheless, they are not actual probability functions, since, for example, some of them could assume negative values. In the years 1969-1970 Refs. [100–103] introduced a formalism in which an infinite amount of different representations are defined. Here however, we focus on one special case, which is the first quasi-probability distribution introduced as long ago as 1932, that is the *Wigner function* [104].

In the following we review the Wigner function and some of its properties in order to illustrate its application for the solution of the master equation. Further details can be seen for example in Refs. [53, 89, 105].

Consider a particle in one dimension with mass m, position $\hat{x}$ and momentum $\hat{p}$, with $[\hat{x}, \hat{p}] = \mathrm{i}\hbar$. We define the Wigner transformation of an operator $\hat{\mu}$ as *Wigner transform*

$$W_\mu(x, p) = \frac{1}{\pi\hbar}\int_{-\infty}^{\infty}\langle x + y|\hat{\mu}|x - y\rangle \mathrm{e}^{-2\mathrm{i}yp/\hbar}\mathrm{d}y, \tag{2.43}$$

where $|x \pm y\rangle$ are eigenstates of the position operator $\hat{x}$ with eigenvalues $x \pm y$, and $x, y, p \in \mathbb{R}$. The Wigner function is the Wigner transform of *Wigner function*

the density operator $\hat{\rho}$ of the system

$$W(x,p) = W_\rho(x,p) = \frac{1}{\pi\hbar}\int_{-\infty}^{\infty}\langle x+y|\hat{\rho}|x-y\rangle \mathrm{e}^{-2\mathrm{i}yp/\hbar}\mathrm{d}y. \tag{2.44}$$

For a harmonic oscillator it is possible to define the Wigner function $W(\alpha,\alpha^*)$, where α and α^* are complex variables that are related to the amplitude of a coherent state $|\alpha\rangle$. In Appendix 2.A we give the Wigner function $W(\alpha,\alpha^*)$ for a harmonic oscillator by means of an equivalent, but easier to generalize, definition.

2.4.1 *Some properties of the Wigner function*

The moments of the Wigner function are equal to the expectation values of symmetrically ordered products of position and momentum operators

$$\mathrm{Tr}\Big[\hat{\rho}\,\{\hat{x}^n\hat{p}^m\}_{\mathrm{sym}}\Big] = \int_{-\infty}^{\infty}\int_{-\infty}^{\infty} W(x,p)x^n p^m \mathrm{d}x\mathrm{d}p, \tag{2.45}$$

where $\{\cdot\}_{\mathrm{sym}}$ is the average of all possible ways of ordering the operators inside the brackets. In particular the marginals of $W(x,p)$ are the probability distribution of position and momentum

$$\mathrm{Tr}[\hat{\rho}\hat{x}] = \int_{-\infty}^{\infty}\langle x|\hat{\rho}|x\rangle x\mathrm{d}x = \int_{-\infty}^{\infty}\int_{-\infty}^{\infty} W(x,p)x\mathrm{d}x\mathrm{d}p = \int_{-\infty}^{\infty} W(x)x\mathrm{d}x, \tag{2.46}$$

where $W(x)$ is the probability distribution of the position

$$W(x) = \langle x|\hat{\rho}|x\rangle = \int_{-\infty}^{\infty} W(x,p)\mathrm{d}p, \tag{2.47}$$

and analogously the probability distribution of the momentum is

$$W(p) = \int_{-\infty}^{\infty} W(x,p)\mathrm{d}x. \tag{2.48}$$

Equation (2.45) also implies the normalization of the Wigner function

$$\int_{-\infty}^{\infty}\int_{-\infty}^{\infty} W(x,p)\mathrm{d}x\mathrm{d}p = \mathrm{Tr}[\hat{\rho}] = 1. \tag{2.49}$$

2.4.2 *Master equation in phase-space*

In Sec. 2.1 we showed that the time evolution of an open quantum system described by the density operator $\hat{\rho}$ is, in the Born-Markov approximation, given by an equation of the form (2.14). We now want to derive an equivalent formalism for the Wigner function, i. e. we want to find the equation of motion for $W(x,p)$.

In order to do so, we apply the Wigner transformation, Eq. (2.43), to the master equation (2.14) obtaining

$$\frac{\partial}{\partial t}W(x,p,t) = \int_{-\infty}^{\infty}\langle x+y|\mathcal{L}\hat{\rho}(t)|x-y\rangle \mathrm{e}^{-2\mathrm{i}yp/\hbar}\mathrm{d}y, \tag{2.50}$$

where the Wigner function $W(x,p,t)$ depends parametrically on the time t via the time dependence of the density operator $\hat{\rho}(t)$, see Eq. (2.44). Now one needs to calculate the right hand side of Eq. (2.50), i. e. the Wigner transform of the operator $\mathcal{L}\hat{\rho}$. This depends on the system under study, however the operator $\mathcal{L}\hat{\rho}$ is a linear combination of system operators acting on $\hat{\rho}$, both from right and left. The action of an operator on a density operator is mirrored by the action of a corresponding differential operator on the Wigner function [105]. It is possible to calculate this correspondence by using the definition of Wigner transformation and Wigner function, Eqs. (2.43) and (2.44). The results are summarized in Tab. 2.1.

DENSITY OPERATOR		WIGNER FUNCTION
$\hat{x}\hat{\rho}$	$\longleftrightarrow$	$\left(x+\frac{\mathrm{i}\hbar}{2}\frac{\partial}{\partial p}\right)W(x,p)$
$\hat{\rho}\hat{x}$	$\longleftrightarrow$	$\left(x-\frac{\mathrm{i}\hbar}{2}\frac{\partial}{\partial p}\right)W(x,p)$
$\hat{p}\hat{\rho}$	$\longleftrightarrow$	$\left(x-\frac{\mathrm{i}\hbar}{2}\frac{\partial}{\partial x}\right)W(x,p)$
$\hat{\rho}\hat{p}$	$\longleftrightarrow$	$\left(x+\frac{\mathrm{i}\hbar}{2}\frac{\partial}{\partial x}\right)W(x,p)$

Table 2.1: Correspondence between the action of an operator on the density operator $\hat{\rho}$ and the action of a differential operator on the Wigner function $W(x,p)$.

Finally, having calculated the Wigner transform of the operator $\mathcal{L}\hat{\rho}$, one can explicitly write Eq. (2.50): It is a partial differential equation for the Wigner function $W(x,p)$. This is the equation of motion that we were looking for.

In Appendix 2.A we present the correspondence as the one in Tab. 2.1 for a harmonic oscillator Wigner function $W(\alpha,\alpha^*)$.

APPENDICES

2.A WIGNER FUNCTION FOR A HARMONIC OSCILLATOR

Consider a harmonic oscillator of frequency ω with annihilation and creation operators $\hat{a}$ and $\hat{a}^\dagger$, with $\left[\hat{a},\hat{a}^\dagger\right]=1$. We define the characteristic function of a system operator $\hat{\mu}$ by

$$\chi_\mu(\lambda,\lambda^*) = \mathrm{Tr}\left[\hat{\mu}\left(\mathrm{e}^{\lambda\hat{a}^\dagger-\lambda^*\hat{a}}\right)\right], \tag{2.51}$$

where λ is a complex variable $\lambda = \lambda_r + i\lambda_i$, with $\lambda_r, \lambda_i \in \mathbb{R}$. The Wigner transformation of the operator $\hat{\mu}$ is the Fourier transform of its characteristic function

Wigner transform

$$W_\mu(\alpha, \alpha^*) = \frac{1}{\pi^2} \int_{-\infty}^{\infty} \int_{-\infty}^{\infty} \chi_\mu(\lambda, \lambda^*) e^{\alpha\lambda^* - \alpha^*\lambda} d^2\lambda, \tag{2.52}$$

where $d^2\lambda = d\lambda_r d\lambda_i$. Equation (2.52) is related to Eq. (2.43) by [105]

$$\frac{1}{2\hbar} W_\mu(\alpha, \alpha^*) = W_\mu(x, p), \tag{2.53}$$

with

$$x = \sqrt{\frac{\hbar}{2m\omega}}(\alpha + \alpha^*), \tag{2.54a}$$

$$p = -i\sqrt{\frac{m\omega\hbar}{2}}(\alpha - \alpha^*). \tag{2.54b}$$

Wigner function

The Wigner function is the Wigner transform of the density operator $\hat{\rho}$

$$W(\alpha, \alpha^*) = \frac{1}{\pi^2} \int_{-\infty}^{\infty} \int_{-\infty}^{\infty} \mathrm{Tr}\left[\hat{\rho}\left(e^{\lambda\hat{a}^\dagger - \lambda^*\hat{a}}\right)\right] e^{\alpha\lambda^* - \alpha^*\lambda} d^2\lambda. \tag{2.55}$$

In the following re report the properties of the Wigner function Eq. (2.55).

2.A.1 *Some properties of the Wigner function*

The moments of the Wigner function $W(\alpha, \alpha^*)$ are equal to the expectation values of symmetrically ordered products of creation and annihilation operators

$$\mathrm{Tr}\left[\hat{\rho}\left\{\hat{a}^n\left(\hat{a}^\dagger\right)^m\right\}_{\mathrm{sym}}\right] = \int_{-\infty}^{\infty} \int_{-\infty}^{\infty} W(\alpha, \alpha^*) \alpha^n (\alpha^*)^m d^2\alpha, \tag{2.56}$$

where $\{\cdot\}_{\mathrm{sym}}$ is the average of all possible ways of ordering the operators and $d^2\alpha = d\alpha_r d\alpha_i$, with $\alpha = \alpha_r + i\alpha_i$ and $\alpha_r, \alpha_i \in \mathbb{R}$.

Equation (2.56) implies the normalization of the Wigner function

$$\int_{-\infty}^{\infty} \int_{-\infty}^{\infty} W(\alpha, \alpha^*) d^2\alpha = \mathrm{Tr}[\hat{\rho}] = 1. \tag{2.57}$$

2.A.2 *Master equation in phase-space*

The equation of motion for the Wigner function $W(\alpha, \alpha^*)$ can be found following the same steps performed in Sec. 2.4.2: It is derived by applying the Wigner transformation, Eq. (2.52), to the master equation describing the system dynamics.

As for $W(x, p)$ in Sec. 2.4.2, it is possible to find the correspondence between the action of an operator on the density operator $\hat{\rho}$ and the

DENSITY OPERATOR		WIGNER FUNCTION
$\hat{a}\hat{\rho}$	$\longleftrightarrow$	$\left(\alpha + \frac{1}{2}\frac{\partial}{\partial\alpha^*}\right)W(\alpha,\alpha^*)$
$\hat{\rho}\hat{a}$	$\longleftrightarrow$	$\left(\alpha - \frac{1}{2}\frac{\partial}{\partial\alpha^*}\right)W(\alpha,\alpha^*)$
$\hat{a}^\dagger\hat{\rho}$	$\longleftrightarrow$	$\left(\alpha^* - \frac{1}{2}\frac{\partial}{\partial\alpha}\right)W(\alpha,\alpha^*)$
$\hat{\rho}\hat{a}^\dagger$	$\longleftrightarrow$	$\left(\alpha^* + \frac{1}{2}\frac{\partial}{\partial\alpha}\right)W(\alpha,\alpha^*)$

Table 2.2: Correspondence between the action of an operator on the density operator $\hat{\rho}$ and the action of a differential operator on the Wigner function $W(\alpha,\alpha^*)$. Notice that if $\alpha = \alpha_\mathrm{r} + \mathrm{i}\alpha_\mathrm{i}$ then $\partial/\partial\alpha = (\partial/\partial\alpha_\mathrm{r} - \mathrm{i}\partial/\partial\alpha_\mathrm{i})/2$ and $\partial/\partial\alpha^* = (\partial/\partial\alpha_\mathrm{r} + \mathrm{i}\partial/\partial\alpha_\mathrm{i})/2$.

action of a differential operator on the Wigner function $W(\alpha,\alpha^*)$. This is summarized in Tab. 2.2.

Finally, after calculating the Wigner transform of the operator $\mathcal{L}\hat{\rho}$, for example by means of Tab. 2.2, one derives a partial differential equation which is the equation of motion for the Wigner function $W(\alpha,\alpha^*)$.

Part II

STORAGE OF A SINGLE PHOTON

We theoretically analyze the dynamics of storage of a single photon in a quantum memory composed of a single atom trapped into a high-finesse optical cavity. In Chapter 3 we optimize the storage efficiency by suitably tailoring a laser pulse driving the atom. In the adiabatic regime we derive an analytical expression for the optimal laser pulse shape that leads to storage with maximal efficiency. In the non-adiabatic regime we employ optimal control theory to derive the optimal pulse shape, the maximal efficiency, and the shortest photon that can be stored with a given efficiency. In Chapter 4 we investigate the storage process when the single photon is replaced by an attenuated laser pulse.

3

OPTIMAL STORAGE OF A SINGLE PHOTON BY A SINGLE INTRA-CAVITY ATOM

The content of this chapter contains results, text and figures from:

- L. Giannelli, T. Schmit, T. Calarco, C. P. Koch, S. Ritter, and G. Morigi,
  "Optimal storage of a single photon by a single intra-cavity atom,
  In: "*New Journal of Physics* 20 (2018), p. 105009,
  DOI: 10.1088/1367-2630/aae725.

3.1 INTRODUCTION

Quantum control of atom-photon interactions is a prerequisite for the realization of quantum networks based on single photons as flying qubits [4, 106]. In these architectures, the quantum information carried by the photons is stored in a controlled way in a stable quantum mechanical excitation of a system, the quantum memory [107–111]. In several experimental realizations the quantum memory is an ensemble of spins and the photon is stored in a spin wave excitation [107]. Alternative approaches employ individually addressable particles, such as single trapped atoms or ions [35, 112]: here, high-aperture lenses [113] or optical resonators [114] increase the probability that the photon qubit is coherently transferred into an electronic excitation. In addition, schemes based on heralded state transfer have been realized [113, 115–117], and fibre-coupled resonators coupled to single atoms have been used to perform SWAP gates [118, 119]. Most recently, storage efficiencies of the order of 22% have been reported for a quantum memory composed by a single atom in an optical cavity [120]. This value lies well below the value one can extract from theoretical works on spin ensembles for photon storage [121]. This calls for a detailed understanding of these dynamics and for elaborating strategies to achieve full control of the atom-photon interface at the single atom level.

The purpose of this work is to provide a systematic theoretical analysis of the efficiency of protocols for a quantum memory for single photons, where information is stored in the electronic excitation of a single atom inside a high-finesse resonator. The qubit can be the photon polarization [35, 122], or a time-bin superposition of photonic states [123], and shall then be transferred into a superposition of atomic spin states.

The scheme is illustrated in Fig. 3.1: a photon propagating along a transmission line impinges on the cavity mirror, the storage protocol

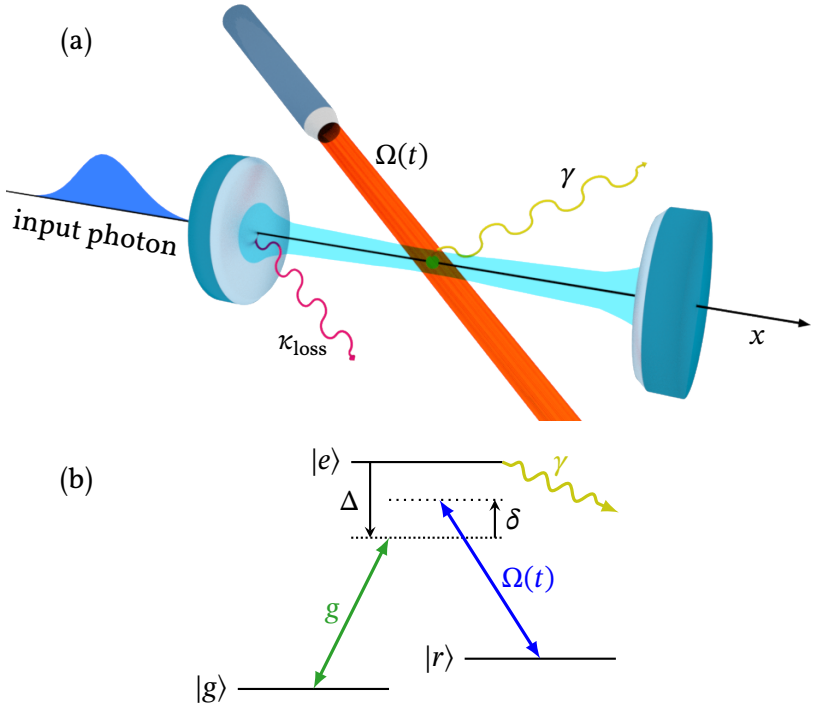

Figure 3.1: Storage of a single photon in the electronic state of a single atom confined inside an optical resonator. (a) The photon wave packet propagates along a transmission line and impinges onto a cavity mirror. (b) The single photon is absorbed by the cavity, which drives the atomic transition $|g\rangle \rightarrow |e\rangle$. An additional laser couples to the atomic transition $|r\rangle \rightarrow |e\rangle$. The dynamics of storage is tailored by optimizing the functional dependence of the laser amplitude on time, $\Omega(t)$: Ideally, the atom undergoes a Raman transition to the final state $|r\rangle$ and the photon is stored. We analyse the storage efficiency including the spontaneous decay with rate γ of the excited state and photon absorption or scattering at the cavity mirrors via an incoherent process at rate κ_{loss}. Further parameters are defined in the text.

coherently transfers the photon into a metastable atomic state, here denoted by $|r\rangle$, with the help of an external laser. The protocols we analyse are based on the seminal proposal by Cirac et al. [106]. Here, we first compare adiabatic protocols, originally developed for atomic ensembles in bad cavities [122, 124] as well as a protocol developed for any coupling regime for a single atom [123]. We then extend the protocol of Ref. [124] to quantum memories composed of single atoms confined inside a high-finesse resonator. We investigate how the storage efficiency is affected by parasitic losses at the cavity mirrors and whether these effects can be compensated by the dynamics induced by the laser pulse driving the atom. We finally extend our study to the non-adiabatic regime, and analyse the efficiency of storage of broadband photon pulses using optimal control.

This Chapter is organized as follows. In Sec. 3.2 we introduce the basic model, which we use in order to determine the efficiency of the storage process. In Sec. 3.3 we analyse the efficiency of protocols based on adiabatic dynamics in presence of irreversible cavity losses. In Sec. 3.4 we investigate the storage efficiency when the photon coherence time does not fulfil the condition for adiabatic quantum dynamics. Here, we use optimal control theory to determine the shortest photon pulse that can be stored. The conclusions are drawn in Sec. 3.5. The appendices provide further details of the analyses presented in Sec. 3.3.

3.2 BASIC MODEL

The basic elements of the dynamics are illustrated in Fig. 3.1. A photon propagates along the transmission line and impinges on the mirror of a high-finesse cavity. Here, it interacts with a cavity mode at frequency ω_c. The cavity mode, in turn, couples to a dipolar transition of a single atom, which is confined within the resonator. We denote by $|g\rangle$ the initial electronic state in which the atom is prepared, it is a metastable state and it performs a transition to the excited state $|e\rangle$ by absorbing a cavity photon. The relevant atomic levels are shown in subplot (b): they are two meta-stable states, $|g\rangle$ and $|r\rangle$, which are coupled by electric dipole transitions to a common excited state $|e\rangle$ forming a Λ level scheme. Transition $|r\rangle \to |e\rangle$ is driven by a laser, which we model by a classical field.

In order to describe the dynamics of the photon impinging onto the cavity mirror we resort to a coherent description of the modes of the electromagnetic field outside the resonator. The incident photon is an excitation of the external modes, and it couples with the single mode of a high-finesse resonator via the finite transmittivity of the mirror on which the photon is incident.

In this section we provide the details of our theoretical model and introduce the physical quantities which are relevant to the discussions in the rest of this paper.

3.2.1 *Master equation*

The state of the system, composed of the cavity mode, the atom, and the modes of the transmission line, is described by the density operator $\hat{\rho}$. Its dynamics is governed by the master equation ($\hbar = 1$)

$$\partial_t \hat{\rho} = -\mathrm{i}\big[\hat{H}(t), \hat{\rho}\big] + \mathcal{L}_{\mathrm{dis}}\hat{\rho}\,, \tag{3.1}$$

where Hamiltonian $\hat{H}(t)$ describes the coherent dynamics of the modes of the electromagnetic field outside the resonator, of the single-mode cavity, of the atom's internal degrees of freedom, and of their mutual coupling. The incoherent dynamics, in turn, is given by superoperator $\mathcal{L}_{\mathrm{dis}}$, and includes spontaneous decay of the atomic excited state, at rate γ, and cavity losses due to the finite transmittivity of the second cavity

mirror as well as due to scattering and/or finite absorption of radiation at the mirror surfaces, at rate κ_{loss}.

We first provide the details of the Hamiltonian. This is composed of two terms, $\hat{H}(t) = \hat{H}_{\text{fields}} + \hat{H}_{\text{I}}(t)$. The first term, $\hat{H}_{\text{fields}}$, describes the coherent dynamics of the fields in absence of the atom. It reads

$$\hat{H}_{\text{fields}} = \sum_k (\omega_k - \omega_{\text{c}}) \hat{b}_k^\dagger \hat{b}_k + \sum_k \lambda_k (\hat{a}^\dagger \hat{b}_k + \hat{b}_k^\dagger \hat{a}), \tag{3.2}$$

and is reported in the reference frame of the cavity mode frequency ω_{c}. Here, operators $\hat{b}_k$ and $\hat{b}_k^\dagger$ annihilate and create, respectively, a photon at frequency ω_k in the transmission line, with $\left[\hat{b}_k, \hat{b}_{k'}^\dagger\right] = \delta_{k,k'}$. The modes $\hat{b}_k$ are formally obtained by quantizing the electromagnetic field in the transmission line and have the same polarization as the cavity mode. They couple with strength λ_k to the cavity mode, which is described by a harmonic oscillator with annihilation and creation operators a and $a^\dagger$, where $\left[\hat{a}, \hat{a}^\dagger\right] = 1$ and $\left[\hat{a}, \hat{b}_k\right] = \left[\hat{a}, \hat{b}_k^\dagger\right] = 0$. In the rotating-wave approximation the interaction is of beam-splitter type and conserves the total number of excitations. The coupling λ_k is related to the radiative damping rate of the cavity mode by the rate $\kappa = L|\lambda(\omega_{\text{c}})|^2/c$, with $\lambda_k = \lambda(\omega_{\text{c}})$ the coupling strength at the cavity-mode resonance frequency [125] and L the length of the transmission line. Note that κ is the cavity decay rate because of transmission into the transmission line and is necessary for the storage, while κ_{loss} is the decay rate into other modes and is only detrimental.

The atom-photon interaction is treated in the dipole and rotating-wave approximation. The transition $|g\rangle \to |e\rangle$ couples with the cavity mode with strength (vacuum Rabi frequency) g. Transition $|r\rangle \to |e\rangle$ is driven by a classical laser with time-dependent Rabi frequency $\Omega(t)$, which is the function to be optimized in order to maximize the probability of transferring the excitation into state $|r\rangle$. The corresponding Hamiltonian reads

$$\hat{H}_{\text{I}} = \delta |r\rangle\langle r| - \Delta |e\rangle\langle e| + [g|e\rangle\langle g|\hat{a} + \Omega(t)|e\rangle\langle r| + \text{H.c.}], \tag{3.3}$$

where $\Delta = \omega_{\text{c}} - \omega_e$ is the detuning between the cavity frequency ω_{c} and the frequency ω_e of the $|g\rangle - |e\rangle$ transition, while $\delta = \omega_r + \omega_{\text{L}} - \omega_{\text{c}}$ is the two-photon detuning which is evaluated using the central frequency ω_{L} of the driving field $\Omega(t)$. Here, we denote by $\omega_r = (E_r - E_g)/\hbar$ the frequency difference (Bohr frequency) between the state $|r\rangle$ (of energy E_r) and the state $|g\rangle$ (of energy E_g). Unless otherwise stated, in the following we assume that the condition of two-photon resonance $\delta = 0$ is fulfilled.

The irreversible processes that we consider in our theoretical description are (i) the radiative decay at rate γ from the excited state $|e\rangle$, where photons are emitted into free field modes other than the modes $\hat{b}_k$ introduced in Eq. (3.2), and (ii) the cavity losses at rate κ_{loss} due to absorption and scattering at the cavity mirrors and to the finite transmittivity of the second mirror. We model each of these phenomena by Born-Markov

processes described by the superoperators $\mathcal{L}_\gamma$ and $\mathcal{L}_{\kappa_{\text{loss}}}$, respectively, such that $\mathcal{L}_{\text{dis}} = \mathcal{L}_\gamma + \mathcal{L}_{\kappa_{\text{loss}}}$ and

$$\mathcal{L}_\gamma \hat{\rho} = \gamma(2|\xi_e\rangle\langle e|\hat{\rho}|e\rangle\langle\xi_e| - |e\rangle\langle e|\hat{\rho} - \hat{\rho}|e\rangle\langle e|)\,, \tag{3.4a}$$

$$\mathcal{L}_{\kappa_{\text{loss}}} \hat{\rho} = \kappa_{\text{loss}}(2\hat{a}\hat{\rho}\hat{a}^\dagger - \hat{a}^\dagger\hat{a}\hat{\rho} - \hat{\rho}\hat{a}^\dagger\hat{a})\,. \tag{3.4b}$$

Here, $|\xi_e\rangle$ is an auxiliary atomic state where the losses of atomic population from the excited state $|e\rangle$ are collected.

3.2.2 *Initial state and target state*

The model is one dimensional, the transmission line is at $x < 0$, and the cavity mirror is at position $x = 0$. The single incident photon is described by a superposition of single excitations of the modes of the external field [126]

$$|\psi_{\text{sp}}\rangle = \sum_k \mathcal{E}_k \hat{b}_k^\dagger |\text{vac}\rangle, \tag{3.5}$$

where $|\text{vac}\rangle$ is the vacuum state and the amplitudes $\mathcal{E}_k$ fulfil the normalization condition $\sum_k |\mathcal{E}_k|^2 = 1$. For the studies performed in this work, we will consider the amplitudes

$$\mathcal{E}_k = \sqrt{\frac{c}{2L}} \int_{-\infty}^{\infty} \mathrm{d}t \mathrm{e}^{\mathrm{i}(kc-\omega_c)t} \mathcal{E}_{\text{in}}(t) \tag{3.6}$$

with c the speed of light, L the length of the transmission line, and

$$\mathcal{E}_{\text{in}}(t) = \frac{1}{\sqrt{T}} \operatorname{sech}\left(\frac{2t}{T}\right) \tag{3.7}$$

the input amplitude at the position $x = 0$, with T the characteristic time determining the coherence time T_c of the photon, $T_c = \pi T/4\sqrt{3}$ (see definition in Eq. (3.10)). Our formalism applies to a generic input envelope, nevertheless the specific choice of Eq. (3.7) allows us to compare our results with previous studies, see Refs. [122–124]. The total state of the system at the initial time $t = t_1$ is given by the input photon in the transmission line, the empty resonator, and the atom in state $|g\rangle$. In particular, the dynamics is analysed in the interval $t \in [t_1, t_2]$, with $t_1 < 0$, $t_2 > 0$ and $|t_1|, t_2 \gg T_c$, such that (i) at the initial time there is no spatial overlap between the single photon and the cavity mirror and (ii) assuming that the cavity mirror is perfectly reflecting, at $t = t_2$ the photon has been reflected away from the mirror.

The initial state is described by the density operator $\rho(t_0) = |\psi_0\rangle\langle\psi_0|$, where

$$|\psi_0\rangle = |g\rangle \otimes |0\rangle_c \otimes |\psi_{\text{sp}}\rangle\,, \tag{3.8}$$

and $|0\rangle_c$ is the Fock state of the resonator with zero photons.

Our target is to store the single photon into the atomic state $|r\rangle$ by shaping the laser field $\Omega(t)$. When comparing different storage approaches, it is essential to have a figure of merit characterizing the performance of the process. In accordance with Ref. [124] we define the efficiency η of the process as the ratio between the probability to find the excitation in the state $|\psi_T\rangle = |r\rangle \otimes |0\rangle_c \otimes |\mathrm{vac}\rangle$ at time t and the number of impinging photons between t_1 and t, namely

$$\eta(t) = \frac{\langle\psi_T|\rho(t)|\psi_T\rangle}{\int_{t_1}^{t} |\mathcal{E}_{\mathrm{in}}(t)|^2 \mathrm{d}t}\,, \tag{3.9}$$

where $t > t_1$ and the denominator is unity for $t \to t_2$. We note that states $|\psi_0\rangle$ and $|\psi_T\rangle$ are connected by the coherent dynamics via the intermediate states $|e\rangle \otimes |0\rangle_c \otimes |\mathrm{vac}\rangle$ and $|g\rangle \otimes |1\rangle_c \otimes |\mathrm{vac}\rangle$. These states are unstable, since they can decay via spontaneous emission or via the parasitic cavity losses. Moreover, the incident photon can be reflected off the cavity. The latter is a unitary process, which results in a finite probability of finding a photon excitation in the transmission line after the photon has reached the mirror. The choice of $\Omega(t)$ shall maximize the transfer $|\psi_0\rangle \to |\psi_T\rangle$ by minimizing the losses as well as reflection at the cavity mirror.

3.2.3 *Relevant quantities*

The transmission line is here modelled by a cavity of length L, with a perfect mirror at $x = -L$. The second mirror at $x = 0$ coincides with the mirror of finite transmittivity, separating the transmission line from the optical cavity. The length L is chosen to be sufficiently large to simulate a continuum of modes for all practical purposes. This requires that the distance between neighbouring frequencies is smaller than all characteristic frequencies of the problem. The smallest characteristic frequency is the bandwidth of the incident photon, which is the inverse of the photon duration in time. Since the initial state is assumed to be a single photon in a pure state, the latter coincides with the photon coherence time T_c [127] which is defined as

$$T_{\mathrm{c}} = \sqrt{\langle t^2\rangle - \langle t\rangle^2} \tag{3.10}$$

with $\langle t^x\rangle \equiv \int_{t_1}^{t_2} t^x |\mathcal{E}_{\mathrm{in}}(t)|^2 \mathrm{d}t$, and

$$\int_{t_1}^{t_2} |\mathcal{E}_{\mathrm{in}}(t)|^2 \mathrm{d}t = 1 - \varepsilon\,, \tag{3.11}$$

where $\varepsilon < 10^{-5}$ for the choice $|t_1| = t_2 = 6T_{\mathrm{c}}$ and $L = 12cT_{\mathrm{c}}$. The modes of the transmission line are standing waves with wave vector along the x axis. For numerical purposes we take a finite number N of modes around the cavity wave number $k_{\mathrm{c}} = \frac{\omega_{\mathrm{c}}}{c}$. Their wave numbers are

$$k_n = k_{\mathrm{c}} + \frac{n\pi}{L}\,, \tag{3.12}$$

while $n = -(N-1)/2, \ldots, (N-1)/2$, and the corresponding frequencies are $\omega_n = ck_n$. We choose N and L so that our simulations are not significantly affected by the finite size of the transmission line and by the cutoff in the mode number N. We further choose N in order to appropriately describe spontaneous decay by the cavity mode. This is tested by initialising the system with no atom and one cavity photon and choosing the parameters so to reproduce the exponential damping of the cavity field.

Note that a single mode of the cavity is sufficient to describe the interaction with a single photon if the photon frequencies lie in a range which is smaller than the free spectral range of the cavity and is centered around the frequency of the cavity mode. In this work we choose the central frequency of the photon to coincide with the cavity mode frequency $\omega_p = \omega_c$ and the spectrally broadest photon we consider (Figs. 3.5 and 3.6) spans about $16 \times 2\pi\, MHz$ around the cavity frequency ω_c. A cavity of $1\, cm$ has a free spectral range of about $15 \times 2\pi\, GHz$ which is three orders of magnitudes larger than the bandwidth of the photon. This justifies the approximation to a single mode cavity. The employed formalism can be applied to photons with other center frequencies as well, if the number of modes N is chosen sufficiently large and their center is appropriately shifted (c.f. eq. (3.12)).

Since the free field modes are included in the unitary evolution, it is possible to constantly monitor their state. The photon distribution in space at time t is given by

$$P(x,t) = \frac{2}{L} \sum_{n,m=1}^{N} \rho_{nm}(t) \sin\Big(n\frac{\pi}{L}x\Big) \sin\Big(m\frac{\pi}{L}x\Big), \tag{3.13}$$

where $\rho_{nm}(t) = \mathrm{Tr}\{\hat{\rho}(t)|1_m\rangle\langle 1_n|\}$ and $|1_n\rangle = b^\dagger_{k_n}|\mathrm{vac}\rangle$.

A further important quantity characterizing the coupling between cavity mode and atom is the cooperativity C, which reads [124]

$$C = \frac{g^2}{\kappa\gamma}\,. \tag{3.14}$$

The cooperativity sets the maximum storage efficiency in the limit in which the cavity can be adiabatically eliminated from the dynamics of the system [124], which corresponds to assuming the condition

$$\gamma C T_c \gg 1\,. \tag{3.15}$$

In this limit, in fact, the state $|g\rangle \otimes |1\rangle_c \otimes |\mathrm{vac}\rangle$ can be eliminated from the dynamics. Then, the efficiency satisfies $\eta(t) \leq \eta_{\max}$ where the maximal efficiency $\eta_{\max}$ reads [124]

$$\eta_{\max} = \frac{C}{1+C}. \tag{3.16}$$

The maximal efficiency $\eta_{\max}$ is reached for any input photon envelope $\mathcal{E}_{\mathrm{in}}(t)$ and detuning Δ, provided the adiabatic condition (3.15) is fulfilled.

In our study we also determine the probability that the photon is in the transmission line,

$$P_r(t) = \sum_k \mathrm{Tr}\{\hat{\rho}(t)|1_k\rangle\langle 1_k|\}, \tag{3.17}$$

the probability that spontaneous emission occurs,

$$P_s(t) = \mathrm{Tr}\{\hat{\rho}(t)|\xi_e\rangle\langle\xi_e|\}, \tag{3.18}$$

and finally, the probability that cavity parasitic losses take place,

$$P_{\mathrm{loss}}(t) = \mathrm{Tr}\{\hat{\rho}(t)|g, 0_c, \mathrm{vac}\rangle\langle g, 0_c, \mathrm{vac}|\}. \tag{3.19}$$

By means of these quantities we gain insight into the processes leading to optimal storage.

3.3 STORAGE IN THE ADIABATIC REGIME

In this section we determine the efficiency of storage protocols derived in Refs. [122–124] for the setup of Ref. [120] in the adiabatic regime. We then analyse how the efficiency of these protocols is modified by the presence of parasitic losses at rate κ_{loss}. In this case, we find also an analytic result which corrects the maximal value of Eq. (3.16).

We remark that in Refs. [122–124] the optimal pulses $\Omega(t)$ were analytically determined using input-output theory [55]. In Refs. [122, 124] the authors consider an atomic ensemble inside the resonator in the adiabatic regime. This regime consists in assuming the bad cavity limit $\kappa \gg g$ and the limit $\gamma T_c C \gg 1$. The first assumption allows one to adiabatically eliminate the cavity field variables from the equations of motion, the second assumption permits one to eliminate also the excited state $|e\rangle$. In Ref. [123] a single atom is considered and there is no such adiabatic approximation, but the coupling with the external field is treated using a phenomenological model.

Here we simulate the full Hamiltonian dynamics of the external field in the transmission line and consider a quantum memory composed of a single atom inside a reasonably good cavity. The parameters we refer to in our study are the ones of the setup of Ref. [120]:

$$(g, \kappa, \gamma) = (4.9, 2.42, 3.03) \times 2\pi\, MHz, \tag{3.20}$$

corresponding to the cooperativity $C = 3.27$ and to the maximal storage efficiency $\eta_{\mathrm{max}} = 0.77$. When we analyse the dependence of the efficiency on γ or κ, we vary the parameters around the values given in Eq. (3.20).

3.3.1 *Ideal resonator*

We first review the requirements and results of the individual protocols of Refs. [122–124] and investigate their efficiency for a single-atom quantum memory. The works of Refs. [122–124] determine the form of the

optimal pulse $\Omega(t)$ for cavities with cooperativities $C \geq 1$. The optimal pulse is found by imposing similar, but not equivalent requirements. In Refs. [122, 123] the authors determine $\Omega(t)$ by imposing impedance matching, namely, that there is no photon reflected back by the cavity mirror. In Ref. [124] the pulse $\Omega(t)$ warrants maximal storage, namely, maximal probability of transferring the photon into the atomic excitation $|r\rangle$. The latter requirement corresponds to maximizing the storage efficiency η defined in Eq. (3.9).

In detail, in Ref. [122] the authors determine the optimal pulse $\Omega(t)$ that suppresses back-reflection from the cavity and warrants that the dynamics follows adiabatically the dark state of the system composed by cavity and atom. For this purpose the authors impose that the cavity field is resonant with the transition $|g\rangle \to |e\rangle$, namely $\Delta = 0$. They further require that the coherence time T_c is larger than the cavity decay time, $\kappa T_c \gtrsim 1$. Under these conditions the optimal pulse $\Omega(t) = \Omega^F(t)$ reads

$$\Omega^F(t) = \frac{g\mathcal{E}_{in}(t)}{\sqrt{c_1 + 2\kappa \int_{t_1}^{t} |\mathcal{E}_{in}(t')|^2 dt' - |\mathcal{E}_{in}(t)|^2}}, \tag{3.21}$$

where c_1 regularize $\Omega^F(t)$ for $t \to t_1$. The work in Ref. [123] imposes the suppression of the back-reflected photon without any adiabatic approximation and finds the optimal pulse $\Omega(t) = \Omega^D(t)$, which takes the form

$$\Omega^D(t) = \frac{g\mathcal{E}_{in}(t) + \left(\dot{\mathcal{F}}(t) + \gamma\mathcal{F}(t)\right)/g}{\sqrt{2\kappa\rho_0 + 2\kappa \int_{t_1}^{t} |\mathcal{E}_{in}(t')|^2 - |\mathcal{E}_{in}(t)|^2 - \mathcal{D}(t)}}, \tag{3.22}$$

with

$$\mathcal{D}(t) = 2\gamma \int_{t_1}^{t} |\mathcal{F}(t')|^2 dt' + |\mathcal{F}(t)|^2 . \tag{3.23}$$

and $\mathcal{F}(t) = \dot{\mathcal{E}}_{in}(t) - \kappa\mathcal{E}_{in}(t)$. Coefficient ρ_0 accounts for a small initial population in the target state $|r\rangle$ and it is relevant in order to avoid divergences in Eq. (3.22) for $t \to t_1$, see Ref. [123] for an extensive discussion. The pulse $\Omega^F(t)$ of Eq. (3.21) can be recovered from Eq. (3.22) by imposing the conditions

$$\dot{\mathcal{F}}(t) + \gamma\mathcal{F}(t) = 0, \tag{3.24a}$$

$$-|\mathcal{F}(t_1)|^2 + 2\kappa\rho_0 = c_1. \tag{3.24b}$$

The control pulse $\Omega^D(t)$ can be considered as a generalization of $\Omega^F(t)$ since it is determined by solely imposing quantum impedance matching.

In Ref. [124] the authors determine the amplitude $\Omega(t)$ that maximizes the efficiency η. This condition is not equivalent to imposing impedance matching. In fact, while in the case of impedance matching major losses

through the excited state $|e\rangle$ are acceptable in order to minimize the probability of photon reflection, in the case of maximum transfer efficiency η those losses are detrimental and thus have to be minimized. The optimal pulse $\Omega(t) = \Omega^{\mathrm{G}}(t)$ is determined for a generic detuning Δ by using an analytical model based on the adiabatic elimination of the excited state $|e\rangle$ of the atom and of the cavity field in the bad cavity limit $\kappa \gg g$. It reads

$$\Omega^{\mathrm{G}}(t) = \frac{\gamma(1+C)+\mathrm{i}\Delta}{\sqrt{2\gamma(1+C)}} \frac{\mathcal{E}_{\mathrm{in}}(t)}{\sqrt{\int_{t_1}^{t}|\mathcal{E}_{\mathrm{in}}(t')|^2\mathrm{d}t'}} \times \exp\left(-\mathrm{i}\frac{\Delta}{2\gamma(1+C)}\ln\int_{t_1}^{t}|\mathcal{E}_{\mathrm{in}}(t')|^2\mathrm{d}t'\right). \tag{3.25}$$

In the limit in which the adiabatic conditions are fulfilled, this control pulse allows for storage with efficiency $\eta_{\max}$, Eq. (3.16). This efficiency approaches unity for cooperativities $C \gg 1$.

We start by integrating numerically the master equation for a single atom (3.1) after setting $\kappa_{\mathrm{loss}} = 0$, namely, by neglecting parasitic losses. We determine the storage efficiency at the time t_2, which we identify by taking $t_2 \gg T_{\mathrm{c}}$ for different choices of the control field $\Omega = \Omega^{\mathrm{G}}, \Omega^{\mathrm{F}}, \Omega^{\mathrm{D}}$ in Hamiltonian (3.3). Numerically, t_2 corresponds to the time the photon would need to be reflected back into the initial position, assuming that the partially reflecting mirror is replaced by a perfect mirror. Our numerical simulations are performed for a single atom in a resonator in the good cavity limit.

Figures 3.2 display the efficiency and the losses as a function of κ, γ, and of the coherence time T_c of the photon (and thus of the adiabatic parameter $\gamma T_{\mathrm{c}} C$). Each curve corresponds to the different control pulses in the Hamiltonian (3.3) according to the three protocols. In subplot (a) we observe that the efficiency reached with the pulse $\Omega^{\mathrm{G}}(t)$ corresponds to the maximum theoretical efficiency $\eta_{\max}$, while the efficiency with Ω^{D} is the smallest. In subplot (b) it is visible that the control pulse $\Omega^{\mathrm{G}}(t)$ warrants the maximum efficiency even down to values of κ of the order of $\kappa \sim g/5$. Subplot (c) displays the efficiency as a function of the adiabatic parameter $\gamma T_{\mathrm{c}} C$: the protocol $\Omega^{\mathrm{G}}(t)$ reaches the maximum theoretical efficiency $\eta_{\max}$ for $\gamma T_{\mathrm{c}} C \gtrsim 20$, while the other protocols have smaller efficiency for all values of T_{c}. Figures 3.2(d)(e)(f) report the probability that the photon is reflected back into the transmission line, eq. (3.17). It is evident that protocol Ω^{D} perfectly suppresses the back reflection probability in every regime here considered. However in the non-adiabatic regime (subplots (c)(f)(i), $\gamma T_{\mathrm{c}} C \lesssim 20$) the protocol Ω^{D}, as well as the protocol Ω^{F}, requires an increasing maximum Rabi frequency for decreasing T_{c}. At the value of about $\gamma T_{\mathrm{c}} C \approx 3.74$ the Rabi frequency is so high that it is not anymore manageable by our numerical solver, for this reason the plots for the protocols Ω^{D} and Ω^{F} are reported for $\gamma T_{\mathrm{c}} C \gtrsim 3.74$. The same happens for small values of κ, subplots (b)(e)(h): in this case the

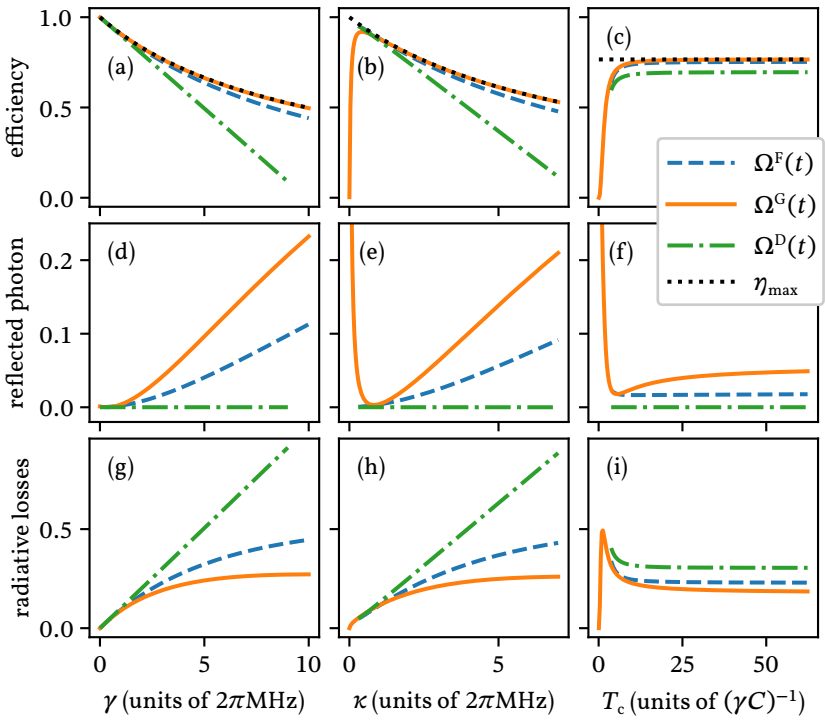

Figure 3.2: Comparison between the protocols of Refs. [122–124]. (Upper row) Storage efficiency η, Eq. (3.9), (central row) probability that the photon is reflected P_r, Eq. (3.17), and (bottom row) probability of spontaneous emission, Eq. (3.18), evaluated at time $t_2 = 6T_c$ by integrating numerically Eq. (3.1) for $\kappa_{loss} = 0$. The quantities are reported as a function of (left column) the decay rate γ from the excited state (for $\kappa = \kappa_0$ and $T_c = T_c^0$), (central column) the decay rate κ of the cavity field (for $\gamma = \gamma_0$ and $T_c = T_c^0$) and (right column) the coherence time of the photon T_c (in units of $1/(\gamma C)$ and for $\kappa = \kappa_0$ and $\gamma = \gamma_0$). The three different lines Ω^F, Ω^D, and Ω^G refer to the evolution with the respective control pulse (see Eqs. (3.21), (3.22), (3.25), respectively). The dotted lines in panels (a)(b)(c) correspond to the maximum efficiency $\eta = C/(1+C)$, Eq. (3.16). Here, $(g, \kappa_0, \gamma_0) = (4.9, 2.42, 3.03) \times 2\pi\, MHz$ and $T_c^0 = 0.5\,\mu s$. The input pulse $\mathcal{E}_{in}(t)$ is given in Eq. (3.7), at the initial time $t_1 = -6T_c$ the pulse has negligible overlap with the cavity mode. The transmission line has length $L = \max(12cT_c, 15c/\kappa)$ and 211 equispaced modes. With this choice the frequency range of the modes included in the simulation is about 40κ around the cavity frequency ω_c.

plots for the protocols Ω^D and Ω^F are reported for $\kappa \gtrsim 0.3 \times 2\pi\, MHz$. The diverging Rabi frequency can be avoided by an appropriate choice of the parameters c_1 and ρ_0 in Eqs. (3.21) and (3.22), respectively. Figures 3.2(g)(h)(i) report the losses via spontaneous emission of the atom, Eq. (3.18): while these losses are acceptable in order to minimize the back-reflected photon, they are detrimental for the intent of populating the target state $|r\rangle$. Protocol Ω^D, which perfectly suppresses the back

reflected photon, has the highest losses via spontaneous emission, which in the end leads to a lower efficiency η. Protocol Ω^{G} in turn, has the lowest radiative losses and it allows for the transfer with the maximal efficiency $\eta_{\max}$. Protocol Ω^{F} tries to minimize reflection of the photon at the cavity mirror. However, since Ω^{F} is derived with some approximations, it does not suppress completely the reflection and its final efficiency is between the ones of the other two protocols.

An important general result of this study is that the bad cavity limit is not essential for reaching the maximal efficiency as long as the dynamics is adiabatic: the relevant parameter is in fact the cooperativity.

3.3.2 *Parasitic losses*

The protocols so far discussed assume an ideal optical resonator. In this section we analyse how their efficiency is modified by the presence of parasitic losses, here described by the superoperator $\mathcal{L}_{\kappa_{\mathrm{loss}}}$ in Eq. (3.4b). In particular, we derive the maximal efficiency the protocols can reach as a function of $\kappa_{\mathrm{loss}} > 0$.

We first numerically determine the efficiency of the individual protocols as a function of κ_{loss} for $T_{\mathrm{c}} = 0.5\,\mu s$. Figure 3.3(a) displays η for $\Omega = \Omega^{\mathrm{G}}, \Omega^{\mathrm{D}}, \Omega^{\mathrm{F}}$. It is evident that the effect of losses is detrimental, for instance it leads to a definite reduction of the maximal efficiency from $\eta = 0.77$ down to $\eta = 0.68$ for $\kappa_{\mathrm{loss}} \sim 0.1\kappa$. This result can be improved by identifying a control field $\Omega = \Omega^{\mathrm{X}}$ which compensates, at least partially, the effects of these parasitic losses. The control field $\Omega^{\mathrm{X}}(t)$ is derived in Sec. 3.3.3 using the input-output formalism: it corresponds to performing the substitution $\kappa \to \kappa + \kappa_{\mathrm{loss}}$ in the functional form $\Omega^{\mathrm{G}}(t)$ of Eq. (3.25). Specifically, it reads

$$\begin{aligned}\Omega^{\mathrm{X}}(t) &= \frac{\gamma(1+C') + \mathrm{i}\Delta}{\sqrt{2\gamma(1+C')}} \frac{\mathcal{E}_{\mathrm{in}}(t)}{\sqrt{\int_{t_1}^{t} |\mathcal{E}_{\mathrm{in}}(t')|^2 \mathrm{d}t'}} \\ &\quad \times \exp\left(-\mathrm{i}\frac{\Delta}{2\gamma(1+C')} \ln \int_{t_1}^{t} |\mathcal{E}_{\mathrm{in}}(t')|^2 \mathrm{d}t'\right),\end{aligned} \tag{3.26}$$

with the modified cooperativity

$$C' = \frac{g^2}{\gamma(\kappa + \kappa_{\mathrm{loss}})}. \tag{3.27}$$

When the control pulse $\Omega^{\mathrm{X}}(t)$ is used, the efficiency of the process corresponds to the maximal efficiency $\eta'_{\max}$, which is now given by

$$\eta'_{\max} = \frac{\kappa}{\kappa + \kappa_{\mathrm{loss}}} \frac{C'}{1+C'}. \tag{3.28}$$

Clearly, $\eta'_{\max} \leq \eta_{\max}$, while the equality holds for $\kappa_{\mathrm{loss}} = 0$.

By inspecting the numerical results, we note that the efficiency obtained using Ω^{X} is always higher than the one reached by the other protocols. Even though for some values of κ_{loss} the efficiencies using different

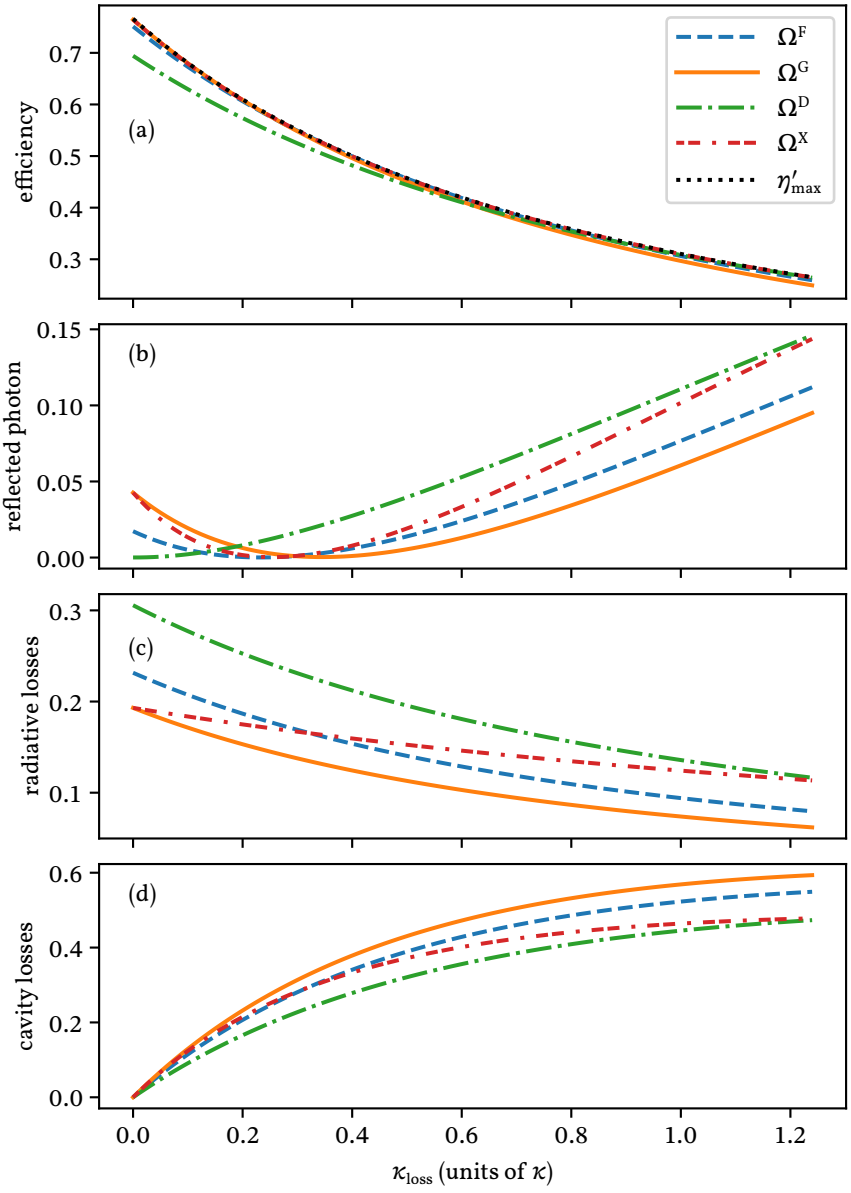

Figure 3.3: Efficiency of storage protocols in the adiabatic regime as a function of the rate of parasitic losses κ_{loss} (in units of κ). (a) Storage efficiency, Eq. (3.9), (b) the probability that the photon is reflected, Eq. (3.17), (c) the probability of spontaneous decay, Eq. (3.18), and (d) the probability of parasitic losses, Eq. (3.19), evaluated at time $t_2 = 6T_c$ and for $(g, \kappa, \gamma) = (4.9, 2.42, 3.03) \times 2\pi\, MHz$, $T_c = 0.5\,\mu s$. The other parameters are the same as in Fig. 3.2. The lines Ω^X, Ω^F, Ω^D, and Ω^G refer to the evolution with the respective control pulse (resp. Eqs. (3.26), (3.21), (3.22), (3.25)). The dotted line in (a) corresponds to the value of η'_{max}, Eq. (3.28).

control fields may approach the one found with Ω^X, yet the dynamics are substantially different. This is visible by inspecting the probability that the photon is reflected, the radiative losses, and the parasitic losses, as a

function of κ_{loss} as shown in Figs. 3.3(b)(c)(d), respectively: Each pulse distributes the losses in a different way, with $\Omega^{\text{X}}(t)$ interpolating among the different strategies in order to maximize the efficiency.

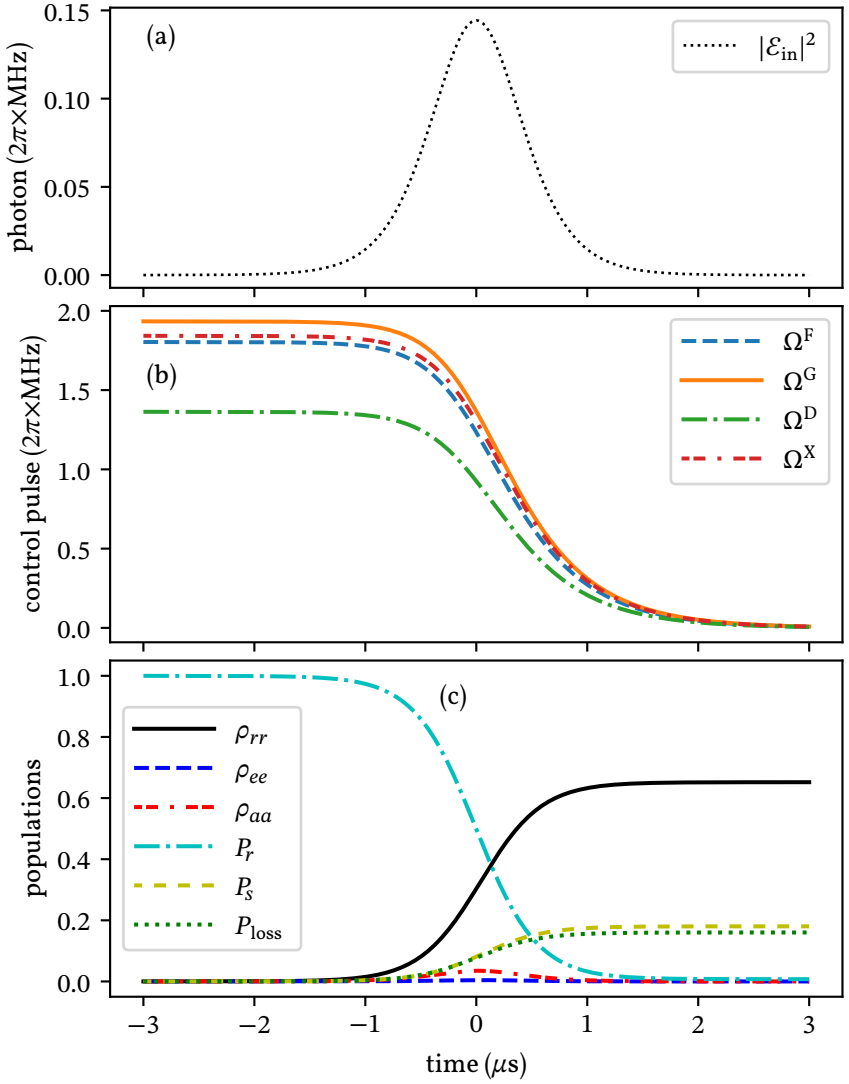

Figure 3.4: Dynamics of storage. (a) Photon envelope $|\mathcal{E}_{\text{in}}(t)|^2$, Eq. (3.7), as a function of time. (b) Time dependence of the control pulses $\Omega^{\text{F}}(t)$, $\Omega^{\text{G}}(t)$, $\Omega^{\text{D}}(t)$, and $\Omega^{\text{X}}(t)$ (resp. Eqs. (3.21), (3.25), (3.22), (3.26)). (c) Time evolution of the diagonal elements of the density matrix when the atom is driven by Ω^{X}. The curves are the population ρ_{rr} of state $|r\rangle$, the population ρ_{ee} of state $|e\rangle$, the probability that there is one photon in the cavity ρ_{aa}, the probability that the photon is in the transmission line P_r, Eq. (3.17), the probability of spontaneous decay, Eq. (3.18) P_s, and the probability of cavity parasitic losses P_{loss}, Eq. (3.19). The parameters are $(g, \kappa, \gamma, \kappa_{\text{loss}}) = (4.9, 2.42, 3.03, 0.33) \times 2\pi\, MHz$, $\Delta = 0$ and $T_{\text{c}} = 0.5\,\mu s$.

Figure 3.4 shows the evolution of the system for $T_c = 0.5\,\mu s$. Fig. 3.4(a) displays the envelope in time $|\mathcal{E}_{in}(t)|^2$ for the photon given in eq. (3.7), which is the one used also in this simulation. Fig. 3.4(b) displays the control pulse shapes of the protocols Ω^F, Ω^G, Ω^D, of Refs. [122–124] and Ω^X derived in this work (the pulse shapes are given analytically in Eqs. (3.21), (3.25), (3.22), (3.26)). Fig. 3.4(c) shows the population of the states and the losses during the evolution when the atom is driven by $\Omega^X(t)$. The efficiency of the transfer, Eq. (3.9), corresponds to the population of the state $|r\rangle$, ρ_{rr}. For the parameters of Ref. [120] the final efficiency is $\eta(t_2) \approx \eta'_{max} \approx 0.653$.

In the next subsection we report the derivation of Ω^X and η'_{max} by means of the input-output formalism.

3.3.3 *Maximal efficiency in presence of parasitic losses*

In this section we generalize the adiabatic protocol of Ref. [124] in order to identify the control field that maximizes the storage efficiency and to determine the maximum storage efficiency one can reach. The derivation presented in this section is based on the input-output formalism and it delivers Eq. (3.26) and Eq. (3.28).

We first justify the result for Eq. (3.28) using a time reversal argument applied in Refs. [124, 128]. Let us consider retrieval of the photon, assuming the atom is initially in state $|r\rangle$ and there is neither external nor cavity field. Then, in order to retrieve the photon, the control pulse $\Omega(t)$ shall drive the transition $|r\rangle \to |e\rangle$ such that at the end of the process the state $|r\rangle$ is completely empty. The excited state $|e\rangle$ dissipates the excitation with probability $1/(1 + C')$, while it can emit into the cavity mode with probability $C'/(1 + C')$. When the cavity mode is populated, a fraction $\kappa_{loss}/(\kappa + \kappa_{loss})$ is lost, while the fraction $\kappa/(\kappa + \kappa_{loss})$ is emitted via the coupling mirror into the transmission line. From this argument one finds that the probability of retrieval is given by Eq. (3.28). Using the time reversal argument, this is also the efficiency of storage.

We now derive this result as well as $\Omega^X(t)$ starting from the retrieval process and then applying the time reversal argument. For this purpose, we restrict the dynamics to the Hilbert space $\mathcal{H}$ composed by the states $\{|g, 1_c, \text{vac}\rangle, |e, 0_c, \text{vac}\rangle, |r, 0_c, \text{vac}\rangle, |g, 0_c, 1_k\rangle : 1 \le k \le N\}$. In $\mathcal{H}$ the probability is not conserved due to leakage via spontaneous decay and via parasitic cavity losses. Therefore, a generic state in $\mathcal{H}$ takes the form $|\phi(t)\rangle = c(t)|g, 1_c, \text{vac}\rangle + e(t)|e, 0_c, \text{vac}\rangle + r(t)|r, 0_c, \text{vac}\rangle + \sum_k \mathcal{E}_k(t)|g, 0_c, 1_k\rangle$, it evolves according to a non-Hermitian Hamiltonian and its norm decays exponentially with time [129]. We assume that at the initial time $t = t_1$ the probability amplitude $r(t_1)$ equals 1, while all other proba-

bility amplitudes vanish. The equations of motion for the probability amplitudes read

$$\dot{c}(t) = -\mathrm{i}g e(t) - \mathrm{i}\sqrt{2\kappa}\mathcal{E}_{\mathrm{in}}(t) - (\kappa + \kappa_{\mathrm{loss}})c(t), \tag{3.29a}$$

$$\dot{e}(t) = (\mathrm{i}\Delta - \gamma)e(t) - \mathrm{i}g c(t) - \mathrm{i}\Omega(t)r(t), \tag{3.29b}$$

$$\dot{r}(t) = -\mathrm{i}\Omega^*(t)e(t)\,, \tag{3.29c}$$

where we used the Markov approximation and the input-output formalism [55]. We now assume the bad-cavity limit $\kappa \gg g$ and adiabatically eliminate the cavity field from the equations of motion (which corresponds to assuming $\dot{c}(t) \approx 0$ over the typical time scales of the other variables). In this limit the input-output operator relation, $\hat{\mathcal{E}}_{\mathrm{out}}(t) = \mathrm{i}\sqrt{2\kappa}\hat{a}(t) - \hat{\mathcal{E}}_{\mathrm{in}}(t)$, takes the form

$$\mathcal{E}_{\mathrm{out}}(t) = G\sqrt{2\gamma C}e(t) + \frac{\kappa - \kappa_{\mathrm{loss}}}{\kappa + \kappa_{\mathrm{loss}}}\mathcal{E}_{\mathrm{in}}(t)\,, \tag{3.30}$$

where

$$G = \kappa/(\kappa + \kappa_{\mathrm{loss}})$$

and C is given in Eq. (3.14). This equation has to be integrated together with the equations

$$\dot{e}(t) = [\mathrm{i}\Delta - \gamma(1 + GC)]e(t) - \mathrm{i}\Omega(t)r(t) - G\sqrt{2\gamma C}\mathcal{E}_{\mathrm{in}}(t)\,, \tag{3.31}$$

$$\dot{r}(t) = -\mathrm{i}\Omega^*(t)e(t)\,. \tag{3.32}$$

Our goal is to determine the retrieval efficiency assuming that at time $t = 0$ there is no input photonic excitation, thus $\mathcal{E}_{\mathrm{in}}(t) = 0$ at all times. Using these assumptions, the above equations can be cast into the form

$$\frac{\mathrm{d}}{\mathrm{d}t}\left(|e(t)|^2 + |r(t)|^2\right) = -2\gamma(1 + C')|e(t)|^2\,. \tag{3.33}$$

The probability that no excitations are left in the atom at time $t_2 > 0$ ($t_2 \gg T_{\mathrm{c}}$) is the retrieval efficiency

$$\begin{aligned}\eta'_{\max} &= \int_{t_1}^{t_2} |\mathcal{E}_{\mathrm{out}}(t)|^2 \mathrm{d}t = 2G^2\gamma C \int_{t_1}^{t_2} |e(t)|^2 \mathrm{d}t = \\ &= \frac{-GC'}{1 + C'}\Big[|e(t)|^2 + |r(t)|^2\Big]_{t_1}^{t_2} = \frac{GC'}{1 + C'}\,.\end{aligned} \tag{3.34}$$

By means of the time reversal argument, this is also the storage efficiency.

The output field can be analytically determined by adiabatically eliminating the excited state from Eqs. (3.30). This leads to the expression

$$\begin{aligned}\mathcal{E}_{\mathrm{out}}(t) = \mathrm{i}\sqrt{2\gamma GC'}&\frac{\Omega(t)}{\mathrm{i}\Delta - \gamma(1 + C')} \\ &\times \exp\left(\int_{t_1}^{t} \frac{|\Omega(t')|^2}{\mathrm{i}\Delta - \gamma(1 + C')}\mathrm{d}t'\right).\end{aligned} \tag{3.35}$$

Integrating the norm squared of Eq. (3.35) one obtains

$$\left(G\frac{C'}{1+C'}\right)^{-1}\int_{t_1}^{t}|\mathcal{E}_{\rm out}(t')|^2\mathrm{d}t' = \\ = 1-\exp\left[\frac{-2\gamma(1+C')}{\gamma^2(1+C')^2+\Delta^2}\int_{t_1}^{t}|\Omega(t')|^2\mathrm{d}t'\right]. \tag{3.36}$$

We solve Eq. (3.36) to find $|\Omega(t)|$, while the phase of $\Omega(t)$ can be determined from Eq. (3.35). Finally, we obtain the control pulse $\Omega^{\rm X}{}_{\rm retr}(t)$ which retrieves the photon with efficiency $\eta'_{\rm max}$. It reads

$$\Omega^{\rm X}{}_{\rm retr}(t) = \frac{\gamma(1+C')-\mathrm{i}\Delta}{\sqrt{2\gamma(1+C')}}\frac{\mathcal{E}_{\rm out}(t)}{\sqrt{\int_t^{t_2}|\mathcal{E}_{\rm out}(t')|^2\mathrm{d}t'}} \\ \times\exp\left(\mathrm{i}\frac{\Delta}{2\gamma(1+C')}\ln\int_t^{t_2}(|\mathcal{E}_{\rm out}(t')|^2/\eta'_{\rm max})\mathrm{d}t'\right). \tag{3.37}$$

Using the time reversal argument, the control pulse $\Omega^{\rm X}(t)=\Omega^{\rm X^*}{}_{\rm retr}(T-t)$ stores the time reversed input photon with $\mathcal{E}_{\rm in}(t)=\mathcal{E}^*_{\rm out}(T-t)/\sqrt{\eta'_{\rm max}}$ and $T=t_2-t_1$, and it takes the form given in Eq. (3.26). This pulse has the same form as the pulse of Eq. (3.25), where now C has been replaced by C' (or equivalently $\kappa\to\kappa+\kappa_{\rm loss}$).

3.3.4 *Photon Retrieval*

The generation of single photons with arbitrary shape of the wavepacket envelope in atom-cavity systems has been discussed theoretically in [124, 130] and demonstrated experimentally in [131, 132].

In Ref. [106, 128] it has been pointed out that photon storage and retrieval are connected by a time reversal transformation. This argument has profound implications. Consider for instance the pulse shape $\Omega(t)$ which optimally stores an input photon with envelope $\mathcal{E}_{\rm in}(t)$. This pulse shape is the time reversal of the pulse shape $\Omega_{\rm retr}(t)=\Omega^*(T-t)$ which retrieves a photon with envelope $\mathcal{E}_{\rm out}(t)=\mathcal{E}^*_{\rm in}(T-t)$ (here $T=t_2-t_1$). In this case, the storage efficiency is equal to the efficiency of retrieval and is limited by the cooperativity through the relation in Eq. (3.28). We have numerically checked that this is fulfilled by considering adiabatic retrieval and storage of a single photon through 5 nodes, consisting of 5 identical cavity-atom systems. We applied $\Omega_{\rm retr}(t)$ for the retrieval and the corresponding $\Omega(t)$ for the storage. Within the numerical error, we verified that the storage efficiency of each retrieved photon remains constant and equal to the one of the first retrieved photon.

3.4 BEYOND ADIABATICITY

In this section we analyse the efficiency of storage of single photon pulses in the regime in which the adiabaticity condition Eq. (3.15) does not hold.

Our treatment extends to single-atom quantum memories the approach that was applied to atomic ensemble in Refs. [133, 134] and allows us to identify the minimum coherence time scale of the photon pulse for which a given target efficiency can be reached.

Our procedure is developed as follows. We use the von-Neumann equation, obtained from Eq. (3.1) after setting $\gamma = \kappa_{\text{loss}} = 0$, and resort to optimal control theory for identifying the control pulse $\Omega(t) = \Omega^{\text{opt}}(t)$ that maximizes the storage efficiency for $\gamma = \kappa_{\text{loss}} = 0$. Specifically, we make use of the GRAPE algorithm [135] implemented in the library QuTiP [136, 137]. We then determine the storage efficiency of the full dynamics, including spontaneous decay and cavity parasitic losses, by numerically integrating the master equation (3.1) using the pulse $\Omega^{\text{opt}}(t)$. We show that the dynamics due to $\Omega^{\text{opt}}(t)$ significantly differs from the adiabatic dynamics, and thereby improve the efficiency for short coherence times.

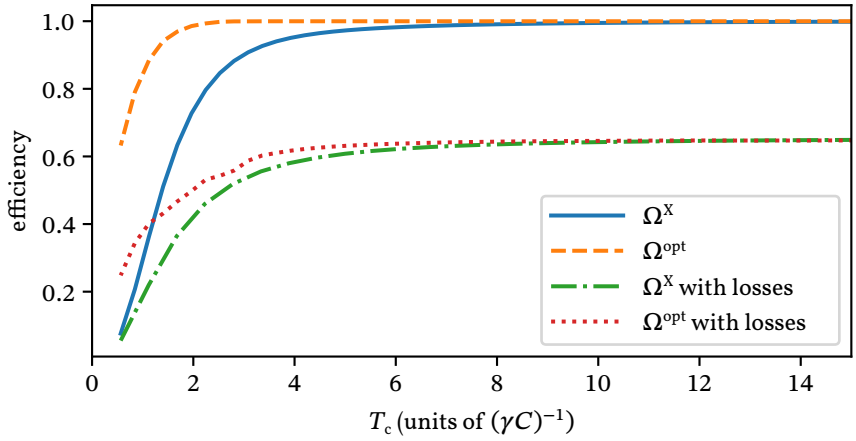

Figure 3.5: Storage efficiency η at $t = t_2$ as a function of the coherence time of the single-photon pulse T_c (in units of $(\gamma C)^{-1}$). The legenda indicates the pulses used in the numerical integration of Eq. (3.1). The parameters are $(g, \kappa) = (4.9, 2.42) \times 2\pi\, MHz$, the lines labeled "with losses" refer to the efficiency of the process when $(\gamma, \kappa_{\text{loss}}) = (3.03, 0.33) \times 2\pi\, MHz$, otherwise $\gamma = \kappa_{\text{loss}} = 0$; $t_2 = -t_1 = 6T_c$. The other parameters are given in Fig. 3.2.

Figure 3.5 displays the storage efficiency η as a function of the photon coherence time T_c when the control pulse is $\Omega^X(t)$, Eq. (3.26), and when instead the control pulse is found by means of the numerical procedure specified above, which we denote by $\Omega^{\text{opt}}(t)$. The storage efficiency is reported for $\gamma = \kappa_{\text{loss}} = 0$ and for $(\gamma, \kappa_{\text{loss}}) = (3.03, 0.33) \times 2\pi\, MHz$. The results show that optimal control, in the way we implement it, does not improve the maximal value of the storage efficiency, which seems to be limited by the value of η'_{max}, Eq. (3.28). We remark that this behaviour is generally encountered when applying optimal-control-based protocols to Markovian dynamics [138]. Nevertheless, the protocols identified us-

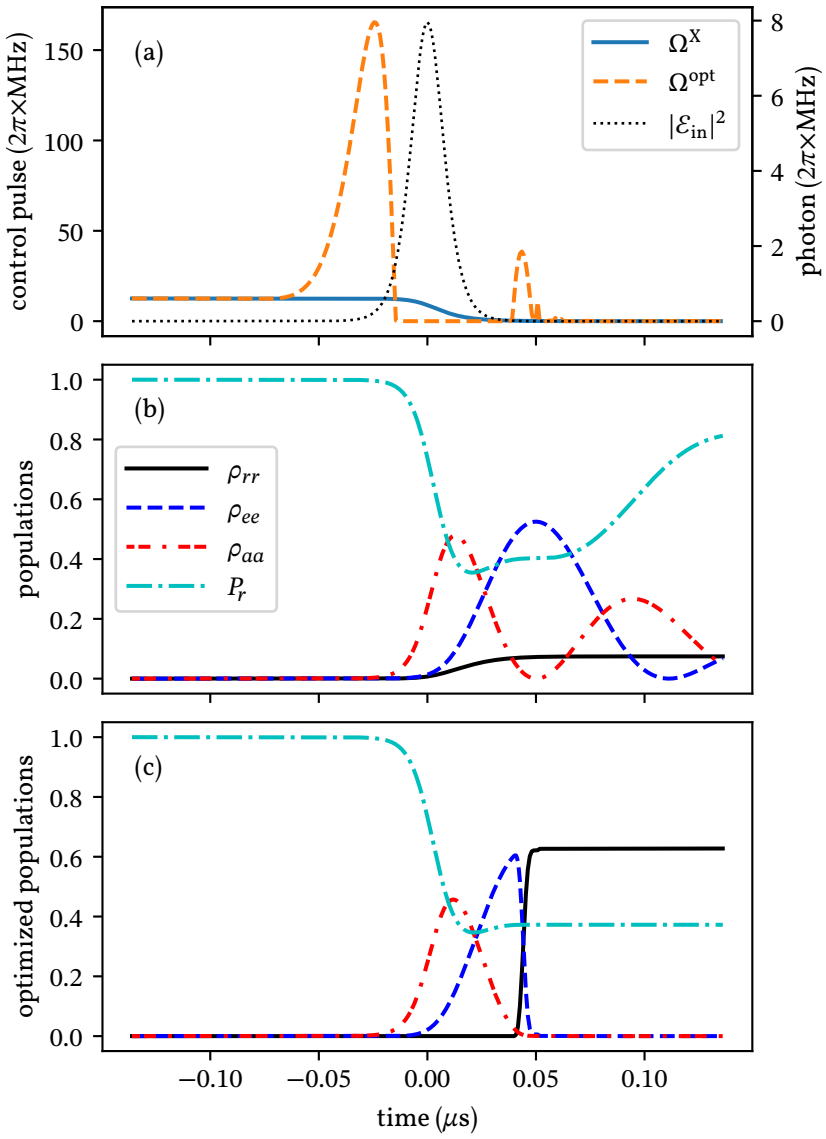

Figure 3.6: (a) Photon envelope $|\mathcal{E}_{\text{in}}(t)|^2$, Eq. (3.7), and optimized pulse $\Omega^{\text{opt}}(t)$ as a function of time (the initial guess pulse $\Omega^{\text{X}}(t)$ is shown for comparison). Subplot (b) and (c) display the time evolution of the diagonal elements of the density matrix when the atom is driven by Ω^{X} and Ω^{opt}, respectively. The curves are the population ρ_{rr} of state $|r\rangle$, the population ρ_{ee} of state $|e\rangle$, the probability that there is one photon in the cavity ρ_{aa}, and the probability that the photon is in the transmission line P_r, Eq. (3.17). The parameters are $(g, \kappa) = (4.9, 2.42) \times 2\pi\, MHz$, $\gamma = \kappa_{\text{loss}} = \Delta = 0$ and $T_{\text{c}} = 0.009\,\mu s$, thus the regime is non adiabatic as $T_{\text{c}} \approx 0.57/(\gamma C)$. At $t = t_2$ the population ρ_{rr} gives $\eta(t_2)$. In this case the system has been simulated for a longer time interval: $t_2 = -t_1 = 15T_{\text{c}}$.

ing optimal control extend the range of values of T_{c}, where the maximal efficiency is reached, down to values where the adiabatic condition is not

fulfilled. We further find that the optimized pulse we numerically identified in absence of losses provides an excellent guideline for optimizing the storage also in presence of losses.

In order to get insight into the optimized dynamics we analyse the time dependence of the control pulse as well as the dynamics of cavity and atomic state populations for $T_c = 0.009\,\mu s$, namely, when the dynamics is non-adiabatic. Figure 3.6(a) shows the time evolution of the pulse $\Omega^{opt}(t)$ resulting from the optimization procedure in the non-adiabatic regime; the pulse $\Omega^{X}(t)$ is shown for comparison. The efficiency of the transfer (when the losses are neglected) with the control pulse Ω^{X} is $\eta^{X} \approx 0.07 < \eta_{max}$ because the process is non adiabatic, while the efficiency reached with the optimized pulse $\Omega^{opt}(t)$ is $\eta^{opt} \approx 0.63$. The value of the solid green line at $t = t_2$ in Fig. 3.6(b) and 3.6(c) corresponds to the leftmost point in Fig. 3.5 for the case without losses. A double bump in the cavity population is visible in Fig. 3.6(b): this is due to the Jaynes-Cummings dynamics, and is thus the periodic exchange of population between the atomic excited state $|e\rangle$ and the cavity field. In Fig. 3.6(a) it is noticeable that the intensity of the optimized pulse exhibits a relatively high peak when the photon is impinging on the cavity. It corresponds to a way to perform impedance matching in order to maximize the transmission at the mirror, and it is related to the same dynamics which gives rise to the divergence of $\Omega^{F}(t)$ and $\Omega^{D}(t)$ which is found when they are applied in the non-adiabatic regime. After this the intensity of the control pulse vanishes and then exhibits a second maximum when the population of the excited state reaches the maximum: we verified that the area about this second "pulse" corresponds to the one of a π pulse, thus transferring the population into state $|r\rangle$.

We now investigate the limit of optimal storage. For this purpose we determine the lower bound T_c^{min} to the coherence time T_c of the photon, for which a given efficiency $\eta = \eta_{tr}$ can be reached. For each value of g and T_c we optimize the control pulse using GRAPE. For each g we determine η as a function of T_c and then extract $T_c^{min} = \min_{T_c}\{T_c : \eta(T_c) \geq \eta_{tr}\}$. We then analyse how the minimum coherence time T_c^{min} scales with the vacuum Rabi frequency g.

Figure 3.7 displays the minimum photon coherence time T_c^{min} required for reaching the storage efficiency (a) $\eta_{tr} = 0.99$ and (b) $\eta_{tr} = 2/3$ as a function of the coupling constant g. We observe two behaviours, separated by the value $g = \kappa$: For $g \ll \kappa$, in the bad cavity limit, we extract the functional behaviour $T_c^{min} \propto 1/\gamma C = \kappa/g^2$. On the contrary, in the good cavity limit, $g > \kappa$, we find that $T_c^{min} \propto 1/\kappa$: The limit to photon storage is here determined by the cavity linewidth. The general behaviour as a function of g interpolates between these two limits. This result shows that the photon can be stored as long as its spectral width is of the order of the linewidth of the dressed atomic state. Fig. 3.7(a) also displays the minimum photon coherence times T_c^{X} and T_c^{D} that allows for a transfer with efficiency $\eta = \eta_{tr} = 0.99$ for the protocols Ω^{X} and Ω^{D}, respectively.

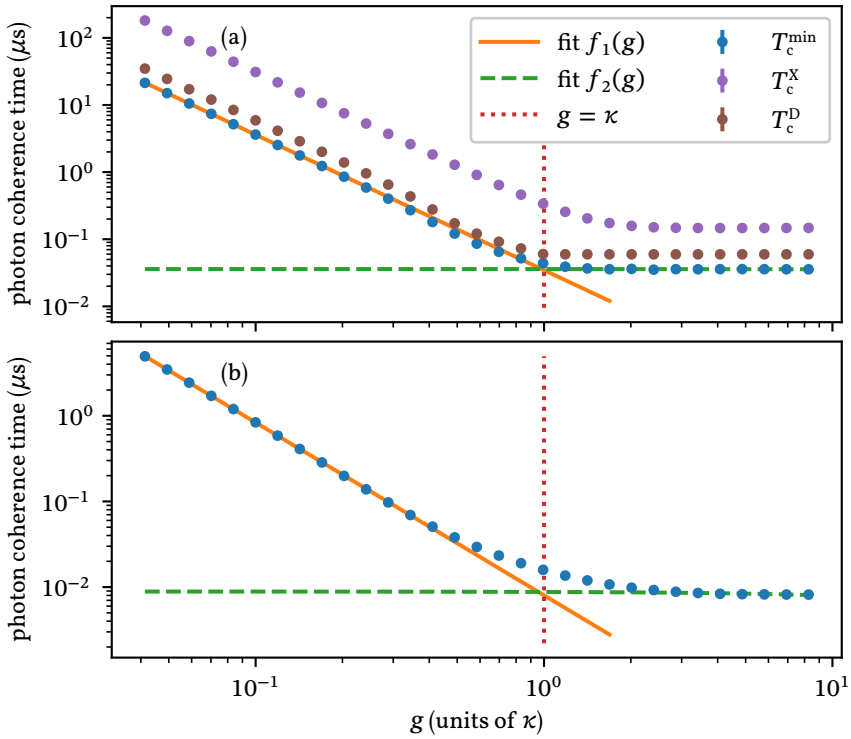

Figure 3.7: Minimum photon coherence time as a function of g (in units of κ). The coherence time T_c^{min} is the lower bound to the coherence time of photons which can be stored with efficiency (a) $\eta_{tr} = 0.99$ and (b) $\eta_{tr} = 2/3$ for $\gamma = \kappa_{loss} = \Delta = 0$. The vertical dotted line shows the value $g = \kappa = 2.42 \times 2\pi\, MHz$. The data in the region $g \ll \kappa$ and $g \gg \kappa$ have been fitted with the functions $f_1(g) = a\kappa/g^2$ and $f_2(g) = a'/\kappa$, respectively. Plot (a) also shows the minimum photon coherence times T_c^X and T_c^D that allows for a storage with $\eta = 0.99$ for the protocols Ω^X and Ω^D, respectively.

The time T_c^D is difficult to evaluate numerically because, for each g, there is a T_c^0 such that for each photon coherence time $T_c \geq T_c^0$ the efficiency is one within the numerical error, and for each $T_c \leq T_c^0$ the Rabi frequency Ω^D is numerically intractable (Ω^D, given in Eq. (3.22), becomes so high that it is not anymore manageable by our numerical solver). We then take $T_c^D = T_c^0$.

3.5 CONCLUSIONS

We have analysed the storage efficiency of a single photon by a single atom inside a resonator. We have focused on the good cavity limit and shown that, as in the bad cavity limit, the storage efficiency is bound by the cooperativity and the maximal value it can reach is given by Eq. (3.16). We have extended these predictions to the case in which the resonator undergoes parasitic losses. For this case we determined the maximal

storage efficiency for an adiabatic protocol as well as the corresponding control field respectively given in Eq. (3.28) and Eq. (3.26). Numerical simulations show that protocols based on optimal control theory do not achieve higher storage efficiencies than $\eta'_{\max}$. Nevertheless they can reach this upper bound even for spectrally-broad photon wave packets where the dynamics is non-adiabatic, as long as the spectral width is of the order of the linewidth of the dressed atomic state.

Our analysis shows that the storage efficiency is limited by parasitic losses. Nevertheless, we have demonstrated that these can be partially compensated by the choice of an appropriate control field. This result has been analytically derived for adiabatic protocols, yet it shows that extending optimal control theory to incoherent dynamics could provide new tools for efficient quantum memories.

Experimental realizations of this process have been attempted in the adiabatic regime [120, 139] as well as in the non-adiabatic regime [140]. While the theoretical predictions for single photon production are experimentally confirmed, the storage efficiency reached in experiments is about 50% lower than the theoretically predicted one [139]. One possible explanation for this discrepancy is the fact that attenuated laser pulses have been employed in place of single photons. Attenuated laser pulses, which are well described theoretically by *weak coherent pulses*, are in fact easier to produce in a lab respect to single photons [139]. In Chapter 4 we address this question by theoretically analyzing the dynamics of storage of an attenuated laser pulse, where the pulse intensity is at the single photon level.

The storage dynamics in the non-adiabatic regime presents various opportunities for improving the storage efficiency. For instance optimal control algorithms different from the one we used can be employed, as for example in Appendix 3.C. Furthermore, storage protocols based on super-adiabatic quantum dynamics [141, 142] may be investigated. Here an additional Hamiltonian is used in order to completely suppress non-adiabatic processes in the unitary evolution.

APPENDICES

3.A INPUT-OUTPUT FORMALISM

In input-output formalism [55] the equation of motion are

$$\begin{aligned}
\dot{\hat{a}} &= -\mathrm{i}g\hat{\sigma}_{ge} - \mathrm{i}\sqrt{2\kappa}\hat{\mathcal{E}}_{\mathrm{in}}(t) - (\kappa + \kappa_{\mathrm{bad}})\hat{a}(t) + \hat{F}_a, \\
\dot{\hat{\sigma}}_{gg} &= \mathrm{i}g\hat{\sigma}_{eg}\hat{a} - \mathrm{i}g\hat{a}^\dagger\hat{\sigma}_{ge}, \\
\dot{\hat{\sigma}}_{rr} &= \mathrm{i}\Omega(t)\hat{\sigma}_{er} - \mathrm{i}\Omega^*(t)\hat{\sigma}_{re}, \\
\dot{\hat{\sigma}}_{ee} &= -\mathrm{i}g\hat{\sigma}_{eg}\hat{a} + \mathrm{i}g\hat{a}^\dagger\hat{\sigma}_{ge} - \mathrm{i}\Omega(t)\hat{\sigma}_{er} + \\
&\quad + \mathrm{i}\Omega^*(t)\hat{\sigma}_{re} - \gamma\hat{\sigma}_{ee} + \hat{F}_{ee}, \\
\dot{\hat{\sigma}}_{ge} &= \mathrm{i}\Delta\hat{\sigma}_{ge} + \mathrm{i}g(\hat{\sigma}_{ee} - \hat{\sigma}_{gg})\hat{a} - \mathrm{i}\Omega(t)\hat{\sigma}_{gr} + \\
&\quad - \frac{\gamma}{2}\hat{\sigma}_{ge} + \hat{F}_{ge}, \\
\dot{\hat{\sigma}}_{er} &= -\mathrm{i}\Delta\hat{\sigma}_{er} + \mathrm{i}g\hat{a}^\dagger\hat{\sigma}_{gr} + \mathrm{i}\Omega^*(t)(\hat{\sigma}_{rr} - \hat{\sigma}_{ee}) + \\
&\quad - \frac{\gamma}{2}\hat{\sigma}_{er} + \hat{F}_{er}, \\
\dot{\hat{\sigma}}_{gr} &= \mathrm{i}g\hat{\sigma}_{er}\hat{a} - \mathrm{i}\Omega^*(t)\hat{\sigma}_{ge},
\end{aligned} \tag{3.38}$$

where $\hat{\sigma}_{jk} = |j\rangle\langle k|$ are atomic operators and $\hat{F}_a, \hat{F}_{ee}, \hat{F}_{ge}$ and $\hat{F}_{er}$ are Langevin noise operators [52]. The input operator for the quantum electromagnetic field is

$$\hat{\mathcal{E}}_{\mathrm{in}}(t) = \sqrt{\frac{Lc}{2\pi^2}} \int_{-\infty}^{\infty} e^{-\mathrm{i}kc(t-t_1)}\hat{b}(k + k_c, t = t_1)\mathrm{d}k, \tag{3.39}$$

here $\hat{b}(k, t = t_1)$ is the annihilation operator of the mode k at the initial time $t = t_1$. The input output relation is given by

$$\hat{\mathcal{E}}_{\mathrm{out}}(t) = \mathrm{i}\sqrt{2\kappa}\hat{a}(t) - \hat{\mathcal{E}}_{\mathrm{in}}(t). \tag{3.40}$$

The equations of motion for $M \gg 1$ atoms in the cavity take the same form as Eqs. (3.38) when one performs the replacement $\hat{\sigma}_{jk} \to \sum_{i=1}^{N} \hat{\sigma}_{jk}^i$ [124]. In this case, one can make the approximations $\langle\tilde{\sigma}_{gg}(t)\rangle \approx M$, $\langle\tilde{\sigma}_{rr}(t)\rangle \approx \langle\tilde{\sigma}_{ee}(t)\rangle \approx \langle\tilde{\sigma}_{er}(t)\rangle = 0$, where $\langle\cdot\rangle = \mathrm{Tr}(\rho_0\cdot)$ and ρ_0 is the initial state. Then, the set of equations (3.38) reduces to the equations of motion of a single photon given in Eqs. (3.29).

We note that the quantum impedance matching condition imposed by the authors of Refs. [122] consists in taking $\mathcal{E}_{\mathrm{out}}(t) = \dot{\mathcal{E}}_{\mathrm{out}}(t) = 0$, according to which the form of the control pulse Ω^{F}, Eq. (3.21), is found.

3.B EFFECT OF PHOTON DETUNING ON STORAGE

The protocol $\Omega^{\mathrm{G}}(t)$ does not have any restriction on Δ: for every Δ there is a pulse $\Omega^{\mathrm{G}}(t)$ that allows for storage with efficiency $\eta_{\max}$ (within the adiabatic regime), see Eq. (3.25). Figure 3.8 displays the storage efficiency and

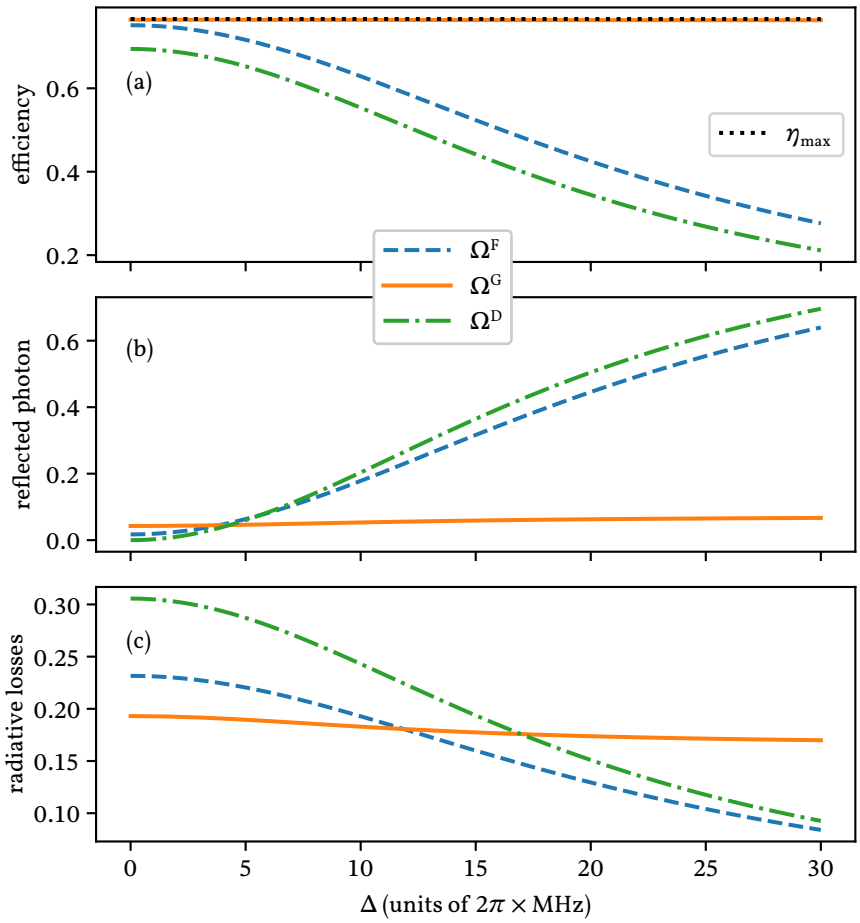

Figure 3.8: (a) Storage efficiency, (b) probability of photon reflection, Eq. (3.17), and (c) probability of spontaneous decay, Eq. (3.18), as a function of the single photon detuning Δ and at time t_2. The parameters are $(g, \kappa, \gamma) = (4.9, 2.42, 3.03) \times 2\pi\, MHz$, $T_c = 0.5\,\mu s$. The input photon $\mathcal{E}_{in}(t)$ is defined as in Eq. (3.7). See Fig. 3.2 for further details.

the losses for each protocol as a function of Δ, as expected the protocol $\Omega^G(t)$ performs in the same way for any values of Δ.

A time-dependent phase $\chi(t)$ of the control pulse $\Omega(t) = |\Omega(t)|e^{i\chi(t)}$ can be implemented as a two-photon detuning

$$\delta = \dot{\chi}(t). \tag{3.41}$$

In fact, by applying the unitary transformation $\hat{U}(t) = \exp(-i|r\rangle\langle r|\chi(t))$, the transformed Hamiltonian is $\hat{H}' = \hat{H}'_I + \hat{H}_{fields}$, where

$$\begin{aligned}\hat{H}'_I = \dot{\chi}(t)|r\rangle\langle r| - \Delta|e\rangle\langle e| + \\ + (g|e\rangle\langle g|\hat{a} + |\Omega(t)||e\rangle\langle r| + \text{H.c.}).\end{aligned} \tag{3.42}$$

For $\Omega^{\mathrm{G}}(t)$ we have

$$\dot{\chi}^{\mathrm{G}}(t) = \frac{-\Delta}{2\gamma(1+C)} \cdot \frac{|\mathcal{E}_{\mathrm{in}}(t)|^2}{\int_{t_1}^{t} |\mathcal{E}_{\mathrm{in}}(t')|^2 \mathrm{d}t'} = \tag{3.43a}$$

$$= \frac{-\Delta |\Omega^{\mathrm{G}}(t)|^2}{\Delta^2 + \gamma^2(1+C)^2} \,. \tag{3.43b}$$

Recall that also $|\Omega^{\mathrm{G}}(t)|$ depends on Δ. This can be understood in terms of AC Stark shift: one-photon detuning $\Delta \neq 0$ is a shift of the control laser out of resonance for the transition $|r\rangle - |e\rangle$ and thereby induces an AC Stark shift on the levels $|e\rangle$ and $|r\rangle$ of the atom; thus the condition of two-photon resonance does not hold anymore. In order to restore the latter, changes in frequency of the carrier and/or of the cavity and/or of the atomic levels are needed and they appear as a two-photon detuning in the Hamiltonian. This also explains why the reflected photon probability for the protocols $\Omega^{\mathrm{F}}(t)$ and $\Omega^{\mathrm{D}}(t)$ (see Fig. 3.8), which do not take into account the one-photon detuning, increases with increasing Δ: the input photon sees the system out of resonance and hence it is mostly reflected.

Eq. (3.43b) gives the energy shift as a function of the Rabi frequency of the control pulse.

3.C OPTIMAL CONTROL WITH INCOHERENT DYNAMICS

We extend the analysis performed in Sec. 3.4 and implement the GRAPE optimal control algorithm for the full dynamics of the systems, i. e. we include the irreversible processes in the optimization procedure. The evolution of the system in this case is obtained by numerically solving Eqs. (3.29) with $\gamma = 3.03 \times 2\pi\, MHz$ and $\kappa_{\mathrm{loss}} = 0.33 \times 2\pi\, MHz$. We identify the control pulse $\Omega(t) = \Omega^{\mathrm{opt}\prime}(t)$ that maximizes the storage efficiency η for several values of the single-photon coherence time T_{c}. Figure 3.9 displays the efficiency of single-photon storage with the pulse $\Omega^{\mathrm{opt}\prime}(t)$ in dependence of T_{c}. For comparison, we also report the efficiencies obtained with the pulses $\Omega^{\mathrm{X}}(t)$ and $\Omega^{\mathrm{opt}}(t)$ already reported in Fig. 3.5, where they were labeled "Ω^{X} with losses" and "Ω^{opt} with losses", respectively. Comparing the efficiency for $\Omega^{\mathrm{opt}\prime}$ with the one for Ω^{opt} it is visible that the inclusion of the irreversible losses during the optimization of the control pulse leads to higher efficiencies.

This result can be understood by comparing the optimized pulse $\Omega^{\mathrm{opt}\prime}$ with the pulse Ω^{opt} obtained in Sec. 3.4, which are shown in Fig. 3.10. We emphasize two main differences: (i) the initial high peak in the Rabi frequency Ω^{opt} appearing around the instant in which the photon impinges on the cavity (see Sec. 3.4 for a discussion) almost disappears in $\Omega^{\mathrm{opt}\prime}$, and (ii) the second pulse in Ω^{opt}, which is a π-pulse and at the instant in time when the population of the excited state $|e\rangle$ is maximal switches the populations between $|e\rangle$ and the target state $|r\rangle$, has been moved at an earlier time and has an area larger than π. We interpret the better

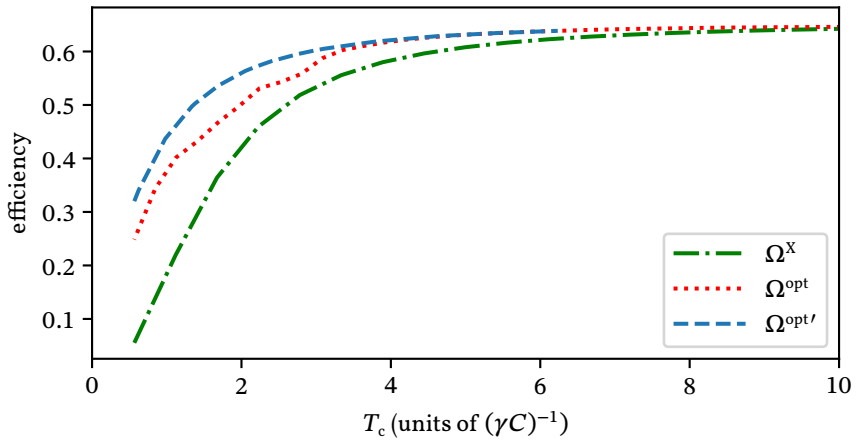

Figure 3.9: Storage efficiency η at $t = t_2 = -t_1 = 15T_c$ as a function of the single-photon coherence time T_c. To compare with Fig. 3.5. The curves labeled Ω^X and Ω^{opt} are the same curves plotted in Fig. 3.5 with labels "Ω^X with losses" and "Ω^{opt} with losses", respectively. $\Omega^{opt\prime}$ refers to the efficiency reached with the control pulse obtained in Sec. 3.C. The parameters are $(g, \kappa, \gamma, \kappa_{loss}, \Delta) = (4.9, 2.42, 3.03, 0.33, 0) \times 2\pi\, MHz$.

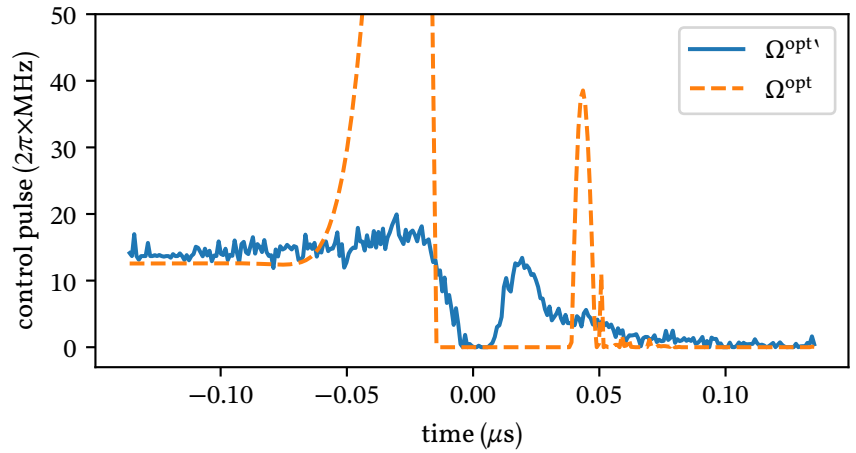

Figure 3.10: Optimized pulse $\Omega^{opt\prime}(t)$ as a function of time. The control pulse $\Omega^{opt}(t)$ obtained in Sec. 3.4 and reported in Fig. 3.6(a) is shown for comparison.

performance of $\Omega^{opt\prime}$ mainly due to point (ii): while in the case of Ω^{opt} the excited state does not decay and thus waiting until it is maximally populated and then moving the excitation to the target state is a good strategy, in the case of $\Omega^{opt\prime}$ the excited state $|e\rangle$ loses population with rate 2γ and thus an earlier pulse, which transfer the excitation to the target state $|r\rangle$ sooner, minimizes the losses due to decay of $|e\rangle$ and is a better strategy.

This analysis can be extended by employing different optimization strategies such as the Krotov [143] and the CRAB [144] algorithms.

4

WEAK COHERENT PULSES FOR SINGLE-PHOTON QUANTUM MEMORIES

The content of this chapter contains results, text and figures from:

- L. Giannelli, T. Schmit, and G. Morigi,
  "Weak coherent pulses for single-photon quantum memories,
  In: "*Physica Scripta* 94 (2019), p. 014012,
  DOI: 10.1088/1402-4896/aaee36.

4.1 INTRODUCTION

Attenuated laser pulses are often employed in place for single photons in order to test the efficiency of the elements of a quantum network. The laser pulses are typically attenuated to the regime where the probability that they contain a single photon is very small, while the probability that two or more photons are detected is practically negligible. Even though photo-detection after a beam splitter shows the granular properties of the light, yet the coherence properties of weak laser pulses are quite different from the ones of a single photon [145]. In particular, they are well described by coherent states of the electromagnetic field, whose correlation functions can be reproduced by a classical coherent field [53, 57, 146]. In this perspective it is therefore legitimate to ask which specific information about the efficiency of a single-photon quantum network can one possibly extract by means of weak laser pulses.

Theoretically, similar questions have been analysed in Ref. [109–111, 121–124, 128]. In [121–124, 128], in particular, the authors consider a quantum memory composed by an atomic ensemble, where the number of atoms is much larger than the mean number of photons of the incident pulse. In this limit the equations describing the dynamics can be brought to the form of the equations describing the interaction of a single photon with the medium, and one can simply extract from the study of one case the efficiency of the other. This scenario changes dramatically if the memory is composed by a single atom [35, 106, 112, 113]. In this case the dynamics is quite different depending on whether the atom interacts with a single photon or with (the superposition of) several photonic excitations.

In this work we theoretically analyse the dynamics of the storage of a *weak coherent pulse* into the excitation of a single-atom confined within an optical resonator like in the setups of [131, 147–149]. The laser pulse propagates along a transmission line and impinges on the mirror of the

resonator, as illustrated in Fig. 3.1(a). A control laser drives the atom in order to optimize the transfer of the propagating pulse into the atomic excitation $|r\rangle$, as shown in Fig. 3.1(b). We determine the efficiency of storage under the assumption that the control laser optimizes the storage of a single photon, which possesses the same time dependent amplitude as the weak coherent pulse. Our goal is to identify the regime and the conditions for which the dynamics of storage of the weak coherent pulse reproduces the one of a single photon. This study draws on the protocols based on adiabatic transfer identified in Refs. [122–124, 150] and in Chapter 3. The theoretical formalism for the interface between the weak coherent pulse propagating along the transmission line and the single atom inside the resonator is quite general and can be extended to describe the storage fidelity of an arbitrary quantum state of light into excitations of the memory.

This Chapter is organized as follows. In Sec. 4.2 we introduce the theoretical model. In Sec. 4.3 we report our results: in Sec 4.3.1 we analyse the storage fidelity of a weak coherent pulse. In Sec. 4.3.2 we analyze the storage fidelity of an arbitrary incident pulse at the single photon level. We then compare them with the storage fidelity of a single photon. The conclusions are drawn in Sec. 4.4. The appendices provide details to the calculations in Secs. 4.2 and 4.3.

4.2 BASIC MODEL

Figure 3.1 reports the basic elements of the dynamics. A weak coherent pulse propagates along the transmission line and impinges on the mirror of a optical high-finesse cavity. Here it is transmitted into a cavity mode at frequency ω_c, which, in turn, interacts with a single atom confined within the resonator. The atom is driven by a laser, whose temporal shape is tailored in order to maximize the transfer of a single photonic excitation, with the same amplitude as the weak coherent pulse, into an atomic excitation $|r\rangle$.

In the following we provide the details of the theoretical model and we introduce the physical quantities which are important for the discussion of the rest of this paper.

4.2.1 *Master equation*

The starting point of our analysis is master equation (3.1) which describes the evolution of the density operator $\hat{\rho}$ for the cavity mode, the atom, and the modes of the transmission line. Here we report the master equation again in order to facilitate the reading of this chapter, for details see Sec. 3.2.1. The evolution of the density operator $\hat{\rho}$ is governed by the master equation ($\hbar = 1$)

$$\partial_t \hat{\rho} = -\mathrm{i}\big[\hat{H}(t), \hat{\rho}\big] + \mathcal{L}_{\mathrm{dis}}\hat{\rho}\,, \tag{4.1}$$

where Hamiltonian $\hat{H}(t)$ determines the coherent evolution and superoperator $\mathcal{L}_{\text{dis}}$ the incoherent dynamics. Hamiltonian $\hat{H}(t) = \hat{H}_{\text{fields}} + \hat{H}_{\text{I}}(t)$ is the sum of the term

$$\hat{H}_{\text{fields}} = \sum_k (\omega_k - \omega_c)\hat{b}_k^\dagger \hat{b}_k + \sum_k \lambda_k(\hat{a}^\dagger \hat{b}_k + \hat{b}_k^\dagger \hat{a}), \tag{4.2}$$

which describes the coherent dynamics of the electromagnetic field in absence of the atom, and the term

$$\hat{H}_{\text{I}} = \delta|r\rangle\langle r| - \Delta|e\rangle\langle e| + [g|e\rangle\langle g|\hat{a} + \Omega(t)|e\rangle\langle r| + \text{H.c.}], \tag{4.3}$$

which describes the dynamics of the atom coupled to the cavity mode with coupling constant g and driven by the laser with Rabi frequency $\Omega(t)$.

4.2.2 *Initial state*

The total state of the system $|\psi_t\rangle$ at the initial time $t = t_1$ is given by a weak coherent pulse in the transmission line, the empty optical cavity, and the atom in state $|g\rangle$:

$$|\psi_{t_1}\rangle = |g\rangle \otimes |0\rangle_c \otimes |\psi^{\text{coh}}\rangle, \tag{4.4}$$

where $|0\rangle_c$ is the Fock state of the resonator with zero photons.

Below we specify in detail the state of the field. The incident light pulse is characterized by the time-dependent operator $\hat{D}$, such that its state at the interface with the optical resonator reads

$$|\psi^{\text{coh}}\rangle = \hat{D}(\{\alpha_k\})|\text{vac}\rangle \tag{4.5}$$

and $|\text{vac}\rangle$ is the vacuum state of the external electromagnetic field. Operator $\hat{D}(\{\alpha_k\})$ takes the form

$$\hat{D}(\{\alpha_k\}) = \otimes_k \exp(\alpha_k \hat{b}_k^\dagger - \alpha_k^* \hat{b}_k)\,, \tag{4.6}$$

where α_k is a complex scalar and the index k runs over all modes of the electromagnetic field with the same polarization. It thus generates a multi-mode coherent state, whose mean photon number n is

$$n = \left\langle \psi^{\text{coh}} \middle| \sum_k \hat{b}_k^\dagger \hat{b}_k \middle| \psi^{\text{coh}} \right\rangle = \sum_k |\alpha_k|^2\,. \tag{4.7}$$

In the following we assume that $n \ll 1$, which is fulfilled when $|\alpha_k|^2 \ll 1$ for all k. We will denote this a *weak coherent pulse*. This state approximates a single-photon state since at first order in n it can be approximated by the expression

$$|\psi^{\text{coh}}\rangle \approx (1 - n/2)|\text{vac}\rangle + \sum_k \alpha_k \hat{b}_k^\dagger |\text{vac}\rangle\,. \tag{4.8}$$

Coefficients α_k are related to the pulse envelope $\mathcal{E}_{\rm in}(t)$ at position $x = 0$ (which is the position of the mirror interfacing the cavity with the transmission line) via the relation

$$\alpha_k = \sqrt{\frac{c}{2L}} \int_{-\infty}^{\infty} \mathrm{d}t e^{\mathrm{i}(kc-\omega_c)t} \mathcal{E}_{\rm in}(t) \tag{4.9}$$

with c the speed of light and L the length of the transmission line. The squared norm of $\mathcal{E}_{\rm in}(t)$ equals the number of impinging photons in Eq. (4.7):

$$\int_{-\infty}^{\infty} |\mathcal{E}_{\rm in}(t)|^2 \mathrm{d}t = n\,. \tag{4.10}$$

In this work we are interested in determining the storage efficiency of a weak coherent pulse by the atom. We compare in particular the storage efficiency with the one of a single photon, whose amplitude is given by the same amplitude $\mathcal{E}_{\rm in}(t)$, apart for a normalization factor giving that the integral in Eq. (4.10) is unity. For this specific study we choose

$$\mathcal{E}_{\rm in}(t) = \frac{\sqrt{n}}{\sqrt{T}} \operatorname{sech}\left(\frac{2t}{T}\right), \tag{4.11}$$

where T is the characteristic time determining the coherence time $T_c = \pi T/4\sqrt{3}$ of the light pulse, defined as

$$T_c = \sqrt{\langle t^2\rangle - \langle t\rangle^2} \tag{4.12}$$

with $\langle t^x\rangle \equiv \int_{t_1}^{t_2} t^x |\mathcal{E}_{\rm in}(t)|^2 \mathrm{d}t$. The dynamics is analysed in the interval $t \in [t_1, t_2]$, with $t_1 < 0 < t_2$ and $|t_1|, t_2 \gg T_c$, such that (i) at the initial time there is no spatial overlap between the input light pulse and the cavity mirror and (ii) at $t = t_2$ the reflected component of the light pulse is sufficiently far away from the mirror so that it has no spatial overlap with the cavity mode. The choice of these parameters has been discussed in detail in Sec. 3.2.3.

4.2.3 *Target dynamics*

The target of the dynamics is to absorb a single photon excitation and populate the atomic state $|r\rangle$. This dynamics is achieved by suitably tailoring the control field $\Omega(t)$. We will consider protocols using control fields $\Omega(t)$ that have been developed for a single-photon wave packet [122–124, 150], see Chapter 3. The figures of merit we take are (i) the probability η to find the excitation in the state $|r\rangle$ of the atom after a fixed interaction time and (ii) the fidelity of the transfer ν, which we define as the ratio between the probability η and the number of impinging photons. This ratio, as we show in the next section, approaches the fidelity of storage of a single photon $\eta^{\rm sp}$ when $n \to 0$.

We give the formal definition of these two quantities. The probability η reads [124]

$$\eta = \mathrm{Tr}\{\hat{\rho}(t_2)|r\rangle\langle r| \otimes \mathbb{1}_{\mathrm{em}}\} = \left\langle r \middle| \mathrm{Tr}_{\mathrm{em}}\{\hat{\rho}(t_2)\} \middle| r \right\rangle \tag{4.13}$$

where $\mathbb{1}_{\mathrm{em}}$ and $\mathrm{Tr}_{\mathrm{em}}$ denote respectively the identity and the trace over the electromagnetic fields (both the fields in the transmission line and in the optical cavity), and $\hat{\rho}(t)$ is the density operator of the system.

The fidelity of the transfer is defined as the ratio between η and the number of impinging photons, namely

$$\nu = \frac{\eta}{\int_{t_1}^{t_2} |\mathcal{E}_{\mathrm{in}}(t)|^2 \mathrm{d}t}, \tag{4.14}$$

which is strictly valid for a coherent pulse. This definition of the fidelity quantitatively describes the probability that the incident pulse is stored by the atom. It agrees with the definition of Ref. [124], where the authors denote this quantity by "efficiency". Indeed, if the initial state is a single photon, the fidelity ν and the efficiency η coincide.

Before we conclude, we remind the reader of the cooperativity C, which determines the maximum fidelity of single-photon storage [124, 150]. The cooperativity C characterizes the strength of the coupling between the cavity mode and the atomic transition, it reads [124]

$$C = \frac{g^2}{\kappa_{\mathrm{tot}}\gamma}, \tag{4.15}$$

where $\kappa_{\mathrm{tot}} = \kappa + \kappa_{\mathrm{loss}}$ is the total cavity decay rate. For protocols based on adiabatic transfer of the single photon into the atomic excitation, the maximum fidelity of single-photon storage reads [124, 150] (see Chapter 3)

$$\eta_{\mathrm{max}}^{\mathrm{sp}} = \frac{\kappa}{\kappa_{\mathrm{tot}}} \frac{C}{1+C}, \tag{4.16}$$

and it approaches $\kappa/\kappa_{\mathrm{tot}}$ for $C \to \infty$. Equation (4.16) is also the probability for emission of a photon into the transmission line when the atom is initially prepared in the excited state $|e\rangle$ and no control pulse is applied.

The parameters we use in our study are the ones of the setup of Reference [120], $(g, \kappa, \gamma, \kappa_{\mathrm{loss}}) = (4.9, 2.42, 3.03, 0.33) \times 2\pi\, MHz$, corresponding to the cooperativity $C \approx 2.88$ and to the maximal storage fidelity $\eta_{\mathrm{max}}^{\mathrm{sp}} \approx 0.65$. Furthermore we choose $T_{\mathrm{c}} = 0.5\,\mu s$ such that the adiabatic condition is fulfilled: $\gamma T_{\mathrm{c}} C \approx 27 \gg 1$ (see Chapter 3).

4.3 STORAGE

In this section we report the results of the storage of weak coherent pulses into a single atom excitation. We first determine efficiency and fidelity by numerically solving the master equation of Eq. (4.1). We compare the results with the corresponding storage fidelity of a single photon

with temporal envelope $\mathcal{E}_{\rm in}(t)$, Eq. (4.11). We then determine analytically the efficiency η and the fidelity ν for weak coherent pulses with mean photon number $n \ll 1$ and quantify the discrepancy between these quantities and the single-photon storage fidelity as a function of n. We further discuss how this method can be extended in order to determine the efficiency of storage of an arbitrary incident pulse.

4.3.1 *Numerical results*

We determine the dynamics of storage by numerically integrating a master equation in the reduced Hilbert space of cavity mode and atomic degrees of freedom, which we obtain from the master equation (4.1) after moving to the reference frame which displaces the multimode coherent state to the vacuum. The procedure extends to an input multimode coherent state an established procedure for describing the interaction of a quantum system with an oscillator in a coherent state, see for instance [52]. We apply the unitary transformation $\hat{D}'(t) = \hat{D}(\{\alpha_k(t)\})$, where operator $\hat{D}$ is given in Eq.(4.6) and the arguments are $\alpha_k \to \alpha_k(t) = \alpha_k e^{-{\rm i}(\omega_k-\omega_c)t}$. In this reference frame the initial state of the electromagnetic field is the vacuum, the full density matrix is given by $\hat{\rho}'(t) = \hat{D}'(t)^\dagger \rho(t) \hat{D}'(t)$ and its coherent dynamics is governed by Hamiltonian

$$\hat{H}'(t) = \hat{H}(t) + \sqrt{2\kappa}\big(\mathcal{E}_{\rm in}(t)\hat{a}^\dagger + \mathcal{E}^*_{\rm in}(t)\hat{a}\big). \tag{4.17}$$

Here $\mathcal{E}_{\rm in}(t)$ carries the information about the initial state of the electromagnetic field and it is related to the amplitudes α_k by the following equation (consistently with Eq. (4.9))

$$\mathcal{E}_{\rm in}(t) = \sqrt{\frac{Lc}{2\pi^2}} \int_{-\infty}^{\infty} \alpha(k+k_c) e^{-{\rm i}kct} {\rm d}k. \tag{4.18}$$

By using the Born-Markov approximation one can now trace out the degrees of freedom of the electromagnetic field outside the resonator. The Hilbert space is then reduced to the cavity mode and atom's degrees of freedom, the density matrix which describes the state of this system is

$$\hat{\tau}(t) = \operatorname*{Tr}_{\rm ff} \hat{\rho}'(t)\,, \tag{4.19}$$

where $\mathrm{Tr}_{\rm ff}$ denotes the partial trace with respect to the degrees of freedom of the external electromagnetic field. Its dynamics is governed by the master equation

$$\partial_t \hat{\tau} = -{\rm i}\big[\hat{H}''(t), \hat{\tau}\big] + \mathcal{L}_\gamma \hat{\tau} + \mathcal{L}_{\kappa_{\rm tot}} \hat{\tau}. \tag{4.20}$$

where

$$H''(t) = \hat{H}_{\rm I}(t) + \sqrt{2\kappa}\big(\mathcal{E}_{\rm in}(t)\hat{a}^\dagger + \mathcal{E}^*_{\rm in}(t)\hat{a}\big), \tag{4.21}$$

$\hat{H}_I(t)$ is given in Eq. (3.3) and superoperators $\mathcal{L}_\gamma$ and $\mathcal{L}_{\kappa_{tot}}$ are defined in Eqs. (3.4), where now the cavity field is damped at rate $\kappa_{tot} = \kappa + \kappa_{loss}$ and κ is the linewidth due to radiative decay of the cavity mode by the finite transmittivity of the mirror at $x = 0$. The initial state is here described by the density operator $\hat{\tau}(t_1) = |g, 0_c\rangle\langle g, 0_c|$, and the storage efficiency is $\eta = \mathrm{Tr}\{\hat{\tau}(t_2)|r\rangle\langle r|\}$.

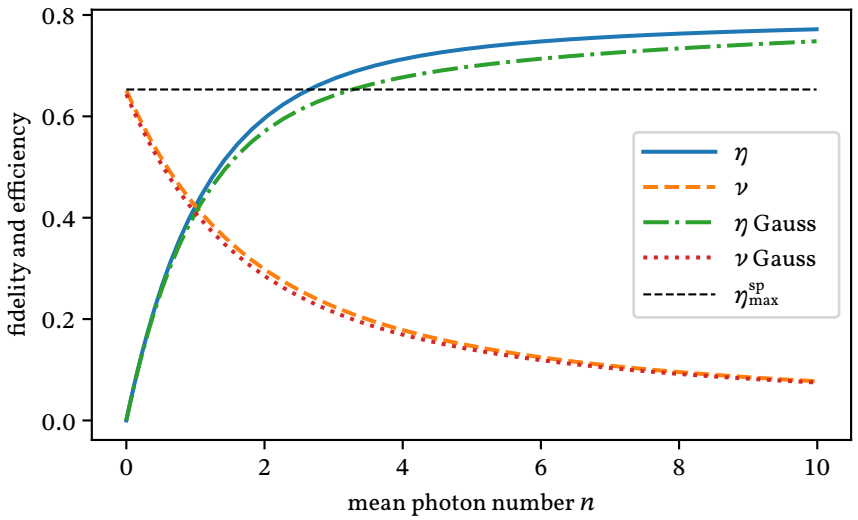

Figure 4.1: Storage efficiency η, Eq. (4.13), and fidelity ν, Eq. (4.14), at time $t = t_2$ as a function of the mean photon number n of the incident weak coherent pulse with shape of Eq. (4.11) (solid and dashed). The figures of merit η and ν have been evaluated by determining numerically the density matrix of the system $\hat{\tau}(t_2)$ from the initial state $\hat{\tau}(t_1) = |g, 0_c\rangle\langle g, 0_c|$ by integrating the master equation (4.20) in the truncated Hilbert space of the cavity field with a maximum of 14 excitations. For comparison we also report the fidelity and efficiency of storage of a weak coherent pulse with Gaussian shape (labels "Gauss"); In this case the control pulse is optimized for the storage of a single photon with Gaussian shape. The dashed line indicates the maximal fidelity of storage of a single photon. The other parameters are given in Sec. 4.2.3.

We integrate numerically the optical Bloch Equation for the matrix elements of Eq. (4.20) taking a truncated Hilbert space for the cavity field, with number states ranging from $m = 0$ to $m = m_{max}$. For the parameters we use in our simulation we find that the mean average number of intracavity photons is below 2. We check the convergence of our simulation for different values of $m = m_{max}$ and fix $m_{max} = 14$. Figure 4.1 displays the storage efficiency η and fidelity ν at time $t = t_2$ for different mean number of photons n of the incident weak coherent pulse. When evaluating the dynamics we employed the control laser pulse $\Omega(t)$ which optimizes the storage of the incident pulse when this is a *single* photon with temporal envelope $\mathcal{E}_{in}(t)$, Eq. (4.11). In detail, the

amplitude of the laser pulse has been determined in Chapter 3 and reads (for $\delta = \Delta = 0$)

$$\Omega(t) = \sqrt{\frac{2\gamma(1+C)}{(e^{4t/T}+1)T}}. \tag{4.22}$$

We observe that the storage efficiency η rapidly increases with n and saturates to the asymptotic value $\eta_\infty \approx 0.79$ for $n \gtrsim 10$. This asymptotic value indicates that the field in the cavity is essentially classical, the dynamics is the one of STIRAP [151], and its efficiency does not reach unity being the control pulse optimal for single-photon storage but *not* for STIRAP. The fidelity ν decreases with n, while in the limit $n \to 0$ it approaches the single-photon storage fidelity. We note that the behavior for $n \gtrsim 1$ depends on the pulse shape (see Fig. 4.1).

In Ref. [120] the authors report the experimental results of measuring the fidelity ν as a function of n. In particular they report the ratio between the fidelity of storing a weak coherent pulse with $n \approx 0.02$ and the fidelity for $n \approx 1$ to be $\nu_{\rm exp}(n = 0.02)/\nu_{\rm exp}(n = 1) \approx 1.27$. We compare these results with our predictions for $n \ll 1$ where the fidelity is independent of the photon shape. Then, we extract the same ratio from Fig. 4.1 and obtain $\nu(n = 0.02)/\nu(n = 1) \approx 1.5$. Even if for $n = 1$ the fidelity depends on the pulse shape, we have verified by comparing with different pulse shapes that the discrepancy is typically small.

4.3.2 *Extracting the single-photon storage fidelity from arbitrary incident pulses*

The method we applied in Sec. 4.3.1 is convenient but valid solely when the input pulse is a coherent state. We now show a more general approach for describing storage of a generic input pulse by an atomic medium (which can also be composed by a single atom) and which allows to obtain a useful description of the dynamics. This approach does not make use of approximations such as treating the atomic polarization as an oscillator [124] and allows one to determine the storage fidelity.

For this purpose we consider master equation (4.1), and recast it in the form [129, 152]

$$\partial_t \hat{\rho} = -\mathrm{i}(\hat{H}_{\rm eff}(t)\hat{\rho} - \hat{\rho}\hat{H}^\dagger_{\rm eff}(t)) + \mathcal{J}\hat{\rho}, \tag{4.23}$$

where $\hat{H}_{\rm eff}(t)$ is a non-Hermitian operator, which reads

$$\hat{H}_{\rm eff}(t) = \hat{H}(t) - \mathrm{i}\gamma|e\rangle\langle e| - \mathrm{i}\kappa_{\rm loss}\hat{a}^\dagger\hat{a}\,, \tag{4.24}$$

and is denoted in the literature as effective Hamiltonian. The last term on the right-hand side of Eq. (4.23) is denoted by *jump term* and is here given by

$$\mathcal{J}\hat{\rho} = 2\big(\gamma|\xi_e\rangle\langle e|\hat{\rho}|e\rangle\langle\xi_e| + \kappa_{\rm loss}\hat{a}\hat{\rho}\hat{a}^\dagger\big). \tag{4.25}$$

This decomposition allows one to visualize the dynamics in terms of an ensemble of trajectories contributing to the dynamics, where each trajectory is characterized by a number of jumps at given instant of time within the interval where the evolution occurs [125, 152]. Of all trajectories, we restrict to the one where no jump occurs since this is the only trajectory which contributes to the target dynamics. In fact, even though trajectories with spontaneous emission events may lead to dynamics where the atom is finally in state $|r\rangle$, yet such trajectories are incoherent and thus irreversible. We therefore discard them since they do not contribute to the fidelity of the process. The corresponding density matrix is $\rho_0(t) = S(t)\rho(t_1)S(t)^\dagger/P_0$, where $S(t) = T : \exp\left(-i\int_{t_1}^t d\tau \hat{H}_{\rm eff}(\tau)/\hbar\right)$ and T is the time ordering operator, while $P_0 = \mathrm{Tr}\{S(t)\rho(t_1)S(t)^\dagger\}$ is the probability that the trajectory occurs. Since the initial state is a pure state, $\hat{\rho}(t_1) = |\psi_{t_1}\rangle\langle\psi_{t_1}|$, then $\hat{\rho}_0(t) = |\psi_t\rangle\langle\psi_t|$ with $|\psi_t\rangle = S(t)|\psi_{t_1}\rangle/\sqrt{P_0}$. The efficiency of storage η, in particular, can be written as

$$\eta = P_0\,\mathrm{Tr}\{|r\rangle\langle r|\rho_0(t_2)\}\,. \tag{4.26}$$

We note that this definition can be extended also to input pulses which are described by mixed states. In fact, consider the density matrix μ of the incident pulse: $\mu = \sum_\alpha p_\alpha |\psi^\alpha\rangle\langle\psi^\alpha|$, with $\sum_\alpha p_\alpha = 1$ and each $|\psi^\alpha\rangle$ a quantum state of the electromagnetic field. The efficiency of storage of the mixed state μ is then

$$\eta^{\rm mix} = \sum_\alpha p_\alpha \eta^\alpha\,. \tag{4.27}$$

Here, η^α is the efficiency of storage of the pure state $|\psi^\alpha\rangle$ which can be computed using Eq. (4.26).

In order to determine η, we first decompose the incident pulse at $t = t_1$ into photonic excitations, namely:

$$|\psi^{\rm coh}\rangle = \sum_{m=0}^{\infty} C_m |\psi^{(m)}\rangle, \tag{4.28}$$

where $\sum_m |C_m|^2 = 1$, and the state $|\psi^{(m)}\rangle$ contains exactly m photons, $\langle\psi^{(l)}|\psi^{(m)}\rangle = \delta_{lm}$. The dynamics transfers the excitations but preserves their total number, since $\hat{H}_{\rm eff}$ commutes with $\sum_k b_k^\dagger b_k + a^\dagger a + |e\rangle\langle e| + |r\rangle\langle r|$. Therefore it does not couple states $|\psi^{(m)}\rangle$ with different number of photons. By this decomposition we can numerically determine the fidelity η for a finite number of initial excitations, as we show in Appendix 4.A. The efficiency η, in particular, can be cast in the form

$$\eta = \sum_{m=0}^{\infty} |C_m|^2 \eta^{(m)}\,, \tag{4.29}$$

where $\eta^{(m)} = \langle\psi^{(m)}|S(t)^\dagger|r\rangle\langle r|S(t)|\psi^{(m)}\rangle$ is the efficiency that one photon from a m-photon state is transferred into the atomic excitation $|r\rangle$. Here,

$\eta^{(1)}$ is the storage fidelity of a single photon $\eta^{\rm sp}$. For a weak coherent pulse $C_m = \sqrt{e^{-n}n^m/m!}$, and for $n \ll 1$ we obtain the expression

$$\eta = n\eta^{(1)} + n^2\big(\eta^{(2)}/2 - \eta^{(1)}\big) + O(n^3)\,. \tag{4.30}$$

such that the fidelity takes the form

$$\nu = \frac{\eta}{n} = \eta^{(1)} + n\big(\eta^{(2)}/2 - \eta^{(1)}\big) + O(n^2)\,. \tag{4.31}$$

If the control pulse $\Omega(t)$ is chosen to be the one which maximize the storage fidelity of a single photon, then $\eta^{(1)} = \eta^{\rm sp}_{\rm max}$, Eq. (4.16). This can be clearly seen in Fig. 4.1.

We now discuss this dynamics if, instead of a single atom, the quantum memory is composed by M atoms within the resonator. In the following we assume that the atoms are identical and that the vacuum Rabi coupling and the control laser pulse intensity and phase do not depend on the atomic positions within the cavity. Let us first consider that the input pulse is a single photon. In this case the dynamics can be mapped to the one described by Eq. (4.1), where in the Hamiltonian (3.3) the states of the Λ transition are replaced by the collective atomic states $|g\rangle \to |g'\rangle = |g_1,\dots,g_M\rangle$, $|e\rangle \to |e'\rangle = \sum_{i=1}^{M}|g_1,\dots,e_i,\dots,g_M\rangle/\sqrt{M}$, and $|r\rangle \to |r'\rangle = \sum_{i=1}^{M}|g_1,\dots,r_i,\dots,g_M\rangle/\sqrt{M}$, where the latter is the target state. For a single incident photon, in fact, these are the only internal states involved in the dynamics. The coupling between the cavity mode and the $|g'\rangle - |e'\rangle$ transition is now $g\sqrt{M}$, leading to a higher cooperativity C and thus to a larger value of $\eta^{\rm sp}_{\rm max}$. In this case the control pulse leading to optimal storage is the same as for a single atom, which couples to the cavity with vacuum Rabi frequency $\tilde{g} = g\sqrt{M}$ (see for example Eq. (4.22) and Chapter 3).

If the incident pulse is not a single photon, further collective excitations of the atoms have to be accounted for and the dynamics cannot be reduced to the coupling of a Λ structure with the cavity field, as is detailed in Appendix 4.A for the case of a weak coherent pulse. Nevertheless, if the number of atoms is much larger than the mean number of excitations in the incident pulse $M \gg n$, the dynamical equations can be reduced to the ones describing storage of the single photon [122–124]. In this limiting case, the optimal control pulses for storage of a single photon can also be applied to storage of the input pulse by the atomic ensemble, as long as the input pulse has the same envelope as the single photon. We refer the interested reader to Ref. [124] for details.

In general, the formalism of the effective Hamiltonian can be applied to determine the control field for storage of an arbitrary input pulse by an atomic ensemble, without having to impose the condition $M \gg n$. For an arbitrary input pulse, $|\psi\rangle = \sum_{m=0}^{\infty} C_m|\psi^{(m)}\rangle$ with $\sum_m |C_m|^2 = 1$, the target state is $\sum_{m=0}^{\infty} C_m|r_m\rangle$, where $|r_m\rangle$ is the Dicke state of the atomic ensemble where m atoms are in $|r\rangle$ and which is coherently coupled to

the Dicke state $|g'\rangle$ by the dynamics. The control pulse $\Omega(t)$ shall then optimize the dynamics by maximizing the fidelity

$$\eta' = \sum_m |C_m|^2 \eta_m^{(m)}, \tag{4.32}$$

where $\eta_m^{(m)} = \langle \psi^{(m)}|S(t)^\dagger|r_m\rangle\langle r_m|S(t)|\psi^{(m)}\rangle$ and $S(t)$ is calculated for the effective Hamiltonian of the atomic ensemble. The control field $\Omega(t)$ can be found by means of an analogous strategy as for ensemble optimal control theory (OCT), finding the control pulse that optimizes the dynamics in each subspace of m excitations so to maximize η' [138, 153–156].

4.4 CONCLUSIONS

We have analysed the storage of a weak coherent pulse into the excitation of a single atom inside a resonator, which acts as a quantum memory. Our specific objective was to characterize the process in order to show under which conditions an attenuated incident pulse can be considered as a single photon for storage purposes. Thus we have identified the conditions and the figures of merit which allow one to extract the single-photon storage fidelity by measuring the probability that the atom has been excited at the end of the process.

We remark that the retrieved information by a single atom will always be a single photon [157]. Nevertheless, the formalism we developed in this work permits one to extend this dynamics to other kind of incident pulses and to quantum memories composed by spin ensembles. For this general case it sets the basis for identifying the optimal control pulses for storage and retrieval of an arbitrary quantum light pulse.

APPENDICES

4.A STORAGE EFFICIENCY FOR $n \ll 1$

In this appendix we provide the details for calculating the dynamics and the fidelity for an incident pulse which is a superposition of different photon number states. We apply the procedure to multimode coherent states, nevertheless it can be generalised in a straighforward manner to a generic initial input pulse.

4.A.1 *Decomposition of a coherent state*

The coherent state in Eq. (4.5) can be decomposed in a linear combination of states each with a fixed number of excitations (see Eq. (4.28) with $C_m = \sqrt{e^{-n}n^m/m!}$): The mean number of photons in the mode k is $|\alpha_k|^2$ and the mean photon number in the coherent state is $n = \sum_{k=1}^N |\alpha_k|^2$,

see Eq. (4.7). State $|\psi^{(m)}\rangle$ contains exactly m excitations of the quantum electromagnetic field and reads

$$|\psi^{(0)}\rangle = |\text{vac}\rangle, \tag{4.33a}$$

$$|\psi^{(1)}\rangle = \sum_{k=1}^{N} \mathcal{E}_k \hat{b}_k^\dagger |\text{vac}\rangle, \tag{4.33b}$$

$$|\psi^{(2)}\rangle = \sum_{k=1}^{N}\sum_{k'=1}^{N} \mathcal{E}_{k,k'} \hat{b}_k^\dagger \hat{b}_{k'}^\dagger |\text{vac}\rangle, \tag{4.33c}$$

$$\vdots$$

$$|\psi^{(m)}\rangle = \sum_{\{k\}_m} \mathcal{E}_{\{k\}_m} \overbrace{\hat{b}_k^\dagger \hat{b}_{k'}^\dagger \dots \hat{b}_{k''\dots''}^\dagger}^{m} |\text{vac}\rangle. \tag{4.33d}$$

Coefficients $\mathcal{E}_{\{k\}_m}$ read

$$\mathcal{E}_k = \frac{\alpha_k}{\sqrt{n}}, \tag{4.34a}$$

$$\mathcal{E}_{k,k'} = \mathcal{E}_{k',k} = \frac{\mathcal{E}_k \mathcal{E}_{k'}}{\sqrt{2}}, \tag{4.34b}$$

$$\vdots \tag{4.34c}$$

$$\mathcal{E}_{\{k\}_m} = \mathcal{E}_{\underbrace{k,k'\dots k''\dots''}_{m}} = \frac{\prod_{i\in\{k\}_m} \mathcal{E}_i}{\sqrt{m!}}, \tag{4.34d}$$

and it is easy to check that the states $|\psi^{(m)}\rangle$ are orthonormal $\langle\psi^{(m)}|\psi^{(n)}\rangle = \delta_{mn}$ and complete.

The storage fidelity when the initial state is the coherent state introduced in Eq. (4.28) is given by (see Eq. (4.29))

$$\eta = e^{-n} \sum_{m=1}^{\infty} \frac{n^m}{m!} \eta^{(m)}. \tag{4.35}$$

4.A.2 *Equations of motion*

We here explicitly derive the equations of motion in the subspaces with $m \leq 2$ excitations.

Zero excitations - Vacuum: The subspace of zero excitations $m = 0$ contains only the state $|g, 0, \text{vac}\rangle$, meaning that the atom is in the ground state $|g\rangle$, the cavity is empty and the electromagnetic field is in the vacuum state. Thus the time evolution in this subspace is $|\phi_t^{(0)}\rangle = |\phi_{t_1}^{(0)}\rangle$.

One excitation - Single photon: A basis for the subspace with one excitation $m = 1$ is

$$\mathcal{B}_1 = \{|g, 1, \text{vac}\rangle, |e, 0, \text{vac}\rangle, |r, 0, \text{vac}\rangle, \\ |g, 0, 1_k\rangle \,:\, k \in \{1, \dots, N\}\}$$

and a general state can be written as

$$|\phi_t^{(1)}\rangle = c_1(t)|g,1,\mathrm{vac}\rangle + e_1(t)|e,0,\mathrm{vac}\rangle + \\ + r_1(t)|r,0,\mathrm{vac}\rangle + \sum_k \mathcal{E}_k(t)|g,0,1_k\rangle. \tag{4.36}$$

The equations of motion in this subspace are ($\lambda_k = \lambda$)

$$\begin{aligned} \dot{c}_1(t) &= -\mathrm{i}g e_1(t) - \mathrm{i}\lambda \sum_k \mathcal{E}_k(t) - \kappa_{\mathrm{loss}} c_1(t), \\ \dot{e}_1(t) &= (\mathrm{i}\Delta - \gamma) e_1(t) - \mathrm{i}g c_1(t) - \mathrm{i}\Omega(t) r_1(t), \\ \dot{r}_1(t) &= -\mathrm{i}\Omega^*(t) e_1(t), \\ \dot{\mathcal{E}}_k(t) &= -\mathrm{i}\Delta_k \mathcal{E}_k(t) - \mathrm{i}\lambda c_1(t), \end{aligned} \tag{4.37}$$

and they constitute a system of $(N+3)$ coupled differential equations with time dependent coefficients. Using the input-output formalism [55] one obtains

$$\begin{aligned} \dot{c}_1(t) &= -\mathrm{i}g e_1(t) - \mathrm{i}\sqrt{2\kappa}\mathcal{E}_{\mathrm{in}}(t) - (\kappa + \kappa_{\mathrm{loss}}) c_1(t), \\ \dot{e}_1(t) &= (\mathrm{i}\Delta - \gamma) e_1(t) - \mathrm{i}g c_1(t) - \mathrm{i}\Omega(t) r_1(t), \\ \dot{r}_1(t) &= -\mathrm{i}\Omega^*(t) e_1(t), \end{aligned} \tag{4.38}$$

where $\kappa = L\lambda^2/c$ is the decay rate of the cavity field and $\mathcal{E}_{\mathrm{in}}(t)$ is defined in Eq. (4.18). Equations (4.37) or Eqs. (4.38) can be easily solved numerically. These equations correspond to the storage of a single photon into a single atom [150] (see Eqs (3.29)) and are equivalent to the approximated equations obtained in Ref. [124] describing the storage of a light pulse in an atomic ensemble composed by a large number $N \gg 1$ of atoms.

Two excitations - Two-photons states: A basis for the subspace with two excitations $m = 2$ is

$$\mathcal{B}_2 = \{|g,2,\mathrm{vac}\rangle, |g,1,1_k\rangle, |g,0,1_k 1_{k'}\rangle, |e,1,\mathrm{vac}\rangle, \\ |e,0,1_k\rangle, |r,1,\mathrm{vac}\rangle, |r,0,1_k\rangle \,:\, k,k' \in \{1,\dots,N\}\}$$

thus a general state in this subspace can be written as

$$\begin{aligned} |\phi_t^{(2)}\rangle = {} & c_2(t)|g,2,\mathrm{vac}\rangle + \sum_k \mathcal{E}_k^c(t)|g,1,1_k\rangle + \\ & + \sum_k \sum_{k' \geq k} \mathcal{E}_{k,k'}(t)|g,0,1_k 1_{k'}\rangle + \\ & + e_2(t)|e,1,\mathrm{vac}\rangle + \sum_k \mathcal{E}_k^e(t)|e,0,1_k\rangle + \\ & + r_2(t)|r,1,\mathrm{vac}\rangle + \sum_k \mathcal{E}_k^r(t)|r,0,1_k\rangle. \end{aligned} \tag{4.39}$$

The state in Eq. (4.39) can be used to describe the interaction of the atom-cavity system with a two-photon state; in fact the term

$$\sum_{k,k'} \mathcal{E}_{k,k'}(t)|g,0,1_k 1_{k'}\rangle$$

describes a two-photon state of the electromagnetic field. Notice that we use the definition $|\cdot,\cdot,1_k1_{k'}\rangle = b_k^\dagger b_{k'}^\dagger|\cdot,\cdot,\mathrm{vac}\rangle$ which implies $|\cdot,\cdot,1_k1_k\rangle = \sqrt{2}|\cdot,\cdot,2_k\rangle$. The equations of motion in this subspace are

$$\begin{aligned}
\dot{c}_2(t) &= -\mathrm{i}\sqrt{2}g e_2(t) - \mathrm{i}\sqrt{2}\lambda\sum_k \mathcal{E}_k^c(t) + \\
&\quad - 2\kappa_{\mathrm{loss}} c_2(t) \\
\dot{e}_2(t) &= (\mathrm{i}\Delta - \gamma - \kappa_{\mathrm{loss}})e_2(t) - \mathrm{i}\sqrt{2}g c_2(t) + \\
&\quad - \mathrm{i}\Omega(t) r_2(t) - \mathrm{i}\lambda\sum_k \mathcal{E}_k^e(t) \\
\dot{r}_2(t) &= -\mathrm{i}\Omega^*(t) e_2(t) - \mathrm{i}\lambda\sum_k \mathcal{E}_k^r(t) - \kappa_{\mathrm{loss}} r_2(t) \\
\dot{\mathcal{E}}_k^c(t) &= -(\mathrm{i}\Delta_k + \kappa_{\mathrm{loss}})\mathcal{E}_k^c(t) - \mathrm{i}g\mathcal{E}_k^e(t) + \\
&\quad - \mathrm{i}\lambda\sum_{k'} A_{k,k'}(t) - \mathrm{i}\sqrt{2}\lambda c_2(t) \\
\dot{\mathcal{E}}_k^e(t) &= \mathrm{i}(\Delta - \Delta_k)\mathcal{E}_k^e(t) - \mathrm{i}g\mathcal{E}_k^c(t) + \\
&\quad - \mathrm{i}\Omega(t)\mathcal{E}_k^r(t) - \mathrm{i}\lambda e_2(t) \\
\dot{\mathcal{E}}_k^r(t) &= -\mathrm{i}\Delta_k\mathcal{E}_k^r(t) - \mathrm{i}\Omega^*(t)\mathcal{E}_k^e(t) - \mathrm{i}\lambda r_2(t) \\
\dot{A}_{k,k'}(t) &= -\mathrm{i}(\Delta_k + \Delta_{k'})A_{k,k'} + \\
&\quad - \mathrm{i}\lambda\big(\mathcal{E}_k^c(t) + \mathcal{E}_{k'}^c(t)\big),
\end{aligned} \tag{4.40}$$

where we have defined $A_{k,k'}(t) = \mathcal{E}_{k,k'}(t) + \mathcal{E}_{k',k}(t)$. Eqs. (4.40) are a system of (N^2+3N+3) coupled differential equations with time dependent coefficients; this system can be solved numerically.

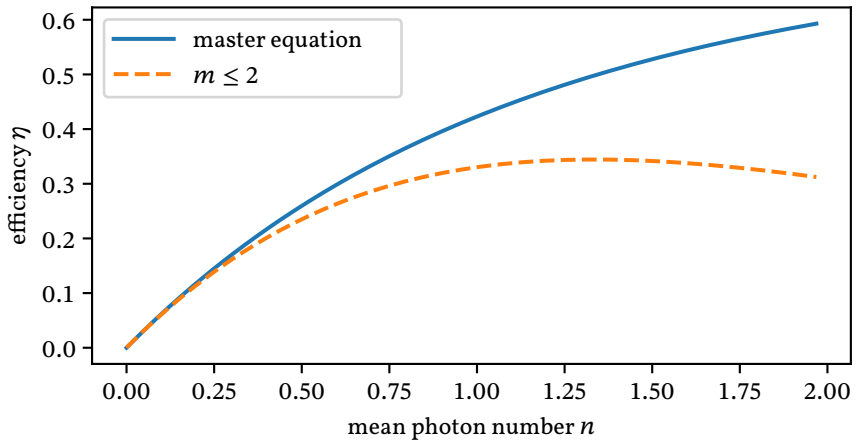

Figure 4.2: Efficiency η of the storage process of a weak coherent pulse. Solution with the master equation formalism of Sec. 4.3.1 (solid line) and approximated solution with truncation to two excitations $m \leq 2$ as described in the current section (dashed).

Calculation of the efficiency: The efficiency η can be calculated with the formalism introduced in this section in two ways: (i) solve Eqs. (4.37)

and Eqs. (4.40) with initial conditions given by the expansion (4.28) and the coefficients given by Eqs. (4.34a) and (4.34b), then the efficiency is

$$\eta = |r_1(t_2)|^2 + |r_2(t_2)|^2 + \sum_k |\mathcal{E}_k^r(t_2)|^2; \tag{4.41}$$

or (ii) solve Eqs. (4.37) and Eqs. (4.40) with initial conditions (4.34a) and (4.34b) separately to obtain the efficiencies $\eta^{(1)}$ and $\eta^{(2)}$ of single and double photon storage; then the efficiency as function of n is given by Eq. (4.30).

Fig. 4.2 reports the efficiency η as a function of n, the solid line represent the result of the numerical integration of the master equation described in Sec. 4.3.1. The dashed line is the solution with the decomposition until $m = 2$ described in this section. It is evident that for $n \ll 1$ the two results coincide.

Part III

HYBRID QUANTUM SYSTEMS

We analyze the dynamics of a hybrid quantum system composed of an NV-center in a diamond crystal which is an optical and a mechanical resonator. By means of the master equation formalism, we investigate the dynamics of a mechanical mode of the diamond structure and identify the regime in which it is radiatively cooled. We determine the steady state temperature and the cooling rate as a function of the system parameters. We further determine the spectrum of resonance fluorescence to identify the scattering processes that lead to cooling.

5

LASER AND CAVITY COOLING OF A MECHANICAL RESONATOR WITH A NITROGEN-VACANCY CENTER IN DIAMOND

The content of this chapter contains results, text and figures from:

- L. Giannelli, R. Betzholz, L. Kreiner, M. Bienert, and G. Morigi, "Laser and cavity cooling of a mechanical resonator with a nitrogen-vacancy center in diamond, In: "*Physical Review A* 94 (2016), p. 053835, DOI: 10.1103/PhysRevA.94.053835.

5.1 INTRODUCTION

A nitrogen-vacancy (NV) center is formed by replacing two adjacent carbon atoms by a nitrogen atom and a vacancy in a diamond crystal. This atomic defect exhibit atom-like properties such as well-defined optical transitions and long lived spin quantum states [158]. Colour centers in diamond, such as NV-centers, are widely studied because of their exceptional properties as bright solid-state quantum emitters at room temperature [158, 159]. Their dynamics is being analysed in a wide variety of setups, which for instance can achieve the strong coupling with high-finesse optical resonators [160–162] and/or the strain coupling with high-Q vibrating structures [161–167] or standing mechanical waves [168, 169]. This experimental progress makes NV centers promising candidates for realizing quantum hybrid devices, namely, devices capable of interfacing photons, phonons, and spin excitations in a controlled way, and can offer a wide range of applications for quantum information processing [56, 170–172] and quantum sensing [56, 173–176]. It thus calls for identifying the perspectives for control of these hybrid devices, which requires a systematic characterization of their dynamics.

In this work, we theoretically analyse laser cooling of a high-Q vibrating mode, which is strain coupled to the electronic transitions of an NV-center in diamond and optomechanically coupled to an optical cavity. This situation can be realised, for instance, when NV center, high-Q mechanical mode, and optical resonators are assembled in a monolithic diamond structure, as illustrated in Fig. 5.1 and recently discussed in Refs. [165, 166]. In this setup the high-Q vibrating mode can be optomechanically cooled by the coupling with the cavity and/or laser-cooled by the strain-coupling with the NV-center transitions between the state

$|g\rangle \equiv |^3A_{20}\rangle$ and the levels $|E_x\rangle \equiv |x\rangle$ and $|E_y\rangle \equiv |y\rangle$, sketched in Fig. 5.1(b). The starting point of our study is the theoretical model of Ref. [177], where the authors investigated the effect of the NV multilevel structure on the dynamics of a high-Q vibrational mode. We extend this model by including the high-finesse mode of an optical cavity, which couples to the electronic transitions of the NV center and to the mechanical resonator by means of radiation pressure, and determine the laser cooling dynamics. We focus in particular on the regime where the linewidth of the resonances induced by the coupling with the cavity is of the same order as the one of the electronic transitions of the NV center. We further determine the effect of pure dephasing, which tends to destroy the coherence of the NV-center excitations, on the cooling dynamics. Surprisingly, we identify regimes where pure dephasing can improve the cooling rate.

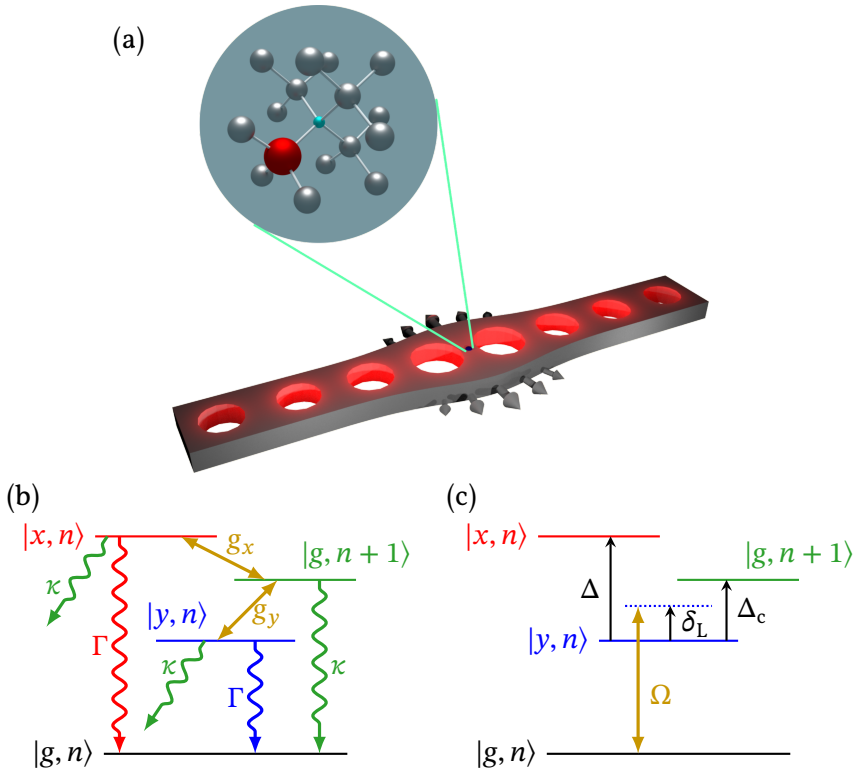

Figure 5.1: (a) A mechanical resonator, which is also a photonic crystal, interacts with a NV center in a diamond bulk via strain coupling. (b) The NV-center internal level structure, including the photonic excitations: the ground state $|g\rangle \equiv |^3A_{20}\rangle$ couples to the excited states $|x\rangle \equiv |E_x\rangle$ and $|y\rangle \equiv |E_y\rangle$, which radiatively decay at rate Γ. A mode of the high-finesse optical cavity decays at rate κ and drives quasi-resonantly the transitions $|g,n+1\rangle \rightarrow |x,n\rangle, |y,n\rangle$ with n the intracavity photon number. Coefficients g_x and g_y denote the corresponding vacuum Rabi frequencies. (c) Sketch of the relevant frequencies $\delta_L, \Delta_c, \Delta$, as a function of which the cooling efficiency is characterised, in presence of a laser driving the transition $|g\rangle \rightarrow |y\rangle$ with Rabi frequency Ω.

This Chapter is organised as follows. In Sec. 5.2 we review some general concepts ruling the cooling dynamics in presence of the strong coupling with a resonator. In Sec. 5.3 the theoretical model is introduced and in Sec. 5.4 the parameter regime is discussed with reference to existing experimental realisation. In Sec. 5.5 the rate equations for the phonon dynamics are derived and in Sec. 5.6 the cooling rate, the asymptotic temperature, and the spectrum of resonance fluorescence are determined and discussed in the presence and in the absence of the coupling with the optical cavity mode. Moreover, the cooling efficiency as a function of the dephasing rate is analysed. The conclusions are drawn in Sec. 5.7.

5.2 GENERAL CONSIDERATIONS

Our study is motivated by an experimentally existing platform, like the one sketched in Fig. 5.1. Our purpose is to investigate whether the optomechanical coupling can help in achieving lower temperatures than the ones that have been predicted by sideband cooling using the strain-coupling with the NV center, see Ref. [177]. In fact, there can be an advantage by resorting to the optical cavity if the final occupation of the mechanical oscillator is lower than by just performing sideband cooling with the NV center, and thus if (i) the cavity-assisted cooling processes are sufficiently faster than the thermalization with the external environment and yet (ii) the final occupation of the oscillator is smaller than the one obtained by solely employing sideband cooling, according to a protocol like the one described in Ref. [177]. This analysis draws from several works where it was studied how the interplay between the mechanical effects due to the coupling of an electronic transition with a laser and with a cavity can increase the cooling efficiency of a mechanical oscillator [178–182]. There it was found that ground state cooling can be achieved as long as the mechanical oscillator frequency, here denoted by ν, is larger than either the linewidth of the electronic transition, Γ, or of the optical resonator, κ. The minimal final mechanical oscillator occupation one can achieve is then controlled by the ratio between the linewidth of the narrower resonance, which we denote here by $\Gamma_{\min} = \min(\kappa, \Gamma)$, and ν. Accordingly, the cooling rate $\tilde{\Gamma}$ is slower and scales with $\Gamma_{\min}$.

These dynamics can be often illustrated by means of a set of rate equations for the occupations p_n of the oscillator's state with n excitations ($n = 0, 1, 2, ...$) [183]:

$$\dot{p}_n = -n(A_+ + A_-)p_n + (n+1)A_- p_{n+1} + nA_+ p_{n-1}\,, \tag{5.1}$$

with $\sum_n p_n = 1$ (see Sec. 5.5 for details how this equation is derived). Here, nA_+ and nA_- are the rates with which the oscillator in state $|n\rangle$ is heated and cooled, respectively, by one phonon, and can have the form of lorentz functions, whose linewidth is determined by the linewidth scattering resonance.

Specific predictions for the relevant quantities, whose dynamics Equation (5.1) describes, can be directly extracted from the equation for the mean phonon occupation number $\langle n \rangle = \langle a^\dagger a \rangle = \sum_n n p_n$ [183]:

$$\dot{\langle n \rangle} = -(\tilde{\Gamma} + \gamma)(\langle n \rangle - n_f). \tag{5.2}$$

Here γ is the thermalization rate and n_f the final phonon occupation of the mechanical mode. Finally

$$\tilde{\Gamma} = A_- - A_+ \tag{5.3}$$

is the cooling rate when $A_- > A_+$, whose maximum amplitude scales as $\tilde{\Gamma} \sim (\omega_r/\nu)\Gamma_{\min}$ with ω_r the frequency scaling the mechanical effects due to the coupling with light (when these are due to the phase or intensity gradient of the light wave, ω_r is the recoil frequency; Here, $\omega_r \sim (\Lambda/\hbar)^2/\nu$, with Λ the strength of the strain coupling). In this regime and for $\gamma = 0$ radiation cools the vibrations to the asymptotic occupation N_0, which is given by

$$N_0 = \frac{A_+}{A_- - A_+} = \frac{A_+}{\tilde{\Gamma}}, \tag{5.4}$$

and whose minimum scales with $N_0 \sim (\Gamma_{\min}/\nu)^2$.

In a solid-state environment, where the heating rate due to the coupling with the external reservoir is not negligible, slowing down the cooling dynamics can be detrimental. This is visible when considering the final occupation:

$$n_f = \frac{\tilde{\Gamma}}{\tilde{\Gamma} + \gamma} N_0 + \frac{\gamma}{\tilde{\Gamma} + \gamma} N_{\text{th}}, \tag{5.5}$$

where N_{th} is the mean phonon occupation at the temperature of the external reservoir. Thus, maximizing the ratio $\Gamma_{\min}/\gamma$ and minimizing the ratio $\Gamma_{\min}/\nu$ is crucial and limits the parameter interval where cavity-assisted cooling can improve the efficiency.

From these considerations one can generally identify the regime where the coupling with a resonator can increase the sideband cooling efficiency. In fact, a large cavity decay rate such that $\kappa > \nu > \Gamma$ would increase the cooling rate $\tilde{\Gamma}$. Yet it can also increase the asymptotic occupation number of the mechanical mode N_0. On the other hand, a very good cavity with $\kappa < \Gamma < \nu$ can allow one to achieve smaller values of N_0, but at the price of decreasing $\tilde{\Gamma}$, so that the final occupation number of the mechanical mode n_f becomes effectively larger.

The parameter regime to explore is quite large. However in general we expect that, in the regime where laser sideband cooling is efficient, the coupling to a resonator at linewidth $\kappa > \Gamma$ can be of help only if it substantially increases the cooling rate keeping $N_0 < 1$. The coupling to a resonator with $\kappa < \Gamma < \nu$ can help in reaching ultralow temperatures, provided thermalization can be neglected. In this Chapter we limit our

analysis by taking the optimal parameters for sideband cooling of an NV center and adding the coupling with a cavity with linewidth $\kappa \sim \Gamma$, in order to search for possible effects which cannot be foreseen drawing from these simple considerations. We refer the reader to Sec. 5.4 where the choice of the parameter regime is discussed in relation to existing experimental implementations. The cooling rate, the asymptotic temperature, and the spectrum of resonance fluorescence are then determined and discussed in Sec. 5.6 in the presence and in the absence of the coupling with the optical cavity mode. The reader who is solely interested in the resulting cooling efficiency can skip Sec. 5.5 and jump directly to Sec. 5.6.

5.3 THE SYSTEM

In this Section we introduce the theoretical model which is at the basis of our study. We describe the interaction of a high-Q mechanical resonator mode of a phononic crystal cavity, with a quantum emitter, specifically, a NV center in diamond, and a high-finesse optical resonator mode of a photonic crystal cavity. The NV center is strain-coupled with the mechanical resonator and the electronic dipole transitions strongly couple with the photonic mode. The mechanical resonator, in turn, is optomechanically coupled to the photonic cavity. The interactions in this system are expected to be strongly enhanced by the co-localization in a single structure ensuring a perfect spatial overlap between the different degrees of freedom, which is achieved by assemblance in a monolithic diamond structure sketched in Fig. 5.1(a). The system is intrinsically dissipative due to radiative decay of the electronic excitations and optical cavity losses. Additionally, the mechanical resonator couples to an external thermal reservoir. We assume that it is continuously driven by a laser field, which directly couples to an electric dipole transition of the defect. In what follows we define the master equation governing the dynamics of the density matrix ρ, which describes the state of the composite system composed by the NV center, and the photonic and phononic resonators.

5.3.1 *Basic equations*

The dynamics of the hybrid system's density operator ρ, describing the state of the system composed by the internal degrees of freedom of the NV-center, of the optical cavity mode and of the mechanical oscillator, is governed by the master equation $\partial_t \rho = \mathcal{L}\rho$, where superoperator $\mathcal{L}$ is defined as ($\hbar = 1$):

$$\mathcal{L}\rho = -\mathrm{i}[H, \rho] + \mathcal{L}_{\mathrm{dis}}\rho\,, \tag{5.6}$$

and which will be conveniently reported in the reference frame rotating with the laser frequency ω_{L}. Below we provide the detailed form of Hamiltonian H and superoperator $\mathcal{L}_{\mathrm{dis}}$.

5.3.1.1 *Unitary dynamics*

We first give the detailed form of the Hamiltonian H, which generates the unitary part of the time evolution. For convenience, we decompose it into the sum of Hermitian operators:

$$H = H_{\mathrm{mec}} + H_{\mathrm{I}} + (a + a^{\dagger})V, \tag{5.7}$$

where a and $a^{\dagger}$ annihilate and create, respectively, a mechanical vibration at frequency ν, while V acts on the cavity and NV-center degrees of freedom and is specified later on. Operator

$$H_{\mathrm{mec}} = \nu a^{\dagger} a \tag{5.8}$$

is the internal energy of the mechanical resonator, while Hamiltonian H_{I} describes the coupled dynamics of the NV center and the optical cavity:

$$\begin{aligned} H_{\mathrm{I}} \;=\; & (\omega_y - \omega_{\mathrm{L}})|y\rangle\langle y| + (\omega_x - \omega_{\mathrm{L}})|x\rangle\langle x| + (\omega_{\mathrm{c}} - \omega_{\mathrm{L}})c^{\dagger}c \\ & + \Big[\frac{\Omega}{2}|y\rangle\langle g| + \big(g_x|x\rangle\langle g| + g_y|y\rangle\langle g|\big)c + \mathrm{H.c.}\Big]. \end{aligned} \tag{5.9}$$

Here, ω_x (ω_y) is the frequency splitting in the laboratory frame between the excited state $|x\rangle$ ($|y\rangle$) and the ground state $|g\rangle$; operators c and $c^{\dagger}$ annihilate and create, respectively, a cavity photon at frequency ω_{c} (in the laboratory frame). The splitting between the $|x\rangle$ and $|y\rangle$ states is, for instance, due to a non-zero strain coupling, which is not related to the mechanical mode we consider. The frequencies appear shifted by ω_{L} since Hamiltonian H_{I} is reported in the reference frame rotating at the laser frequency. The second line of Eq. (5.9) describes, from left to right, the external laser driving the transition $|g\rangle \rightarrow |y\rangle$ with Rabi frequency Ω, while the optical mode drives the transitions $|g\rangle \rightarrow |x\rangle$ and $|g\rangle \rightarrow |y\rangle$ with vacuum Rabi frequency g_x and g_y, respectively. We note that the laser polarization can be chosen to selectively drive one electronic transition, as we do in our model, while in general the cavity mode's polarization has a finite projection to the dipole moment of both transitions, since this depends on the preparation of the sample. Therefore, we generally assume $g_x, g_y \neq 0$ unless otherwise stated. The relevant NV center and cavity states are reported in Fig. 5.1(b)-(c) with the relative detunings with respect to the laser frequencies. These are defined as:

$$\begin{aligned} \delta_{\mathrm{L}} &= \omega_{\mathrm{L}} - \omega_{\mathrm{y}}, \\ \Delta &= \omega_{\mathrm{x}} - \omega_{\mathrm{y}}, \\ \Delta_{\mathrm{c}} &= \omega_{\mathrm{c}} - \omega_{\mathrm{y}}\,. \end{aligned} \tag{5.10}$$

Finally, operator V is the sum of the strain and of the optomechanical coupling of the mechanical resonator with NV center and optical cavity, respectively. We decompose it hence into the sum $V = V_{\mathrm{strain}} + V_{\mathrm{om}}$, where V_{strain} acts on the NV degrees of freedom and reads [184]

$$V_{\mathrm{strain}} = \sum_{j=I,X,Z} \Lambda_j A_j\,, \tag{5.11}$$

where Λ_j are the strain coupling constants and the operators A_j are defined as:

$$\begin{aligned} A_I &= |x\rangle\langle x| + |y\rangle\langle y|\,, \\ A_X &= |x\rangle\langle y| + |y\rangle\langle x|\,, \\ A_Z &= |x\rangle\langle x| - |y\rangle\langle y|\,. \end{aligned} \tag{5.12}$$

The optomechanical coupling reads $V_{\mathrm{om}} = -\chi c^\dagger c$ with χ the optomechanical coupling constant [88, 185].

5.3.1.2 *Dissipation*

The irreversible processes we consider in our theoretical description are: (i) the radiative decay of the NV excitations and pure dephasing of the electronic coherences, (ii) cavity losses, and (iv) the mechanical damping rate due to the coupling of the mechanical resonator with an external thermal reservoir. We model each of these phenomena by a Born-Markov process described by the corresponding superoperator, such that superoperator $\mathcal{L}_{\mathrm{dis}}$ in Eq. (5.6) can be cast in the form

$$\mathcal{L}_{\mathrm{dis}} = \mathcal{L}_\Gamma + \mathcal{L}_\kappa + \mathcal{L}_\gamma\,. \tag{5.13}$$

The individual terms read

$$\mathcal{L}_\Gamma = \frac{\Gamma}{2}\sum_{\xi=x,y}\mathcal{D}[|g\rangle\langle\xi|] + \frac{\Gamma_\phi}{2}\sum_{\xi=x,y}\mathcal{D}[|\xi\rangle\langle\xi|]\,, \tag{5.14}$$

$$\mathcal{L}_\kappa = \frac{\kappa}{2}\mathcal{D}[c]\,, \tag{5.15}$$

$$\mathcal{L}_\gamma = \frac{\gamma}{2}(N_{\mathrm{th}}+1)\mathcal{D}[a] + \frac{\gamma}{2}N_{\mathrm{th}}\mathcal{D}[a^\dagger]\,, \tag{5.16}$$

where we used the definition

$$\mathcal{D}[o]\rho = 2o\rho o^\dagger - o^\dagger o\rho - \rho o^\dagger o\,, \tag{5.17}$$

with $o = |g\rangle\langle\xi|, |\xi\rangle\langle\xi|, c, a, a^\dagger$. The coefficients are the radiative decay rate Γ of the NV-center excited states, the dephasing rate of the electronic coherences Γ_ϕ, cavity losses at rate κ, and the damping rate of the mechanical oscillator γ. Finally, $N_{\mathrm{th}} = (\exp(\nu/k_{\mathrm{B}}T)-1)^{-1}$ is the equilibrium phonon occupation number of the bath to which the oscillator couples, with T the bath's temperature.

5.3.2 *Spectrum of resonance fluorescence*

In what follows we will use the master equation, Eq. (5.6), in order to analyze the cooling efficiency of the mechanical resonator and the spectrum of the light emitted by the NV center at the steady state of the cooling dynamics. In order to better characterize the parameter regime where cooling is efficient we choose an analytical approach, which is based on

a perturbative expansion of the Lioville operator and allows us to determine the cooling regime, the corresponding rate and the asymptotic temperature. This approach is reported in the following Section.

Moreover, in the regimes of interest we determine the spectrum of the scattered light, for the purpose of identifying the relevant features in the photons which are emitted by the NV center outside of the resonator. The spectrum of resonance fluorescence is, apart from a constant proportionality factor, the Fourier transform of the auto-correlation function of the electric field [186]:

$$\mathcal{S}(\omega) \propto \mathrm{Re} \int_0^\infty \mathrm{d}\tau \, \mathrm{e}^{-\mathrm{i}\omega\tau} \langle E^{(-)}(\tau) E^{(+)}(0) \rangle_{\mathrm{st}} \tag{5.18}$$

where $E^{(-)}(t)$ and $E^{(+)}(t)$ are the negative and positive frequency component of the electric field at time t and $\langle \cdot \rangle_{\mathrm{st}} \equiv \mathrm{Tr}\{\cdot \rho_{\mathrm{st}}\}$ denotes the trace taken over the steady state density matrix ρ_{st} which solves $\mathcal{L}\rho_{\mathrm{st}} = 0$. The intensity of the scattered field (away from the forward direction) is proportional to the source field, hence in the far-field the electric field is proportional to the sum of the operators $\vec{d}_j |g\rangle\langle j| + \mathrm{H.c.}$, for $j = x, y$ where $\vec{d}_x$ and $\vec{d}_y$ are the dipole moments of the transitions $|g\rangle \to |x\rangle$ and $|g\rangle \to |y\rangle$, respectively (notice that $\left|\vec{d}_x\right| = \left|\vec{d}_y\right|$). Since the dipole moments are mutually orthogonal, the spectrum integrated over the full solid angle 4π is the incoherent sum of the two components coming from the $|g\rangle\langle x|$ and $|g\rangle\langle y|$ operators, i. e. the interference term integrates to zero. With the help of the quantum regression theorem [89] one can cast the spectrum into the form

$$\mathcal{S}(\omega) \propto \sum_{j=x,y} \Re \mathrm{Tr}\left\{ |j\rangle\langle g| [i(\omega - \omega_{\mathrm{L}}) - \mathcal{L}]^{-1} |g\rangle\langle j| \rho_{\mathrm{st}} \right\}. \tag{5.19}$$

In this work we numerically determine the spectrum for the parameter regimes of interest.

5.4 PARAMETER REGIME

In order to justify the experimental relevance of the cooling dynamics we discuss in the rest of this Chapter, we now relate the theoretical model to existing experimental realisations and identify the parameter regime which we will consider in our analysis.

Optical resonator. A structure like the one discussed here can be found for instance in a so-called phoxonic crystal (PxC), which co-localizes confined optical and mechanical resonator modes [165]. Photonic crystals are formed by a periodic modulation of the refractive index (in this case air holes in diamond), resulting in the formation of optical bands similar to electronic band structures in solids. A local defect like e. g. a variation of the hole diameters along the PxC structure perturbs the perfect periodicity and gives rise to an optical cavity mode. So far, fabrication imperfections limit experimental quality factors to 10^4 at visible wavelengths

suitable for the interaction with colour centers in diamond and up to 10^5 in the telecom band around 1550 nm [166, 187–189]. Nevertheless, simulations of one-dimensional photonic crystal cavities designed for visible light predict quality factors up to 10^7 and mode volumes around 1 cubic wavelength with cavity loss rate in the range $\kappa \sim 10\,MHz - 1\,GHz$ [165].

Mechanical resonator: In a PxC a periodic variation of the elastic modulus creates a mechanical band structure and a suitable variation of the regular pattern allows for a localized mode of the mechanical resonator. Recent experiments with structures at mechanical frequencies of 6 GHz with optical properties suitable for telecom wavelengths show mechanical quality factors of 10^3 [189]. Numerical modeling shows that modes with frequencies in the range $10 - 20\,GHz$ with quality factors reaching 10^7 can be achieved with an effective mass of $10^{-16}\,kg$ for structure dimensions matching visible wavelengths with the confined optical mode [165]. The parameters we choose are consistent with assuming mechanical frequencies of the order of $1 - 10\,GHz$ and a quality factor of the order of $10^6 - 10^7$, giving a damping rate γ of few kHz. The strain coupling constants are taken to be of the order of $1 - 10\,MHz$ [177, 190, 191]. The optomechanical coupling constant χ is taken to be of the order of few MHz [165].

NV center. Figure 5.1(b)-(c) reports the relevant level structure of the NV center in diamond. In absence of strain coupling, the $m_s = 0$ ground state $|^3A_{20}\rangle$ can be selectively coupled to the excited states $|E_{x,y}\rangle$, which have zero spin angular momentum. While the ground state is much less sensitive to lattice distortion, these excited states are highly susceptible to external perturbations [158, 191, 192]. Axial strain (parallel to the NV center axis, equivalent $\langle 111\rangle$ crystal direction) leads to an additional splitting between ground and excited states as well as between the $m_s = 0$ and $m_s = \pm 1$ levels in the ground state. Radial strain (perpendicular to NV axis) mixes the excited state levels E_x and E_y and leads to a splitting of the new states E_x^* and E_y^* ($m_s = +1^*$ and $m_s = -1^*$). The effect of strain coupling on the excited states is several orders of magnitude larger than on the ground state and hence dominates the strain-induced modification of the NV's optical properties. Therefore, we restrict our model to the interaction between the mechanical resonator mode and the transition coupling the ground state $|g\rangle \equiv |^3A_{20}\rangle$ to the excited states $|x\rangle \equiv |E_x\rangle$ and $|y\rangle \equiv |E_y\rangle$. For the excited states we take the radiative decay rate $\Gamma \sim 100\,MHz$ [193, 194]. The interaction between the NV transitions and the 71 meV lattice phonon modes [195] changes the energy of the $|x\rangle$ and $|y\rangle$ states and can thus give rise to a dephasing mechanism of the electronic coherence [160, 196]. In our model we neglect the mixing between the states and consider only pure dephasing with rates of the order of $\Gamma_\phi \sim 100\,MHz$, which can be achieved in bulk diamond at temperatures lower than $10\,K$ [184, 197]. We restrict the frequency of the mechanical resonator mode to $\nu = 2\pi \times 1\,GHz$ in order to avoid coupling to NV excited states other that E_x and E_y. As the optical cavity mode

should still be near resonant on the optical transition of the NV at 637 *nm* this doesn't correspond to a real structure design for the full threefold hybrid-system. However, we still model this artificial parameter set in order to obtain qualitative results on the nature of the interaction.

Cooling regime: The analysis of the cooling efficiency is performed by determining the cooling rate $\tilde{\Gamma}$ and the ideal asymptotic occupation number of the mechanical mode N_0 as a function of the tunable parameters, which we take here to be the frequency splitting of the electronic excited states and the laser frequency, corresponding to changing δ_L, Δ_c, and Δ. The analysis is performed by searching for the parameter regime where the asymptotic occupation number $N_0 < 1$ and the cooling rate $\tilde{\Gamma}$ is maximized, in order to realise regimes where the radiative cooling can overcome thermalization by the external reservoir. This constrains the range of parameters. A necessary condition for performing ground state cooling is the presence of a resonance whose linewidth L is smaller than the trap frequency [198], which poses an upper bound to L. Moreover, the cooling rate shall exceed the thermalization rate. Since the cooling rate is proportional to the effective linewidth of the cooling transition, this condition sets a lower bound to L. If one performs optomechanical cooling by driving the optical resonator, then $L = \kappa$. In absence of the resonator, the mechanical oscillator can be cooled by driving the NV center transitions with a laser and $L = \Gamma$. When the NV center transitions also couple with the optical cavity, then L is a linear interpolation of the cavity linewidth κ and of the NV transition linewidth Γ, and varies between Γ and κ [180, 181] (smaller linewidths could be achieved by coupling to other stable electronic transitions, which in our system are not considered [199, 200]).

In order to get a relatively small phonon occupation of the bath N_{th} we take a large mechanical frequency, $\nu \sim 2\pi \times 1\,GHz$, and thus for our parameter choice $\Gamma < \nu$. We then fix the cavity linewidth $\kappa \simeq \Gamma$.

5.5 EFFECTIVE DYNAMICS OF THE MECHANICAL RESONATOR

For the parameter regime we consider all characteristic frequencies characterizing the coupling of the mechanical resonator with NV center and optical cavity are much smaller than the mechanical resonator eigenfrequency $\Lambda_I, \Lambda_X, \Lambda_Z, \chi\bar{n}_c \ll \nu$ ($\bar{n}_c$ being the mean intracavity photon occupation number). This justifies a perturbative treatment, which allows us to eliminate the degrees of freedom of NV and optical cavity from the dynamics of the mechanical oscillator in second-order perturbation theory. By means of this procedure we derive an effective master equation for the mechanical resonator only, which allows us to determine the parameter regime where the vibrations are cooled, the corresponding cooling rate and the asymptotic vibrational state. The details of the derivation are reported in Appendix 5.A.

5.5.1 *Perturbative expansion*

We derive a closed master equation for the mechanical oscillator starting from Eq. (5.6) and assuming that the coupling frequencies, which scale the operator $a + a^\dagger$, are much smaller than ν. This can be summarized by the inequality $\alpha \ll \nu$, with $\alpha = \Lambda_I, \Lambda_X, \Lambda_Z, \chi\bar{n}_c$ and $\bar{n}_c$ the mean intracavity photon occupation number. We then perform perturbation theory in second order in the small parameter α/ν. We further assume that the incoherent dynamics of the oscillator due to the coupling with the environment is sufficiently slow that the occurrence of these processes during a scattering process can be discarded. This requires that $\gamma N_{\rm th} \ll \alpha$, which for the parameters considered in this work is valid also at room temperature, so that we treat it in first order.

According to these considerations we split the Liouville operator as

$$\mathcal{L} = \mathcal{L}_0 + \mathcal{V} + \mathcal{L}_\gamma\,,$$

with $\mathcal{L}_0 = \mathcal{L}_{\rm E} + \mathcal{L}_{\rm I}$, where $\mathcal{L}_{\rm E}$ and $\mathcal{L}_{\rm I}$ are the Liouville operators that generate the uncoupled mechanical oscillator and internal (NV center + optical cavity) dynamics, respectively, while $\mathcal{V}$ describes the coupling between mechanical and internal degrees of freedom. In detail,

$$\mathcal{L}_{\rm E}\rho = -{\rm i}[H_{\rm mec}, \rho], \tag{5.20a}$$
$$\mathcal{L}_{\rm I}\rho = -{\rm i}[H_{\rm I}, \rho] + \mathcal{L}_\Gamma\rho + \mathcal{L}_\kappa\rho, \tag{5.20b}$$
$$\mathcal{V}\rho = -{\rm i}[V(a + a^\dagger), \rho]\,. \tag{5.20c}$$

We formally eliminate the coupling between mechanical resonator and internal degrees of freedom as done for instance in Refs. [90, 180, 181, 201, 202]. We first introduce the superoperators $\mathcal{P}_k$ such that

$$\mathcal{P}_k\rho = \sigma_{\rm st}\sum_{n=0}^{\infty} |n\rangle\langle n+k|\langle n|\mu|n+k\rangle\,, \tag{5.21}$$

with $\mu = {\rm Tr}_{\rm I}\{\rho(t)\}$ the reduced density matrix, ${\rm Tr}_{\rm I}\{\cdot\}$ being the trace over the internal degrees of freedom, $|n\rangle$ the eigenstates of the mechanical oscillator, $k = 0, \pm1, \pm2, \ldots$ ($k \geq -n$) and $\sigma_{\rm st}$ the steady state for the internal degrees of freedom: $\mathcal{L}_{\rm I}\sigma_{\rm st} = 0$. Applying $\mathcal{P}_k$ to the master equation (5.6), with the definitions of the superoperators (5.20), in a second-order perturbative expansion in parameter α/ν and first order in $\gamma(N_{\rm th}+1)$, leads to the equation

$$\frac{\partial}{\partial t}\mathcal{P}_k\rho = \left\{ik\nu + \mathcal{P}_k\mathcal{V}\big(ik\nu - \mathcal{L}_0\big)^{-1}\mathcal{Q}_k\mathcal{V}\mathcal{P}_k\right\}\mathcal{P}_k\rho + \mathcal{L}_\gamma\mathcal{P}_k\rho, \tag{5.22}$$

with $\mathcal{Q}_k = \mathbb{1} - \mathcal{P}_k$ and $\mathbb{1}$ is here the superoperator whose action is the identity on both sides of the density matrix. The master equation for the reduced density matrix μ is obtained after tracing out the internal degrees of freedom in Eq. (5.22) and reads

$$\dot{\mu} = -{\rm i}\bar{\nu}\big[a^\dagger a, \mu\big] + \frac{A_-}{2}\mathcal{D}[a]\mu + \frac{A_+}{2}\mathcal{D}[a^\dagger]\mu + \mathcal{L}_\gamma\mu\,. \tag{5.23}$$

The rates $A_\pm$ are defined as

$$A_\pm = 2\,\Re s(\mp\nu), \tag{5.24}$$

$$\bar{\nu} = \nu + \Im s(\nu) + \Im s(-\nu)\,, \tag{5.25}$$

with

$$s(\upsilon) = \int_0^\infty dt\, \mathrm{e}^{\mathrm{i}\upsilon t}\langle V \exp\left(\mathcal{L}_I t\right) V\rangle_{\mathrm{st}}\,, \tag{5.26}$$

which is the Fourier component at frequency ν of the autocorrelation function of operator V, where the average $\langle\cdot\rangle_{\mathrm{st}}$ is taken in the steady state σ_{st}.

The diagonal elements of Eq. (5.23) give a set of rate equations for the occupation $p_n = \langle n|\mu|n\rangle$ of the phonon state $|n\rangle$, which are reported in Eq. (5.1).

5.6 RESULTS

In this section we characterize the parameter regimes in which the mechanical resonator is cooled by photon scattering process in the setup of Fig. 5.1(a). We focus on the range of parameters discussed in Sec. 5.4. We consider laser cooling of the mechanical resonator by strain coupling with the NV center and analyse how the cooling dynamics is affected by the presence of the optical resonator and of dephasing. The results we report are compared to the predictions in absence of the optical resonator and for vanishing dephasing. This latter case has been extensively discussed in Ref. [177] and we refer the interested reader to it for a detailed discussion of the predicted dynamics in that specific limit.

5.6.1 *Cavity-assisted cooling*

We now analyse how laser cooling dynamics of the mechanical resonator by strain coupling with the NV center is affected by the presence of the optical resonator. In order to better understand the role of the resonator, we first discard thermal effects and dephasing (setting $\gamma = \Gamma_\phi = 0$).

Figure 5.2 displays the cooling rate $\tilde{\Gamma}$ and the mean vibrational number at the asymptotics N_0 as a function of δ_{L} and Δ in absence (left panels) and in presence of the optical cavity (right panel). Both plots show that the cooling rate is maximum, and the final occupation minimum, along the lines $\delta_{\mathrm{L}} = -\nu$ and $\delta_{\mathrm{L}} = \Delta - \nu$. In the first case cooling is achieved by setting the laser frequency to the value $\omega_{\mathrm{L}} = \omega_y - \nu$, hence resonantly driving the transition $|g, n\rangle \to |y, n-1\rangle$ (red sideband). In the second case the laser frequency is $\omega_{\mathrm{L}} = \omega_x - \nu$, so that the transition $|g, n\rangle \to |x, n-1\rangle$ is resonantly driven by an effective process, which combines the laser and the strain coupling. For most values of the detuning Δ the excitation of the intermediate state $|y\rangle$ is virtual, except for $\Delta = \omega_x - \omega_y = \nu$. This

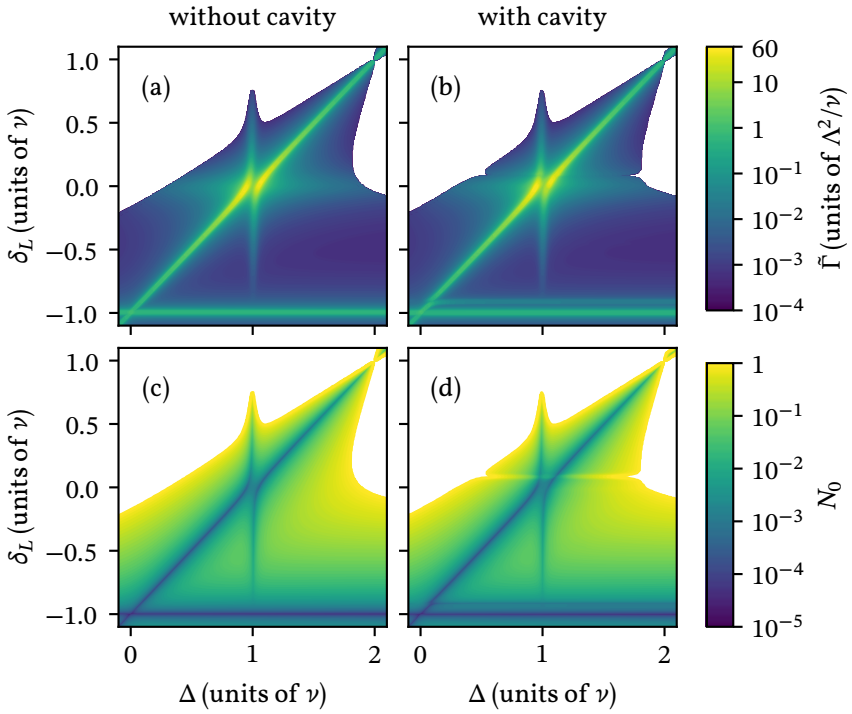

Figure 5.2: Predictions on the cooling efficiency extracted from the rate equation, Eq. (5.1), for laser cooling of the mechanical resonator by driving the NV center with a laser (left panel) and by additionally coupling the dipole transitions to an optical cavity (right panel). (a) and (b) show the cooling rate $\tilde{\Gamma}$, Eq. (5.3) in units of Λ^2/ν, (c) and (d) the asymptotic occupation N_0 of the vibrational mode, according to Eq. (5.4), as a function of the excited level splitting Δ and the laser detuning δ_L (in units of ν). The white region are heating regions ($\tilde{\Gamma} < 0$) or where $N_0 > 1$. The parameters for the left panel are $\Omega = 0.1\nu$, $\Gamma = 1.6 \times 10^{-2}\nu$, $\Gamma_\phi = 0$, $\Lambda_I = 0$, $\Lambda_X = \Lambda_Z = \chi = \Lambda = 0.1\Gamma$ and $g_x = g_y = 0$. In the right panel we take the same parameters except for $g_x = g_y = \kappa = \Gamma$. The cavity frequency is fixed to the value $\Delta_c = 8.5 \times 10^{-2}\nu$ (see text).

latter case corresponds to the vertical line visible in both figures, where cooling results to be efficient. These properties have been identified and discussed in Ref. [177] and do not depend on the coupling with the resonator. The curves in Fig. 5.3 show the cooling rate and the minimum phonon occupation as a function of δ_L after fixing the detuning $\Delta = \nu$. Some (relatively small) differences are visible close to the values $\delta_L = 0$ and $\delta_L = -\nu$, which are due to the level splitting induced by the strong coupling with the resonator: for this choice of Δ_c, in fact, the cavity drives almost resonantly the transition $|g\rangle \to |y\rangle$.

We have tested that the value of the detuning Δ_c, and thus of the cavity frequency, in Figs. 5.2 and 5.3, leads to the best results by comparing cooling rate and final temperature for different values of Δ_c. The results

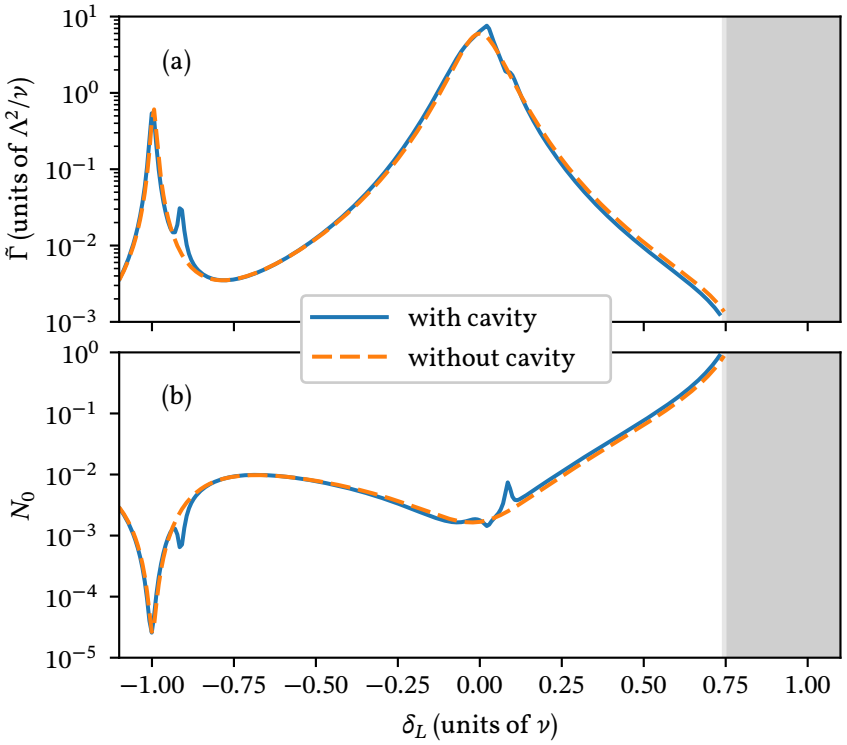

Figure 5.3: (a) Cooling rate $\tilde{\Gamma}$ and (b) asymptotic occupation N_0 of the vibrational mode as a function of δ_L for the same parameters as in Fig. 5.2 and $\Delta = \nu$. The dashed (solid) line corresponds to the predictions in absence (presence) of the coupling to the cavity. The shaded region indicates the regime where the resonator is heated by the radiative processes ($\tilde{\Gamma} < 0$) or where $N_0 > 1$.

of this analysis are summarized in Fig. 5.4, which displays (a) the maximum cooling rate (maximized by varying Δ and δ_L by keeping Δ_c fixed). The mean phonon occupation in (b) and the mean intracavity photon number in (c) are reported for the corresponding values of Δ and δ_L, at which $\tilde{\Gamma}$ is maximum. These plots show that maximal cooling rates are found for $\Delta_c \simeq 0$. We verified that the curves do not differ substantially if instead we search for Δ_c by minimizing the mean phonon number. Therefore, the contour plots in Fig. 5.2(b) and (d) show the optimal cooling rate and temperature in presence of the resonator. On the basis of the comparison with the plots on the left panels, we can thus conclude that the coupling with the cavity does not substantially improve the cooling efficiency for the chosen parameter regime.

We now analyse how the spectrum of resonance fluorescence is modified by the coupling with the resonator. We focus on the light emitted once the system has reached the stationary state. Figure 5.5 displays the resonance fluorescence spectrum in absence and in presence of the optical cavity for the parameters of Fig. 5.3 with $\delta_L = 0$. To better understand how the cavity modifies the dynamics, we first discuss the spectrum in

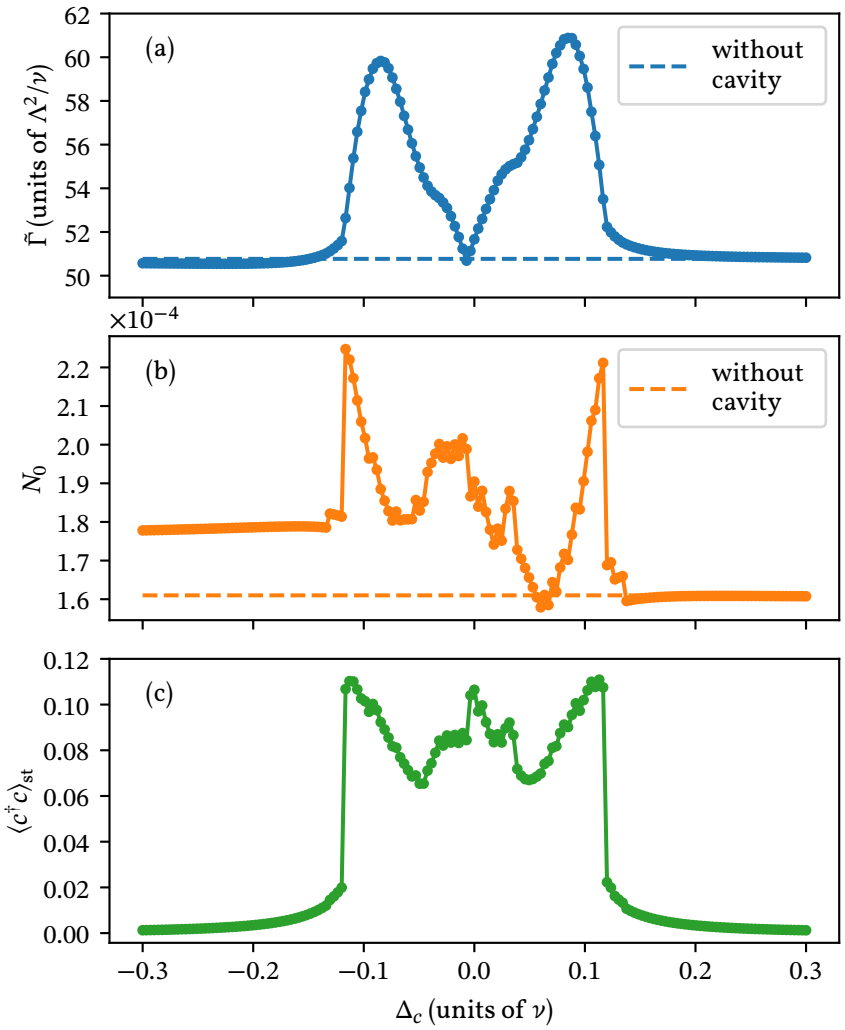

Figure 5.4: (a) Maximum cooling rate $\tilde{\Gamma}_{\max}$ in presence of the resonator as a function of Δ_c. The value $\tilde{\Gamma}_{\max}$ has been calculated by varying δ_L and Δ and keeping Δ_c fixed. Subplot (b) displays the corresponding value of N_0 and (c) the mean intracavity photon number. The parameters are: $\Omega = 0.1\nu$, $\Gamma_\phi = 0$, $\Gamma = \kappa = g_x = g_y = 1.6 \times 10^{-2}\nu$, $\Lambda_I = 0$, $\Lambda_X = \Lambda_Z = \chi = \Lambda = 0.1\Gamma$. The dashed lines in (a) and (b) indicate the maximum cooling rate and corresponding value of N_0 in absence of the optical resonator. In the latter case $\tilde{\Gamma}_{\max}$ is maximum for $\Delta \approx 0.93\nu$ and $\delta_L \approx -3.5 \times 10^{-2}\nu$.

absence of the cavity. In this case we observe the three broad resonances around $\omega = \omega_L$. These are due to inelastic processes in which the motion is not involved and can be interpreted as a Mollow-type triplet [203]. We further observe the narrow resonances at $\omega = \omega_L \mp \nu$, which are the red and the blue motional sidebands of the elastic peak. Subplots 5.5(b) and 5.5(c) report the details of the sidebands of the elastic peak. These spectral components correspond to the photons emitted in the processes where a phonon is created $(\omega_L - \nu)$ or destroyed $(\omega_L + \nu)$ in the mechani-

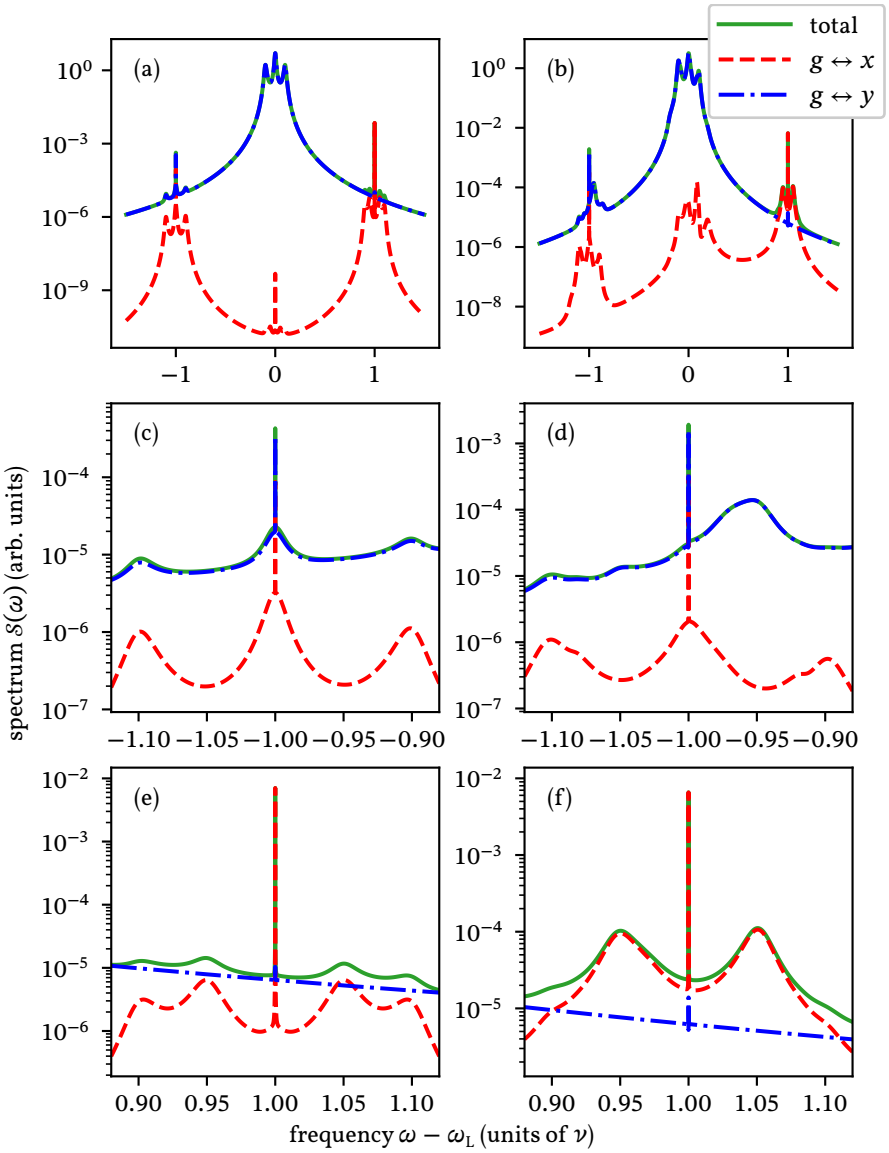

Figure 5.5: Spectrum of light emitted by the NV center at the asymptotics of the laser cooling dynamics. The left panels correspond to the parameter regime of Fig. 5.2(a)(c) (no cavity), the right panels to the parameter regime of Fig. 5.2(b)(d) (cavity assisted cooling). The dashed (dashed-dotted) line correspond to the emission from the transition $g \leftrightarrow x$ ($g \leftrightarrow y$), the solid line correspond to the sum of these two contributions. Here, we took $\Delta = \nu$ and $\delta_L = 0$. Panels (c), (d), (e) and (f) show the details of the sidebands.

cal resonator. The motional sideband has a width of the order of $\propto \Lambda_X^2$, and appears on a broader background with linewidth $\approx \Gamma$. Our analysis shows that this structure is due to the fact that mechanical effects are dominated by the strain coupling A_X, which mixes the two excited states. For our parameter choice, where $\Delta = \nu$, this coupling is weak but resonant so that the effect of the strain coupling is particularly enhanced. Figure 5.5(d)-(f) displays corresponding spectra of resonance

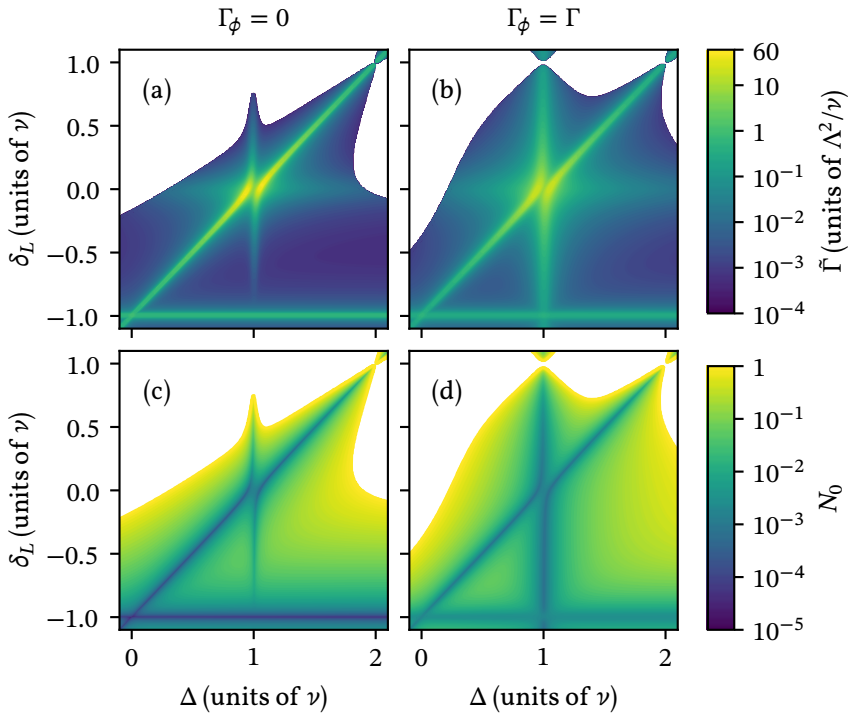

Figure 5.6: Predictions on the cooling efficiency extracted from the rate equation, Eq. (5.1), for laser cooling of the mechanical resonator by driving the NV center with a laser in absence (left panel) and in presence of pure dephasing (right panel). (a) and (b) show the cooling rate $\tilde{\Gamma}$, Eq. (5.3) in units of Λ^2/ν, (c) and (d) the asymptotic occupation N_0 of the vibrational mode, according to Eq. (5.4), as a function of the excited level splitting Δ and the laser detuning δ_L (in units of ν). The white area are heating regions ($\tilde{\Gamma} < 0$) or where $N_0 > 1$. The parameters are $\Omega = 0.1\nu$, $\Gamma = 1.6\times10^{-2}\nu$, $\Lambda_I = 0$, $\Lambda_X = \Lambda_Z = \chi = \Lambda = 0.1\Gamma$, and (left panel) $\Gamma_\phi = 0$, (right panel) $\Gamma_\phi = \Gamma$.

fluorescence in presence of the cavity. The significantly different features are due to the modified dressed state structure because of the strong coupling between cavity and NV center, while for both cases the cooling (heating) processes are dominated by emission along the transition $|x\rangle \to |g\rangle$ ($|y\rangle \to |g\rangle$).

The summary of this analysis is that the effect of the optical resonator on the cooling dynamics can consist in a very small improvement of the cooling efficiency. This result, which seems to contrast with previous investigations where the effect of the cavity on the cooling efficiency was relevant [180, 181, 200], can be understood when considering that (i) the loss rate of the resonator and the radiative decay rate of the electronic excitations have been chosen to be of the same order of magnitude, and (ii) the cooperativity $C = g^2/\kappa\Gamma \sim 1$, so that the level splitting induced by the coupling with the resonator is of the order of the loss rate κ. Because of (i) the coupling with the resonator gives rise to an effective level

structure where the linewidths of all excited levels is of the same order of magnitude. Since for sideband cooling the linewidth determines both the cooling rate as well as the final temperature, the improvement of the cooling efficiency by coupling this level structure to a resonator is incremental. Because of (ii), the level splitting induced by the coupling with the cavity does not exceed the linewidth of the resonances, so that the regime of optimal detunings is essentially the same as without the cavity.

5.6.2 *Dephasing-assisted cooling*

We now analyse the effect of other noise sources on the cooling efficiency, and consider in particular dephasing, which is an important source of loss of coherence in solid-state systems. We here discard the coupling with the optical resonator and calculate the cooling efficiency when $\Gamma_\phi \neq 0$.

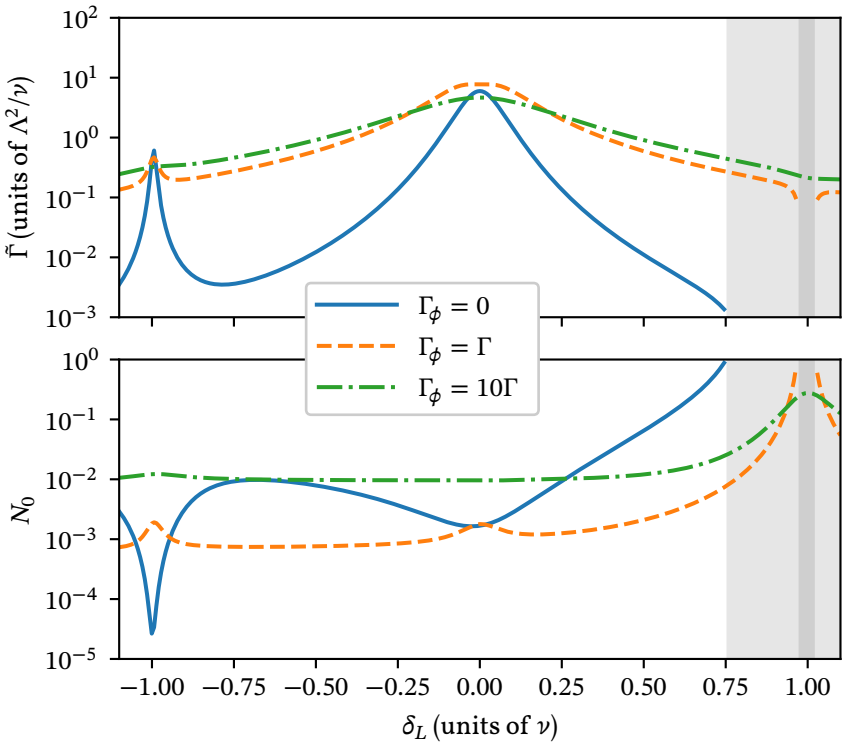

Figure 5.7: (a) Cooling rate $\tilde{\Gamma}$ and (b) asymptotic occupation N_0 of the vibrational mode as a function of δ_L for the same parameters as in Fig. 5.6 and $\Delta = \nu$. The solid line corresponds to the predictions in absence of dephasing. The dashed (dashed-dotted) line corresponds to the predictions when the dephasing rate is $\Gamma_\phi = \Gamma$ ($\Gamma_\phi = 10\Gamma$). The shaded region indicates the regime where the resonator is heated by the radiative processes ($\tilde{\Gamma} < 0$) or where $N_0 > 1$.

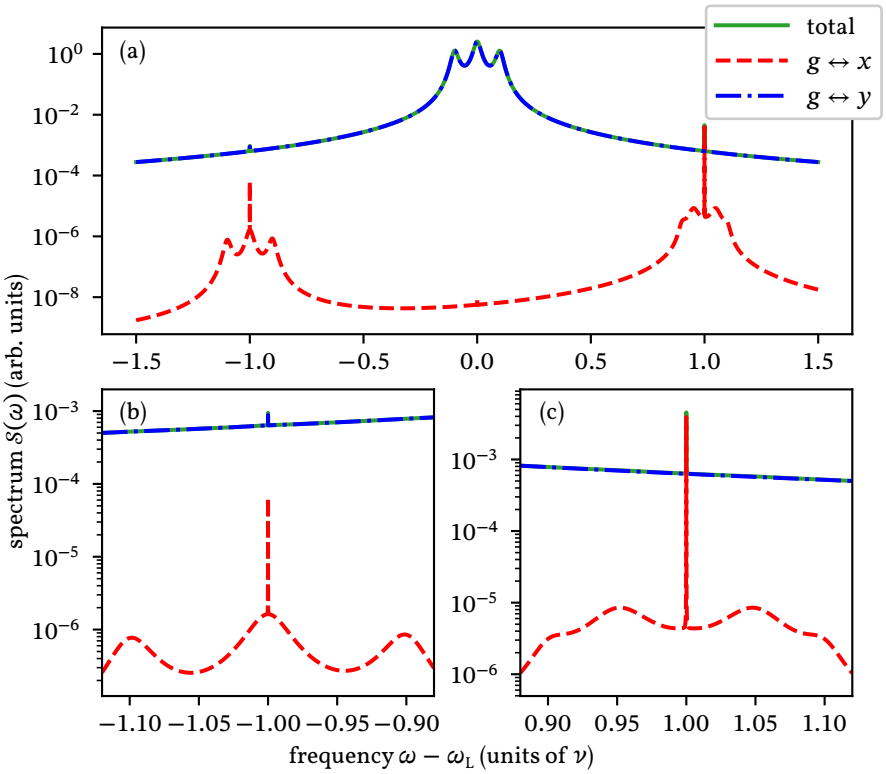

Figure 5.8: Spectrum of light emitted by the NV center at the asymptotics of the laser cooling dynamics. The parameters are the same as in Fig. 5.6(b)(d) (dephasing assisted cooling with $\Gamma_\phi = \Gamma$). The dashed (dashed-dotted) line correspond to the emission from the transition $g \leftrightarrow x$ ($g \leftrightarrow y$), the solid line correspond to the sum of these two contributions. Here, we took $\Delta = \nu$ and $\delta_L = 0$. Panels (b) and (c) show the details of the sidebands.

Figure 5.6 compares the cooling rate and final occupation for $\Gamma_\phi = 0$ (left panel) and $\Gamma_\phi = \Gamma$ (right panel). We observe that pure dephasing decreases the cooling efficiency when cooling is achieved by tuning the laser to the red sideband of the dressed states. Nevertheless, the cooling region is larger and the dependence on the exact values of the experimental parameters is less pronounced. Moreover, the cooling performance is enhanced in most parts of parameter landscape. Figures 5.7(a) and (b) compare the cuts along the line $\Delta = \nu$: one clearly sees that the case of $\Gamma_\phi = \Gamma$ outperforms the case when $\Gamma_\phi = 0$. This occurs over almost the full range of δ_L in terms of both cooling rate and minimal phonon number. We have checked that the value $\Gamma_\phi = \Gamma$ is close to the optimal dephasing rate. We also found the range of values in which the dephasing has a beneficial effect on the cooling spans till several Γ (see dotted line, which shows the predictions for $\Gamma_\phi = 10\Gamma$).

The effect of dephasing is also visible in the spectrum of resonance fluorescence. We observe in Fig. 5.8 for $\delta_L = 0$ a broadening of the background at the motional sidebands, which now scale with $\approx \Gamma + \Gamma_\phi$.

This linewidth is indeed the cooling rate, which results to be enhanced by the presence of pure dephasing.

We understand this behaviour since pure dephasing increases the width of the excited states $|x\rangle$ and $|y\rangle$ without increasing their decay rate. Thus it increases the excitation probability. Since this cooling scheme is optimal when population is transferred to the excited state, then pure dephasing leads to larger transition rates, and thus larger cooling rate. This reasoning works within a certain parameter interval: dephasing rates exceeding the Rabi frequency, in fact, tend to suppress population transfer and thus are detrimental.

The beneficial role of pure dephasing on the cooling efficiency can be best illustrated by analysing the final mean occupation for different temperatures of the bath. Figure 5.9 illustrates how dephasing can improve the cooling efficiency over a large parameter regime, flattening out the minimum of n_f (Eq. (5.5)) as a function of the frequency of the driving laser.

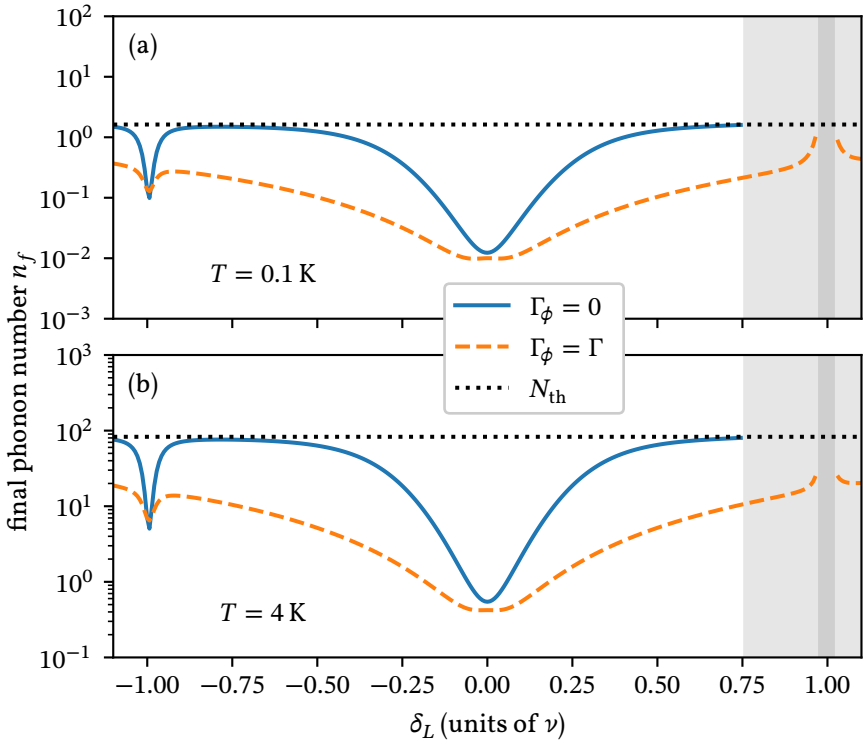

Figure 5.9: Final phonon number of the mechanical resonator with $\nu = 2\pi \times 1\,GHz$ and a quality factor $Q = \nu/\gamma = 10^7$, Eq. (5.5), for (a) $T = 0.1\,K$ ($N_{\text{th}} \approx 1.6$) and (b) $T = 4\,K$ ($N_{\text{th}} \approx 83$), for the same parameter regime of Fig. 5.7(b). The solid (dashed) line corresponds to the predictions in absence (presence) of pure dephasing. The black dotted lines correspond to $n_f = N_{\text{th}}$. The shaded region indicates the regime where the resonator is heated by the radiative processes.

5.7 CONCLUSIONS

We have analysed the cooling efficiency of a mechanical resonator which is laser cooled by the strain coupling with a NV center. The cooling dynamics is essentially due to the strain coupling with the NV center and the parameter regime is such that the resolved-sideband cooling can be performed by driving the NV center electronic resonances. In this regime we have analysed the effect of the coupling to an optical resonator, and found that it does only incrementally improve the cooling efficiency. We have further shown that pure dephasing can make the cooling dynamics more robust against parameter fluctuations, without affecting the overall efficiency, as long as the dephasing rate does not exceed the driving strength of the laser.

In our analysis the optomechanical coupling was a small effect. It can be increased in configurations where the cavity is driven: in this case the optomechanical coupling would cool the resonator according to the dynamics explored in Refs. [204, 205]. Another possibility is to drive both optical cavity and NV center for large cooperativity: In this situation phonon excitation or absorption can be realised by means of two excitation paths, that can interfere. This interference depends on the relative phase between the lasers and could be a control parameter for realising multi-wave mixing.

A further interesting possibility is the analysis of entanglement and coherent quantum information transfer between the different components of this hybrid quantum system.

This setup could also be investigated to develop a quantum memory: by using the system analyzed here, a photonic excitation traveling in space or in an optical fiber can be transferred and stored into the nuclear spin of the nitrogen atom [206] intrinsic to the NV-center or into the nuclear spin of an adjacent carbon atom [207].

Recently a similar setup has been analyzed experimentally in Ref. [208] in which the authors manipulate the NV-center electronic states by driving the mechanical resonator.

APPENDICES

5.A ELIMINATION OF THE INTERNAL DEGREES OF FREEDOM

In this section we report the details of the calculation covered in Sec. 5.5.

5.A.1 *Perturbation theory*

We consider the parameter regime

$$\gamma N_{\rm th} \ll \alpha \ll \nu, \tag{5.27}$$

with $\alpha = \Lambda_I, \Lambda_X, \Lambda_Z, \chi\bar{n}_c$ ($\bar{n}_c$ being the mean cavity photon occupation number) and perform perturbation theory in second order in the small parameter α/ν.

We solve the right and left eigenvalues equations for the Liouvillian operator Eq. (5.6)

$$\mathcal{L}\hat{\rho}_\lambda = \lambda\hat{\rho}_\lambda \tag{5.28a}$$

$$\check{\rho}_\lambda^\dagger\mathcal{L} = \lambda\check{\rho}_\lambda^\dagger \tag{5.28b}$$

perturbatively with the expansion

$$\begin{aligned}\mathcal{L} &= \mathcal{L}^{(0)} + \mathcal{L}^{(1)} + \mathcal{L}^{(2)} + \dots\\ \lambda &= \lambda^{(0)} + \lambda^{(1)} + \lambda^{(2)} + \dots\\ \hat{\rho}_\lambda &= \hat{\rho}_\lambda^{(0)} + \hat{\rho}_\lambda^{(1)} + \hat{\rho}_\lambda^{(2)} + \dots\\ \check{\rho}_\lambda &= \check{\rho}_\lambda^{(0)} + \check{\rho}_\lambda^{(1)} + \check{\rho}_\lambda^{(2)} + \dots .\end{aligned} \tag{5.29}$$

Sobstituting Eqs. (5.29) in Eqs. (5.28) we obtain the following equations for the order α

$$\sum_{\beta=0}^{\alpha}\mathcal{L}^{(\beta)}\hat{\rho}_\lambda^{(\alpha-\beta)} = \sum_{\beta=0}^{\alpha}\lambda^{(\beta)}\hat{\rho}_\lambda^{(\alpha-\beta)} \tag{5.30a}$$

$$\sum_{\beta=0}^{\alpha}\left(\check{\rho}_\lambda^{(\beta)}\right)^\dagger\mathcal{L}^{(\alpha-\beta)} = \sum_{\beta=0}^{\alpha}\lambda^{(\alpha-\beta)}\left(\check{\rho}_\lambda^{(\beta)}\right)^\dagger. \tag{5.30b}$$

In the spirit of Eq. (5.27) and Eqs. (5.29) and (5.30) we decompose the master equation as

$$\mathcal{L}\rho = \mathcal{L}^{(0)}\rho + \mathcal{L}^{(1)}\rho \tag{5.31}$$

where (see Eq. (5.20) of the main text)

$$\mathcal{L}^{(0)} = \mathcal{L}_E + \mathcal{L}_I, \tag{5.32a}$$

$$\mathcal{L}_E\rho = -i[H_{mec}, \rho], \tag{5.32b}$$

$$\mathcal{L}_I\rho = -i[H_I, \rho] + \mathcal{L}_\Gamma\rho + \mathcal{L}_\kappa\rho, \tag{5.32c}$$

$$\mathcal{L}^{(1)}\rho = \mathcal{V}\rho = -i[V(a + a^\dagger), \rho] = -i[Vx, \rho], \tag{5.32d}$$

$$\mathcal{L}^{(i)} = 0 \quad \forall i > 1, \tag{5.32e}$$

here we have defined for simplicity $x = a + a^\dagger$. The superoperator $\mathcal{L}_E$ describes the dynamics of the external degrees of freedom, i. e., the mechanical oscillator. The superoperator $\mathcal{L}_I$ describes the dynamics of the internal degrees of freedom, i. e., the NV-center, the optical cavity and their coupling. The superoperator $\mathcal{V}$ describes the coupling between the internal and external degrees of freedom.

5.A.1.1 *Zeroth order*

At zeroth order Eqs. (5.30) (with $\alpha = 0$) become

$$\mathcal{L}^{(0)}\hat{\rho}_\lambda^{(0)} = \lambda^{(0)}\hat{\rho}_\lambda^{(0)} \tag{5.33a}$$

$$(\check{\rho}_\lambda^{(0)})^\dagger\mathcal{L}^{(0)} = \lambda^{(0)}(\check{\rho}_\lambda^{(0)})^\dagger. \tag{5.33b}$$

According to Eq. (5.32) the internal and external degree of freedom are decoupled in zeroth order and the eigenvalue $\lambda^{(0)}$ will then be the sum $\lambda^{(0)} = \lambda_I + \lambda_E$ of the eigenvalues of $\mathcal{L}_\mathrm{I}$ and $\mathcal{L}_\mathrm{E}$, respectively. Correspondingly, the zeroth order eigenelements are product states of internal eigenelements $\hat{\rho}^{\lambda_I}, \check{\rho}^{\lambda_I}$ and external eigenelements $\hat{\mu}^{\lambda_I}, \check{\mu}^{\lambda_I}$ fulfilling the equations

$$\mathcal{L}_\mathrm{I}\hat{\rho}^{\lambda_I} = \lambda_I\hat{\rho}^{\lambda_I}, \quad \left(\check{\rho}^{\lambda_I}\right)^\dagger\mathcal{L}_\mathrm{I} = \lambda_I\left(\check{\rho}^{\lambda_I}\right)^\dagger \tag{5.34a}$$

$$\mathcal{L}_\mathrm{E}\hat{\mu}^{\lambda_E} = \lambda_E\hat{\mu}^{\lambda_E}, \quad \left(\check{\mu}^{\lambda_E}\right)^\dagger\mathcal{L}_\mathrm{E} = \lambda_E\left(\check{\mu}^{\lambda_E}\right)^\dagger. \tag{5.34b}$$

The right and the left eigenelements of the external degree of freedom can be written in the form [91–93, 209]

$$\begin{aligned}\hat{\mu}^k(n) &= \left|n + \frac{|k|-k}{2}\right\rangle\!\!\left\langle n + \frac{|k|+k}{2}\right| \\ \left(\check{\mu}^k(n)\right)^\dagger &= \left|n + \frac{|k|+k}{2}\right\rangle\!\!\left\langle n + \frac{|k|-k}{2}\right|\end{aligned} \tag{5.35}$$

with external eigenvalue $\lambda_E = \mathrm{i}k\nu$ and $k = 0, \pm1, \pm2, \ldots$. It is important to notice that each external eigenelement is infinite degenerate and the elements are spanned by the quantum number $n = 0, 1, 2, \ldots$. Nevertheless the external eigenelements are orthogonal and complete [91–93, 209]. Due to this degeneracy the eigenelements of $\mathcal{L}^{(0)}$ are not uniquely determined. In fact, they can be written as

$$\hat{\rho}^{(0)}_\lambda = \hat{\rho}^{\lambda_I}\hat{\mu}^{\lambda_E} \tag{5.36a}$$

$$\check{\rho}^{(0)}_\lambda = \check{\rho}^{\lambda_I}\check{\mu}^{\lambda_E} \tag{5.36b}$$

with

$$\hat{\mu}^{\lambda_E} = \sum_{n=0}^{\infty} c_n\hat{\mu}^k(n) \quad \text{and} \quad \check{\mu}^{\lambda_E} = \sum_{n=0}^{\infty} d_n\check{\mu}^k(n), \tag{5.37}$$

and any superposition with coefficients c_n and d_n of the external eigenelements can be used to satisfy Eq. (5.33). The only restriction on the coefficients c_n and d_n comes by the orthogonality condition

$$\mathrm{Tr}\left(\hat{\rho}^{(0)}_\lambda(\check{\rho}^{(0)}_{\lambda'})^\dagger\right) = \delta_{\lambda,\lambda'} \tag{5.38}$$

and the completeness relation

$$\sum_{\lambda_0}\hat{\rho}^{(0)}_\lambda \otimes \check{\rho}^{(0)}_\lambda = \mathbb{1} \tag{5.39}$$

which requires $\sum_n c_n d_n^* = 1$.

We now introduce the zeroth order projectors

$$\mathcal{P}^\lambda_0 = \hat{\rho}^{(0)}_\lambda \otimes \check{\rho}^{(0)}_\lambda = \mathcal{P}_I^{\lambda_I}\mathcal{P}_E^{\lambda_E} \tag{5.40}$$

which can be decomposed in the internal and external part due to the uncoupled dinamics. The internal projectors are

$$\mathcal{P}_I^{\lambda_I} = \hat{\rho}^{\lambda_I} \otimes \check{\rho}^{\lambda_I}. \tag{5.41}$$

The external projector must take account for the degeneracy of external eigenelements, thus the projector which project onto the subspace relative to the eigenvalue λ_E is

$$\mathcal{P}_k = \mathcal{P}_E^{\lambda_E} = \sum_{n=0}^{\infty} \hat{\mu}^{\lambda_E}(n) \otimes \check{\mu}^{\lambda_E}(n), \quad \lambda_E = \mathrm{i}k\nu. \tag{5.42}$$

It can be shown that the completeness relation

$$\sum_{\lambda_E} \mathcal{P}_E^{\lambda_E} = \mathbb{1}_E \tag{5.43}$$

holds. We further assume that the completeness relation for the internal projectors $\sum_{\lambda_I} \mathcal{P}_I^{\lambda_I} = \mathbb{1}_I$ holds, such that the zeroth orders projectors fulfill

$$\sum_{\lambda_0} \mathcal{P}_0^{\lambda} = \mathbb{1}, \tag{5.44}$$

that is, they are complete in the composite system of internal and external degrees of freedom.

5.A.1.2 *First order*

the general procedure is: (i) use eqs. (5.30) to derive equations for order α. (ii) project the equation for the right eigenvectors with $\mathcal{P}_0^{\lambda}$ on the left to obtain the eigenvalue correction of order α. (iii) project the equation for the right eigenvectors with $\mathcal{Q}_0^{\lambda}$ on the left to obtain the right eigenvectors correction of order α. (iv) project the equation obtained from (i) for the left eigenvectors with $\mathcal{Q}_0^{\lambda}$ on the right to obtain the left eigenvector correction of order α. (v) the corrections of order α calculated here will be used in the calculation for the order $\alpha + 1$ following the same steps.

Equations (5.30) for $\alpha = 1$ lead to

$$\mathcal{L}^{(0)}\hat{\rho}_\lambda^{(1)} + \mathcal{L}^{(1)}\hat{\rho}_\lambda^{(0)} = \lambda^{(0)}\hat{\rho}_\lambda^{(1)} + \lambda^{(1)}\hat{\rho}_\lambda^{(0)} \tag{5.45a}$$

$$(\check{\rho}_\lambda^{(1)})^\dagger\mathcal{L}^{(0)} + (\check{\rho}_\lambda^{(0)})^\dagger\mathcal{L}^{(1)} = \lambda^{(0)}(\check{\rho}_\lambda^{(1)})^\dagger + \lambda^{(1)}(\check{\rho}_\lambda^{(0)})^\dagger. \tag{5.45b}$$

Let's consider the projector $\mathcal{P}_0^{\lambda}$ introduced in Eq. (5.40) and the orthogonal projector $\mathcal{Q}_0^{\lambda} = 1 - \mathcal{P}_0^{\lambda}$. Since the subspaces on which they project are orthogonal we have

$$\mathcal{P}_0^{\lambda}\mathcal{Q}_0^{\lambda} = \mathcal{Q}_0^{\lambda}\mathcal{P}_0^{\lambda} = 0 \tag{5.46}$$

and since $\left\{\hat{\rho}_\lambda^{(0)}, \check{\rho}_\lambda^{(0)}\right\}$ are eigenstates of $\mathcal{L}^{(0)}$

$$\left[\mathcal{P}_0^{\lambda}, \mathcal{L}^{(0)}\right] = \left[\mathcal{Q}_0^{\lambda}, \mathcal{L}^{(0)}\right] = 0 \tag{5.47}$$

and consequently

$$\mathcal{P}_0^{\lambda}\mathcal{L}^{(0)}\mathcal{Q}_0^{\lambda} = \mathcal{Q}_0^{\lambda}\mathcal{L}^{(0)}\mathcal{P}_0^{\lambda} = 0. \tag{5.48}$$

Notice also that $\mathcal{L}^{(0)}\mathcal{P}_0^{\lambda} = \mathcal{P}_0^{\lambda}\mathcal{L}^{(0)} = \lambda^{(0)}\mathcal{P}_0^{\lambda}$. Now we project Eq. (5.45a) with $\mathcal{P}_0^{\lambda}$ and $\mathcal{Q}_0^{\lambda}$. Using the properties just given we have

$$\mathcal{P}_0^{\lambda}\mathcal{L}^{(1)}\hat{\rho}_\lambda^{(0)} = \lambda^{(1)}\mathcal{P}_0^{\lambda}\hat{\rho}_\lambda^{(0)} \tag{5.49a}$$

$$\mathcal{L}^{(0)}\mathcal{Q}_0^{\lambda}\hat{\rho}_\lambda^{(1)} + \mathcal{Q}_0^{\lambda}\mathcal{L}^{(1)}\hat{\rho}_\lambda^{(0)} = \lambda^{(0)}\mathcal{Q}_0^{\lambda}\hat{\rho}_\lambda^{(1)}. \tag{5.49b}$$

From Eq. (5.49a) we obtain

$$\hat{\rho}_\lambda^{(0)} \otimes \check{\rho}_\lambda^{(0)} \mathcal{L}^{(1)} \hat{\rho}_\lambda^{(0)} = \lambda^{(1)} \hat{\rho}_\lambda^{(0)} \otimes \check{\rho}_\lambda^{(0)} \hat{\rho}_\lambda^{(0)}$$
$$\Longrightarrow$$
$$\hat{\rho}_\lambda^{(0)} \operatorname{Tr}\left\{(\check{\rho}_\lambda^{(0)})^\dagger \mathcal{L}^{(1)} \hat{\rho}_\lambda^{(0)}\right\} = \lambda^{(1)} \hat{\rho}_\lambda^{(0)} \cancelto{1}{\operatorname{Tr}\left\{(\check{\rho}_\lambda^{(0)})^\dagger \hat{\rho}_\lambda^{(0)}\right\}}$$

and we obtain for the first order correction to the eigenvalue $\lambda^{(0)}$

$$\lambda^{(1)} = -\mathrm{i} \operatorname{Tr}\left\{(\check{\rho}_\lambda^{(0)})^\dagger \left[V x, \hat{\rho}_\lambda^{(0)}\right]\right\}. \tag{5.50}$$

Eq. (5.50) is identically zero in fact

$$\begin{aligned}
\lambda^{(1)} &= -\mathrm{i} \operatorname{Tr}\left\{(\check{\rho}_\lambda^{(0)})^\dagger \left[V x, \hat{\rho}_\lambda^{(0)}\right]\right\} = \\
&= -\mathrm{i} \operatorname{Tr}\left\{(\check{\rho}_\lambda^{(0)})^\dagger V \left[x, \hat{\rho}_\lambda^{(0)}\right]\right\} - \mathrm{i} \operatorname{Tr}\left\{(\check{\rho}_\lambda^{(0)})^\dagger \left[V, \hat{\rho}_\lambda^{(0)}\right] x\right\} = \\
&= -\mathrm{i} \operatorname{Tr}\left\{(\check{\rho}^{\lambda_I})^\dagger (\check{\mu}^{\lambda_E})^\dagger V \left[x, \hat{\rho}^{\lambda_I} \hat{\mu}^{\lambda_E}\right]\right\} + \\
&\quad - \mathrm{i} \operatorname{Tr}\left\{(\check{\rho}^{\lambda_I})^\dagger (\check{\mu}^{\lambda_E})^\dagger \left[V, \hat{\rho}^{\lambda_I} \hat{\mu}^{\lambda_E}\right] x\right\} = \\
&= -\mathrm{i} \operatorname{Tr}\left\{(\check{\rho}^{\lambda_I})^\dagger (\check{\mu}^{\lambda_E})^\dagger V (\hat{\rho}^{\lambda_I} \left[x, \hat{\mu}^{\lambda_E}\right] + \cancelto{0}{\left[x, \hat{\rho}^{\lambda_I}\right]} \hat{\mu}^{\lambda_E})\right\} + \\
&\quad - \mathrm{i} \operatorname{Tr}\left\{(\check{\rho}^{\lambda_I})^\dagger (\check{\mu}^{\lambda_E})^\dagger (\hat{\rho}^{\lambda_I} \cancelto{0}{\left[V, \hat{\mu}^{\lambda_E}\right]} + \left[V, \hat{\rho}^{\lambda_I}\right] \hat{\mu}^{\lambda_E}) x\right\} = \\
&= -\mathrm{i} \operatorname{Tr}\left\{(\check{\rho}^{\lambda_I})^\dagger (\check{\mu}^{\lambda_E})^\dagger V \hat{\rho}^{\lambda_I} \left[x, \hat{\mu}^{\lambda_E}\right]\right\} + \\
&\quad - \mathrm{i} \operatorname{Tr}\left\{(\check{\rho}^{\lambda_I})^\dagger (\check{\mu}^{\lambda_E})^\dagger \left[V, \hat{\rho}^{\lambda_I}\right] \hat{\mu}^{\lambda_E} x\right\} = \\
&= -\mathrm{i} \operatorname*{Tr}_I\left\{(\check{\rho}^{\lambda_I})^\dagger V \hat{\rho}^{\lambda_I}\right\} \cancelto{0}{\operatorname*{Tr}_E\left\{(\check{\mu}^{\lambda_E})^\dagger \left[x, \hat{\mu}^{\lambda_E}\right]\right\}} + \\
&\quad - \mathrm{i} \operatorname*{Tr}_I\left\{(\check{\rho}^{\lambda_I})^\dagger \left[V, \hat{\rho}^{\lambda_I}\right]\right\} \cancelto{0}{\operatorname*{Tr}_E\left\{(\check{\mu}^{\lambda_E})^\dagger \hat{\mu}^{\lambda_E} x\right\}} = \\
&= 0.
\end{aligned} \tag{5.51}$$

To perform this calculation we have used eqs. (5.36) and that the commutators $\left[x, \hat{\rho}^{\lambda_I}\right]$ and $\left[V, \hat{\mu}^{\lambda_E}\right]$ are identically zero because $x = a + a^\dagger$ acts only on the external subspace, while V acts only on the internal subspace. For the last line we used that either $x\hat{\mu}^{\lambda_E}$ or $\hat{\mu}^{\lambda_E} x$ are out of the subspace corresponding to $\lambda_E = \mathrm{i}k\nu$ but rather in the subspace with $\lambda'_E = \mathrm{i}(k \pm 1)\nu$ and so the trace with $(\check{\mu}^{\lambda_E})^\dagger$ vanishes due to orthogonality.

Plugging the solution $\lambda^{(1)} = 0$ in Eq. (5.49a) we get

$$\mathcal{P}_0^\lambda \mathcal{L}^{(1)} \hat{\rho}_\lambda^{(0)} = 0 \tag{5.52a}$$

and multiplying on the right by $\check{\rho}_\lambda^{(0)}$

$$\mathcal{P}_0^\lambda \mathcal{L}^{(1)} \mathcal{P}_0^\lambda = 0. \tag{5.52b}$$

Equations (5.52) express the fact that the action of $\mathcal{L}^{(1)}$ leads out of the subspace selected by $\mathcal{P}_0^\lambda$ ($\mathcal{L}^{(1)}$ only couples subspaces relative to different eigenvalues).

From Eq. (5.49b) we obtain

$$\left(\lambda^{(0)} - \mathcal{L}^{(0)}\right)\mathcal{Q}_0^\lambda \hat{\rho}_\lambda^{(1)} = \mathcal{Q}_0^\lambda \mathcal{L}^{(1)} \hat{\rho}_\lambda^{(0)} \tag{5.53}$$

Since $\mathcal{Q}_0^\lambda$ projects out all contribution which potentially could lead to $\left(\lambda^{(0)} - \mathcal{L}^{(0)}\right) = 0$, we can safely form the inverse of it and find

$$\begin{aligned} \mathcal{Q}_0^\lambda \hat{\rho}_\lambda^{(1)} = \hat{\rho}_\lambda^{(1)} &= \frac{1}{\lambda^{(0)} - \mathcal{L}^{(0)}} \mathcal{Q}_0^\lambda \mathcal{L}^{(1)} \hat{\rho}_\lambda^{(0)} = \\ &= \frac{\mathbb{1} - \mathcal{P}_0^\lambda}{\lambda^{(0)} - \mathcal{L}^{(0)}} \mathcal{L}^{(1)} \hat{\rho}_\lambda^{(0)} = \frac{\mathbb{1}}{\lambda^{(0)} - \mathcal{L}^{(0)}} \mathcal{L}^{(1)} \hat{\rho}_\lambda^{(0)} \end{aligned} \tag{5.54}$$

where we have assumed that the first order contribution $\hat{\rho}_\lambda^{(1)}$ is orthogonal to the zeroth order part, that is $\mathcal{P}_0^\lambda \hat{\rho}_\lambda^{(1)} = 0$. Analogously we can derive the first order correction to the left eigenvector

$$(\check{\rho}_\lambda^{(1)})^\dagger \mathcal{Q}_0^\lambda = (\check{\rho}_\lambda^{(1)})^\dagger = (\check{\rho}_\lambda^{(0)})^\dagger \mathcal{L}^{(1)} \frac{\mathbb{1} - \mathcal{P}_0^\lambda}{\lambda^{(0)} - \mathcal{L}^{(0)}} = (\check{\rho}_\lambda^{(0)})^\dagger \mathcal{L}^{(1)} \frac{\mathbb{1}}{\lambda^{(0)} - \mathcal{L}^{(0)}}, \tag{5.55}$$

by multiplying Eq. (5.45b) on the right with $\mathcal{Q}_0^\lambda$ and using $\lambda^{(1)} = 0$. Results Eq. (5.54) and Eq. (5.55) can be used to write the first order correction to the projector

$$\begin{aligned} P_1^\lambda &= \hat{\rho}_0^\lambda \otimes \check{\rho}_1^\lambda + \hat{\rho}_1^\lambda \otimes \check{\rho}_0^\lambda \\ &= P_0^\lambda \mathcal{L}^{(1)} \frac{\mathbb{1} - \mathcal{P}_0^\lambda}{\lambda^{(0)} - \mathcal{L}^{(0)}} + \frac{\mathbb{1} - \mathcal{P}_0^\lambda}{\lambda^{(0)} - \mathcal{L}^{(0)}} \mathcal{L}^{(1)} P_0^\lambda \\ &= P_0^\lambda \mathcal{L}^{(1)} \frac{\mathbb{1}}{\lambda^{(0)} - \mathcal{L}^{(0)}} + \frac{\mathbb{1}}{\lambda^{(0)} - \mathcal{L}^{(0)}} \mathcal{L}^{(1)} P_0^\lambda. \end{aligned} \tag{5.56}$$

5.A.1.3 *Second Order*

From Eq. (5.30) with $\alpha = 2$ we obtain

$$\mathcal{L}^{(0)} \hat{\rho}_\lambda^{(2)} + \mathcal{L}^{(1)} \hat{\rho}_\lambda^{(1)} = \lambda^{(0)} \hat{\rho}_\lambda^{(2)} + \lambda^{(2)} \hat{\rho}_\lambda^{(0)} \tag{5.57a}$$

$$(\check{\rho}_\lambda^{(2)})^\dagger \mathcal{L}^{(0)} + (\check{\rho}_\lambda^{(1)})^\dagger \mathcal{L}^{(1)} = \lambda^{(0)} (\check{\rho}_\lambda^{(2)})^\dagger + \lambda^{(2)} (\check{\rho}_\lambda^{(0)})^\dagger. \tag{5.57b}$$

We project Eq. (5.57a) with $\mathcal{P}_0^\lambda$ obtaining

$$\begin{aligned} &\mathcal{P}_0^\lambda \mathcal{L}^{(0)} \hat{\rho}_\lambda^{(2)} + \mathcal{P}_0^\lambda \mathcal{L}^{(1)} \hat{\rho}_\lambda^{(1)} = \lambda^{(0)} \mathcal{P}_0^\lambda \hat{\rho}_\lambda^{(2)} + \lambda^{(2)} \mathcal{P}_0^\lambda \hat{\rho}_\lambda^{(0)} \Rightarrow \\ &\cancel{\lambda^{(0)} \mathcal{P}_0^\lambda \hat{\rho}_\lambda^{(2)}} + \mathcal{P}_0^\lambda \mathcal{L}^{(1)} \hat{\rho}_\lambda^{(1)} = \cancel{\lambda^{(0)} \mathcal{P}_0^\lambda \hat{\rho}_\lambda^{(2)}} + \lambda^{(2)} \mathcal{P}_0^\lambda \hat{\rho}_\lambda^{(0)} \Rightarrow \\ &\mathcal{P}_0^\lambda \mathcal{L}^{(1)} \hat{\rho}_\lambda^{(1)} = \lambda^{(2)} \mathcal{P}_0^\lambda \hat{\rho}_\lambda^{(0)} = \lambda^{(2)} \hat{\rho}_\lambda^{(0)} \end{aligned} \tag{5.58}$$

Now we apply the scalar product with $\check{\rho}_\lambda^0$ from left and obtain

$$\begin{aligned} \lambda^{(2)} &= \mathrm{Tr}\left\{(\check{\rho}_\lambda^0)^\dagger (\hat{\rho}_\lambda^0 \otimes \check{\rho}_\lambda^0) \mathcal{L}^{(1)} \hat{\rho}_\lambda^{(1)}\right\} = \\ &= \mathrm{Tr}\left\{\cancel{\mathrm{Tr}\left[(\check{\rho}_\lambda^0)^\dagger \hat{\rho}_\lambda^0\right]} (\check{\rho}_\lambda^0)^\dagger \mathcal{L}^{(1)} \hat{\rho}_\lambda^{(1)}\right\} = \mathrm{Tr}\left\{(\check{\rho}_\lambda^0)^\dagger \mathcal{L}^{(1)} \hat{\rho}_\lambda^{(1)}\right\}. \end{aligned} \tag{5.59}$$

Projecting Eq. (5.57a) with $\mathcal{Q}_0^\lambda$ we obtain

$$\mathcal{Q}_0^\lambda \mathcal{L}^{(0)} \hat{\rho}_\lambda^{(2)} + \mathcal{Q}_0^\lambda \mathcal{L}^{(1)} \hat{\rho}_\lambda^{(1)} = \lambda^{(0)} \mathcal{Q}_0^\lambda \hat{\rho}_\lambda^{(2)} + \lambda^{(2)} \mathcal{Q}_0^\lambda \hat{\rho}_\lambda^{(0)}. \tag{5.60}$$

Notice that

$$\mathcal{Q}_0^\lambda \mathcal{L}^{(0)} \hat{\rho}_\lambda^{(2)} = (\mathbb{1} - \mathcal{P}_0^\lambda) \mathcal{L}^{(0)} \hat{\rho}_\lambda^{(2)} = \mathcal{L}^{(0)} \hat{\rho}_\lambda^{(2)} - \lambda^{(0)} \mathcal{P}_0^\lambda \hat{\rho}_\lambda^{(2)} \tag{5.61a}$$

and

$$\lambda^{(0)} \mathcal{Q}_0^\lambda \hat{\rho}_\lambda^{(2)} = \lambda^{(0)} (\mathbb{1} - \mathcal{P}_0^\lambda) \hat{\rho}_\lambda^{(2)} = \lambda^{(0)} \hat{\rho}_\lambda^{(2)} - \lambda^{(0)} \mathcal{P}_0^\lambda \hat{\rho}_\lambda^{(2)}. \tag{5.61b}$$

Inserting Eq. (5.61a) and Eq. (5.61b) into Eq. (5.60) we obtain

$$\mathcal{Q}_0^\lambda \mathcal{L}^{(1)} \hat{\rho}_\lambda^{(1)} - \lambda^{(2)} \mathcal{Q}_0^\lambda \hat{\rho}_\lambda^{(0)} = (\lambda^{(0)} - \mathcal{L}^{(0)}) \hat{\rho}_\lambda^{(2)}. \tag{5.62}$$

Then the second order correction to the right eigenvector is then

$$\begin{aligned} \hat{\rho}_\lambda^{(2)} &= \frac{\mathbb{1} - \mathcal{P}_0^\lambda}{\lambda^{(0)} - \mathcal{L}^{(0)}} \mathcal{L}^{(1)} \hat{\rho}_\lambda^{(1)} - \cancelto{0}{\lambda^{(2)} \frac{\mathbb{1} - \mathcal{P}_0^\lambda}{\lambda^{(0)} - \mathcal{L}^{(0)}} \hat{\rho}_\lambda^{(0)}} \\ &= \frac{\mathbb{1} - \mathcal{P}_0^\lambda}{\lambda^{(0)} - \mathcal{L}^{(0)}} \mathcal{L}^{(1)} \frac{\mathbb{1} - \mathcal{P}_0^\lambda}{\lambda^{(0)} - \mathcal{L}^{(0)}} \mathcal{L}^{(1)} \hat{\rho}_\lambda^{(0)} \\ &= \frac{\mathbb{1} - \mathcal{P}_0^\lambda}{\lambda^{(0)} - \mathcal{L}^{(0)}} \mathcal{L}^{(1)} \frac{\mathbb{1}}{\lambda^{(0)} - \mathcal{L}^{(0)}} \mathcal{L}^{(1)} \hat{\rho}_\lambda^{(0)}. \end{aligned} \tag{5.63}$$

The second order correction to the left eigenvector can be derived analogously by multiplying Eq. (5.57b) on the right by $\mathcal{Q}_0^\lambda$ and reads

$$(\check{\rho}_\lambda^{(2)})^\dagger = (\check{\rho}_\lambda^{(0)})^\dagger \mathcal{L}^{(1)} \frac{\mathbb{1}}{\lambda^{(0)} - \mathcal{L}^{(0)}} \mathcal{L}^{(1)} \frac{\mathbb{1} - P_0^\lambda}{\lambda^{(0)} - \mathcal{L}^{(0)}}. \tag{5.64}$$

Notice that we have used the fact $(\mathbb{1} - \mathcal{P}_0^\lambda) \hat{\rho}_\lambda^{(0)} = 0$. The second order correction to the projector is

$$\begin{aligned} \mathcal{P}_2^\lambda &= \hat{\rho}_0^\lambda \otimes \check{\rho}_2^\lambda + \hat{\rho}_1^\lambda \otimes \check{\rho}_1^\lambda + \hat{\rho}_2^\lambda \otimes \check{\rho}_0^\lambda \\ &= \mathcal{P}_0^\lambda \mathcal{L}^{(1)} \frac{\mathbb{1}}{\lambda^{(0)} - \mathcal{L}^{(0)}} \mathcal{L}^{(1)} \frac{\mathbb{1} - \mathcal{P}_0^\lambda}{\lambda^{(0)} - \mathcal{L}^{(0)}} + \\ &\quad + \frac{\mathbb{1}}{\lambda^{(0)} - \mathcal{L}^{(0)}} \mathcal{L}^{(1)} \mathcal{P}_0^\lambda \mathcal{L}^{(1)} \frac{\mathbb{1}}{\lambda^{(0)} - \mathcal{L}^{(0)}} + \\ &\quad + \frac{\mathbb{1} - \mathcal{P}_0^\lambda}{\lambda^{(0)} - \mathcal{L}^{(0)}} \mathcal{L}^{(1)} \frac{\mathbb{1}}{\lambda^{(0)} - \mathcal{L}^{(0)}} \mathcal{L}^{(1)} \mathcal{P}_0^\lambda. \end{aligned} \tag{5.65}$$

5.A.1.4 *Lifting the degeneracy*

We showed in Secs. 5.A.1.2 and 5.A.1.3 that the first correction to the eigenvalue $\lambda^{(0)}$ appears in second order perturbation theory. We now calculate this correction and see that the degeneracy that occurs in zeroth order is lifted.

Consider an effective eigenvalue equation in the subspace fixed by $\lambda^{(0)} = \lambda_I + \lambda_E$. We look for the basis elements which span the degenerated subspace and fulfill simultaneously the second order eigenvalue

equations (5.57). In order to do this we plug Eq. (5.54) into Eq. (5.58) to obtain

$$\begin{aligned}\lambda^{(2)}\hat{\rho}_\lambda^{(0)} &= \mathcal{P}_0^\lambda \mathcal{L}^{(1)}\hat{\rho}_\lambda^{(1)} = \mathcal{P}_0^{(\lambda)}\mathcal{L}^{(1)}\frac{\mathbb{1}}{\lambda^{(0)}-\mathcal{L}^{(0)}}\mathcal{L}^{(1)}\hat{\rho}_\lambda^{(0)} = \\ &= \mathcal{P}_0^\lambda \mathcal{L}^{(1)}\frac{\mathbb{1}}{\lambda^{(0)}-\mathcal{L}^{(0)}}\mathcal{L}^{(1)}\mathcal{P}_0^\lambda\hat{\rho}_\lambda^{(0)} = \tilde{\mathcal{L}}(\lambda^{(0)})\hat{\rho}_\lambda^{(0)}\end{aligned} \tag{5.66}$$

with

$$\tilde{\mathcal{L}}(\lambda^{(0)}) = \mathcal{P}_0^\lambda \mathcal{L}^{(1)}\frac{\mathbb{1}}{\lambda^{(0)}-\mathcal{L}^{(0)}}\mathcal{L}^{(1)}\mathcal{P}_0^\lambda. \tag{5.67}$$

Eq. (5.66) lives in the subspace selected by $\mathcal{P}_0^\lambda$ and depends parametrically on the eigenvalue $\lambda^{(0)}$ and its relative subspace. It is the eigenvalue equation in the degenerated subspace belonging to $\lambda^{(0)}$ that determines the second order correction $\lambda^{(2)}$ to the chosen $\lambda^{(0)}$ and fixes the correct choice of eigenelements $\hat{\rho}^{\lambda_0,\lambda_2} = \hat{\rho}^{\lambda_I}\hat{\mu}^{\lambda_E,\lambda_2}$ which diagonalize $\tilde{\mathcal{L}}(\lambda^{(0)})$. Now we take the scalar product of Eq. (5.66) with $\check{\rho}^{\lambda_I}$ on the left, i. e. we multiply on the left with $(\check{\rho}^{\lambda_I})^\dagger$ and take the trace over the internal degree of freedom. We obtain then an eigenvalue equation for the external degrees of freedom

$$\lambda^{(2)}\operatorname*{Tr}_I\left[(\check{\rho}^{\lambda_I})^\dagger\hat{\rho}^{\lambda_I}\hat{\mu}^{\lambda_E,\lambda_2}\right] = \operatorname*{Tr}_I\left[(\check{\rho}^{\lambda_I})^\dagger\mathcal{P}_I^{\lambda_I}\mathcal{P}_E^{\lambda_E}\mathcal{L}^{(1)}\frac{\mathbb{1}}{\lambda^{(0)}-\mathcal{L}^{(0)}}\mathcal{L}^{(1)}\hat{\rho}^{\lambda_I}\hat{\mu}^{\lambda_E,\lambda_2}\right]. \tag{5.68}$$

We define

$$\tilde{\mathcal{L}}_E(\lambda^{(0)}) = \operatorname*{Tr}_I\left[(\check{\rho}^{\lambda_I})^\dagger\mathcal{P}_I^{\lambda_I}\mathcal{P}_E^{\lambda_E}\mathcal{L}^{(1)}\frac{\mathbb{1}}{\lambda^{(0)}-\mathcal{L}^{(0)}}\mathcal{L}^{(1)}\hat{\rho}^{\lambda_I}\right]. \tag{5.69}$$

such that we can write

$$\lambda^{(2)}\hat{\mu}^{\lambda_E,\lambda_2} = \tilde{\mathcal{L}}_E(\lambda^{(0)})\hat{\mu}^{\lambda_E,\lambda_2}. \tag{5.70}$$

Thus the states $\hat{\mu}^{\lambda_E,\lambda_2}$ are eigenstates of $\tilde{\mathcal{L}}_E(\lambda^{(0)})$ with respect to the eigenvalue $\lambda^{(2)}$, and eigenstates of $\mathcal{L}_E$ with respect to the eigenvalue λ_E. Now we calculate explicitly the action of the superoperator $\tilde{\mathcal{L}}_E(\lambda^{(0)})$ on the operator $\hat{\mu}^{\lambda_E}$. Using Eq. (5.32d), the equivalence

$$\frac{\mathbb{1}}{\lambda^{(0)}-\mathcal{L}^{(0)}} = \int_0^\infty e^{(\mathcal{L}^{(0)}-\lambda^{(0)})t}\mathrm{d}t \tag{5.71}$$

and noting that

$$(\check{\rho}^{\lambda_I})^\dagger\mathcal{P}_I^{\lambda_I} = (\check{\rho}^{\lambda_I})^\dagger\hat{\rho}^{\lambda_I}\otimes\check{\rho}^{\lambda_I} = \operatorname{Tr}\left[(\check{\rho}^{\lambda_I})^\dagger\hat{\rho}^{\lambda_I}\right](\check{\rho}^{\lambda_I})^\dagger = (\check{\rho}^{\lambda_I})^\dagger \tag{5.72}$$

we have

$$\tilde{\mathcal{L}}_E(\lambda^{(0)})\hat{\mu}^{\lambda_E} = -\int_0^\infty \mathrm{d}t\, e^{-\lambda^{(0)}t}\operatorname*{Tr}_I\left\{(\check{\rho}^{\lambda_I})^\dagger\mathcal{P}_E^{\lambda_E}\left[Vx, e^{\mathcal{L}_I t}e^{\mathcal{L}_E t}\left[Vx,\hat{\rho}^{\lambda_I}\hat{\mu}^{\lambda_E}\right]\right]\right\}. \tag{5.73}$$

The calculation is performed in Sec. 5.A.1.6. The result is (Eq. (5.95) and Eq. (5.96))

$$\begin{aligned}\tilde{\mathcal{L}}_E(\lambda^{(0)})\hat{\mu}^{\lambda_E} = {} & s^{\lambda_I}(\nu)\big(a\hat{\mu}^{\lambda_E}a^\dagger - a^\dagger a\hat{\mu}^{\lambda_E}\big) + \\ & + s^{\lambda_I}(-\nu)\big(a^\dagger\hat{\mu}^{\lambda_E}a - aa^\dagger\hat{\mu}^{\lambda_E}\big) + \\ & + s'^{\lambda_I}(\nu)\big(a^\dagger\hat{\mu}^{\lambda_E}a - \hat{\mu}^{\lambda_E}aa^\dagger\big) + \\ & + s'^{\lambda_I}(-\nu)\big(a\hat{\mu}^{\lambda_E}a^\dagger - \hat{\mu}^{\lambda_E}a^\dagger a\big) + \\ & - t^{\lambda_I}\big(a\hat{\mu}^{\lambda_E}a^\dagger + a^\dagger\hat{\mu}^{\lambda_E}a\big) + \\ & + t'^{\lambda_I}\big(\hat{\mu}^{\lambda_E}a^\dagger a + \hat{\mu}^{\lambda_E}aa^\dagger\big)\end{aligned} \tag{5.74}$$

with

$$s^{\lambda_I}(\upsilon) = \int_0^\infty \mathrm{d}t\, e^{(\mathrm{i}\upsilon-\lambda_I)t}\operatorname*{Tr}_I\big[(\check{\rho}^{\lambda_I})^\dagger V e^{\mathcal{L}_I t}V\hat{\rho}^{\lambda_I}\big], \tag{5.75a}$$

$$s'^{\lambda_I}(\upsilon) = \int_0^\infty \mathrm{d}t\, e^{(\mathrm{i}\upsilon-\lambda_I)t}\operatorname*{Tr}_I\big[(\check{\rho}^{\lambda_I})^\dagger V e^{\mathcal{L}_I t}\hat{\rho}^{\lambda_I}V\big], \tag{5.75b}$$

$$t^{\lambda_I} = \int_0^\infty \mathrm{d}t\, e^{-\lambda_I t}\operatorname*{Tr}_I\big[(\check{\rho}^{\lambda_I})^\dagger\big[V, e^{\mathcal{L}_I t}V\hat{\rho}^{\lambda_I}\big]\big], \tag{5.75c}$$

$$t'^{\lambda_I} = \int_0^\infty \mathrm{d}t\, e^{-\lambda_I t}\operatorname*{Tr}_I\big[(\check{\rho}^{\lambda_I})^\dagger\big[V, e^{\mathcal{L}_I t}\hat{\rho}^{\lambda_I}V\big]\big]. \tag{5.75d}$$

5.A.1.5 *Effective dynamics of the mechanical oscillator*

We now consider the internal part of the system to be always in the steady state and always decoupled from the external part, i. e., $\lambda_I = 0$ and

$$\rho(t) = \hat{\rho}^{\lambda_I=0}\otimes\hat{\mu}^{\lambda_E}(t) = \hat{\rho}^{\lambda_I=0}\otimes\sum_{\lambda_2} c_{\lambda_2}\hat{\mu}^{\lambda_E,\lambda_2}\mathrm{e}^{(\lambda_E+\lambda^{(2)})t} \tag{5.76}$$

where $\hat{\rho}^{\lambda_I=0} = \hat{\rho}_I^{ss}$ is the steady state of the internal degree of freedom solution of $\mathcal{L}_I\hat{\rho}^{\lambda_I} = 0$ and $\hat{\mu}^{\lambda_E}(t) = \mathrm{Tr}_I\left[\mathcal{P}_I^{\lambda_I=0}\rho(t)\right]$ is the reduced density matrix of the mechanical oscillator. In the last step of Eq. (5.76) we have expanded the state $\hat{\mu}^{\lambda_E}(t)$ as a superposition of $\hat{\mu}^{\lambda_E,\lambda_2}$ eigenstates of $\tilde{\mathcal{L}}_E(\lambda_E)$ with eigenvalue $\lambda^{(2)}$ (see Eq. (5.70)).

The effective dynamics is then given by

$$\frac{\partial}{\partial t}\hat{\mu}^{\lambda_E}(t) = \big[\mathcal{L}_E + \tilde{\mathcal{L}}_E(\lambda_E)\big]\hat{\mu}^{\lambda_E}(t) \tag{5.77}$$

where $\tilde{\mathcal{L}}_E(\lambda_E)\hat{\mu}^{\lambda_E}(t)$ is given by Eq. (5.74) and Eq. (5.75) with $\lambda_I = 0$. Equation (5.77) (apart from a trace and the term $\mathcal{L}_\gamma$ which will be considered later) is Eq. (5.22) reported in the main text. Notice that the left eigenvector relative to the eigenvalue $\lambda_I = 0$ is $(\check{\rho}^{\lambda_I=0})^\dagger = \mathbb{1}$. Using this fact

with eqs. (5.75c) and (5.75d) it is clear that $t^{\lambda_I=0} = t'^{\lambda_I=0} = 0$ because the trace of a commutator is zero. We define

$$s(\upsilon) = s^{\lambda_I=0}(\upsilon) = \frac{1}{\hbar^2}\int_0^\infty \mathrm{d}t\, e^{\mathrm{i}\upsilon t}\langle V(t)V(0)\rangle_{ss}, \tag{5.78a}$$

$$s^*(\upsilon) = s'^{\lambda_I=0}(-\upsilon) = \frac{1}{\hbar^2}\int_0^\infty \mathrm{d}t\, e^{-\mathrm{i}\upsilon t}\langle V(0)V(t)\rangle_{ss}, \tag{5.78b}$$

where we used the *quantum regression theorem* to write the coefficient $s(\upsilon)$ in the form of steady state expectation value. We define also

$$\frac{A_\pm}{2} = \Re s(\mp\nu) \tag{5.79a}$$

$$\bar{\nu} = \Im s(\nu) + \Im s(-\nu) \tag{5.79b}$$

and Eq. (5.77) is explicitly given by

$$\begin{aligned}\frac{\partial}{\partial t}\hat{\mu}^{\lambda_E} = &-\mathrm{i}(\nu+\bar{\nu})\big[a^\dagger a, \hat{\mu}^{\lambda_E}\big] + \frac{A_-}{2}\big(2a\hat{\mu}^{\lambda_E}a^\dagger - \big\{a^\dagger a, \hat{\mu}^{\lambda_E}\big\}\big) + \\ &+ \frac{A_+}{2}\big(2a^\dagger\hat{\mu}^{\lambda_E}a - \big\{aa^\dagger, \hat{\mu}^{\lambda_E}\big\}\big).\end{aligned} \tag{5.80}$$

Eq. (5.80) is a generalized master equation of a damped harmonic oscillator with renormalized frequency $(\nu+\bar{\nu})$ and generalized feeding rates $A_\pm$. Apart from the term $\mathcal{L}_\gamma\hat{\mu}^{\lambda_E}$ which will be added later, it is Eq. (5.23) reported in the main text. Notice that each subspace relative to λ_E is effectively damped. We define the *cooling rate*

$$\tilde{\Gamma} = A_- - A_+, \tag{5.81}$$

and the *minimal phonon number*

$$N_0 = \frac{A_+}{A_- - A_+} = \frac{A_+}{\tilde{\Gamma}}. \tag{5.82}$$

The equation describing the effective dynamics can then be written as

$$\frac{\partial}{\partial t}\mu = -\mathrm{i}(\nu+\bar{\nu})\big[a^\dagger a, \mu\big] + \frac{\tilde{\Gamma}}{2}(N_0+1)\mathcal{D}[a]\mu + \frac{\tilde{\Gamma}}{2}N_0\mathcal{D}[a^\dagger]\mu + \mathcal{L}_\gamma\mu, \tag{5.83}$$

where $\mathcal{D}[o]\rho = 2o\rho o^\dagger - \big\{o^\dagger o, \rho\big\}$ and we added the mechanical dissipation due to the coupling with the thermal bath of phonons described by $\mathcal{L}_\gamma$.

5.A.1.6 *Calculation of the action of the operator $\tilde{\mathcal{L}}_E(\lambda^{(0)})$ on $\hat{\mu}^{\lambda_E}$*

Here we perform the calculations used in Sec. 5.A.1.4. We want to calculate Eq. (5.73) which we report here

$$\tilde{\mathcal{L}}_E(\lambda^{(0)})\hat{\mu}^{\lambda_E} = -\int_0^\infty \mathrm{d}t\, e^{-\lambda^{(0)}t}\operatorname*{Tr}_I\Big\{(\check{\rho}^{\lambda_I})^\dagger\mathcal{P}_E^{\lambda_E}\big[Vx, e^{\mathcal{L}_I t}e^{\mathcal{L}_E t}\big[Vx, \hat{\rho}^{\lambda_I}\hat{\mu}^{\lambda_E}\big]\big]\Big\}. \tag{5.84}$$

We first evaluate

$$\begin{aligned}\big[Vx,\hat{\rho}^{\lambda_I}\hat{\mu}^{\lambda_E}\big] &= V\big[x,\hat{\rho}^{\lambda_I}\hat{\mu}^{\lambda_E}\big]+\big[V,\hat{\rho}^{\lambda_I}\hat{\mu}^{\lambda_E}\big]x = \\ &= V\Big(\hat{\rho}^{\lambda_I}\big[x,\hat{\mu}^{\lambda_E}\big]+\cancelto{0}{\big[x,\hat{\rho}^{\lambda_I}\big]\hat{\mu}^{\lambda_E}}\Big)+ \\ &\quad+\Big(\hat{\rho}^{\lambda_I}\cancelto{0}{\big[V,\hat{\mu}^{\lambda_E}\big]}+\big[V,\hat{\rho}^{\lambda_I}\big]\hat{\mu}^{\lambda_E}\Big)x \\ &= V\hat{\rho}^{\lambda_I}\big[x,\hat{\mu}^{\lambda_E}\big]+\big[V,\hat{\rho}^{\lambda_I}\big]\hat{\mu}^{\lambda_E}x,\end{aligned} \tag{5.85}$$

where some commutators vanish because they are commutators between operators that act on different degrees of freedom (internal and external).

Now we calculate

$$\begin{aligned}&\Big[Vx,e^{\mathcal{L}^{(0)}t}\big[Vx,\hat{\rho}^{\lambda_I}\hat{\mu}^{\lambda_E}\big]\Big] = \\ &\quad=\Big[Vx,e^{\mathcal{L}^{(0)}t}V\hat{\rho}^{\lambda_I}\big[x,\hat{\mu}^{\lambda_E}\big]+e^{\mathcal{L}^{(0)}t}\big[V,\hat{\rho}^{\lambda_I}\big]\hat{\mu}^{\lambda_E}x\Big] = \\ &\quad=V\Big[x,e^{\mathcal{L}^{(0)}t}V\hat{\rho}^{\lambda_I}\big[x,\hat{\mu}^{\lambda_E}\big]\Big]+\Big[V,e^{\mathcal{L}^{(0)}t}V\hat{\rho}^{\lambda_I}\big[x,\hat{\mu}^{\lambda_E}\big]\Big]x+ \\ &\qquad+V\Big[x,e^{\mathcal{L}^{(0)}t}\big[V,\hat{\rho}^{\lambda_I}\big]\hat{\mu}^{\lambda_E}x\Big]+\Big[V,e^{\mathcal{L}^{(0)}t}\big[V,\hat{\rho}^{\lambda_I}\big]\hat{\mu}^{\lambda_E}x\Big]x = \\ &\quad=Ve^{\mathcal{L}_It}V\hat{\rho}^{\lambda_I}\big[x,e^{\mathcal{L}_Et}\big[x,\hat{\mu}^{\lambda_E}\big]\big]+\big[V,e^{\mathcal{L}_It}V\hat{\rho}^{\lambda_I}\big]e^{\mathcal{L}_Et}\big[x,\hat{\mu}^{\lambda_E}\big]x+ \\ &\qquad+Ve^{\mathcal{L}_It}\big[V,\hat{\rho}^{\lambda_I}\big]\big[x,e^{\mathcal{L}_Et}\hat{\mu}^{\lambda_E}x\big]+\big[V,e^{\mathcal{L}_It}\big[V,\hat{\rho}^{\lambda_I}\big]\big]e^{\mathcal{L}_Et}\hat{\mu}^{\lambda_E}x^2\end{aligned} \tag{5.86}$$

where in the last step we sorted internal and external quantities. Then

$$\begin{aligned}&\operatorname*{Tr}_I\Big\{(\check{\rho}^{\lambda_I})^\dagger\mathcal{P}_E^{\lambda_E}\big[Vx,e^{\mathcal{L}_It}e^{\mathcal{L}_Et}\big[Vx,\hat{\rho}^{\lambda_I}\hat{\mu}^{\lambda_E}\big]\big]\Big\} = \\ &\quad=\operatorname*{Tr}_I\big[(\check{\rho}^{\lambda_I})^\dagger Ve^{\mathcal{L}_It}V\hat{\rho}^{\lambda_I}\big]\mathcal{P}_E^{\lambda_E}\big[x,e^{\mathcal{L}_Et}\big[x,\hat{\mu}^{\lambda_E}\big]\big]+ \\ &\qquad+\operatorname*{Tr}_I\big[(\check{\rho}^{\lambda_I})^\dagger\big[V,e^{\mathcal{L}_It}V\hat{\rho}^{\lambda_I}\big]\big]\mathcal{P}_E^{\lambda_E}e^{\mathcal{L}_Et}\big[x,\hat{\mu}^{\lambda_E}\big]x+ \\ &\qquad+\operatorname*{Tr}_I\big[(\check{\rho}^{\lambda_I})^\dagger Ve^{\mathcal{L}_It}\big[V,\hat{\rho}^{\lambda_I}\big]\big]\mathcal{P}_E^{\lambda_E}\big[x,e^{\mathcal{L}_Et}\hat{\mu}^{\lambda_E}x\big]+ \\ &\qquad+\operatorname*{Tr}_I\big[(\check{\rho}^{\lambda_I})^\dagger\big[V,e^{\mathcal{L}_It}\big[V,\hat{\rho}^{\lambda_I}\big]\big]\big]\mathcal{P}_E^{\lambda_E}e^{\mathcal{L}_Et}\hat{\mu}^{\lambda_E}x^2.\end{aligned} \tag{5.87}$$

We want to calculate each external expression in Eq. (5.87). In order to do so, it is useful to express the action of $\mathcal{P}_E^{\lambda_E}$ on a general operator X. With the use of Eq. (5.35) and Eq. (5.42) we have

$$\begin{aligned}\mathcal{P}_E^{\lambda_E}X &= \sum_{n=0}^{\infty}\hat{\mu}^{\lambda_E}(n)\otimes\check{\mu}^{\lambda_E}(n)X = \\ &=\sum_{n=0}^{\infty}\hat{\mu}^{\lambda_E}(n)\operatorname{Tr}\big[[\check{\mu}^{\lambda_E}(n)]^\dagger X\big] = \\ &=\sum_{n=0}^{\infty}\Big|n+\frac{|k|-k}{2}\Big\rangle\Big\langle n+\frac{|k|+k}{2}\Big|\Big\langle n+\frac{|k|-k}{2}\Big|X\Big|n+\frac{|k|+k}{2}\Big\rangle = \\ &=\sum_{n=\frac{|k|-k}{2}}^{\infty}|n\rangle\langle n+k|\langle n|X|n+k\rangle.\end{aligned}$$

(5.88)

We will also use Eq. (5.37) which can be rewritten as

$$\hat{\mu}^{\lambda_E=ik\nu} = \sum_{n=0}^{\infty} c_n \hat{\mu}^k(n) = \sum_{n=\frac{|k|-k}{2}}^{\infty} c_n |n\rangle\langle n+k| \tag{5.89}$$

and the completeness relation Eq. (5.43). Now we calculate each external expression of Eq. (5.87). We first evaluate

$$\begin{aligned} e^{\mathcal{L}_E t}\hat{\mu}^{\lambda_E}x^2 &= \sum_{\lambda'_E} \mathcal{P}_E^{\lambda'_E} e^{\mathcal{L}_E t}\hat{\mu}^{\lambda_E}x^2 = \sum_{\lambda'_E} e^{\lambda'_E t}\mathcal{P}_E^{\lambda'_E}\hat{\mu}^{\lambda_E}x^2 = \\ &= \sum_{\lambda'_E=ik'\nu} e^{\lambda'_E t}\sum_m |m\rangle\langle m+k'|\langle m|\hat{\mu}^{\lambda_E}x^2|m+k'\rangle = \\ &= \sum_{\lambda'_E=ik'\nu} e^{\lambda'_E t}\sum_{m,n} |m\rangle\langle m+k'|\cancelto{\delta_{mn}}{\langle m|n\rangle} c_n\langle n+k|x^2|m+k'\rangle = \\ &= \sum_{\lambda'_E=ik'\nu} e^{\lambda'_E t}\sum_m c_m|m\rangle\langle m+k'|\langle m+k|x^2|m+k'\rangle, \end{aligned} \tag{5.90}$$

and $\mathcal{P}_E^{\lambda_E} e^{\mathcal{L}_E t}\hat{\mu}^{\lambda_E}x^2 =$

$$\begin{aligned} &= \mathcal{P}_E^{\lambda_E}\sum_{\lambda'_E=ik'\nu} e^{\lambda'_E t}\sum_m c_m|m\rangle\langle m+k'|\langle m+k|x^2|m+k'\rangle = \\ &= \sum_{n,k',m} e^{ik'\nu t}c_m|n\rangle\langle n+k|\cancelto{\delta_{nm}}{\langle n|m\rangle}\langle m+k'|n+k\rangle\langle m+k|x^2|m+k'\rangle = \\ &= \sum_{n,k'} e^{ik'\nu t}c_n|n\rangle\langle n+k|\cancelto{\delta_{kk'}}{\langle n+k'|n+k\rangle}\langle n+k|x^2|n+k'\rangle = \\ &= e^{ik\nu t}\sum_n c_n|n\rangle\langle n+k|\left\langle n+k\middle|aa^\dagger + a^\dagger a + \cancelto{0}{a^2} + \cancelto{0}{(a^\dagger)^2}\middle|n+k\right\rangle = \\ &= e^{ik\nu t}\sum_n c_n|n\rangle\langle n+k|\cancelto{1}{\langle n+k|n+k\rangle}\left(\left(\sqrt{n+k+1}\right)^2 + \left(\sqrt{n+k}\right)^2\right) = \\ &= e^{ik\nu t}\sum_n c_n|n\rangle\langle n+k|(aa^\dagger + a^\dagger a) = \\ &= e^{\lambda_E t}\hat{\mu}^{\lambda_E}(aa^\dagger + a^\dagger a). \end{aligned} \tag{5.91}$$

Now we evaluate $e^{\mathcal{L}_E t} x \hat{\mu}^{\lambda_E} x =$

$$
\begin{aligned}
&= \sum_{\lambda'_E} \mathcal{P}_E^{\lambda'_E} e^{\mathcal{L}_E t} x \hat{\mu}^{\lambda_E} x = \sum_{\lambda'_E} e^{\lambda'_E t} \mathcal{P}_E^{\lambda'_E} x \hat{\mu}^{\lambda_E} x = \\
&= \sum_{\lambda'_E = \mathrm{i}k'\nu} e^{\lambda'_E t} \sum_m |m\rangle\langle m+k'| \langle m| x \hat{\mu}^{\lambda_E} x |m+k'\rangle = \\
&= \sum_{\lambda'_E = \mathrm{i}k'\nu} e^{\lambda'_E t} \sum_{m,n} c_n |m\rangle\langle m+k'| \langle m|x|n\rangle\langle n+k|x|m+k'\rangle = \\
&= \sum_{\lambda'_E = \mathrm{i}k'\nu} e^{\lambda'_E t} \sum_{m,n} c_n |m\rangle\langle m+k'| (\sqrt{n}\delta_{m,n-1} + \sqrt{n+1}\delta_{m,n+1}) \cdot \\
&\qquad \cdot \langle n+k|x|m+k'\rangle = \\
&= \sum_{\lambda'_E = \mathrm{i}k'\nu} e^{\lambda'_E t} \sum_n c_n \Big[\sqrt{n} |n-1\rangle\langle n-1+k'| \langle n+k|x|n-1+k'\rangle + \\
&\qquad + \sqrt{n+1} |n+1\rangle\langle n+1+k'| \langle n+k|x|n+1+k'\rangle \Big],
\end{aligned}
\tag{5.92}
$$

and $\mathcal{P}_E^{\lambda_E} e^{\mathcal{L}_E t} x \hat{\mu}^{\lambda_E} x =$

$$
\begin{aligned}
&= \mathcal{P}_E^{\lambda_E} \sum_{\lambda'_E = \mathrm{i}k'\nu} e^{\lambda'_E t} \sum_n c_n \Big[\sqrt{n} |n-1\rangle\langle n-1+k'| \langle n+k|x|n-1+k'\rangle + \\
&\qquad + \sqrt{n+1} |n+1\rangle\langle n+1+k'| \langle n+k|x|n+1+k'\rangle \Big] = \\
&= \sum_{k',n,m} e^{\mathrm{i}k'\nu t} c_n |m\rangle\langle m+k| \cdot \\
&\qquad \cdot \Big[\sqrt{n} \langle m|n-1\rangle \overset{\delta_{m,n-1}}{\langle n-1+k'|m+k\rangle} \langle n+k|x|n-1+k'\rangle + \\
&\qquad + \sqrt{n+1} \langle m|n+1\rangle \overset{\delta_{m,n+1}}{\langle n+1+k'|m+k\rangle} \langle n+k|x|n+1+k'\rangle \Big] = \\
&= \sum_{k',n} e^{\mathrm{i}k'\nu t} c_n \Big[\sqrt{n} |n-1\rangle\langle n-1+k| \cdot \\
&\qquad \cdot \overset{\delta_{k,k'}}{\langle n-1+k'|n-1+k\rangle} \langle n+k|x|n-1+k'\rangle + \\
&\qquad + \sqrt{n+1} |n+1\rangle\langle n+1+k| \cdot \\
&\qquad \cdot \overset{\delta_{k,k'}}{\langle n+1+k'|n+1+k\rangle} \langle n+k|x|n+1+k'\rangle \Big] = \\
&= e^{\mathrm{i}k\nu t} \sum_n c_n \Big[\sqrt{n} |n-1\rangle\langle n-1+k| \langle n+k|x|n-1+k\rangle + \\
&\qquad + \sqrt{n+1} |n+1\rangle\langle n+1+k| \langle n+k|x|n+1+k\rangle \Big] = \\
&= e^{\lambda_E t} \sum_n c_n \Big[\sqrt{n} |n-1\rangle\langle n+k-1| \sqrt{n+k} + \\
&\qquad + \sqrt{n+1} |n+1\rangle\langle n+k+1| \sqrt{n+k+1} \Big] = \\
&= e^{\lambda_E t} \sum_n c_n \big[a|n\rangle\langle n+k|a^\dagger + a^\dagger |n\rangle\langle n+k|a \big] = \\
&= e^{\lambda_E t} (a \hat{\mu}^{\lambda_E} a^\dagger + a^\dagger \hat{\mu}^{\lambda_E} a)
\end{aligned}
\tag{5.93}
$$

The other terms are calculated in a similar way, the results are

$$\begin{aligned}\mathcal{P}_E^{\lambda_E}\big[x, e^{\mathcal{L}_E t}\big[x, \hat{\mu}^{\lambda_E}\big]\big] = e^{\lambda_E t}\big[e^{-\mathrm{i}\nu t}\big(aa^\dagger\hat{\mu}^{\lambda_E} + \hat{\mu}^{\lambda_E}a^\dagger a\big) + \\ + e^{\mathrm{i}\nu t}\big(a^\dagger a\hat{\mu}^{\lambda_E} + \hat{\mu}^{\lambda_E}aa^\dagger\big) + \\ - \big(e^{-\mathrm{i}\nu t} + e^{\mathrm{i}\nu t}\big)\big(a\hat{\mu}^{\lambda_E}a^\dagger + a^\dagger\hat{\mu}^{\lambda_E}a\big)\big],\end{aligned} \tag{5.94a}$$

$$\mathcal{P}_E^{\lambda_E} e^{\mathcal{L}_E t}\big[x, \hat{\mu}^{\lambda_E}\big]x = e^{\lambda_E t}\big(a\hat{\mu}^{\lambda_E}a^\dagger + a^\dagger\hat{\mu}^{\lambda_E}a - \hat{\mu}^{\lambda_E}aa^\dagger - \hat{\mu}^{\lambda_E}a^\dagger a\big), \tag{5.94b}$$

$$\begin{aligned}\mathcal{P}_E^{\lambda_E}\big[x, e^{\mathcal{L}_E t}\hat{\mu}^{\lambda_E}x\big] = e^{\lambda_E t}\big[e^{-\mathrm{i}\nu t}\big(a\hat{\mu}^{\lambda_E}a^\dagger - \hat{\mu}^{\lambda_E}a^\dagger a\big) + \\ + e^{\mathrm{i}\nu t}\big(a^\dagger\hat{\mu}^{\lambda_E}a - \hat{\mu}^{\lambda_E}aa^\dagger\big)\big],\end{aligned} \tag{5.94c}$$

$$\mathcal{P}_E^{\lambda_E} e^{\mathcal{L}_E t}\hat{\mu}^{\lambda_E}x^2 = e^{\lambda_E t}\hat{\mu}^{\lambda_E}(aa^\dagger + a^\dagger a). \tag{5.94d}$$

Inserting Eqs. (5.94) in Eq. (5.87) and then in Eq. (5.84), recasting the terms we finally obtain

$$\begin{aligned}\tilde{\mathcal{L}}_E(\lambda^{(0)})\hat{\mu}^{\lambda_E} = s^{\lambda_I}(\nu)\big(a\hat{\mu}^{\lambda_E}a^\dagger - a^\dagger a\hat{\mu}^{\lambda_E}\big) + s^{\lambda_I}(-\nu)\big(a^\dagger\hat{\mu}^{\lambda_E}a - aa^\dagger\hat{\mu}^{\lambda_E}\big) + \\ + s'^{\lambda_I}(\nu)\big(a^\dagger\hat{\mu}^{\lambda_E}a - \hat{\mu}^{\lambda_E}aa^\dagger\big) + s'^{\lambda_I}(-\nu)\big(a\hat{\mu}^{\lambda_E}a^\dagger - \hat{\mu}^{\lambda_E}a^\dagger a\big) + \\ - t^{\lambda_I}\big(a\hat{\mu}^{\lambda_E}a^\dagger + a^\dagger\hat{\mu}^{\lambda_E}a\big) + t'^{\lambda_I}\big(\hat{\mu}^{\lambda_E}a^\dagger a + \hat{\mu}^{\lambda_E}aa^\dagger\big)\end{aligned} \tag{5.95}$$

where

$$s^{\lambda_I}(\upsilon) = \int_0^\infty \mathrm{d}t\, e^{(\mathrm{i}\upsilon - \lambda_I)t}\operatorname*{Tr}_I\big[(\check{\rho}^{\lambda_I})^\dagger V e^{\mathcal{L}_I t}V\hat{\rho}^{\lambda_I}\big], \tag{5.96a}$$

$$s'^{\lambda_I}(\upsilon) = \int_0^\infty \mathrm{d}t\, e^{(\mathrm{i}\upsilon - \lambda_I)t}\operatorname*{Tr}_I\big[(\check{\rho}^{\lambda_I})^\dagger V e^{\mathcal{L}_I t}\hat{\rho}^{\lambda_I}V\big], \tag{5.96b}$$

$$t^{\lambda_I} = \int_0^\infty \mathrm{d}t\, e^{-\lambda_I t}\operatorname*{Tr}_I\big[(\check{\rho}^{\lambda_I})^\dagger\big[V, e^{\mathcal{L}_I t}V\hat{\rho}^{\lambda_I}\big]\big], \tag{5.96c}$$

$$t'^{\lambda_I} = \int_0^\infty \mathrm{d}t\, e^{-\lambda_I t}\operatorname*{Tr}_I\big[(\check{\rho}^{\lambda_I})^\dagger\big[V, e^{\mathcal{L}_I t}\hat{\rho}^{\lambda_I}V\big]\big], \tag{5.96d}$$

which is the solution reported in Eqs. (5.74) and (5.75).

Part IV

SPINOR SELF-ORDERING

We theoretically analyze the dynamics of cold atomic spins in a single-mode standing-wave cavity as a function of the intensity and phase of two transverse lasers, driving the atoms. We identify and discuss the conditions under which stable spatial patterns form, where atomic position and magnetization are correlated. We discuss the properties of the light emitted by the cavity as a method to reveal the state of the atomic vapor.

6

SPINOR SELF-ORDERING OF MAGNETIC ATOMS IN AN OPTICAL CAVITY

6.1 INTRODUCTION

A remarkable aspect of light-matter interactions inside optical cavities is the appearance of collective phenomena induced by multiple scattering of photons. Cavity photons exchange information between atoms across the cavity volume and mediate effective long-range interactions between them [210]. This leads to prominent collective effects such as synchronization [211–213] and spontaneous spatial ordering [214–216].

Among several setups, spontaneous pattern formation (*self-organization*) in cavities has been the object of several theoretical and experimental studies [214–222]. Self-organization occurs when an ensemble of polarizable particles is confined in an optical resonator and is driven by an external laser. If the laser intensity exceed a threshold value, the particles spontaneously order in space in a periodic structure (Bragg grating) with period λ_c, where λ_c is the cavity-mode wavelength. In this configuration the laser light that is scattered by the atoms into the cavity mode constructively interferes and leads to the build up of cavity field. In turn, the cavity field stabilizes the Bragg grating by means of the mechanical effects of light. In this process the atomic internal state remains in good approximation unchanged and can be eliminated from the dynamics.

Recent studies investigated setups where spatial self-organization is accompanied by correlations with internal degrees of freedom [47, 223–229]. One example are setups where different electronic ground states of the atoms are coupled via a Raman transition with cavity and laser photons, as for instance in Ref. [226]. Here the authors considered a Bose Einstein condensate with two effective internal states (spin states) confined in a optical cavity. Transitions between the spin states are induced via Raman scattering of two external pumping lasers into the cavity mode (see Fig. 6.1). For sufficiently high laser intensities, the system reaches an ordered state. This state involves a periodic spatial density with period $\lambda_c/2$ and a periodic spin structure with period λ_c. Experimental evidence of this phenomenon, called *spinor self-ordering*, has been discussed in Ref. [227]. Spatial-spin textures in ultra-cold gases have also been observed in Ref. [225].

In this Chapter we address the question whether spatial-spin structures can also arise in the dynamics of a thermal cloud of atoms confined in an optical cavity. Our analysis shows that the cloud can be cooled into spinor self-ordered structures. Furthermore we show how some

properties of the self-ordered state can be controlled by means of the external lasers. These properties can be measured at the cavity output.

In Section 6.2 we introduce the system and the basic equations describing its dynamics. In Section 6.3 we discuss the quantities that are relevant to characterize the state of the system. In Section 6.4 we analyze numerically the dynamics of the system, the properties of the self-ordered state and show how some properties can be externally controlled and measured. Finally in Section 6.5 we summarize the results and draw the conclusions.

6.2 SYSTEM AND MODEL

In this section we provide the details of our theoretical model and introduce the physical quantities which are relevant to the discussions in the rest of this chapter.

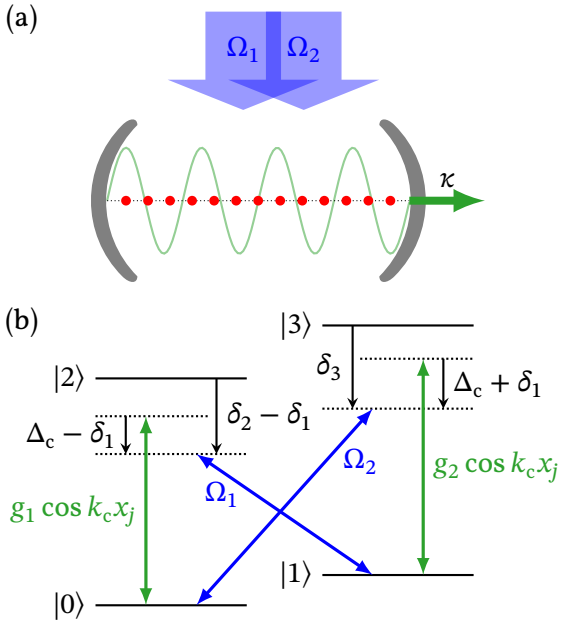

Figure 6.1: Sketch of the system. (a) N atoms tightly trapped in a lossy cavity and driven by 2 lasers with Rabi frequency Ω_1 and Ω_2; κ is the linewidth of the cavity. (b) Level scheme of the atoms. The relevant levels are the ground states $|0\rangle$ and $|1\rangle$ and the excited states $|2\rangle$ and $|3\rangle$. The external lasers drive the transitions $1 \leftrightarrow 2$ and $0 \leftrightarrow 3$ with Rabi frequency Ω_1 and Ω_2, respectively; while the transitions $0 \leftrightarrow 2$ and $1 \leftrightarrow 3$ are coupled to the cavity mode with strength $g_1 \cos(k_c \hat{x}_j)$ and $g_2 \cos(k_c \hat{x}_j)$, respectively; here $\hat{x}_j$ is the position of the atom and k_c is the wave vector of the cavity mode. The pump frequencies ω_{L1} and ω_{L2} and the cavity frequency ω_c are assumed to be far detuned from of the frequencies of the atomic transitions $0 \leftrightarrow 2$, $0 \leftrightarrow 3$, $1 \leftrightarrow 2$ and $1 \leftrightarrow 3$. The detunings δ_1, δ_2, δ_3 and Δ_c are defined in Appendix 6.A.

The physical system is illustrated in Figure 6.1: N atoms are confined inside a lossy cavity and are illuminated by two external pumping lasers.

We assume a tight trap along the transverse directions so that the atomic motion is confined along the cavity axis. The relevant states of the atoms are the ground states $|0\rangle$ and $|1\rangle$, and the excited states $|2\rangle$ and $|3\rangle$. The coupling of the atoms with the external lasers and the cavity mode form a double Λ configuration scheme. The first Λ scheme is formed by the transitions $0 \leftrightarrow 2 \leftrightarrow 1$: the $2 \leftrightarrow 1$ transition is driven by the first laser, while the transition $0 \leftrightarrow 2$ couples to the cavity mode. Similarly, the second Λ scheme is formed by the transitions $0 \leftrightarrow 3 \leftrightarrow 1$: transition $0 \leftrightarrow 3$ is driven by the second laser, while transition $3 \leftrightarrow 1$ is coupled to the same cavity mode. We assume the laser frequencies and the cavity frequency to be far detuned from the frequencies of the atomic transitions $0 \leftrightarrow 2$, $0 \leftrightarrow 3$, $1 \leftrightarrow 2$ and $1 \leftrightarrow 3$. This setting induces two-photon Raman transitions between the states $|0\rangle$ and $|1\rangle$, which form spin states. This setting has been considered in several other works, as for example Refs. [47, 226–229].

6.2.1 *Hamiltonian for N four-level atoms*

The Hamiltonian of the system composed by N transversally driven atoms and the cavity includes the kinetic and internal energies of the atoms, the interaction between the atoms and the lasers, the cavity energy and the interaction between the cavity and the atoms. The Hamiltonian can be cast into the sum of three terms

$$\hat{H}_{\text{sys}} = \hat{H}_{\text{at}} + \hat{H}_{\text{cav}} + \hat{H}_{\text{int}}. \tag{6.1}$$

The first term, $\hat{H}_{\text{at}}$, describes the dynamics of N four-level atoms driven by two lasers. In a convenient rotating frame (see Appendix 6.A) it reads ($\hbar = 1$)

$$\hat{H}_{\text{at}} = \sum_{j=1}^{N}\left(\frac{\hat{p}_j^2}{2m} - \sum_{\tau=1,2,3}\delta_\tau|\tau\rangle_j\langle\tau|\right) + \sum_{j=1}^{N}\Big(\Omega_1|2\rangle_j\langle 1| + \Omega_2|3\rangle_j\langle 0| + \text{h.c.}\Big). \tag{6.2}$$

Here $\hat{p}_j$ is the momentum operator of the atom j, m is the mass of the atoms and δ_τ are atomic detunings (see Appendix 6.A). The lasers drive the transitions $1 \leftrightarrow 2$ and $0 \leftrightarrow 3$ with Rabi frequencies Ω_1 and Ω_2, respectively.

The term $\hat{H}_{\text{cav}}$ describes the dynamics of the cavity mode and reads

$$\hat{H}_{\text{cav}} = -\Delta_c\hat{a}^\dagger\hat{a} \tag{6.3}$$

where Δ_c is the cavity detuning (see Appendix 6.A), and the operators $\hat{a}$ and $\hat{a}^\dagger$ annihilate and create, respectively, a cavity photon at frequency ω_c, with $[\hat{a}, \hat{a}^\dagger] = 1$.

The atom-photon interaction is treated in dipole and rotating-wave approximation. The transitions $0 \leftrightarrow 2$ and $1 \leftrightarrow 3$ are coupled to a cavity

mode with space-dependent strength $g_1 \cos(k_c \hat{x}_j)$ and $g_2 \cos(k_c \hat{x}_j)$, respectively. Here g_i are the vacuum Rabi frequencies, $\hat{x}_j$ is the position operator of the j-th atom and is the canonical conjugate operator of the momentum $\hat{p}_j$ with $[\hat{x}_j, \hat{p}_l] = i\hbar\delta_{jl}$, $k_c = 2\pi/\lambda_c$ is the wave vector of the cavity mode and λ_c its wavelength. The corresponding Hamiltonian reads

$$\hat{H}_{\text{int}} = \sum_{j=1}^{N} \cos(k_c \hat{x}_j)(g_1 \hat{a}^\dagger |0\rangle_j\langle 2| + g_2 \hat{a}^\dagger |1\rangle_j\langle 3| + \text{h.c.}). \tag{6.4}$$

We consider a cavity with losses at rate κ. In the following of this chapter we will use both the master equation and the Heisenberg-Langevin equation formalism. When using the master equation formalism we model the cavity losses with the superoperator

$$\mathcal{L}_\kappa \hat{\rho} = \kappa(2\hat{a}\hat{\rho}\hat{a}^\dagger - \hat{a}^\dagger\hat{a}\hat{\rho} - \hat{\rho}\hat{a}^\dagger\hat{a}), \tag{6.5}$$

where $\hat{\rho}$ is the density matrix of the system. When using the Heisenberg-Langevin equation formalism the cavity losses will be taken into account with a damping term $-\kappa\hat{a}$ and the corresponding Gaussian noise $\sqrt{2\kappa}\hat{a}^{\text{in}}$. The details will be clear when we introduce the two formalism.

6.2.2 *Adiabatic elimination of the excited states*

When the laser frequencies ω_{L1} and ω_{L2} and the cavity frequency ω_c are far detuned from atomic transition frequencies, i. e., $\delta_2, \delta_3 \gg \delta_1, \Delta_c$, the excited states $|2\rangle$ and $|3\rangle$ of the atoms can be adiabaticaly eliminated from the dynamics. We now follow the derivation given in [218]. Let us first assume that the particles do not move so that the couplings $g_{1,2} \cos(k_c \hat{x}_j)$ with the cavity field are fixed. In this case the states $|2\rangle$ and $|3\rangle$ of the atoms can be eliminated in second order in an expansion in the parameter $1/\delta$, $\delta = \min(|\delta_2|, |\delta_3|)$, assuming that [230] $\delta \gg |\delta_1|, |\Delta_c|, \kappa, \sqrt{N\bar{n}}g_1$, $\sqrt{N\bar{n}}g_2, \sqrt{N}\Omega_1, \sqrt{N}\Omega_2$, with $\bar{n}$ the mean photon number in the cavity. If the center-of-mass motions is considered, then the coupling strengths $g_{1,2} \cos(k_c \hat{x}_j)$ vary with time. Furthermore atoms with different velocities experience different Doppler shifts, which modify the resonance condition. These effects can be neglected when the corresponding time scales are longer than the typical time scale in which the excited states are occupied, i. e., when $\omega_r, k_c \bar{p}_j/m \ll \delta$ (with $\bar{p}_j = \sqrt{\langle \hat{p}_j^2 \rangle}$) [183, 231]. Here we have used the recoil frequency

$$\omega_r = \frac{\hbar k_c^2}{2m}, \tag{6.6}$$

which scales the exchange of mechanical energy between photons and atoms.

We adiabatically eliminate the excited states $|2\rangle$ and $|3\rangle$ by means of a projection method [201] (the calculations are shown in Appendix 6.B)

and obtain the effective Hamiltonian of the system composed by the two ground states $|0\rangle$ and $|1\rangle$, which are the spin states, and the cavity mode. This Hamiltonian is the sum of the kinetic and internal energies of the spins, the cavity energy and the interaction of the spins with the cavity mode and can be cast as a sum of three terms

$$\hat{H} = \hat{H}_{\mathrm{S}} + \hat{H}_{\mathrm{C}} + \hat{H}_{\mathrm{I}}. \tag{6.7}$$

The first term describes the dynamics of free spins and reads

$$\hat{H}_{\mathrm{S}} = \sum_{j=1}^{N}\left(\frac{\hat{p}_j^2}{2m} + \Delta_{\mathrm{e}}\hat{\sigma}_j^\dagger\hat{\sigma}_j\right), \tag{6.8}$$

where $\hat{\sigma}_j = |0\rangle_j\langle 1|$ is the lowering operator for the j-th spin. The Stark-shifted energy splitting between the states $|0\rangle$ and $|1\rangle$ is $\Delta_{\mathrm{e}} = |\Omega_1|^2/\delta_2 - |\Omega_2|^2/\delta_3 - \delta_1$. The second term describes the cavity energy and reads

$$\hat{H}_{\mathrm{C}} = -\left[\Delta_{\mathrm{c}} - \sum_{j=1}^{N}\left(U_1\hat{\sigma}_j\hat{\sigma}_j^\dagger + U_2\hat{\sigma}_j^\dagger\hat{\sigma}_j\right)\cos^2(k_{\mathrm{c}}\hat{x}_j)\right]\hat{a}^\dagger\hat{a}. \tag{6.9}$$

It contains the shift of the cavity frequency due to the interaction with the atoms, which scales with the frequencies $U_1 = |g_1|^2/\delta_2$ and $U_2 = |g_2|^2/\delta_3$. The last term describes the interaction of the spins with the cavity and reads

$$\hat{H}_{\mathrm{I}} = \sum_{j=1}^{N}\left(S_1\hat{a}^\dagger\hat{\sigma}_j + S_1^*\hat{\sigma}_j^\dagger\hat{a} + S_2\hat{a}^\dagger\hat{\sigma}_j^\dagger + S_2^*\hat{a}\hat{\sigma}_j\right)\cos\left(k_{\mathrm{c}}\hat{x}_j\right), \tag{6.10}$$

where the coupling strength are $S_1 = \Omega_1 g_1/\delta_2$ and $S_2 = \Omega_2 g_2/\delta_3$.

6.2.3 *Heisenberg-Langevin equations*

Using Hamiltonian (6.7) we now write the Heisenberg-Langevin equations for the position and momentum operators $\hat{x}_j$ and $\hat{p}_j$ and for the Hermitian operators

$$\hat{\sigma}_j^x = \hat{\sigma}_j + \hat{\sigma}_j^\dagger, \quad \hat{\sigma}_j^y = \mathrm{i}\left(\hat{\sigma}_j - \hat{\sigma}_j^\dagger\right), \quad \hat{\sigma}_j^z = |1\rangle_j\langle 1| - |0\rangle_j\langle 0|, \tag{6.11a}$$

$$\hat{a}_{\mathrm{r}} = \frac{\hat{a} + \hat{a}^\dagger}{2}, \quad \hat{a}_{\mathrm{i}} = \mathrm{i}\frac{\hat{a}^\dagger - \hat{a}}{2}. \tag{6.11b}$$

The operators (6.11a) are Pauli operators and fulfill the commutation and anti-commutation relations

$$[\hat{\sigma}_j^n, \hat{\sigma}_l^m] = \sum_{q=x,y,z} 2\mathrm{i}\hat{\sigma}_j^q\varepsilon_{nmq}\delta_{jl}, \tag{6.12a}$$

$$\{\hat{\sigma}_j^n, \hat{\sigma}_l^m\} = 2\left[\delta_{nm}\delta_{jl}\mathbb{1} + \hat{\sigma}_j^n\hat{\sigma}_l^m(1 - \delta_{jl})\right]. \tag{6.12b}$$

Here ε_{nmq} is the Levi-Civita symbol and $n, m, q \in \{x, y, z\}$. The operators (6.11b) fulfill the commutation relation $[\hat{a}_{\mathrm{r}}, \hat{a}_{\mathrm{i}}] = \mathrm{i}/2$.

The Heisenberg-Langevin equations read ($\hbar = 1$)

$$\frac{\mathrm{d}}{\mathrm{d}t}\hat{x}_j = \frac{\hat{p}_j}{m}, \tag{6.13a}$$

$$\frac{\mathrm{d}}{\mathrm{d}t}\hat{p}_j = k_\mathrm{c}\sin\!\big(k_\mathrm{c}\hat{x}_j\big)\Big\{\big(R^+\hat{\sigma}_j^x\hat{a}_\mathrm{r} - R^-\hat{\sigma}_j^y\hat{a}_\mathrm{i} + I^+\hat{\sigma}_j^x\hat{a}_\mathrm{i} + I^-\hat{\sigma}_j^y\hat{a}_\mathrm{r}\big) + \\ + \cos\!\big(k_\mathrm{c}\hat{x}_j\big)\Big[U_1\big(1-\hat{\sigma}_j^z\big) + U_2\big(1+\hat{\sigma}_j^z\big)\Big]\Big(\hat{a}_\mathrm{r}^2 + \hat{a}_\mathrm{i}^2 - \frac{1}{2}\Big)\Big\}, \tag{6.13b}$$

$$\frac{\mathrm{d}}{\mathrm{d}t}\hat{\sigma}_j^x = -\Big[\Delta_\mathrm{e} - (U_1-U_2)\cos^2\!\big(k_\mathrm{c}\hat{x}_j\big)\Big(\hat{a}_\mathrm{r}^2 + \hat{a}_\mathrm{i}^2 - \frac{1}{2}\Big)\Big]\hat{\sigma}_j^y + \\ + 2\cos\!\big(k_\mathrm{c}\hat{x}_j\big)\hat{\sigma}_j^z[I^-\hat{a}_\mathrm{r} - R^-\hat{a}_\mathrm{i}], \tag{6.13c}$$

$$\frac{\mathrm{d}}{\mathrm{d}t}\hat{\sigma}_j^y = \Big[\Delta_\mathrm{e} - (U_1-U_2)\cos^2\!\big(k_\mathrm{c}\hat{x}_j\big)\Big(\hat{a}_\mathrm{r}^2 + \hat{a}_\mathrm{i}^2 - \frac{1}{2}\Big)\Big]\hat{\sigma}_j^x + \\ - 2\cos\!\big(k_\mathrm{c}\hat{x}_j\big)\hat{\sigma}_j^z[R^+\hat{a}_\mathrm{r} + I^+\hat{a}_\mathrm{i}], \tag{6.13d}$$

$$\frac{\mathrm{d}}{\mathrm{d}t}\hat{\sigma}_j^z = -2\cos\!\big(k_\mathrm{c}\hat{x}_j\big)\big[I^-\hat{\sigma}_j^x\hat{a}_\mathrm{r} - I^+\hat{\sigma}_j^y\hat{a}_\mathrm{i} - R^-\hat{\sigma}_j^x\hat{a}_\mathrm{i} - R^+\hat{\sigma}_j^y\hat{a}_\mathrm{r}\big], \tag{6.13e}$$

$$\frac{\mathrm{d}}{\mathrm{d}t}\hat{a}_\mathrm{r} = -\left[\Delta_\mathrm{c} - \sum_{j=1}^{N}\left(U_1\frac{1-\hat{\sigma}_j^z}{2} + U_2\frac{1+\hat{\sigma}_j^z}{2}\right)\cos^2\!\big(k_\mathrm{c}\hat{x}_j\big)\right]\hat{a}_\mathrm{i} + \\ + \sum_{j=1}^{N}\frac{\cos\!\big(k_\mathrm{c}\hat{x}_j\big)}{2}\big[\hat{\sigma}_j^x I^+ - \hat{\sigma}_j^y R^-\big] - \kappa\hat{a}_\mathrm{r} + \sqrt{2\kappa}\hat{a}_\mathrm{r}^\mathrm{in}, \tag{6.13f}$$

$$\frac{\mathrm{d}}{\mathrm{d}t}\hat{a}_\mathrm{i} = \left[\Delta_\mathrm{c} - \sum_{j=1}^{N}\left(U_1\frac{1-\hat{\sigma}_j^z}{2} + U_2\frac{1+\hat{\sigma}_j^z}{2}\right)\cos^2\!\big(k_\mathrm{c}\hat{x}_j\big)\right]\hat{a}_\mathrm{r} + \\ - \sum_{j=1}^{N}\frac{\cos\!\big(k_\mathrm{c}\hat{x}_j\big)}{2}\big[\hat{\sigma}_j^x R^+ + \hat{\sigma}_j^y I^-\big] - \kappa\hat{a}_\mathrm{i} + \sqrt{2\kappa}\hat{a}_\mathrm{i}^\mathrm{in}. \tag{6.13g}$$

where $R^\pm = \Re(S_1) \pm \Re(S_2)$ and $I^\pm = \Im(S_1) \pm \Im(S_2)$. The noise terms are

$$\hat{a}_\mathrm{r}^\mathrm{in} = \frac{\hat{a}_\mathrm{in} + \hat{a}_\mathrm{in}^\dagger}{2}, \qquad \hat{a}_\mathrm{i}^\mathrm{in} = \mathrm{i}\frac{\hat{a}_\mathrm{in}^\dagger - \hat{a}_\mathrm{in}}{2}, \tag{6.14}$$

and have the correlations

$$\langle\hat{a}_\mathrm{r}^\mathrm{in}(t)\hat{a}_\mathrm{r}^\mathrm{in}(t')\rangle = \langle\hat{a}_\mathrm{i}^\mathrm{in}(t)\hat{a}_\mathrm{i}^\mathrm{in}(t')\rangle = \frac{\delta(t-t')}{4}, \\ \langle\hat{a}_\mathrm{r}^\mathrm{in}(t)\hat{a}_\mathrm{i}^\mathrm{in}(t')\rangle = \mathrm{i}\frac{\delta(t-t')}{4}, \\ \langle\hat{a}_\mathrm{i}^\mathrm{in}(t)\hat{a}_\mathrm{r}^\mathrm{in}(t')\rangle = -\mathrm{i}\frac{\delta(t-t')}{4}. \tag{6.15}$$

The noise operators $\hat{a}_\mathrm{in}$ and $\hat{a}_\mathrm{in}^\dagger$ in Eq. (6.14) are Gaussian noises with $\langle\hat{a}_\mathrm{in}(t)\rangle = \langle\hat{a}_\mathrm{in}^\dagger(t)\rangle = \langle\hat{a}_\mathrm{in}^\dagger(t)\hat{a}_\mathrm{in}(t')\rangle = 0$ and $\langle\hat{a}_\mathrm{in}(t)\hat{a}_\mathrm{in}^\dagger(t')\rangle = \delta(t-t')$. The expectation values $\langle\cdot\rangle$ are taken over the tensor product between the initial density matrix of the system and the external Markovian environment with vanishing mean number of photons [232].

We perform our study by replacing the operators in Eqs. (6.13) with scalar functions, i. e. $\langle \hat{o}(t) \rangle = o(t)$ for any symmetrically ordered operator $\hat{o}$, and the average is taken over the initial state of the system (see Appendix 6.C.2 for a description of the initial state). We include cavity shot-noise as diagonal stochastic terms in the equations for the cavity field [233, 234]. With these approximation Eqs. (6.13) become a system of stochastic differential equations. A comparison of these stochastic differential equations with the equations obtained by a semiclassical approximation is attempted in Section 6.D.

6.3 PRELIMINAR DISCUSSION

6.3.1 *Relevant quantities*

We consider the case $|S_1| = |S_2| = S$ and without loss of generality we choose $S_1 = S \in \mathbb{R}$ and $S_2 = S\mathrm{e}^{-\mathrm{i}2\phi}$. Here $2\phi \in [-\pi, \pi)$ is the relative phase between the Rabi frequencies Ω_1 and Ω_2 of the external lasers, and S is the Raman coupling strength. In this case the interaction term, Eq. (6.10), can be written as

$$H_{\mathrm{I}} = NS\mathrm{e}^{-\mathrm{i}\phi}\hat{\Phi}\hat{a}^\dagger + NS\mathrm{e}^{\mathrm{i}\phi}\hat{\Phi}\hat{a} = NS\hat{\Phi}\left(\mathrm{e}^{\mathrm{i}\phi}\hat{a} + \mathrm{e}^{-\mathrm{i}\phi}\hat{a}^\dagger\right), \tag{6.16}$$

where the operator $\hat{\Phi}$ is defined as

$$\hat{\Phi} = \cos(\phi)\hat{X} + \sin(\phi)\hat{Y}, \quad \phi \in [-\frac{\pi}{2}, \frac{\pi}{2}). \tag{6.17}$$

We call $\hat{X}$ and $\hat{Y}$ the generalized collective spin operators [213, 235] defined by

$$\hat{X} = \frac{1}{N}\sum_{j=1}^{N} \hat{\sigma}_j^x \cos\left(k_{\mathrm{c}}\hat{x}_j\right), \tag{6.18a}$$

$$\hat{Y} = \frac{1}{N}\sum_{j=1}^{N} \hat{\sigma}_j^y \cos\left(k_{\mathrm{c}}\hat{x}_j\right). \tag{6.18b}$$

If the motion of the atoms is neglected and the atomic positions are fixed at the cavity field maxima, i. e. $\cos\left(k_{\mathrm{c}}\hat{x}_j\right) = 1, \forall j = 1, \ldots, N$, then the generalized collective spin operators $\hat{X}$ and $\hat{Y}$ reduce to the x and y components of the collective spin[1] $\hat{\boldsymbol{J}} = (\hat{J}_x, \hat{J}_y, \hat{J}_z)$ where

$$\hat{J}_i = \frac{1}{N}\sum_{j=1}^{N} \hat{\sigma}_j^i, \quad i = x, y, z. \tag{6.19}$$

In this case the system is equivalent to the Dicke model [237–239] and the average values $\langle \hat{J}_x \rangle$ and $\langle \hat{J}_y \rangle$ being different from zero indicates the build-up of macroscopic coherence in the spins of different atoms [240].

1 Typically the spins $\hat{S}_i = N\hat{J}_i$, with $i = x, y, z$ are called collective spin operators because they fulfill the well-known commutation relations $[S_i, S_j] = \sum_{l=x,y,z} 2\epsilon_{ijl}S_l$ [236].

This phenomenon is called superradiance. For this particular case, i. e. when the atoms are fixed at the cavity field maxima, the average values of $\langle \hat{J}_x \rangle = \langle \hat{X} \rangle$ and $\langle \hat{J}_y \rangle = \langle \hat{Y} \rangle$ can be different from zero if the spins, on average, are partially aligned along the x or the y direction, respectively.

However, other spatial spin structures can give rise to a non-vanishing value of $\langle \hat{X} \rangle$ and $\langle \hat{Y} \rangle$. For instance, if the atoms are localized at the anti-nodes of the cavity field mode, we can observe a non-vanishing value of $\langle \hat{X} \rangle$ or $\langle \hat{Y} \rangle$ if the spins organize in a ferromagnetic pattern. This spatial-spin pattern is an example of correlations between internal and external degrees of freedom since

$$\langle \hat{X} \rangle = \frac{1}{N} \sum_{j=1}^{N} \langle \hat{\sigma}_j^x \cos(k_c \hat{x}_j) \rangle \neq \frac{1}{N} \sum_{j=1}^{N} \langle \hat{\sigma}_j^x \rangle \langle \cos(k_c \hat{x}_j) \rangle, \tag{6.20}$$

or similarly for $\langle \hat{Y} \rangle$. The correlations between the positions of the atoms and their spin can be measured by the generalized collective spin operators $\hat{X}$ and $\hat{Y}$, Eq. (6.18). In these operators, in fact, the spins $\hat{\sigma}_j^i$ are weighted with the amplitude of the cavity field at the position of the atom j itself.

We interpret the expectation values

$$X = \langle \hat{X} \rangle, \tag{6.21a}$$

$$Y = \langle \hat{Y} \rangle \tag{6.21b}$$

as the components of a two dimensional vector (X, Y) that in the special case $\cos(k_c \hat{x}_j) = 1, \forall j = 1, \ldots, N$ is the projection of the Bloch vector $\langle \hat{\boldsymbol{J}} \rangle$, Eq. (6.19), in the $x - y$ plane. We then define the collective spin phase as

$$\phi_s = \arg(X + iY), \tag{6.22}$$

which is the angle between the generalized collective spin vector (X, Y) and the x-axis in the $x - y$ plane, see Fig. 6.2.

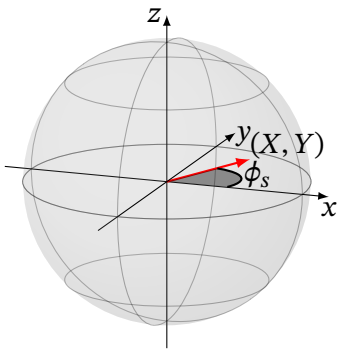

Figure 6.2: Representation of the collective spin phase ϕ_s, eq. (6.22), on the Bloch sphere.

So far we only discussed a static picture of the atoms. In general the atoms are moving, thus the position of the atoms, and their coupling with the cavity field mode, will vary with time. One important question

that we address in our work is weather correlations $\langle \hat{X} \rangle, \langle \hat{Y} \rangle \neq 0$ can arise in presence of motion. To quantify the motion of the atoms we introduce the average kinetic energy per particle

$$E_{\text{kin}} = \frac{1}{N} \sum_{j=1}^{N} \frac{\langle \hat{p}_j^2 \rangle}{2m}. \tag{6.23}$$

Moreover, to analyze the atomic spatial pattern in the cavity field mode we introduce the bunching parameter

$$\mathcal{B} = \frac{1}{N} \langle \sum_{j=1}^{N} \cos(k_c x_j)^2 \rangle \tag{6.24}$$

which characterizes the spatial distribution of the atoms: If the atoms are uniformly distributed then $\mathcal{B} \approx 0.5$, if the atoms are localized at the cavity intensity maxima (minima) then $\mathcal{B} \approx 1$ ($\mathcal{B} \approx 0$).

6.3.2 *Spinor self-ordered state and broken symmetry*

We show numerically in Sec. 6.4.1 the existence of a pumping threshold S_c: If the system is driven below threshold $S < S_c$, then the cavity mode is empty and there is no correlations between the position and the phase of the spins of the atoms. If the system is driven above threshold $S > S_c$ then the cavity mode is populated and there is a build-up of correlations between atomic positions and spins phase. The latter is called the spinor self-ordered state. Here we discuss qualitatively some properties of the spinor self-ordered state in order to make the rest of the discussion clearer.

The spinor self-ordered state involves spatial density ordering with periodicity $\lambda_c/2$ with the atoms localized at the cavity intensity maxima, and spatial spin ordering with periodicity λ_c: all atoms localized at odd anti-nodes of the cavity field have their spin aligned along the direction θ (on the equator of the Bloch sphere), and all atoms localized at even anti-nodes have their spin aligned along $\theta + \pi$, see Fig. 6.3. The angle θ, in this idealized picture, is one of ϕ_s or $\phi_s + \pi$, Eq. (6.22). In this configuration the atoms scatter light in phase into the cavity mode. The discrete $\mathbb{Z}_2$ symmetry associated with the transformation $(\hat{a}, \hat{\sigma}_j,) \to (-\hat{a}, -\hat{\sigma}_j)$, i. e. with the sign change of the cavity field and with the flip of all the spins, is broken by the transition into the self-ordered state. The breaking of the $\mathbb{Z}_2$ symmetry corresponds to the expectation value of the operator $\hat{\Phi}$

$$\Phi = \langle \hat{\Phi} \rangle = \cos(\phi) X + \sin(\phi) Y \tag{6.25}$$

being positive or negative, while $\Phi = 0$ below threshold $S < S_c$. The quantity Φ being different from zero indicates the build-up of correlations between the atomic positions and their spin phase. We identify Φ as an order parameter.

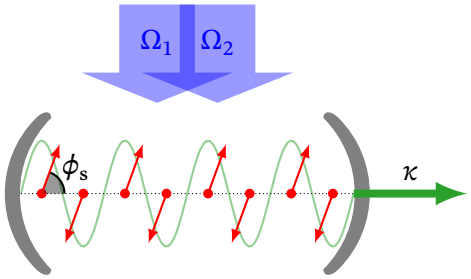

Figure 6.3: Sketch of the spinor self-ordered state: The spin of the atoms localized at the maxima of the cavity field assume the opposite direction respect to the spin of the atoms which localize at the cavity-field minima. In this configuration the atoms scatter light in phase into the cavity mode. The state represented in this sketch is only one of the two possible (for a fixed ϕ), the other being the one with all the spins pointing in the opposite direction.

Some properties of the self-ordered state can be qualitatively understood by looking for the states which minimize the energy. Neglecting U_1, U_2 and the noise terms due to cavity losses, the steady state of the cavity field is

$$\hat{a} \simeq \frac{NSe^{-i\phi}\hat{\Phi}}{\Delta_c + i\kappa}, \tag{6.26}$$

i. e. the cavity field amplitude $\langle \hat{a} \rangle$ is proportional to the order parameter Φ. The interaction energy, Eq. (6.16), scales then as $\hat{H}_I \propto \Delta_c \hat{\Phi}^2$. Since we choose $\Delta_c < 0$, the energy is minimal if $|\Phi|$ is maximal. Notice that the energy remains constant upon a sign change of the order parameter Φ. The fact that the system, in order to minimize the energy, can randomly choose the sign of Φ is associated with the breaking of the $\mathbb{Z}_2$ symmetry discussed earlier.

The maximization of $|\Phi|$ has several implications on the properties of the self-ordered state. First, according to Eq. (6.26), maximizing $|\Phi|$ corresponds to maximizing the scattering of light into the cavity mode and having non-zero population into the cavity mode. Furthermore, since Φ is the scalar product between the vector (X, Y) and the vector $(\cos\phi, \sin\phi)$, maximizing $|\Phi|$ means having the vector (X, Y) co-linear with $(\cos\phi, \sin\phi)$, i. e.

$$\phi_s = \begin{cases} \phi & \text{if } \Phi > 0, \\ \phi + \pi & \text{if } \Phi < 0, \end{cases} \tag{6.27}$$

the definition of ϕ_s is given in Eq. (6.22). Table 6.1 reports the sign of the order parameter Φ and of the expectation values X and Y for the two states which break the $\mathbb{Z}_2$ symmetry, in dependence of the sign of the phase ϕ. The condition given in Eq. (6.27) allows us to control the spin phase ϕ_s by controlling ϕ. This is shown numerically in Sec. 6.4.5.

PHASE ϕ	X AND Y	ORDER PARAMETER Φ
$\phi > 0$	$X > 0,\ Y > 0$	$\Phi > 0$
	$X < 0,\ Y < 0$	$\Phi < 0$
$\phi < 0$	$X > 0,\ Y < 0$	$\Phi > 0$
	$X < 0,\ Y > 0$	$\Phi < 0$

Table 6.1: Sign of the expectation values X and Y and of the order parameter Φ calculated in the states which break the $\mathbb{Z}_2$ symmetry, in dependence of the sign of the phase $\phi \in [-\pi/2, \pi/2)$.

Furthermore Eq. (6.26) allows us also to calculate the phase ϕ_c of the cavity field as a function of ϕ, which in the case $\Delta_c < 0$ reads

$$\phi_c = \begin{cases} \arctan\left(\frac{-\kappa}{\Delta_c}\right) - \phi - \pi & \text{if } \Phi > 0, \\ \arctan\left(\frac{-\kappa}{\Delta_c}\right) - \phi & \text{if } \Phi < 0. \end{cases} \tag{6.28}$$

In the following we will investigate numerically the time evolution of the system and its ordering properties in dependence of the pumping strength S and of the phase ϕ.

6.4 NUMERICAL RESULTS

We numerically integrate the stochastic differential equations obtained in Sec. 6.2.3 with the Monte-Carlo based method of Ref. [241]. The initial state that we use is unordered. It consists of the atoms uniformly distributed in space and in a thermal state. The initial internal atomic state is randomly chosen such that it is close to the ground state $|0\rangle$ with high probability. For more details see Sec. 6.C.2. All the simulations are performed with $N = 100$ particles. The other parameters are reported case by case.

6.4.1 *Threshold*

We calculate the steady state of the system for several values of the pumping strength S and report in Figs. 6.4 the cavity population $\langle \hat{a}^\dagger \hat{a} \rangle$, the absolute value of the order parameter $|\Phi|$ and the bunching parameter $\mathcal{B}$, for different values of the energy spitting Δ_e between the spins states, Eq. (6.8). We observe the existence of a Δ_e-dependent pumping threshold $S_c(\Delta_e)$. When the system is driven below threshold $S < S_c(\Delta_e)$, the cavity mode is empty (see Fig. 6.4(a)), there is no correlations between spins and position (see Fig. 6.4(b)) and the atoms are uniformly distributed in space (see Fig. 6.4(c)). In this state, the laser light scattered by the atoms inside the cavity has a random phase and destructively interfere.

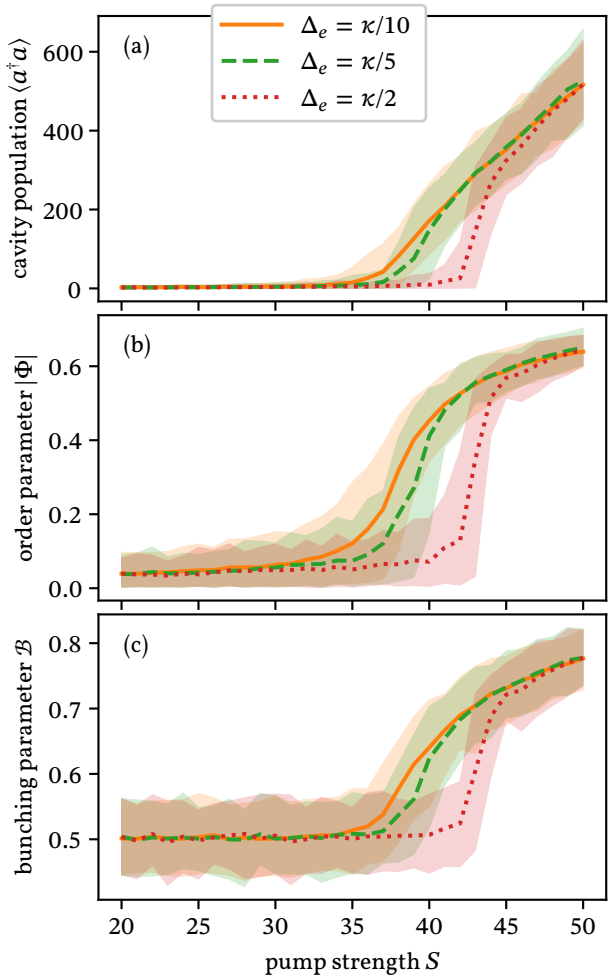

Figure 6.4: Spinor self-ordering as a function of the pumping strength S. (a) Cavity population $\langle \hat{a}^\dagger \hat{a} \rangle$, (b) order parameter $|\Phi|$, Eq. (6.17), and (c) bunching parameter $\mathcal{B}$, Eq. (6.24); for $\Delta_e = \kappa/10$ (dashed green) over 183 trajectories, $\Delta_e = \kappa/5$ (dotted red) over 102 trajectories and $\Delta_e = \kappa/2$ (dashed dotted purple) over 102 trajectories. The shaded regions contain 90% of the trajectories. All the quantities are calculated at time $t = 800\omega_r^{-1}$. The parameters used are $\kappa = 100\omega_r$, $\Delta_c = -\kappa$, $U_1 = U_2 = 0$ and $N = 100$.

If the pumping strength is larger than the threshold $S > S_c(\Delta_e)$, then the atoms self-organize and scatter the laser light constructively into the cavity: the cavity field builds up (see Fig. 6.4(a)), the atomic positions and spins phase are correlated (see Fig. 6.4(b)) and the atoms localize (see Fig. 6.4(c)). In the following we first show the dynamics that, above threshold $S > S_c$, leads to the ordered state and then characterize some of its properties.

6.4.2 *Dynamics*

We show in Fig. 6.5 the typical time evolution of some observables of the system when driven above threshold $S > S_c$. The state which breaks

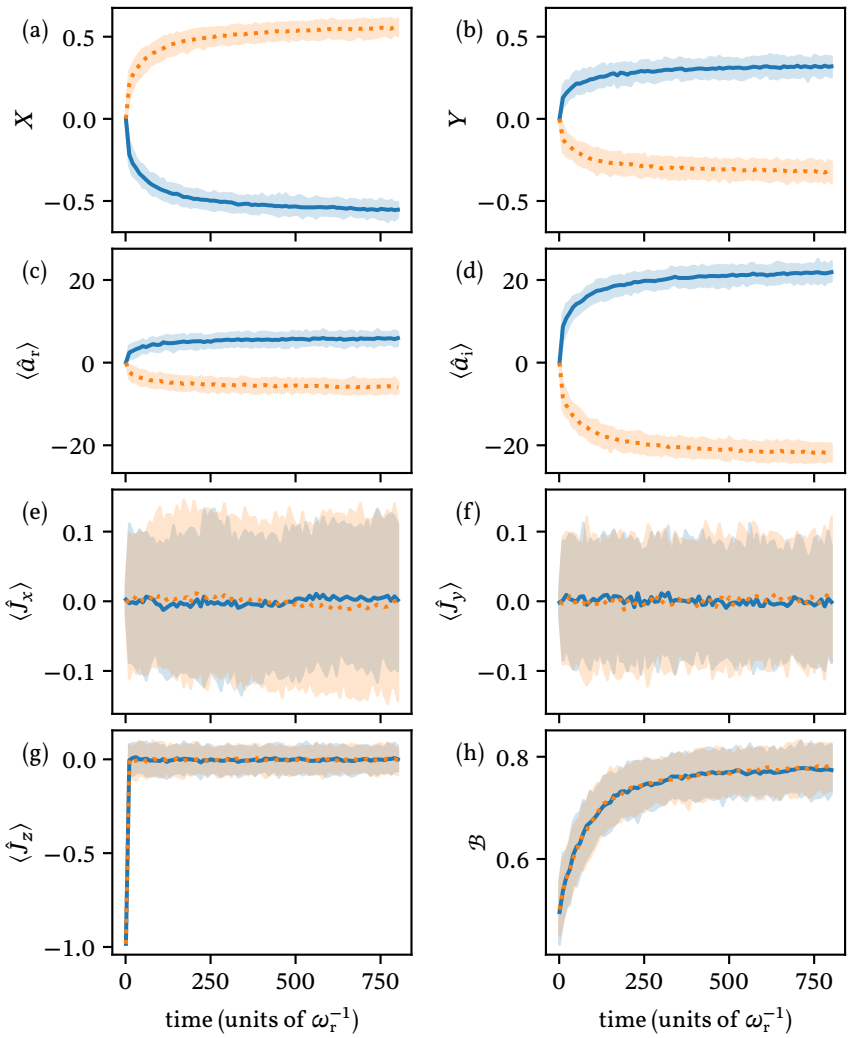

Figure 6.5: Dynamics of the system calculated with 192 trajectories for $N = 100$ particles. (a) Order parameter X, (b) order parameter Y, (c) real and (d) imaginary part of the cavity field, (e) collective spin $\langle J_x \rangle$, (f) collective spin $\langle J_y \rangle$, (g) collective spin $\langle J_z \rangle$ and (h) bunching parameter $\langle \mathcal{B} \rangle$. The shaded region contains 90% of the trajectories. The solid blue line corresponds to the state with $\Phi < 0$, the dotted orange line corresponds to $\Phi > 0$. The parameters used are $E_{\mathrm{kin}}(0) = \hbar\kappa$, $\kappa = 100\omega_r$, $\Delta_c = -\kappa$, $\Delta_e = \kappa/10$, $U_1 = U_2 = 0$, $\phi = -\pi/6$ and $S = 0.5\kappa$.

the $\mathbb{Z}_2$ symmetry with $\Phi < 0$ corresponds to the solid blue line, while the state with $\Phi > 0$ corresponds to the dotted orange line. In this plot $\phi = -\pi/6$ and the generalized collective spins X and Y, shown in panels (a) and (b), fulfill the conditions given in Tab. 6.1, as expected. Panels (c)

and (d) show the real and imaginary part of the cavity field, respectively. The phase of the cavity field is $\phi_c^+ \approx -7\pi/12$ for $\Phi > 0$, and $\phi_c^- \approx 5\pi/12$ for $\Phi < 0$, in agreement with Eq. (6.28). The collective spins $\langle \hat{J}_i \rangle$, Eq. (6.19), have zero expectation values both in the initial state, which is unordered, and in the ordered state (see panels (e-g)). Figure 6.5(h) displays the bunching parameter $\mathcal{B}$: In the initial state it has the value $\mathcal{B}(t = 0) \approx 0.5$ as expected for an uniform spatial density, while in the final state $\mathcal{B}(t = 800\omega_r^{-1}) \approx 0.8$ indicating that the atoms have localized at the cavity intensity maxima.

6.4.3 *Cooling*

Figure 6.6(a) shows the mean kinetic energy per atom, Eq. (6.23), as a function of time: The initial momentum distribution of the atoms is Gaussian with mean kinetic energy $E_{kin}(0) = 10\hbar\kappa$. The atomic motion is cooled and the atoms reach the mean kinetic energy of $E_{kin}(400\omega_r^{-1}) \approx \hbar\kappa$. This coincides with the temperature limit of cavity cooling [74, 75]. Figure 6.6(b) shows the Gaussian momentum distribution of the initial state and the momentum distribution of the final state. It is evident that the momentum distribution in the final state has a smaller width indicating that the atoms are colder. We observe that the atoms are cooled when the system is driven with a pumping strength S that can be both below and above the threshold S_c.

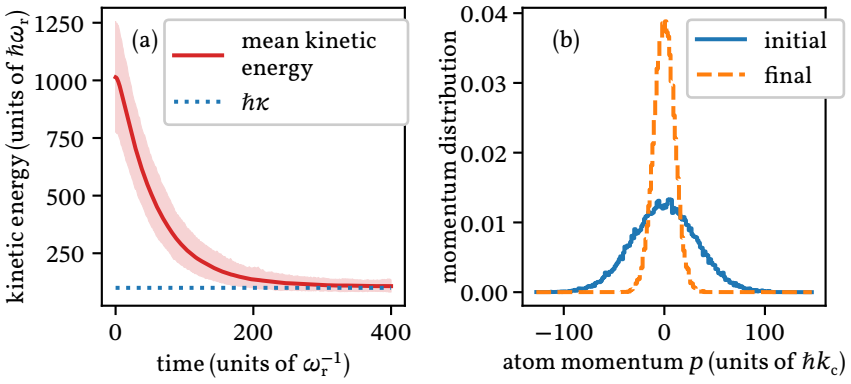

Figure 6.6: (a) Mean kinetic energy E_{kin} (solid red line) of $N = 100$ atoms as a function of time, calculated over 399 trajectories. The shaded region contains 90% of the trajectories. The dotted blue line corresponds to $E_{kin} = \hbar\kappa$. (b) Momentum distribution of the atoms in the initial ($t = 0$) state (solid blue) and in the final ($t = 400\omega_r^{-1}$) state (dashed orange). The initial distribution of momenta is a Gaussian distribution with kinetic energy $E_{kin}(0) = 10\hbar\kappa$. The parameters used are $\kappa = 100\omega_r$, $\Delta_c = -\kappa$, $\Delta_e = \kappa/100$, $U_1 = U_2 = 0$, $S = 0.2\kappa$ and $\phi = 0$. In this parameters range the system is unordered.

6.4.4 *Spin-position correlations*

The correlations between the position of the atoms and their spin phase in either of the broken symmetry states are reported in Fig. 6.7. The data correspond to Fig. 6.5 at the final time $t = 800\omega_r^{-1}$. The two states are connected by the transformation that flips the spins and change the phase of the cavity field by a factor π, as discussed in Sec. 6.3.2. The spin flip is evident in Fig. 6.7 when comparing the top panels (which report the correlations for the state with $\Phi < 0$) with the lower panels (which report the correlations for the state with $\Phi > 0$). The phase of the cavity field also changes by a factor π, in fact it is ${\phi_c}^- \simeq 5\pi/12$ for $\Phi < 0$ and ${\phi_c}^+ \simeq -7\pi/12$ for $\Phi > 0$, as discussed in Sec. 6.4.2. Figure 6.7 also shows that, in both states with $\Phi \gtrless 0$, the spatial density has periodicity $\lambda_c/2$ and that the phase of the spins has periodicity λ_c.

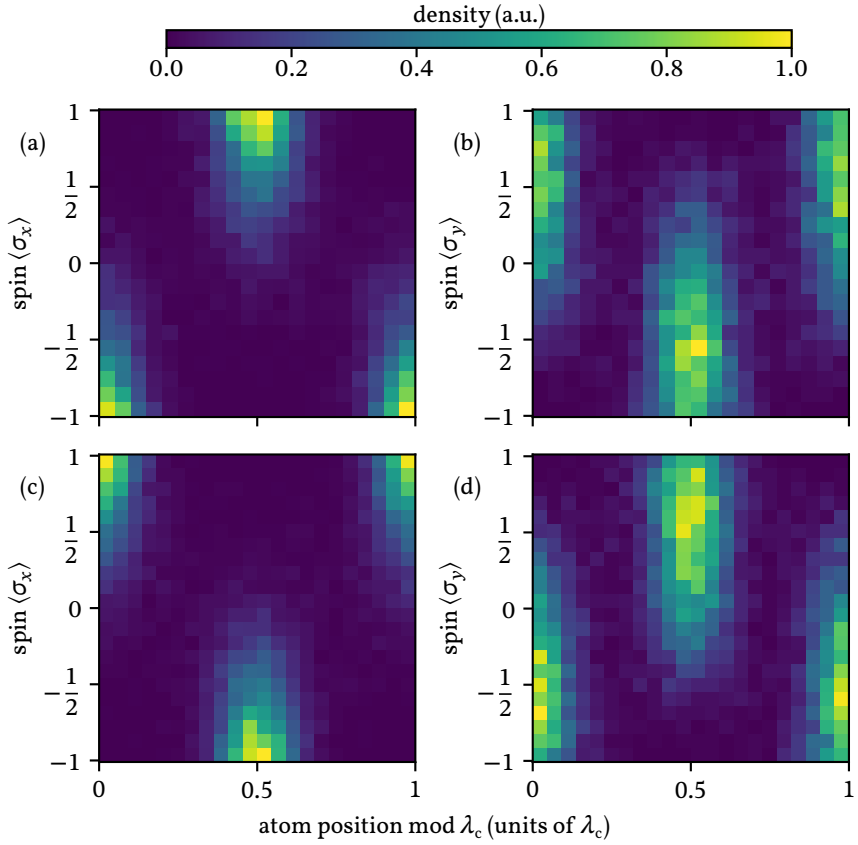

Figure 6.7: Atomic spin-position correlations of the final state for the data used in Figure 6.5. The top (lower) panels show the correlations of the final state with $\Phi < 0$ ($\Phi > 0$). (a) and (c) display the correlations between $\langle\hat{\sigma}^x\rangle$ and the position modulus λ_c, (b) and (d) display the correlations between $\langle\hat{\sigma}^y\rangle$ and the position modulus λ_c.

6.4.5 *Control of the spin phase*

Equation (6.27) shows that the collective spin phase ϕ_s, equation (6.22), can be controlled via the relative phase 2ϕ of the two pumping lasers. Furthermore the phase ϕ also determines the phase ϕ_c of the cavity field, see Eqs. (6.26) and (6.28). We report in Figs. 6.8 the collective spin phase ϕ_s and the cavity field phase ϕ_c obtained from our numerical simulations, for various values of the phase ϕ. The numerical results coincide with our analytical predictions.

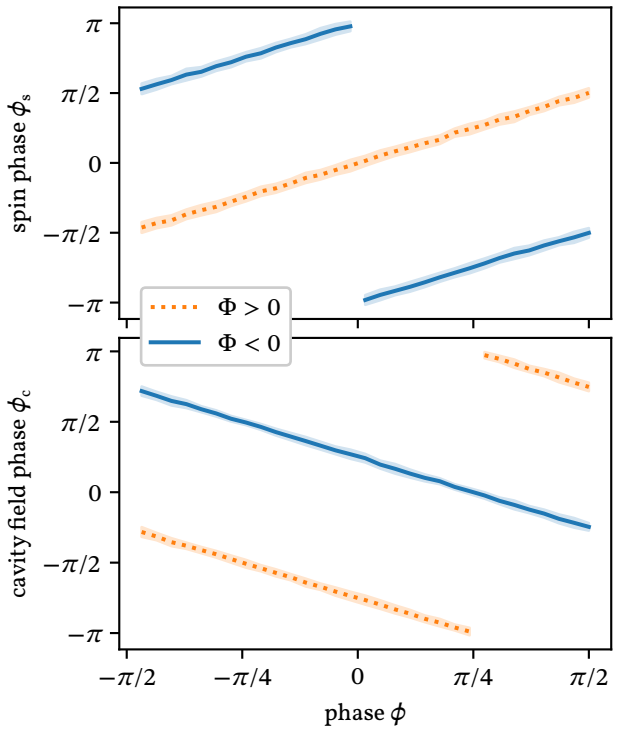

Figure 6.8: (a) Collective spin phase ϕ_s, Eq. (6.22), and (b) cavity field phase ϕ_c, Eq. (6.28), as functions of the phase ϕ, calculated over 183 trajectories. The solid blue line corresponds to the state with $\Phi < 0$, the dotted orange line corresponds to $\Phi > 0$. The shaded regions correspond to the standard deviation calculated over the trajectories. All the quantities are calculated at time $t = 800\omega_r^{-1}$. The parameters used are $S = 0.5\kappa$, $\Delta_e = \kappa/10$, $\kappa = 100\omega_r$, $\Delta_c = -\kappa$, $U_1 = U_2 = 0$ and $N = 100$.

The interaction Hamiltonian (6.16) (and thus the total Hamiltonian (6.7) of the system), considered as a function of ϕ, is periodic with period π. However, Fig. 6.8 shows that the steady states in the ordered phase are periodic with period 2π.

6.5 CONCLUSIONS

In this chapter we studied the dynamics of a cloud of thermal atoms with two internal states in a lossy cavity. Raman transition between the two energy levels of each atom are induced by two transversal pumping lasers and a mode of the cavity. We observed the existence of an ordered phase above a certain pumping threshold. In this ordered phase the atomic density exhibits modulation with half cavity wavelength $\lambda_c/2$ and the spins assume opposite phase when they localize in the cavity field minima or maxima. The transition into the ordered state breaks the $\mathbb{Z}_2$ symmetry associated with the change of the sign of the cavity field and with the spin flip of all the atoms. We showed that cooling to kinetic energy of the order of $\hbar\kappa$ happens in both the organized and the non-organized state. Furthermore the spin orientation inside the cavity can be controlled by the relative phase of the pumping lasers. The latter also fixes the cavity field phase which can be measured at the cavity output. The organized structure emerges from the interplay between the coherent drive of the atoms and the noisy environment of the cavity, and from the interplay between the motion and the internal states of the atoms.

This system can be used to explore the dynamics of strong long range interacting spins. Envisaged applications also include sensors [242], quantum-enhanced metrology [243] and quantum simulation [244, 245] of quantum magnetism [47, 246] and opto-magnonic systems [48, 49]. Further developments may include the coupling of the atoms to several cavity modes and may be used to engineer quantum spin glasses [223, 224].

APPENDICES

6.A HAMILTONIAN IN THE ROTATING FRAME

The single-particle Hamiltonian in the dipole and rotating wave approximation reads ($\hbar = 1$)

$$\begin{aligned}\hat{H}^{(1)} = \frac{\hat{p}^2}{2m} + \sum_{\tau=1,2,3} \omega_\tau |\tau\rangle\langle\tau| + \left(\Omega_1 e^{-i\omega_{L1}t}|2\rangle\langle 1| + \Omega_2 e^{-i\omega_{L2}t}|3\rangle\langle 0| + \text{h.c.}\right) + \\ + \omega_c \hat{a}^\dagger \hat{a} + \cos(k_c x)\left(g_1 \hat{a}^\dagger |0\rangle\langle 2| + g_2 \hat{a}^\dagger |1\rangle\langle 3| + \text{h.c.}\right);\end{aligned} \tag{6.29}$$

here, $\{0, \hbar\omega_1, \hbar\omega_2, \hbar\omega_3\}$ are the energies of the atomic electronic states, ω_{L1} and ω_{L2} are the frequencies of the pumping lasers, $\hat{x}$ and $\hat{p}$ are the position and momentum operator of the atom along the cavity axis such that $[x, p] = i$, m is the mass of the atom, and $\hat{a}$ is the annihilation operator of a cavity mode with frequency ω_c which fulfills $\left[a, a^\dagger\right] = 1$.

We can express the single-particle Hamiltonian (6.29) in the rotating frame defined by the unitary operator

$$\hat{U}(t) = \exp\left\{\mathrm{i}\left[\left(\frac{\omega_{\mathrm{L1}}+\omega_{\mathrm{L2}}}{2}\right)\left(\hat{a}^\dagger\hat{a} + |2\rangle\langle 2|\right) + \left(\frac{\omega_{\mathrm{L2}}-\omega_{\mathrm{L1}}}{2}\right)|1\rangle\langle 1| + \omega_{\mathrm{L2}}|3\rangle\langle 3|\right]t\right\} \tag{6.30}$$

by means of $\hat{H}^{(1)} = \hat{U}\hat{\tilde{H}}^{(1)}\hat{U}^\dagger + \mathrm{i}\left(\partial_t\hat{U}\right)\hat{U}^\dagger$:

$$\begin{aligned}\hat{H}^{(1)} = \frac{\hat{p}^2}{2m} &- \delta_1|1\rangle\langle 1| - \delta_2|2\rangle\langle 2| - \delta_3|3\rangle\langle 3| + \left(\Omega_1|2\rangle\langle 1| + \Omega_2|3\rangle\langle 0| + \mathrm{h.c.}\right) + \\ &- \Delta_{\mathrm{c}}\hat{a}^\dagger\hat{a} + \cos(k_{\mathrm{c}}\hat{x})\left(g_1\hat{a}^\dagger|0\rangle\langle 2| + g_2\hat{a}^\dagger|1\rangle\langle 3| + \mathrm{h.c.}\right),\end{aligned} \tag{6.31}$$

where the detunings are defined as

$$\begin{aligned}\delta_1 &= \left(\frac{\omega_{\mathrm{L2}}-\omega_{\mathrm{L1}}}{2}\right) - \omega_1, \quad & \delta_2 &= \left(\frac{\omega_{\mathrm{L1}}+\omega_{\mathrm{L2}}}{2}\right) - \omega_2, \\ \delta_3 &= \omega_{\mathrm{L2}} - \omega_3, & \Delta_{\mathrm{c}} &= \left(\frac{\omega_{\mathrm{L1}}+\omega_{\mathrm{L2}}}{2}\right) - \omega_{\mathrm{c}}.\end{aligned} \tag{6.32}$$

6.B ADIABATIC ELIMINATION OF THE EXCITED STATES

The single-particle Hamiltonian (6.31) can be written as $\hat{H}^{(1)} = \hat{H}_{\mathrm{S}} + \hat{H}_{\mathrm{F}} + \hat{H}_{\mathrm{int}}$, where

$$\hat{H}_{\mathrm{S}} = \frac{\hat{p}^2}{2m} - \delta_1|1\rangle\langle 1| - \Delta_{\mathrm{c}}\hat{a}^\dagger\hat{a} \tag{6.33a}$$

$$\hat{H}_{\mathrm{F}} = -\delta_2|2\rangle\langle 2| - \delta_3|3\rangle\langle 3| \tag{6.33b}$$

$$\begin{aligned}\hat{H}_{\mathrm{int}} = &\left(\Omega_1|2\rangle\langle 1| + \Omega_2|3\rangle\langle 0| + \mathrm{h.c.}\right) + \\ &+ \cos(k_{\mathrm{c}}\hat{x})\left(g_1\hat{a}^\dagger|0\rangle\langle 2| + g_2\hat{a}^\dagger|1\rangle\langle 3| + \mathrm{h.c.}\right)\end{aligned} \tag{6.33c}$$

and we consider the master equation

$$\frac{\partial\hat{\rho}}{\partial t} = \mathcal{L}\hat{\rho} = \left(\mathcal{L}_{\mathrm{S}} + \mathcal{L}_{\mathrm{F}} + \mathcal{L}_{\mathrm{int}}\right)\hat{\rho} \tag{6.34}$$

with

$$\mathcal{L}_{\mathrm{S}}\hat{\rho} = -\mathrm{i}[H_{\mathrm{S}}, \hat{\rho}] + \mathcal{L}_\kappa\hat{\rho}, \tag{6.35a}$$

$$\mathcal{L}_\kappa\hat{\rho} = \kappa\left(2\hat{a}\hat{\rho}\hat{a}^\dagger - \hat{a}^\dagger\hat{a}\hat{\rho} - \hat{\rho}\hat{a}^\dagger\hat{a}\right) \tag{6.35b}$$

$$\mathcal{L}_{\mathrm{F}}\hat{\rho} = -\mathrm{i}[H_{\mathrm{F}}, \hat{\rho}], \tag{6.35c}$$

$$\mathcal{L}_{\mathrm{int}}\hat{\rho} = -\mathrm{i}[H_{\mathrm{int}}, \hat{\rho}], \tag{6.35d}$$

where $\hat{\rho}$ is the density matrix of the system. We neglect the radiative decay of the excited states $|2\rangle$ and $|3\rangle$, this is a good approximation if δ_2 and δ_3 are the largest frequencies in the system. Let $\mathcal{L}_0 = \mathcal{L}_{\mathrm{S}} + \mathcal{L}_{\mathrm{F}}$ and $\mathcal{L}_1 = \mathcal{L}_{\mathrm{int}}$, we now perform an expansion in $\mathcal{L}_1$.

6.B.1 *Projectors on the slow and fast subspace*

We introduce the projector $P = |0\rangle\langle 0| + |1\rangle\langle 1|$ on the *slow* subspace where $\mathcal{L}_S$ acts, and the superoperators $\mathcal{P}$ and $\mathcal{Q}$ defined as $\mathcal{P}\hat{o} = P\hat{o}P$ and $\mathcal{Q} = \mathbb{1} - \mathcal{P}$, where $\hat{o}$ is an operator. They have the following properties:

1. $\mathcal{P}^2 = \mathcal{P}$ and $\mathcal{Q}^2 = \mathcal{Q}$, i. e. they are projectors:

$$\begin{aligned}
&\mathcal{P}^2\hat{\rho} = PP\hat{\rho}PP = P\hat{\rho}P = \mathcal{P}\hat{\rho},\\
&\mathcal{Q}^2\hat{\rho} = (\mathbb{1} - \mathcal{P})^2\hat{\rho} = \hat{\rho} + \mathcal{P}^2\hat{\rho} - 2\mathcal{P}\hat{\rho} = \hat{\rho} - \mathcal{P}\hat{\rho} = \mathcal{Q}\hat{\rho};
\end{aligned}$$

2. $\mathcal{P}\mathcal{Q} = \mathcal{Q}\mathcal{P} = 0$:

$$\begin{aligned}
&\mathcal{P}\mathcal{Q}\hat{\rho} = \mathcal{P}(\mathbb{1} - \mathcal{P})\hat{\rho} = (\mathcal{P} - \mathcal{P})\hat{\rho} = 0,\\
&\mathcal{Q}\mathcal{P}\hat{\rho} = (\mathbb{1} - \mathcal{P})\mathcal{P}\hat{\rho} = (\mathcal{P} - \mathcal{P})\hat{\rho} = 0;
\end{aligned}$$

3. $[\mathcal{P}, \mathcal{L}_0] = [\mathcal{Q}, \mathcal{L}_0] = 0$:

$$\begin{aligned}
\mathcal{L}_0\mathcal{P}\hat{\rho} &= -\mathrm{i}[H_S + H_F, P\hat{\rho}P] + \mathcal{L}_\kappa P\hat{\rho}P =\\
&= -\mathrm{i}[(H_S + H_F)P\hat{\rho}P - P\hat{\rho}P(H_S + H_F)] + P\mathcal{L}_\kappa\hat{\rho}P =\\
&= -\mathrm{i}[P(H_S + H_F)\hat{\rho}P - P\hat{\rho}(H_S + H_F)P] + P\mathcal{L}_\kappa\hat{\rho}P =\\
&= -\mathrm{i}P[H_S + H_F, \hat{\rho}]P + P\mathcal{L}_\kappa\hat{\rho}P = \mathcal{P}\mathcal{L}_0\hat{\rho},\\
[\mathcal{Q}, \mathcal{L}_0] &= [\mathbb{1} - \mathcal{P}, \mathcal{L}_0] = 0;
\end{aligned}$$

4. $\mathcal{P}\mathcal{L}_F = \mathcal{L}_F\mathcal{P} = 0$;

5. $\mathcal{Q}\mathcal{L}_F = \mathcal{L}_F\mathcal{Q} = \mathcal{L}_F$;

6. $[\mathcal{L}_S, \mathcal{P}] = 0$;

7. $\mathcal{P}\mathcal{L}_1\mathcal{P} = 0$:

$$\begin{aligned}
\mathcal{P}\mathcal{L}_1\mathcal{P}\hat{\rho} &= -\mathrm{i}P[H_{\mathrm{int}}, P\hat{\rho}P]P = -\mathrm{i}P(H_{\mathrm{int}}P\hat{\rho}P - P\hat{\rho}PH_{\mathrm{int}})P =\\
&= -\mathrm{i}[PH_{\mathrm{int}}P, P\hat{\rho}P] = -\mathrm{i}[0, P\hat{\rho}P] = 0;
\end{aligned}$$

8. $\mathcal{Q}\mathcal{L}_1\mathcal{P} = \mathcal{L}_1\mathcal{P}$:

$$\mathcal{Q}\mathcal{L}_1\mathcal{P} = (\mathbb{1} - \mathcal{P})\mathcal{L}_1\mathcal{P} = \mathcal{L}_1\mathcal{P} - \mathcal{P}\mathcal{L}_1\mathcal{P} = \mathcal{L}_1\mathcal{P}.$$

6.B.2 *Effective master equation for the slow subspace*

The density matrix $\hat{\rho}$ can be split in $\hat{\rho} = (\mathcal{P} + \mathcal{Q})\hat{\rho} = v + w$, where $v = \mathcal{P}\hat{\rho} = P\hat{\rho}P$ and $w = \mathcal{Q}\hat{\rho}$.

We now consider the interaction picture defined by the transformation $\tilde{\hat{\rho}} = \mathrm{e}^{-\mathcal{L}_0 t}\hat{\rho}$ and project master equation (6.34) with $\mathcal{P}$ and $\mathcal{Q}$ obtaining (notice that $\tilde{\mathcal{P}} = \mathrm{e}^{-\mathcal{L}_0 t}\mathcal{P}\mathrm{e}^{\mathcal{L}_0 t} = \mathcal{P}$ and $\tilde{\mathcal{Q}} = \mathcal{Q}$)

$$\dot{\tilde{v}} = \mathcal{P}\tilde{\mathcal{L}}_1\tilde{v} + \mathcal{P}\tilde{\mathcal{L}}_1\tilde{w}, \tag{6.36a}$$

$$\dot{\tilde{w}} = \mathcal{Q}\tilde{\mathcal{L}}_1\tilde{v} + \mathcal{Q}\tilde{\mathcal{L}}_1\tilde{w}, \tag{6.36b}$$

where $\tilde{v} = \mathcal{P}\tilde{\hat{\rho}} = \mathcal{P}e^{-\mathcal{L}_0 t}\hat{\rho} = e^{-\mathcal{L}_0 t}\mathcal{P}\hat{\rho} = e^{-\mathcal{L}_0 t}v$, $\tilde{w} = e^{-\mathcal{L}_0 t}w$, $\tilde{\mathcal{L}}_1 = e^{-\mathcal{L}_0 t}\mathcal{L}_1 e^{\mathcal{L}_0 t}$. Note that the first term on the right side of equation (6.36a) vanishes $\mathcal{P}\tilde{\mathcal{L}}_1\mathcal{P} = 0$. We formally solve equation (6.36b) and obtain

$$\tilde{w}(t) = \tilde{w}(0) + \int_0^t \mathcal{Q}\tilde{\mathcal{L}}_1(t')\tilde{v}(t')\mathrm{d}t' + \int_0^t \mathcal{Q}\tilde{\mathcal{L}}_1(t')\tilde{w}(t')\mathrm{d}t'. \tag{6.37}$$

Assuming $\tilde{w}(0) = 0$, namely, the state of the atom at $t = 0$ is in the $\{|0\rangle, |1\rangle\}$ subspace, by iteration we obtain

$$\tilde{w}(t) = \int_0^t \mathcal{Q}\tilde{\mathcal{L}}_1(t')\tilde{v}(t')\mathrm{d}t' + \int_0^t \mathcal{Q}\tilde{\mathcal{L}}_1(t')\int_0^{t'} \mathcal{Q}\tilde{\mathcal{L}}_1(t'')\tilde{v}(t'')\mathrm{d}t''\mathrm{d}t' + \mathcal{O}(\mathcal{L}_1^3), \tag{6.38}$$

and substituting in equation (6.36a)

$$\dot{\tilde{v}}(t) = \mathcal{P}\tilde{\mathcal{L}}_1(t)\int_0^t \mathcal{Q}\tilde{\mathcal{L}}_1(t')\tilde{v}(t')\mathrm{d}t' + \mathcal{O}(\mathcal{L}_1^3). \tag{6.39}$$

Moving back to the Schrödinger picture the equation for v is

$$\begin{aligned} \dot{v}(t) &\approx \mathcal{L}_0 v(t) + \mathcal{P}\mathcal{L}_1 \int_0^t e^{\mathcal{Q}\mathcal{L}_0(t-t')}\mathcal{Q}\mathcal{L}_1 v(t')\mathrm{d}t' = \\ &= \mathcal{L}_S v(t) + \mathcal{P}\mathcal{L}_{\mathrm{int}} \int_0^t e^{\mathcal{Q}\mathcal{L}_0\tau}\mathcal{Q}\mathcal{L}_{\mathrm{int}} v(t-\tau)\mathrm{d}\tau. \end{aligned} \tag{6.40}$$

Now we perform some approximations using the fact that the parameters in $\mathcal{L}_S$ are smaller then the parameters in $\mathcal{L}_F$. Since $[\mathcal{L}_S, \mathcal{L}_F] = 0$, we have

$$e^{\mathcal{L}_0\tau} = e^{(\mathcal{L}_S+\mathcal{L}_F)\tau} = e^{\mathcal{L}_F\tau}\left[\mathbb{1} + \mathcal{L}_S\tau + \mathcal{O}(\mathcal{L}_S^2\tau^2)\right], \tag{6.41}$$

and we expand $v(t-\tau)$ around $\tau = 0$

$$v(t-\tau) = v(t) - \dot{v}(t)\tau + \dots. \tag{6.42}$$

The last term in equation (6.40) becomes

$$\begin{aligned} &\mathcal{P}\mathcal{L}_{\mathrm{int}} \int_0^t e^{\mathcal{Q}\mathcal{L}_F\tau}(\mathbb{1} + \mathcal{Q}\mathcal{L}_S\tau + \dots)\mathcal{Q}\mathcal{L}_{\mathrm{int}}[v(t) - \dot{v}(t)\tau + \dots]\mathrm{d}\tau = \\ &\qquad = \mathcal{P}\mathcal{L}_{\mathrm{int}} \int_0^t e^{\mathcal{Q}\mathcal{L}_F\tau}\mathcal{Q}\mathcal{L}_{\mathrm{int}} v(t)\mathrm{d}\tau + \\ &+ \mathcal{P}\mathcal{L}_{\mathrm{int}} \int_0^t e^{\mathcal{Q}\mathcal{L}_F\tau}\tau[\mathcal{Q}\mathcal{L}_S\mathcal{Q}\mathcal{L}_{\mathrm{int}} v(t) - \mathcal{Q}\mathcal{L}_{\mathrm{int}}\dot{v}(t)]\mathrm{d}\tau + \\ &\qquad - \mathcal{P}\mathcal{L}_{\mathrm{int}} \int_0^t e^{\mathcal{Q}\mathcal{L}_F\tau}\tau^2\mathcal{Q}\mathcal{L}_S\mathcal{Q}\mathcal{L}_{\mathrm{int}}\dot{v}(t)\mathrm{d}\tau + \dots. \end{aligned} \tag{6.43}$$

The first term in the right side of equation (6.43) is of the order $\frac{g^2}{\delta}$, the second term is of the order $\frac{g^2\Delta}{\delta^2}$, and the third term is of the order $\frac{g^2\Delta^2}{\delta^3}$, where $g = \max(g_1, g_2, \Omega_1, \Omega_2)$, $\Delta = \max(\delta_1, \Delta_c, \kappa)$ and $\delta = \min(\delta_2, \delta_3)$. Keeping only the first order we obtain

$$\dot{v}(t) = \mathcal{L}_S v(t) + \mathcal{P}\mathcal{L}_{\text{int}} \int_0^t e^{\mathcal{Q}\mathcal{L}_F \tau} \mathcal{Q}\mathcal{L}_{\text{int}} v(t) d\tau. \tag{6.44}$$

Note that

$$\begin{aligned} e^{\mathcal{L}_F \tau}\mathcal{L}_{\text{int}} v(t) &= -ie^{\mathcal{L}_F \tau}[H_{\text{int}}, v(t)] = -ie^{-iH_F\tau}[H_{\text{int}}, v(t)]e^{iH_F\tau} = \\ &= -i[e^{-iH_F\tau}H_{\text{int}}e^{iH_F\tau}, v(t)], \end{aligned} \tag{6.45}$$

thus

$$\begin{aligned} \int_0^t e^{\mathcal{L}_F \tau}\mathcal{L}_{\text{int}} v(t) d\tau &= -i\int_0^t [e^{-iH_F\tau}H_{\text{int}}e^{iH_F\tau}, v(t)]d\tau = \\ &= -i[\int_0^t e^{-iH_F\tau}H_{\text{int}}e^{iH_F\tau}d\tau, v(t)], \end{aligned} \tag{6.46}$$

and

$$\begin{aligned} e^{-iH_F\tau}H_{\text{int}}e^{iH_F\tau} = &\left(\Omega_1 e^{i\delta_2\tau}|2\rangle\langle 1| + \Omega_2 e^{i\delta_3\tau}|3\rangle\langle 0| + \text{h.c.}\right) + \\ &+ \cos(k_c x)\left(g_1 e^{-i\delta_2\tau}a^\dagger|0\rangle\langle 2| + g_2 e^{-i\delta_3\tau}a^\dagger|1\rangle\langle 3| + \text{h.c.}\right), \end{aligned} \tag{6.47}$$

thus

$$\begin{aligned} &\int_0^t e^{-iH_F\tau}H_{\text{int}}e^{iH_F\tau}d\tau = \\ &= \left[\frac{\Omega_1}{i\delta_2}\left(e^{i\delta_2 t} - 1\right)|2\rangle\langle 1| + \frac{\Omega_2}{i\delta_3}\left(e^{i\delta_3 t} - 1\right)|3\rangle\langle 0| + \text{h.c.}\right] + \\ &\quad + \cos(k_c x)\left[\frac{g_1}{i\delta_2}\left(1 - e^{-i\delta_2 t}\right)a^\dagger|0\rangle\langle 2| + \frac{g_2}{i\delta_3}\left(1 - e^{-i\delta_3 t}\right)a^\dagger|1\rangle\langle 3| + \text{h.c.}\right]. \end{aligned} \tag{6.48}$$

Now we use coarse graining in order to eliminate fast rotating terms in equation (6.44): we choose a time scale Δt such that $\delta_2^{-1}, \delta_3^{-1} \ll \Delta t \ll \delta_1^{-1}, \Delta_c^{-1}, \kappa^{-1}$ and we apply to equation (6.44) the operator $(\Delta t)^{-1}\int_t^{t+\Delta t} dt'$ on the left. In this way the fast oscillating terms average out on the timescale Δt and one obtains

$$\dot{v}(t) = \mathcal{L}_S v(t) + \mathcal{P}\mathcal{L}_{\text{int}}(-i[H', v(t)]), \tag{6.49}$$

where

$$\begin{aligned} H' = &\left[\frac{i\Omega_1}{\delta_2}|2\rangle\langle 1| + \frac{i\Omega_2}{\delta_3}|3\rangle\langle 0| + \text{h.c.}\right] + \\ &+ \cos(k_c x)\left[\frac{-ig_1}{\delta_2}a^\dagger|0\rangle\langle 2| + \frac{-ig_2}{\delta_3}a^\dagger|1\rangle\langle 3| + \text{h.c.}\right]. \end{aligned} \tag{6.50}$$

Now

$$\begin{aligned}\mathcal{P}\mathcal{L}_{\text{int}}(-\mathrm{i}[H',\upsilon]) &= \mathcal{P}\{-\mathrm{i}[H_{\text{int}},-\mathrm{i}[H',\upsilon]]\} = \mathcal{P}\{-[H_{\text{int}},[H',\upsilon]]\} = \\ &= -PH_{\text{int}}H'P\upsilon P + PH_{\text{int}}P\upsilon H'P + \\ &\quad + PH'\upsilon PH_{\text{int}}P - P\upsilon PH'H_{\text{int}}P = \\ &= -PH_{\text{int}}H'P\upsilon - \upsilon PH'H_{\text{int}}P,\end{aligned} \tag{6.51}$$

and

$$\begin{aligned}PH_{\text{int}}H'P = \mathrm{i}\Bigg\{&\frac{|\Omega_2|^2}{\delta_3}|0\rangle\langle 0| + \frac{|\Omega_1|^2}{\delta_2}|1\rangle\langle 1| + \\ &+ a^\dagger a\cos^2(k_{\text{c}}x)\left[\frac{|g_1|^2}{\delta_2}|0\rangle\langle 0| + \frac{|g_2|^2}{\delta_3}|1\rangle\langle 1|\right] + \\ &+ \cos(k_{\text{c}}x)\left[\frac{\Omega_1 g_1}{\delta_2}a^\dagger|0\rangle\langle 1| + \frac{\Omega_2 g_2}{\delta_3}a^\dagger|1\rangle\langle 0| + \text{h. c.}\right]\Bigg\} = \\ &= \mathrm{i}H_{\text{eff}},\end{aligned} \tag{6.52}$$

with $H_{\text{eff}} = H_{\text{eff}}^\dagger$. Now notice that $(H_{\text{int}}H')^\dagger = H'H_{\text{int}}$ because H_{int} and H' are hermitian. Thus

$$\begin{aligned}&PH'H_{\text{int}}P = (PH_{\text{int}}H'P)^\dagger = -\mathrm{i}H_{\text{eff}}, \\ &\mathcal{P}\mathcal{L}_{\text{int}}(-\mathrm{i}[H',\upsilon]) = -\mathrm{i}[H_{\text{eff}},\upsilon].\end{aligned}$$

Equation (6.49) becomes

$$\dot{\upsilon}(t) = -\mathrm{i}[H_{\text{S}} + H_{\text{eff}},\upsilon(t)] + \mathcal{L}_\kappa\upsilon(t). \tag{6.53}$$

Shifting the energy by means of the unitary operator

$$U(t) = \mathbb{1}\exp\left(\mathrm{i}\frac{|\Omega_2|^2}{\delta_3}t\right),$$

finally one gets the master equation for the density matrix $\upsilon(t)$

$$\dot{\upsilon}(t) = -\mathrm{i}[H_{(1)},\upsilon(t)] + \mathcal{L}_\kappa\upsilon(t), \tag{6.54}$$

where

$$\begin{aligned}H_{(1)} =& \frac{p^2}{2m} + \Delta_{\text{e}}|1\rangle\langle 1| - \left[\Delta_{\text{c}} - \cos^2(k_{\text{c}}x)(U_1|0\rangle\langle 0| + U_2|1\rangle\langle 1|)\right]a^\dagger a + \\ &+ \cos(k_{\text{c}}x)\left[S_1 a^\dagger|0\rangle\langle 1| + S_2 a^\dagger|1\rangle\langle 0| + \text{h. c.}\right]\end{aligned} \tag{6.55}$$

and

$$\Delta_{\text{e}} = \frac{|\Omega_1|^2}{\delta_2} - \frac{|\Omega_2|^2}{\delta_3} - \delta_1, \tag{6.56a}$$

$$U_1 = \frac{|g_1|^2}{\delta_2}, \tag{6.56b}$$

$$U_2 = \frac{|g_2|^2}{\delta_3}, \tag{6.56c}$$

$$S_1 = \frac{\Omega_1 g_1}{\delta_2}, \tag{6.56d}$$

$$S_2 = \frac{\Omega_2 g_2}{\delta_3}. \tag{6.56e}$$

The master equation for N atoms is derived in the same way [230] and it reads

$$\dot{\hat{\rho}}(t) = -\mathrm{i}[H, \hat{\rho}(t)] + \mathcal{L}_\kappa \hat{\rho}(t), \tag{6.57}$$

where the Hamiltonian H is

$$\begin{aligned} H = &\sum_{j=1}^{N}\left(\frac{p_j^2}{2m} + \Delta_\mathrm{e}\hat{\sigma}_j^\dagger\hat{\sigma}_j\right) - \left[\Delta_\mathrm{c} - \sum_{j=1}^{N}\left(U_1\hat{\sigma}_j\hat{\sigma}_j^\dagger + U_2\hat{\sigma}_j^\dagger\hat{\sigma}_j\right)\cos^2(k_\mathrm{c}x_j)\right]a^\dagger a + \\ &+ \sum_{j=1}^{N}\left(S_1 a^\dagger\hat{\sigma}_j + S_1^*\hat{\sigma}_j^\dagger a + S_2 a^\dagger\hat{\sigma}_j^\dagger + S_2^* a\hat{\sigma}_j\right)\cos(k_\mathrm{c}x_j). \end{aligned} \tag{6.58}$$

Here $\hat{\sigma}_j = |0\rangle_j\langle 1|$ is the lowering operator for the j-th atom, x_j and p_j are the position and momentum of the atom j, respectively. The conditions of validity are $\delta \gg |\delta_1|, |\Delta_\mathrm{c}|, \kappa, \sqrt{N\bar{n}}g_1, \sqrt{N\bar{n}}g_2, \sqrt{N}\Omega_1, \sqrt{N}\Omega_2$.

6.C DETAILS OF THE NUMERICAL COMPUTATIONS

6.C.1 *Units*

The recoil frequency is defined as

$$\omega_\mathrm{r} = \frac{\hbar k_\mathrm{c}^2}{2m} \tag{6.59}$$

where k_c is the wavenumber of the cavity mode and m is the mass of an atom. We use the recoil frequency ω_r as unit of frequency. Its inverse ω_r^{-1} is used as unit of time. We use $\hbar k_\mathrm{c}$ as unit of momentum and k_c^{-1} as unit of position. With this choice we have that

$$\frac{\mathrm{d}\hat{x}}{\mathrm{d}t} = 2\hat{p} \tag{6.60}$$

where the position $\hat{x}$, the time t and the momentum $\hat{p}$ are expressed in this unit system.

6.C.2 *Initial state*

The initial state of each atom in each trajectory are chosen randomly. The initial position $x_j(0)$ of each atom is uniformly distributed in the interval $[0, 2\pi)$. Notice that this is not a restriction since we use the unit

system described in Sec. 6.C.1. During the evolution the positions are not bounded. The initial momentum $p_j(0)$ of each atom follows a Gaussian distribution with zero mean and variance $E_{\rm kin}(0)$, where $E_{\rm kin}(0)$ is the mean initial kinetic energy. The initial spin state is

$$|\psi_{\rm s}(0)\rangle = \sin(\gamma/2)e^{i\beta}|0\rangle + \cos(\gamma/2)|1\rangle, \tag{6.61}$$

where γ is a random variable uniformly distributed in $[\pi, 1.1\pi)$, and β is a random variable uniformly distributed in $[0, 2\pi)$. The initial values of the spin variables are thus

$$\begin{aligned}\sigma_j^x(0) &= \langle\psi_{\rm s}(0)|\hat{\sigma}_j^x|\psi_{\rm s}(0)\rangle,\\ \sigma_j^y(0) &= \langle\psi_{\rm s}(0)|\hat{\sigma}_j^y|\psi_{\rm s}(0)\rangle,\\ \sigma_j^z(0) &= \langle\psi_{\rm s}(0)|\hat{\sigma}_j^z|\psi_{\rm s}(0)\rangle.\end{aligned} \tag{6.62}$$

The cavity is initially empty $\langle\hat{a}^\dagger(0)\hat{a}(0)\rangle = 0$. Figure 6.9 shows a sample of initial conditions for 19200 atoms.

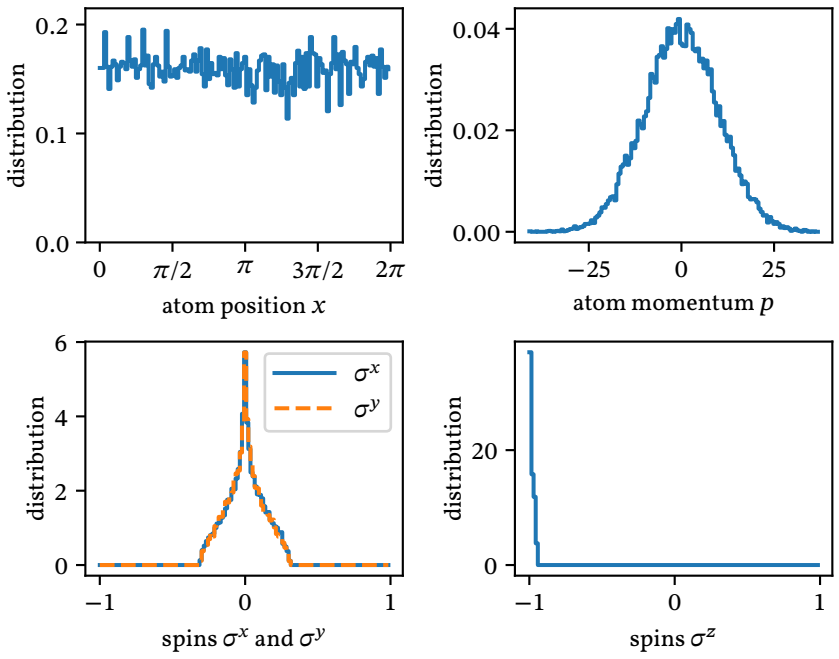

Figure 6.9: Sample of initial conditions for 19200 atoms. The distribution are normalized such that the area behind each curve is 1. The kinetic energy is $E_{\rm kin}(0) = \hbar\kappa$, with $\kappa = 100\omega_{\rm r}$.

6.D SEMI-CLASSICAL TREATMENT

In this section we report the main steps of a calculation based on the Wigner representation [105] in order to derive semi-classical equations of motion for the system [218, 233]. The details are given in the following

subsections. We use the tools introduced in Sec. 2.4 and 2.A. Let $\hat{\rho}(t)$ be the density matrix describing the cavity field degree of freedom together with the internal (spin states $|0\rangle$ and $|1\rangle$) and external (motional) degrees of freedom of the atoms. Consider the operator $\hat{W}_t(\boldsymbol{x}, \boldsymbol{p}, \alpha_\mathrm{r}, \alpha_\mathrm{i})$ defined by

$$\hat{W}_t(\boldsymbol{x}, \boldsymbol{p}, \alpha_\mathrm{r}, \alpha_\mathrm{i}) = \frac{1}{(\pi\hbar)^N \pi^2} \int \mathrm{d}^2\eta \left\{ \mathrm{e}^{\eta^* \alpha - \eta \alpha^*} \times \right. \\ \left. \times \operatorname{Tr}_{\mathrm{cav}} \left[\mathrm{e}^{\eta a^\dagger - \eta^* a} \int_{-\infty}^{\infty} \mathrm{d}^N \boldsymbol{y} \, \langle \boldsymbol{x} + \boldsymbol{y} | v(t) | \boldsymbol{x} - \boldsymbol{y} \rangle \mathrm{e}^{\frac{-2\mathrm{i}\boldsymbol{y}\cdot\boldsymbol{p}}{\hbar}} \right] \right\} \tag{6.63}$$

where $\epsilon = (\epsilon_1, \ldots, \epsilon_N)$ with $\epsilon = \boldsymbol{x}, \boldsymbol{p}, \boldsymbol{y}, \eta$ is a complex variable, $\alpha = \alpha_\mathrm{r} + \mathrm{i}\alpha_\mathrm{i}$, and $\mathrm{Tr}_{\mathrm{cav}}\{\cdot\}$ denotes the trace over the cavity field degree of freedom. $\hat{W}_t(\boldsymbol{x}, \boldsymbol{p}, \alpha_\mathrm{r}, \alpha_\mathrm{i})$ is an operator for the atomic spins, and a function of the atoms' positions $\boldsymbol{x}$, canonically conjugated momenta $\boldsymbol{p}$ and cavity field amplitudes α_r and α_i. The Wigner transformation, corresponding to Eq. (6.63), of the master equation (6.57) leads to a partial differential equation for the operator $\hat{W}$. We want to treat the atomic motion and the cavity field semi-classically. Let us now discuss the conditions under which this is valid.

The atomic motion can be treated semi-classically when the width of the momentum distribution Δp_j of a single atom is much larger than the photon momentum $\hbar k_\mathrm{c}$, where k_c is the wavenumber of the cavity mode

$$\hbar k_\mathrm{c} \ll \Delta p_j. \tag{6.64}$$

In this limit, single photon emission or absorption does not change the momentum distribution considerably. Accordingly, the small parameter $\hbar k_\mathrm{c}/\Delta p_j \ll 1$ introduces a hierarchy of approximations which we truncate at second order. Furthermore we require that the atomic position uncertainty Δx_j is larger than the value set by the Heisenberg uncertainty principle, $\Delta x_j > \hbar/\Delta p_j$. Details of this calculation are reported in Sec. 6.D.1.

A sufficient condition in order to treat the cavity field semi-classically is to assume that the field is in a coherent state $|\alpha\rangle$ with mean number of photon $|\alpha|^2 \gg 1$. This allows us to neglect third-order derivatives [233]. Details of this calculation are reported in Sec. 6.D.2.

At this point we have a partial differential equation for the operator $\hat{W}_t(\boldsymbol{x}, \boldsymbol{p}, \alpha_\mathrm{r}, \alpha_\mathrm{i})$, given in Eq. (6.74), with up to second-order derivatives in position, momentum and cavity field variables.

In the next step we trace out the spins degrees of freedom: we consider the equations of motion for the expectation values of the products of spin operators $\langle \hat{\sigma}_j^n \ldots \hat{\sigma}_l^m \rangle = \mathrm{Tr}\{\hat{\sigma}_j^n \ldots \hat{\sigma}_l^m \hat{W}\}$, where $j \neq l$ and $j, l \in \{1, \ldots, N\}$ indexes the atom and $n, m = x, y, z$ indexes the spin component.

Our assumption is that a probability density $f_t(\boldsymbol{x}, \boldsymbol{p}, \boldsymbol{s}, a_r, a_i)$ exists, where

$$\boldsymbol{s} = (s_1^x, \ldots, s_N^x, s_1^y, \ldots, s_N^y, s_1^z, \ldots, s_N^z), \tag{6.65}$$

and that the function f_t has the following properties:

1. it is solution of a Fokker-Plank equation which is equivalent to the stochastic differential equations obtained in Sec. 6.2.3,

2. the difference between expectation values of the products of variables s_j^n and the expectation values of the corresponding product of spin operators $\hat{\sigma}_j^n$ is of the order $O(N^{-1})$, i. e.

$$\int \prod_{r=1}^{w} s_{j_r}^{n_r} \frac{\partial}{\partial t} f_t \mathrm{d}^{3N}\boldsymbol{s} - \mathrm{Tr}\left\{\hat{\sigma}_{j_1}^{n_1} \ldots \hat{\sigma}_{j_r}^{n_r} \ldots \hat{\sigma}_{j_w}^{n_w} \frac{\partial}{\partial t}\hat{W}\right\} \simeq O(N^{-1}), \quad (6.66)$$

   with $n_r \in \{x, y, z\}$, $j_r \in \{1, \ldots N\}$, $j_r \neq j_q$ if $r \neq q$ and $w \ll N$.

We report in the following sections the calculation only up to the product of one spin operator, i. e. for $\mathrm{Tr}\{\hat{W}\}$ and $\mathrm{Tr}\{\hat{\sigma}_l^m \hat{W}\}$.

6.D.1 *Semiclassical approximation for the atomic motion*

Let $\hat{\rho}(t)$ be the density matrix describing the cavity field degrees of freedom and the internal (spin states $|0\rangle$ and $|1\rangle$) and external (motional) degrees of freedom of the atoms. In order to treat the atomic motion semiclassically we consider the operator

$$\hat{W}_t(\boldsymbol{x}, \boldsymbol{p}) = \frac{1}{(\pi\hbar)^N} \int_{-\infty}^{\infty} \cdots \int_{-\infty}^{\infty} \langle \boldsymbol{x} + \boldsymbol{y}|\rho(t)|\boldsymbol{x} - \boldsymbol{y}\rangle \mathrm{e}^{\frac{-2\mathrm{i}\boldsymbol{y}\cdot\boldsymbol{p}}{\hbar}} \mathrm{d}^N\boldsymbol{y}, \quad (6.67)$$

where $\boldsymbol{\epsilon} = (\epsilon_1, \ldots, \epsilon_N)$ is a N-dimensional vector with $\boldsymbol{\epsilon} = \boldsymbol{x}, \boldsymbol{p}, \boldsymbol{y}$, N is the number of particles. $\hat{W}_t(\boldsymbol{x}, \boldsymbol{p})$ is an operator for the cavity field degrees of freedom and the spin states of the atoms. The Wigner transforma-

tion, corresponding to Eq. (6.67), of master equation (6.57) leads to the equation

$$\begin{aligned}\frac{\partial}{\partial t}\hat{W}_t(\boldsymbol{x},\boldsymbol{p}) = &-\sum_j \frac{p_j}{m}\frac{\partial}{\partial x_j}\hat{W}_t(\boldsymbol{x},\boldsymbol{p}) - \mathrm{i}\Delta_\mathrm{e}\sum_j[\hat{\sigma}_j^\dagger\hat{\sigma}_j,\hat{W}_t(\boldsymbol{x},\boldsymbol{p})] + \\ &+\mathrm{i}\Delta_\mathrm{c}[a^\dagger a,\hat{W}_t(\boldsymbol{x},\boldsymbol{p})] + \\ &-\frac{\mathrm{i}}{4}\sum_j\Big\{\big(U_1\hat{\sigma}_j\hat{\sigma}_j^\dagger + U_2\hat{\sigma}_j^\dagger\hat{\sigma}_j\big)a^\dagger a\Big[2\hat{W}_t(\boldsymbol{x},\boldsymbol{p}) + \\ &\quad+\mathrm{e}^{2\mathrm{i}k_\mathrm{c}x_j}\hat{W}_t(\boldsymbol{x},\boldsymbol{p}-\boldsymbol{k}_j) + \mathrm{e}^{-2\mathrm{i}k_\mathrm{c}x_j}\hat{W}_t(\boldsymbol{x},\boldsymbol{p}+\boldsymbol{k}_j)\Big] + \\ &\quad-\Big[2\hat{W}_t(\boldsymbol{x},\boldsymbol{p}) + \mathrm{e}^{2\mathrm{i}k_\mathrm{c}x_j}\hat{W}_t(\boldsymbol{x},\boldsymbol{p}+\boldsymbol{k}_j) + \\ &\quad+\mathrm{e}^{-2\mathrm{i}k_\mathrm{c}x_j}\hat{W}_t(\boldsymbol{x},\boldsymbol{p}-\boldsymbol{k}_j)\Big]\big(U_1\hat{\sigma}_j\hat{\sigma}_j^\dagger + U_2\hat{\sigma}_j^\dagger\hat{\sigma}_j\big)a^\dagger a\Big\} + \\ &-\frac{\mathrm{i}}{2}\sum_j\Big\{\big(S_1a^\dagger\hat{\sigma}_j + S_1^*\hat{\sigma}_j^\dagger a + S_2a^\dagger\hat{\sigma}_j^\dagger + S_2^*a\hat{\sigma}_j\big)\times \\ &\quad\times\Big[\mathrm{e}^{\mathrm{i}k_\mathrm{c}x_j}\hat{W}_t(\boldsymbol{x},\boldsymbol{p}-\boldsymbol{k}_j/2) + \mathrm{e}^{-\mathrm{i}k_\mathrm{c}x_j}\hat{W}_t(\boldsymbol{x},\boldsymbol{p}+\boldsymbol{k}_j/2)\Big] + \\ &\quad-\Big[\mathrm{e}^{\mathrm{i}k_\mathrm{c}x_j}\hat{W}_t(\boldsymbol{x},\boldsymbol{p}+\boldsymbol{k}_j/2) + \mathrm{e}^{-\mathrm{i}k_\mathrm{c}x_j}\hat{W}_t(\boldsymbol{x},\boldsymbol{p}-\boldsymbol{k}_j/2)\Big]\times \\ &\quad\times\big(S_1a^\dagger\hat{\sigma}_j + S_1^*\hat{\sigma}_j^\dagger a + S_2a^\dagger\hat{\sigma}_j^\dagger + S_2^*a\hat{\sigma}_j\big)\Big\} + \\ &+\kappa\big(2a\hat{W}_t(\boldsymbol{x},\boldsymbol{p})a^\dagger - a^\dagger a\hat{W}_t(\boldsymbol{x},\boldsymbol{p}) - \hat{W}_t(\boldsymbol{x},\boldsymbol{p})a^\dagger a\big),\end{aligned} \tag{6.68}$$

where $\boldsymbol{k}_j = (0,\dots,k_j = k_\mathrm{c},\dots,0)$. Now, in order to perform the semi-classical approximation, we expand the Wigner operator $\hat{W}_t(\boldsymbol{x},\boldsymbol{p}\pm\hbar\boldsymbol{k}_j/2)$ in power series about $\boldsymbol{p}$

$$\begin{aligned}\hat{W}_t(\boldsymbol{x},\boldsymbol{p}\pm\hbar\boldsymbol{k}_j/2) = \hat{W}_t(\boldsymbol{x},\boldsymbol{p}) \pm \frac{\hbar k_\mathrm{c}}{2}\frac{\partial}{\partial p_j}\hat{W}_t(\boldsymbol{x},\boldsymbol{p}) + \\ +\frac{(\hbar k_\mathrm{c})^2}{8}\frac{\partial^2}{\partial p_j^2}\hat{W}_t(\boldsymbol{x},\boldsymbol{p}) + \mathcal{O}\left(\left(\frac{\hbar k_\mathrm{c}}{\Delta p}\right)^3\right).\end{aligned} \tag{6.69}$$

We assume that the typical width of the momentum distribution is much larger than the photon momentum $\Delta p \gg \hbar k_\mathrm{c}$, and truncate expansion (6.69) at second order. Substituting in Eq. (6.68) we obtain

$$\frac{\partial}{\partial t}\hat{W}_t(\boldsymbol{x},\boldsymbol{p}) = [\mathcal{L}_0+\mathcal{L}_1+\mathcal{L}_2]\hat{W}_t(\boldsymbol{x},\boldsymbol{p}), \tag{6.70}$$

where

$$\begin{aligned}\mathcal{L}_0\hat{W}_t(\boldsymbol{x},\boldsymbol{p}) = &-\mathrm{i}\Delta_\mathrm{e}\sum_j[\hat{\sigma}_j^\dagger\hat{\sigma}_j,\hat{W}_t(\boldsymbol{x},\boldsymbol{p})] + \mathrm{i}\Delta_\mathrm{c}[a^\dagger a,\hat{W}_t(\boldsymbol{x},\boldsymbol{p})] + \\ &+\mathrm{i}\sum_j[\hat{D}_j,\hat{W}_t(\boldsymbol{x},\boldsymbol{p})] + \\ &+\kappa\big(2a\hat{W}_t(\boldsymbol{x},\boldsymbol{p})a^\dagger - a^\dagger a\hat{W}_t(\boldsymbol{x},\boldsymbol{p}) - \hat{W}_t(\boldsymbol{x},\boldsymbol{p})a^\dagger a\big),\end{aligned} \tag{6.71a}$$

$$\mathcal{L}_1\hat{W}_t(\boldsymbol{x},\boldsymbol{p}) = -\sum_j \frac{p_j}{m}\frac{\partial}{\partial x_j}\hat{W}_t(\boldsymbol{x},\boldsymbol{p}) - \frac{1}{2}\sum_j\Big\{\frac{\partial}{\partial x_j}\hat{D}_j, \frac{\partial}{\partial p_j}\hat{W}_t(\boldsymbol{x},\boldsymbol{p})\Big\}, \tag{6.71b}$$

$$\mathcal{L}_2\hat{W}_t(\boldsymbol{x},\boldsymbol{p}) = -\frac{\mathrm{i}}{8}\sum_j\left[\frac{\partial^2}{\partial x_j^2}\hat{D}_j, \frac{\partial^2}{\partial p_j^2}\hat{W}_t(\boldsymbol{x},\boldsymbol{p})\right]. \tag{6.71c}$$

Here we used the work operator

$$\begin{aligned}\hat{D}_j = &-\frac{1}{2}\big(1+\cos(2k_{\mathrm{c}}x_j)\big)\big(U_1\hat{\sigma}_j\hat{\sigma}_j^\dagger + U_2\hat{\sigma}_j^\dagger\hat{\sigma}_j\big)a^\dagger a + \\ &-\cos(k_{\mathrm{c}}x_j)\big(S_1 a^\dagger\hat{\sigma}_j + S_1^*\hat{\sigma}_j^\dagger a + S_2 a^\dagger\hat{\sigma}_j^\dagger + S_2^* a\hat{\sigma}_j\big),\end{aligned} \tag{6.72}$$

such that $\hat{F}_j = \frac{\partial}{\partial x_j}\hat{D}_j$ is the force operator on the j-th atom. Equation (6.70) is a partial differential equation with up to second order derivatives in the variables t, x_j and p_j of the operator $\hat{W}_t(\boldsymbol{x},\boldsymbol{p})$.

6.D.2 *Semiclassical approximation for the cavity field*

Consider now the operator

$$\hat{W}_t(\boldsymbol{x},\boldsymbol{p},\alpha_{\mathrm{r}},\alpha_{\mathrm{i}}) = \frac{1}{\pi^2}\int \mathrm{d}^2\eta\, \mathrm{e}^{\eta^*\alpha-\eta\alpha^*}\operatorname*{Tr}_{\mathrm{cav}}\big\{\hat{W}_t(\boldsymbol{x},\boldsymbol{p})\mathrm{e}^{\eta a^\dagger-\eta^* a}\big\}, \tag{6.73}$$

where η is a complex variable, $\alpha = \alpha_{\mathrm{r}} + \mathrm{i}\alpha_{\mathrm{i}}$ with $\alpha_{\mathrm{r}},\alpha_{\mathrm{i}} \in \mathbb{R}$, and $\mathrm{Tr}_{\mathrm{cav}}\{\cdot\}$ is the trace over the cavity field degrees of freedom. $\hat{W}_t(\boldsymbol{x},\boldsymbol{p},\alpha_{\mathrm{r}},\alpha_{\mathrm{i}})$ is an operator for the spins degrees of freedom. Now we perform the Wigner transformation, corresponding to Eq. (6.73), of equation (6.70). In order to simplify the calculation we consider the case $U_1 = U_2 = 0$. We assume that the cavity field is in the coherent state $|\alpha\rangle$ with $|\alpha|^2 \gg 1$ so that

we can neglect third order derivatives. The equation for the operator $\hat{W}_t(\boldsymbol{x}, \boldsymbol{p}, \alpha_\mathrm{r}, \alpha_\mathrm{i}) \equiv \hat{W}$ then reads

$$\begin{aligned}
\frac{\partial}{\partial t}\hat{W} = & -\sum_j \frac{p_j}{m}\frac{\partial}{\partial x_j}\hat{W} - \mathrm{i}\Delta_\mathrm{e}\sum_j\left[\frac{\mathbb{1}+\hat{\sigma}_j^z}{2}, \hat{W}\right] + \frac{\kappa}{4}\left(\frac{\partial^2}{\partial\alpha_\mathrm{r}^2} + \frac{\partial^2}{\partial\alpha_\mathrm{i}^2}\right)\hat{W} + \\
& + \frac{1}{2}\frac{\partial}{\partial\alpha_\mathrm{r}}\left\{\kappa\alpha_\mathrm{r} + \Delta_\mathrm{c}\alpha_\mathrm{i} - \sum_j \frac{\cos(k_\mathrm{c}x_j)}{2}\left[I^+\hat{\sigma}_j^x - R^-\hat{\sigma}_j^y\right], \hat{W}\right\} + \\
& + \frac{1}{2}\frac{\partial}{\partial\alpha_\mathrm{i}}\left\{\kappa\alpha_\mathrm{i} - \Delta_\mathrm{c}\alpha_\mathrm{r} + \sum_j \frac{\cos(k_\mathrm{c}x_j)}{2}\left[R^+\hat{\sigma}_j^x + I^-\hat{\sigma}_j^y\right], \hat{W}\right\} + \\
& - \mathrm{i}\sum_j \cos(k_\mathrm{c}x_j)\left(1 + \frac{k_\mathrm{c}^2}{8}\frac{\partial^2}{\partial p_j^2}\right)\left[\hat{\sigma}_j^x[\alpha_\mathrm{r}R^+ + \alpha_\mathrm{i}I^+], \hat{W}\right] + \\
& - \mathrm{i}\sum_j \cos(k_\mathrm{c}x_j)\left(1 + \frac{k_\mathrm{c}^2}{8}\frac{\partial^2}{\partial p_j^2}\right)\left[\hat{\sigma}_j^y[\alpha_\mathrm{r}I^- - \alpha_\mathrm{i}R^-], \hat{W}\right] + \\
& - \sum_j \frac{k_\mathrm{c}}{2}\sin(k_\mathrm{c}x_j)\frac{\partial}{\partial p_j}\Big\{\left\{\hat{\sigma}_j^x[\alpha_\mathrm{r}R^+ + \alpha_\mathrm{i}I^+], \hat{W}\right\} + \\
& \quad + \left\{\hat{\sigma}_j^y[\alpha_\mathrm{r}I^- - \alpha_\mathrm{i}R^-], \hat{W}\right\} - \frac{\mathrm{i}}{4}\left[I^+\hat{\sigma}_j^x - R^-\hat{\sigma}_j^y, \frac{\partial}{\partial\alpha_\mathrm{r}}\hat{W}\right] + \\
& \quad + \frac{\mathrm{i}}{4}\left[R^+\hat{\sigma}_j^x + I^-\hat{\sigma}_j^y, \frac{\partial}{\partial\alpha_\mathrm{i}}\hat{W}\right]\Big\},
\end{aligned} \tag{6.74}$$

where $R^+ = \Re(S_1) + \Re(S_2)$, $R^- = \Re(S_1) - \Re(S_2)$, $I^+ = \Im(S_1) + \Im(S_2)$ and $I^- = \Im(S_1) - \Im(S_2)$. Equation (6.74) is a partial differential equation with up to second order derivatives in the variables t, x_j, p_j, α_r and α_i of the operator $\hat{W} \equiv \hat{W}_t(\boldsymbol{x}, \boldsymbol{p}, \alpha_\mathrm{r}, \alpha_\mathrm{i})$.

We now calculate the time evolution of the functions $\mathrm{Tr}\{\hat{W}_t(\boldsymbol{x}, \boldsymbol{p}, \alpha_\mathrm{r}, \alpha_\mathrm{i})\}$ and $\mathrm{Tr}\{\hat{\sigma}_j^l\hat{W}_t(\boldsymbol{x}, \boldsymbol{p}, \alpha_\mathrm{r}, \alpha_\mathrm{i})\}$, where $\mathrm{Tr}\{\cdot\}$ denotes the trace over the spins degrees of freedom. Tracing equation (6.74) we obtain

$$\begin{aligned}
\frac{\partial}{\partial t}\mathrm{Tr}(\hat{W}) = & \left[-\sum_j \frac{p_j}{m}\frac{\partial}{\partial x_j} + \frac{\kappa}{4}\left(\frac{\partial^2}{\partial\alpha_\mathrm{r}^2} + \frac{\partial^2}{\partial\alpha_\mathrm{i}^2}\right) + \right. \\
& \left. + \frac{\partial}{\partial\alpha_\mathrm{r}}(\kappa\alpha_\mathrm{r} + \Delta_\mathrm{c}\alpha_\mathrm{i}) + \frac{\partial}{\partial\alpha_\mathrm{i}}(\kappa\alpha_\mathrm{i} - \Delta_\mathrm{c}\alpha_\mathrm{r})\right]\mathrm{Tr}(\hat{W}) + \\
& - \sum_j\left[k_\mathrm{c}\sin(k_\mathrm{c}x_j)\frac{\partial}{\partial p_j}\left(\alpha_\mathrm{r}R^+ + \alpha_\mathrm{i}I^+\right) + \right. \\
& \quad \left. + \frac{\cos(k_\mathrm{c}x_j)}{2}\left(I^+\frac{\partial}{\partial\alpha_\mathrm{r}} - R^+\frac{\partial}{\partial\alpha_\mathrm{i}}\right)\right]\mathrm{Tr}(\hat{\sigma}_j^x\hat{W}) + \\
& - \sum_j\left[k_\mathrm{c}\sin(k_\mathrm{c}x_j)\frac{\partial}{\partial p_j}(\alpha_\mathrm{r}I^- - \alpha_\mathrm{i}R^-) + \right. \\
& \quad \left. - \frac{\cos(k_\mathrm{c}x_j)}{2}\left(R^-\frac{\partial}{\partial\alpha_\mathrm{r}} + I^-\frac{\partial}{\partial\alpha_\mathrm{i}}\right)\right]\mathrm{Tr}(\hat{\sigma}_j^y\hat{W}).
\end{aligned} \tag{6.75}$$

Using equation (6.74) we calculate $\mathrm{Tr}(\hat{\sigma}_l^x \hat{W})$:

$$\begin{aligned}
\frac{\partial}{\partial t}\mathrm{Tr}(\hat{\sigma}_l^x \hat{W}) = \Bigg[& \frac{\kappa}{4}\left(\frac{\partial^2}{\partial \alpha_\mathrm{r}^2} + \frac{\partial^2}{\partial \alpha_\mathrm{i}^2}\right) - \sum_j \frac{p_j}{m}\frac{\partial}{\partial x_j} + \\
& + \frac{\partial}{\partial \alpha_\mathrm{r}}(\kappa\alpha_\mathrm{r} + \Delta_\mathrm{c}\alpha_\mathrm{i}) + \frac{\partial}{\partial \alpha_\mathrm{i}}(\kappa\alpha_\mathrm{i} - \Delta_\mathrm{c}\alpha_\mathrm{r})\Bigg]\mathrm{Tr}(\hat{\sigma}_l^x \hat{W}) + \\
& - \Delta_\mathrm{e}\,\mathrm{Tr}(\hat{\sigma}_l^y \hat{W}) + \\
& - \frac{\cos(k_\mathrm{c} x_l)}{2}\Bigg[\frac{\partial}{\partial \alpha_\mathrm{r}} I^+ - \frac{\partial}{\partial \alpha_\mathrm{i}} R^+ + \\
& \quad - k_\mathrm{c}\sin(k_\mathrm{c} x_l)\frac{\partial}{\partial p_l}(\alpha_\mathrm{r} R^+ + \alpha_\mathrm{i} I^+)\Bigg]\mathrm{Tr}(\hat{W}) \\
& + \Bigg[2\cos(k_\mathrm{c} x_l)\left(1 + \frac{k_\mathrm{c}^2}{8}\frac{\partial^2}{\partial p_l^2}\right)(\alpha_\mathrm{r} I^- - \alpha_\mathrm{i} R^-) + \\
& \quad + \frac{k_\mathrm{c}}{4}\sin(k_\mathrm{c} x_l)\frac{\partial}{\partial p_l}\left(R^-\frac{\partial}{\partial \alpha_\mathrm{r}} + I^-\frac{\partial}{\partial \alpha_\mathrm{i}}\right)\Bigg]\mathrm{Tr}(\hat{\sigma}_l^z \hat{W}) + \\
& - \sum_{j\neq l}\Bigg[\frac{\cos(k_\mathrm{c} x_j)}{2}\left(I^+\frac{\partial}{\partial \alpha_\mathrm{r}} - R^+\frac{\partial}{\partial \alpha_\mathrm{i}}\right) + \\
& \quad + k_\mathrm{c}\sin(k_\mathrm{c} x_j)\frac{\partial}{\partial p_j}(\alpha_\mathrm{r} R^+ + \alpha_\mathrm{i} I^+)\Bigg]\mathrm{Tr}(\hat{\sigma}_l^x \hat{\sigma}_j^x \hat{W}) + \\
& + \sum_{j\neq l}\Bigg[\frac{\cos(k_\mathrm{c} x_j)}{2}\left(R^-\frac{\partial}{\partial \alpha_\mathrm{r}} + I^-\frac{\partial}{\partial \alpha_\mathrm{i}}\right) + \\
& \quad - k_\mathrm{c}\sin(k_\mathrm{c} x_j)\frac{\partial}{\partial p_j}(\alpha_\mathrm{r} I^- - \alpha_\mathrm{i} R^-)\Bigg]\mathrm{Tr}(\hat{\sigma}_l^x \hat{\sigma}_j^y \hat{W}).
\end{aligned} \tag{6.76}$$

Equations (6.75) and (6.76) are partial differential equations with up to second order derivatives in the variables t, x_j, p_j, α_r and α_i of the scalar functions $\mathrm{Tr}(\hat{W})$ and $\mathrm{Tr}(\hat{\sigma}_l^x \hat{W})$, respectively.

6.D.3 *Simulated Focker-Planck equation*

The system of stochastic differential equation introduced in Sec. 6.2.3 is equivalent to the following Focker-Planck equation

$$\begin{aligned}\frac{\partial f_t}{\partial t} = &-\sum_j \Bigg\{ \frac{p_j}{m}\frac{\partial}{\partial x_j} + \frac{\kappa}{4}\left(\frac{\partial^2}{\partial \alpha_\mathrm{r}^2} + \frac{\partial^2}{\partial {\alpha_\mathrm{i}}^2}\right) + \kappa\frac{\partial}{\partial \alpha_\mathrm{r}}\alpha_\mathrm{r} + \kappa\frac{\partial}{\partial \alpha_\mathrm{i}}\alpha_\mathrm{i} + \\ &+ k_\mathrm{c}\sin(k_\mathrm{c}x_j)\left(R^+ s_j^x\alpha_\mathrm{r} - R^- s_j^y\alpha_\mathrm{i} + I^+ s_j^x\alpha_\mathrm{i} + I^- s_j^y\alpha_\mathrm{r}\right)\frac{\partial}{\partial p_j} + \\ &+ \Big[-\Delta_\mathrm{e} s_j^y + 2\cos(k_\mathrm{c}x_j)s_j^z\left(I^-\alpha_\mathrm{r} - R^-\alpha_\mathrm{i}\right)\Big]\frac{\partial}{\partial s_j^x} + \\ &+ \Big[\Delta_\mathrm{e} s_j^x - 2\cos(k_\mathrm{c}x_j)s_j^z\left(R^+\alpha_\mathrm{r} + I^+\alpha_\mathrm{i}\right)\Big]\frac{\partial}{\partial s_j^y} + \\ &- 2\cos(k_\mathrm{c}x_j)\left(I^- s_j^x\alpha_\mathrm{r} - I^+ s_j^y\alpha_\mathrm{i} - R^- s_j^x\alpha_\mathrm{i} - R^+ s_j^y\alpha_\mathrm{r}\right)\frac{\partial}{\partial s_j^z}\Bigg\} f_t + \\ &- \left[-\Delta_\mathrm{c}\alpha_\mathrm{i} + \sum_{j=1}^{N}\frac{\cos(k_\mathrm{c}x_j)}{2}\left(s_j^x I^+ - s_j^y R^-\right)\right]\frac{\partial}{\partial \alpha_\mathrm{r}} f_t + \\ &- \left[\Delta_\mathrm{c}\alpha_\mathrm{r} - \sum_{j=1}^{N}\frac{\cos(k_\mathrm{c}x_j)}{2}\left(s_j^x R^+ + s_j^y I^-\right)\right]\frac{\partial}{\partial \alpha_\mathrm{i}} f_t.\end{aligned} \tag{6.77}$$

for the probability density $f_t \equiv f_t(\boldsymbol{x}, \boldsymbol{p}, \boldsymbol{s}, \alpha_\mathrm{r}, \alpha_\mathrm{i})$, where $\boldsymbol{x}$ and $\boldsymbol{p}$ are N-dimensional vectors and $\boldsymbol{s} = (s_1^x, \dots, s_N^x, s_1^y, \dots, s_N^y, s_1^z, \dots, s_N^z)$.

We define the functions

$$W(t, \boldsymbol{x}, \boldsymbol{p}, \alpha_\mathrm{r}, \alpha_\mathrm{i}) = \int f_t \mathrm{d}^{3N}\boldsymbol{s}, \tag{6.78a}$$

$$W_l^m(t, \boldsymbol{x}, \boldsymbol{p}, \alpha_\mathrm{r}, \alpha_\mathrm{i}) = \int s_l^m f_t \mathrm{d}^{3N}\boldsymbol{s}, \tag{6.78b}$$

$$W_{lj}^{mn}(t, \boldsymbol{x}, \boldsymbol{p}, \alpha_\mathrm{r}, \alpha_\mathrm{i}) = \int s_l^m s_j^n f_t \mathrm{d}^{3N}\boldsymbol{s}, \tag{6.78c}$$

where $l, j = 1, \dots, N$ and $m, n = x, y, z$. Using Eq. (6.77) we now calculate the equations for the functions W and ${W_l}^m$, Eqs. (6.78a) and (6.78b). Integrating equation (6.77) in $\mathrm{d}^{3N}\boldsymbol{s}$ one obtains

$$\begin{aligned}\frac{\partial W}{\partial t} = \Bigg[&- \sum_j \frac{p_j}{m}\frac{\partial}{\partial x_j} + \frac{\kappa}{4}\left(\frac{\partial^2}{\partial \alpha_{\mathrm{r}}^2} + \frac{\partial^2}{\partial {\alpha_{\mathrm{i}}}^2}\right) + \\ &+ \frac{\partial}{\partial \alpha_{\mathrm{r}}}(\kappa\alpha_{\mathrm{r}} + \Delta_{\mathrm{c}}\alpha_{\mathrm{i}}) + \frac{\partial}{\partial \alpha_{\mathrm{i}}}(\kappa\alpha_{\mathrm{i}} - \Delta_{\mathrm{c}}\alpha_{\mathrm{r}})\Bigg] W + \\ &- \sum_j \Bigg[k_{\mathrm{c}} \sin\!\left(k_{\mathrm{c}} x_j\right)\left(R^+\alpha_{\mathrm{r}} + I^+\alpha_{\mathrm{i}}\right)\frac{\partial}{\partial p_j} + \\ &\quad + \frac{\cos\!\left(k_{\mathrm{c}} x_j\right)}{2}\left(I^+\frac{\partial}{\partial \alpha_{\mathrm{r}}} - R^+\frac{\partial}{\partial \alpha_{\mathrm{i}}}\right)\Bigg] {W_j}^x + \\ &- \sum_j \Bigg[k_{\mathrm{c}} \sin\!\left(k_{\mathrm{c}} x_j\right)\frac{\partial}{\partial p_j}\left(I^-\alpha_{\mathrm{r}} - R^-\alpha_{\mathrm{i}}\right) + \\ &\quad - \frac{\cos\!\left(k_{\mathrm{c}} x_j\right)}{2}\left(R^-\frac{\partial}{\partial \alpha_{\mathrm{r}}} + I^-\frac{\partial}{\partial \alpha_{\mathrm{i}}}\right)\Bigg] {W_j}^y .\end{aligned} \tag{6.79}$$

Integrating equation (6.77) in $s_l^x \mathrm{d}^{3N}\boldsymbol{s}$ one obtains

$$\begin{aligned}\frac{\partial {W_l}^x}{\partial t} = \Bigg[&- \sum_j \frac{p_j}{m}\frac{\partial}{\partial x_j} + \frac{\kappa}{4}\left(\frac{\partial^2}{\partial \alpha_{\mathrm{r}}^2} + \frac{\partial^2}{\partial {\alpha_{\mathrm{i}}}^2}\right) + \\ &\quad + \frac{\partial}{\partial \alpha_{\mathrm{r}}}(\kappa\alpha_{\mathrm{r}} + \Delta_{\mathrm{c}}\alpha_{\mathrm{i}}) + \frac{\partial}{\partial \alpha_{\mathrm{i}}}(\kappa\alpha_{\mathrm{i}} - \Delta_{\mathrm{c}}\alpha_{\mathrm{r}})\Bigg] {W_l}^x + \\ &- \Delta_{\mathrm{e}} {W_l}^y + 2\cos\!\left(k_{\mathrm{c}} x_j\right)\left(I^-\alpha_{\mathrm{r}} - R^-\alpha_{\mathrm{i}}\right) {W_l}^z + \\ &- \sum_j \Bigg[k_{\mathrm{c}} \sin\!\left(k_{\mathrm{c}} x_j\right)\left(R^+\alpha_{\mathrm{r}} + I^+\alpha_{\mathrm{i}}\right)\frac{\partial}{\partial p_j} + \\ &\quad + \frac{\cos\!\left(k_{\mathrm{c}} x_j\right)}{2}\left(I^+\frac{\partial}{\partial \alpha_{\mathrm{r}}} - R^+\frac{\partial}{\partial \alpha_{\mathrm{i}}}\right)\Bigg] {W_{lj}}^{xx} + \\ &- \sum_j \Bigg[k_{\mathrm{c}} \sin\!\left(k_{\mathrm{c}} x_j\right)\frac{\partial}{\partial p_j}\left(I^-\alpha_{\mathrm{r}} - R^-\alpha_{\mathrm{i}}\right) + \\ &\quad - \frac{\cos\!\left(k_{\mathrm{c}} x_j\right)}{2}\left(R^-\frac{\partial}{\partial \alpha_{\mathrm{r}}} + I^-\frac{\partial}{\partial \alpha_{\mathrm{i}}}\right)\Bigg] {W_{lj}}^{xy} .\end{aligned} \tag{6.80}$$

6.D.4 *Discussion*

We now identify the function W with $\mathrm{Tr}\left(\hat{W}\right)$, and the function ${W_l}^x$ with $\mathrm{Tr}\left(\hat{\sigma}_l^x \hat{W}\right)$, and compare Eq (6.75) with Eq. (6.79) and Eq. (6.76) with Equation (6.80). They differ of terms of the order of $O(N^{-1})$. Further analysis is required in order to complete this treatment and verify our assumptions.

Part V

SUMMARY AND CONCLUSIONS

SUMMARY AND CONCLUSIONS

In this thesis we have investigated the dynamics of several quantum systems with potential applications in quantum technologies [2, 3].

In Part II we have analyzed the system composed of a single atom trapped in an high-finesse optical cavity for the purpose of realizing a quantum memory for single photons. The atom couples to the cavity photon field and is driven by a laser. The input photon, propagating in the transmission line, impinges on one of the mirrors of the cavity. Photon storage is realized by the controlled transfer of the photonic excitation into a metastable state of the atom and occurs via a Raman transition by suitably tailoring the laser pulse. We take into account irreversible losses due to the finite lifetime of the excited state of the atom, due to absorption and reflection at the cavity mirrors and due to the finite transmittivity of the second mirror. We first analyze the adiabatic regime where we compare three different protocols [122–124] and derive a new protocol which takes into account all the irreversible losses. We also generalize a result of [124] showing that, in the adiabatic regime, there is an upper bound to the storage efficiency which is mainly determined by the cooperativity and the parasitic cavity losses. Furthermore we derive the shape of the laser pulse that leads to storage of the single photon with the maximal efficiency. We then explore the non-adiabatic regime by means of optimal control theory (OCT): the optimized control pulse does not lead to efficiencies higher then the one in the adiabatic limit, however the maximal efficiency can also be reached in a parameter regime where the dynamics is not adiabatic. We also numerically determine the lower bound to the coherence time of the photon for which a given efficiency can be reached, and show that this is limited by the linewidth of the cavity. Finally we analyze how such a quantum memory for single photons can be tested with other types of light pulses. In particular, we analyze the storage of attenuated laser pulses because, due to the simplicity of their production, they are often employed in experimental setups [120, 139]. We determine how the storage efficiency of a single photon is related to the storage efficiency of a weak coherent pulse. The method we develop can be easily extended to other type of light pulses.

In Part III we have analyzed a solid-state system consisting of a nitrogen-vacancy (NV) center embedded in a monolithic diamond structure which is both an optical and a mechanical resonator (also called phoxonic crystal cavity [165]). The NV-center is driven by an external laser and interacts with the optical cavity photon field and with the strain field of the mechanical oscillator. The optical cavity and the mechanical oscillator are coupled by radiation pressure. Furthermore, the NV-center excited states exhibit pure dephasing due to the phononic environment

of the diamond crystal [160, 195]. We have characterized the dynamics of cooling of the mechanical resonator with respect to controllable external parameters, such as the laser detunings. We have determined the cooling regime, the cooling rate, the asymptotic temperatures, and the spectrum of resonance fluorescence for experimentally relevant parameter regimes. For these parameters we show that the addition of an optical cavity in general does not improve the cooling efficiency, while pure dephasing of the NV-center's electronic transitions makes the cooling more robust respect to change of external parameters. Cooling of mechanical degrees of freedom is relevant for quantum information processing [38–40], and for ultrasensitive detection applications [42–46].

In Part IV we investigate the system composed of a thermal ensemble of atoms confined in an optical cavity. The atoms are driven by two external lasers and coherently scatter light into the cavity mode, which, in turn, dissipate lights. Transitions between two internal states of the atoms are induced by Raman scattering of cavity and laser photons. We numerically predict the existence of a spinor self-ordered state which involves a periodic spatial density with period $\lambda_c/2$, where λ_c is the cavity wavelength, and an anti-ferromagnetic ordering of the atomic spins with period λ_c. The transition into the self-ordered state occurs with the breaking of the discrete $\mathbb{Z}_2$ symmetry associated with the sign change of the cavity field and with the flip of all the spins. This phenomenon occurs above a threshold value of the pumping lasers strength. Furthermore we show how some properties of the spinor self-ordered state can be manipulated by means of the external lasers, and how the light emitted by the cavity can be used to reveal the state of the system. Envisaged applications of this system include sensors [242], quantum-enhanced metrology [243] and quantum simulators [244, 245].

All the systems we analyze in this thesis are presently intensively investigated in experimental setups [120, 165, 225, 227, 247].

All the analysis presented in this thesis can be extended in various directions, which are already discussed in each Chapter. However here we point out some possible common paths. The methods developed in Parts III and II, for example, can be used to investigate the development of a quantum memory in the solid state system composed of a NV-center in a phoxonic crystal cavity, where the nuclear spin of the nitrogen atom [206] intrinsic to the NV-center or the nuclear spin of an adjacent carbon atom [207] is used to store the photonic excitation. Here, the mechanical resonator could also be driven [208] in order to improve the storage efficiency. Another possibility, is to analyze spin synchronization of an ensemble of NV-centers embedded in a phoxonic crystal. Also, synchronization of different mechanical modes of the diamond structure can be explored. The setup of Part IV can be investigated to build a robust quantum memory since the symmetry broken states are robust against fluctuations of external parameters.

Within the last two decades, many advances have been made in the development of quantum technologies. It is, however, still difficult to predict what the exact physical components of future quantum technologies will be. Also for this reason, research in several different fields and platforms is very important. This thesis is a contribution towards the control of quantum systems for the development quantum technologies.

[1] R. Feynman, R. Leighton, and M. Sands. "Lectures on Physics, vol. III: Quantum Mechanics." In: *Reading, MA: Addison-Wesley* (1965) (cited on page 1).

[2] S. Wehner, D. Elkouss, and R. Hanson. "Quantum internet: A vision for the road ahead." In: *Science* 362 (2018), eaam9288 (cited on pages 1, 145).

[3] A. Acín, I. Bloch, H. Buhrman, T. Calarco, C. Eichler, J. Eisert, D. Esteve, N. Gisin, S. J. Glaser, F. Jelezko, et al. "The quantum technologies roadmap: a European community view." In: *New Journal of Physics* 20 (2018), p. 080201 (cited on pages 1, 145).

[4] H. J. Kimble. "The quantum internet." In: *Nature* 453 (2008), p. 1023 (cited on pages 1, 2, 31).

[5] C. H. Bennett and G. Brassard. *Proceedings of the IEEE International Conference on Computers, Systems and Signal Processing*. 1984 (cited on page 1).

[6] A. K. Ekert. "Quantum cryptography based on Bell's theorem." In: *Physical review letters* 67 (1991), p. 661 (cited on page 1).

[7] P. Komar, E. M. Kessler, M. Bishof, L. Jiang, A. S. Sørensen, J. Ye, and M. D. Lukin. "A quantum network of clocks." In: *Nature Physics* 10 (2014), p. 582 (cited on page 1).

[8] D. Gottesman, T. Jennewein, and S. Croke. "Longer-baseline telescopes using quantum repeaters." In: *Physical review letters* 109 (2012), p. 070503 (cited on page 1).

[9] R. P. Feynman. "Simulating physics with computers." In: *International journal of theoretical physics* 21 (1982), pp. 467–488 (cited on page 1).

[10] Y. I. Manin. "Computable and uncomputable." In: *Sovetskoye Radio, Moscow* (1980) (cited on page 1).

[11] P. W. Shor. "Algorithms for quantum computation: Discrete logarithms and factoring." In: *Proceedings 35th annual symposium on foundations of computer science*. Ieee. 1994, pp. 124–134 (cited on page 1).

[12] A. K. Lenstra, H. W. Lenstra Jr, M. S. Manasse, and J. M. Pollard. "The number field sieve." In: *Proceedings of the twenty-second annual ACM symposium on Theory of computing*. ACM. 1990, pp. 564–572 (cited on page 1).

[13] J. Preskill. "Quantum computing and the entanglement frontier." In: *arXiv preprint arXiv:1203.5813* (2012) (cited on page 1).

[14] F. Arute et al. "Quantum supremacy using a programmable superconducting processor." In: *Nature* 574 (2019), pp. 505–510. ISSN: 1476-4687 (cited on page 1).

[15] E. Pednault, J. A. Gunnels, G. Nannicini, L. Horesh, and R. Wisnieff. *Leveraging Secondary Storage to Simulate Deep 54-qubit Sycamore Circuits*. 2019. arXiv: 1910.09534 [quant-ph] (cited on page 1).

[16] S. Aaronson and L. Chen. *Complexity-Theoretic Foundations of Quantum Supremacy Experiments*. 2016. arXiv: 1612.05903 [quant-ph] (cited on page 1).

[17] T. H. Johnson, S. R. Clark, and D. Jaksch. "What is a quantum simulator?" In: *EPJ Quantum Technology* 1 (2014), p. 10. ISSN: 2196-0763 (cited on page 1).

[18] I. M. Georgescu, S. Ashhab, and F. Nori. "Quantum simulation." In: *Reviews of Modern Physics* 86 (2014), p. 153 (cited on page 1).

[19] F. Yamaguchi and Y. Yamamoto. "Quantum simulation of the t–J model." In: *Superlattices and microstructures* 32 (2002), pp. 343–345 (cited on page 1).

[20] E. Manousakis. "A quantum-dot array as model for copper-oxide superconductors: A dedicated quantum simulator for the many-fermion problem." In: *Journal of low temperature physics* 126 (2002), pp. 1501–1513 (cited on page 1).

[21] A. Klein and D. Jaksch. "Simulating high-temperature superconductivity model Hamiltonians with atoms in optical lattices." In: *Physical Review A* 73 (2006), p. 053613 (cited on page 1).

[22] D. A. Lidar and O. Biham. "Simulating Ising spin glasses on a quantum computer." In: *Physical Review E* 56 (1997), p. 3661 (cited on page 1).

[23] D. I. Tsomokos, S. Ashhab, and F. Nori. "Fully connected network of superconducting qubits in a cavity." In: *New Journal of Physics* 10 (2008), p. 113020 (cited on page 1).

[24] B. P. Lanyon, J. D. Whitfield, G. G. Gillett, M. E. Goggin, M. P. Almeida, I. Kassal, J. D. Biamonte, M. Mohseni, B. J. Powell, M. Barbieri, et al. "Towards quantum chemistry on a quantum computer." In: *Nature chemistry* 2 (2010), p. 106 (cited on page 2).

[25] G. R. Fleming, S. Huelga, and M. B. Plenio. "Focus on quantum effects and noise in biomolecules." In: *New Journal of Physics* 13 (2011), p. 115002 (cited on page 2).

[26] P. K. Ghosh, A. Y. Smirnov, and F. Nori. "Quantum effects in energy and charge transfer in an artificial photosynthetic complex." In: *The Journal of chemical physics* 134 (2011), 06B611 (cited on page 2).

[27] V. Giovannetti, S. Lloyd, and L. Maccone. "Quantum metrology." In: *Physical review letters* 96 (2006), p. 010401 (cited on page 2).

[28] V. Giovannetti, S. Lloyd, and L. Maccone. "Advances in quantum metrology." In: *Nature photonics* 5 (2011), p. 222 (cited on page 2).

[29] C. L. Degen, F. Reinhard, and P. Cappellaro. "Quantum sensing." In: *Reviews of modern physics* 89 (2017), p. 035002 (cited on page 2).

[30] H. J. Kimble, Y. Levin, A. B. Matsko, K. S. Thorne, and S. P. Vyatchanin. "Conversion of conventional gravitational-wave interferometers into quantum nondemolition interferometers by modifying their input and/or output optics." In: *Physical Review D* 65 (2001), p. 022002 (cited on page 2).

[31] M. A. Taylor and W. P. Bowen. "Quantum metrology and its application in biology." In: *Physics Reports* 615 (2016), pp. 1–59 (cited on page 2).

[32] S. Haroche. "Nobel Lecture: Controlling photons in a box and exploring the quantum to classical boundary." In: *Reviews of Modern Physics* 85 (2013), p. 1083 (cited on page 2).

[33] R. Blatt and D. Wineland. "Entangled states of trapped atomic ions." In: *Nature* 453 (2008), p. 1008 (cited on page 2).

[34] I. Bloch, J. Dalibard, and S. Nascimbene. "Quantum simulations with ultracold quantum gases." In: *Nature Physics* 8 (2012), p. 267 (cited on page 2).

[35] A. Reiserer and G. Rempe. "Cavity-based quantum networks with single atoms and optical photons." In: *Reviews of Modern Physics* 87 (2015), p. 1379 (cited on pages 2, 31, 57).

[36] M. Atatüre, D. Englund, N. Vamivakas, S.-Y. Lee, and J. Wrachtrup. "Material platforms for spin-based photonic quantum technologies." In: *Nature Reviews Materials* 3 (2018), p. 38 (cited on page 2).

[37] M. H. Devoret and R. J. Schoelkopf. "Superconducting circuits for quantum information: an outlook." In: *Science* 339 (2013), pp. 1169–1174 (cited on page 2).

[38] S. Mancini, D. Vitali, and P. Tombesi. "Scheme for teleportation of quantum states onto a mechanical resonator." In: *Physical review letters* 90 (2003), p. 137901 (cited on pages 3, 146).

[39] K. Stannigel, P. Rabl, A. S. Sørensen, P. Zoller, and M. D. Lukin. "Optomechanical transducers for long-distance quantum communication." In: *Physical review letters* 105 (2010), p. 220501 (cited on pages 3, 146).

[40] K. Stannigel, P. Komar, S. Habraken, S. Bennett, M. D. Lukin, P. Zoller, and P. Rabl. "Optomechanical quantum information processing with photons and phonons." In: *Physical review letters* 109 (2012), p. 013603 (cited on pages 3, 146).

[41] G. Kurizki, P. Bertet, Y. Kubo, K. Mølmer, D. Petrosyan, P. Rabl, and J. Schmiedmayer. "Quantum technologies with hybrid systems." In: *Proceedings of the National Academy of Sciences* 112 (2015), pp. 3866–3873 (cited on page 3).

[42] M. LaHaye, O. Buu, B. Camarota, and K. Schwab. "Approaching the quantum limit of a nanomechanical resonator." In: *Science* 304 (2004), pp. 74–77 (cited on pages 3, 146).

[43] J. D. Teufel, T. Donner, M. Castellanos-Beltran, J. W. Harlow, and K. W. Lehnert. "Nanomechanical motion measured with an imprecision below that at the standard quantum limit." In: *Nature nanotechnology* 4 (2009), p. 820 (cited on pages 3, 146).

[44] A. G. Krause, M. Winger, T. D. Blasius, Q. Lin, and O. Painter. "A high-resolution microchip optomechanical accelerometer." In: *Nature Photonics* 6 (2012), p. 768 (cited on pages 3, 146).

[45] Y.-W. Hu, Y.-F. Xiao, Y.-C. Liu, and Q. Gong. "Optomechanical sensing with on-chip microcavities." In: *Frontiers of Physics* 8 (2013), pp. 475–490 (cited on pages 3, 146).

[46] T. P. Purdy, R. W. Peterson, and C. Regal. "Observation of radiation pressure shot noise on a macroscopic object." In: *Science* 339 (2013), pp. 801–804 (cited on pages 3, 146).

[47] F. Mivehvar, H. Ritsch, and F. Piazza. "Cavity-quantum-electrodynamical toolbox for quantum magnetism." In: *Physical Review Letters* 122 (2019), p. 113603 (cited on pages 3, 111, 113, 127).

[48] D. Lachance-Quirion, Y. Tabuchi, A. Gloppe, K. Usami, and Y. Nakamura. "Hybrid quantum systems based on magnonics." In: *Applied Physics Express* 12 (2019), p. 070101 (cited on pages 3, 127).

[49] S. V. Kusminskiy. *Quantum Magnetism, Spin Waves, and Optical Cavities*. Springer, 2019 (cited on pages 3, 127).

[50] M. K. E. L. Planck. "Zur theorie des gesetzes der energieverteilung im normalspectrum." In: *Verhandl. Dtsc. Phys. Ges.* 2 (1900), p. 237 (cited on page 7).

[51] A. Einstein. "Über einen die Erzeugung und Verwandlung des Lichtes betreffenden heuristischen Gesichtspunkt." In: *Annalen der physik* 322 (1905), pp. 132–148 (cited on page 7).

[52] C. Cohen-Tannoudji, J. Dupont-Roc, and G. Grynberg. *Atom–Photon Interactions: Basic Processes and Applications, 2004*. Weinheim: WILEY-VCH Verlag GmbH & Co. KGaA (cited on pages 7, 9, 10, 15, 53, 62).

[53] W. P. Schleich. *Quantum optics in phase space*. Weinheim: WILEY-VCH Verlag GmbH & Co. KGaA, 2001 (cited on pages 7, 9–11, 23, 57).

[54] M. O. Scully and M. S. Zubairy. *Quantum optics*. Cambridge University Press, 1997 (cited on page 7).

[55] D. F. Walls and G. J. Milburn. *Quantum optics*. Springer Science & Business Media, 2007 (cited on pages 7, 11, 38, 46, 53, 69).

[56] M. Aspelmeyer, T. J. Kippenberg, and F. Marquardt. "Cavity optomechanics." In: *Reviews of Modern Physics* 86 (2014), p. 1391 (cited on pages 7, 10, 13, 75).

[57] R. J. Glauber. "Coherent and incoherent states of the radiation field." In: *Physical Review* 131 (1963), p. 2766 (cited on pages 9, 57).

[58] H. Kogelnik and T. Li. "Laser Beams and Resonators." In: *Appl. Opt.* 5 (1966), pp. 1550–1567 (cited on page 10).

[59] A. Neuzner, M. Körber, O. Morin, S. Ritter, and G. Rempe. "Interference and dynamics of light from a distance-controlled atom pair in an optical cavity." In: *Nature Photonics* 10 (2016), p. 303 (cited on page 10).

[60] H. Gothe, D. Sholokhov, A. Breunig, M. Steinel, and J. Eschner. "Continuous-wave virtual-state lasing from cold ytterbium atoms." In: *Phys. Rev. A* 99 (2019), p. 013415 (cited on page 10).

[61] F. Brennecke, T. Donner, S. Ritter, T. Bourdel, M. Köhl, and T. Esslinger. "Cavity QED with a Bose–Einstein condensate." In: *Nature* 450 (2007), p. 268 (cited on page 10).

[62] E. T. Jaynes and F. W. Cummings. "Comparison of quantum and semiclassical radiation theories with application to the beam maser." In: *Proceedings of the IEEE* 51 (1963), pp. 89–109 (cited on page 11).

[63] H. J. Metcalf and P. van der Straten. *Laser Cooling and Trapping*. New York: Springer-Verlag, 1999 (cited on page 12).

[64] D. Wineland and H. Dehmelt. "Proposed $10^{14}\Delta_\nu < \nu$ laser fluorescence spectroscopy on TI^+ mono-ion oscillator III." In: *Bulletin of the American Physical Society* 20 (1975), p. 637 (cited on page 12).

[65] T. W. Hänsch and A. L. Schawlow. "Cooling of gases by laser radiation." In: *Optics Communications* 13 (1975), pp. 68–69 (cited on page 12).

[66] D. J. Wineland, R. E. Drullinger, and F. L. Walls. "Radiation-pressure cooling of bound resonant absorbers." In: *Physical Review Letters* 40 (1978), p. 1639 (cited on page 12).

[67] W. Happer. "Optical pumping." In: *Reviews of Modern Physics* 44 (1972), p. 169 (cited on page 12).

[68] W. D. Phillips. "Nobel Lecture: Laser cooling and trapping of neutral atoms." In: *Reviews of Modern Physics* 70 (1998), p. 721 (cited on page 12).

[69] P. D. Lett, R. N. Watts, C. I. Westbrook, W. D. Phillips, P. L. Gould, and H. J. Metcalf. "Observation of atoms laser cooled below the Doppler limit." In: *Physical review letters* 61 (1988), p. 169 (cited on page 12).

[70] C. Cohen-Tannoudji and W. D. Phillips. "New mechanisms for laser cooling." In: *Phys. Today* 43 (1990), pp. 33–40 (cited on page 12).

[71] B. Sheehy, S. Shang, P. Van Der Straten, S. Hatamian, and H. Metcalf. "Magnetic-field-induced laser cooling below the Doppler limit." In: *Physical review letters* 64 (1990), p. 858 (cited on page 12).

[72] J. Dalibard and C. Cohen-Tannoudji. "Laser cooling below the Doppler limit by polarization gradients: simple theoretical models." In: *JOSA B* 6 (1989), pp. 2023–2045 (cited on page 12).

[73] Y. Castin, J. Dalibard, and C. Cohen-Tannoudji. "The limits of Sisyphus cooling." In: *Light induced kinetic effects on atoms, ions and Molecules. Proceeding of the LIKE Workshops, ETS Editrice, Pisa*. 1991, pp. 5–24 (cited on page 12).

[74] P. Horak, G. Hechenblaikner, K. M. Gheri, H. Stecher, and H. Ritsch. "Cavity-induced atom cooling in the strong coupling regime." In: *Physical review letters* 79 (1997), p. 4974 (cited on pages 12, 124).

[75] V. Vuletić and S. Chu. "Laser cooling of atoms, ions, or molecules by coherent scattering." In: *Physical Review Letters* 84 (2000), p. 3787 (cited on pages 12, 124).

[76] G. Morigi, P. W. Pinkse, M. Kowalewski, and R. de Vivie-Riedle. "Cavity cooling of internal molecular motion." In: *Physical review letters* 99 (2007), p. 073001 (cited on page 12).

[77] P. Maunz, T. Puppe, I. Schuster, N. Syassen, P. W. Pinkse, and G. Rempe. "Cavity cooling of a single atom." In: *Nature* 428 (2004), p. 50 (cited on page 12).

[78] M. Hosseini, Y. Duan, K. M. Beck, Y.-T. Chen, and V. Vuletić. "Cavity cooling of many atoms." In: *Physical review letters* 118 (2017), p. 183601 (cited on page 12).

[79] P. Asenbaum, S. Kuhn, S. Nimmrichter, U. Sezer, and M. Arndt. "Cavity cooling of free silicon nanoparticles in high vacuum." In: *Nature communications* 4 (2013), p. 2743 (cited on page 12).

[80] N. Kiesel, F. Blaser, U. Delić, D. Grass, R. Kaltenbaek, and M. Aspelmeyer. "Cavity cooling of an optically levitated submicron particle." In: *Proceedings of the National Academy of Sciences* 110 (2013), pp. 14180–14185 (cited on page 12).

[81] J. Kepler. *De cometis libelli tres*. Typis Andreæ Apergeri, 1619 (cited on page 12).

[82] J. C. Maxwell. *A treatise on electricity and magnetism*. Vol. 2. Oxford: Clarendon Press, 1873 (cited on page 12).

[83] P. Lebedew. "Untersuchungen über die Druckkräfte des Lichtes." In: *Annalen der Physik* 311 (1901), pp. 433–458 (cited on page 12).

[84] E. F. Nichols and G. F. Hull. "A preliminary communication on the pressure of heat and light radiation." In: *Physical Review (Series I)* 13 (1901), p. 307 (cited on page 12).

[85] A. N. Cleland. *Foundations of nanomechanics: from solid-state theory to device applications*. Springer Science & Business Media, 2003 (cited on page 13).

[86] H. B. G. Casimir and D. Polder. "The Influence of Retardation on the London-van der Waals Forces." In: *Phys. Rev.* 73 (1948), pp. 360–372 (cited on page 14).

[87] G. Klimchitskaya, U. Mohideen, and V. Mostepanenko. "The Casimir force between real materials: Experiment and theory." In: *Reviews of Modern Physics* 81 (2009), p. 1827 (cited on page 14).

[88] C. Law. "Interaction between a moving mirror and radiation pressure: A Hamiltonian formulation." In: *Physical Review A* 51 (1995), p. 2537 (cited on pages 14, 81).

[89] H. J. Carmichael. *Statistical methods in quantum optics 1: master equations and Fokker-Planck equations*. Springer Science & Business Media, 2002 (cited on pages 15, 20, 23, 82).

[90] J. Javanainen, M. Lindberg, and S. Stenholm. "Laser cooling of trapped ions: dynamics of the final stages." In: *JOSA B* 1 (1984), pp. 111–115 (cited on pages 15, 85).

[91] H.-J. Briegel and B.-G. Englert. "Quantum optical master equations: The use of damping bases." In: *Physical Review A* 47 (1993), p. 3311 (cited on pages 15, 22, 97).

[92] S. M. Barnett and S. Stenholm. "Spectral decomposition of the Lindblad operator." In: *Journal of Modern Optics* 47 (2000), pp. 2869–2882 (cited on pages 15, 21, 22, 97).

[93] B.-G. Englert and G. Morigi. "Five lectures on dissipative master equations." In: *Coherent evolution in noisy environments*. Springer, 2002, pp. 55–106 (cited on pages 15, 22, 97).

[94] M. Jakob and S. Stenholm. "Variational functions in driven open quantum systems." In: *Physical Review A* 67 (2003), p. 032111 (cited on pages 15, 22).

[95] G. Lindblad. "On the generators of quantum dynamical semigroups." In: *Communications in Mathematical Physics* 48 (1976), pp. 119–130 (cited on pages 18, 22).

[96] A. Rivas and S. F. Huelga. *Open quantum systems*. Springer, 2012 (cited on page 18).

[97] V. F. Weisskopf and E. P. Wigner. "Calculation of the natural brightness of spectral lines on the basis of Dirac's theory." In: *Z. Phys.* 63 (1930), pp. 54–73 (cited on page 19).

[98] M. Lax. "Formal theory of quantum fluctuations from a driven state." In: *Physical Review* 129 (1963), p. 2342 (cited on page 20).

[99] M. Lax. "Quantum noise. X. Density-matrix treatment of field and population-difference fluctuations." In: *Physical Review* 157 (1967), p. 213 (cited on page 20).

[100] K. E. Cahill and R. J. Glauber. "Density operators and quasiprobability distributions." In: *Physical Review* 177 (1969), p. 1882 (cited on page 23).

[101] G. S. Agarwal and E. Wolf. "Calculus for functions of noncommuting operators and general phase-space methods in quantum mechanics. I. Mapping theorems and ordering of functions of noncommuting operators." In: *Physical Review D* 2 (1970), p. 2161 (cited on page 23).

[102] G. Agarwal and E. Wolf. "Calculus for functions of noncommuting operators and general phase-space methods in quantum mechanics. II. Quantum mechanics in phase space." In: *Physical Review D* 2 (1970), p. 2187 (cited on page 23).

[103] G. Agarwal and E. Wolf. "Calculus for functions of noncommuting operators and general phase-space methods in quantum mechanics. III. A generalized Wick theorem and multitime mapping." In: *Physical Review D* 2 (1970), p. 2206 (cited on page 23).

[104] E. Wigner. "On the Quantum Correction For Thermodynamic Equilibrium." In: *Phys. Rev.* 40 (1932), pp. 749–759 (cited on page 23).

[105] C. Gardiner and P. Zoller. *Quantum noise: a handbook of Markovian and non-Markovian quantum stochastic methods with applications to quantum optics*. Vol. 56. Springer Science & Business Media, 2004 (cited on pages 23, 25, 26, 134).

[106] J. I. Cirac, P. Zoller, H. J. Kimble, and H. Mabuchi. "Quantum state transfer and entanglement distribution among distant nodes in a quantum network." In: *Physical Review Letters* 78 (1997), p. 3221 (cited on pages 31, 32, 47, 57).

[107] M. Afzelius, N. Gisin, and H. De Riedmatten. "Quantum memory for photons." In: *Phys. Today* 68 (2015), pp. 42–47 (cited on page 31).

[108] K. Heshami, D. G. England, P. C. Humphreys, P. J. Bustard, V. M. Acosta, J. Nunn, and B. J. Sussman. "Quantum memories: emerging applications and recent advances." In: *Journal of modern optics* 63 (2016), pp. 2005–2028 (cited on page 31).

[109] A. Kalachev. "Quantum storage on subradiant states in an extended atomic ensemble." In: *Physical Review A* 76 (2007), p. 043812 (cited on pages 31, 57).

[110] A. Kalachev. "Quantum memory for light using extended atomic ensembles in a tunable cavity." In: *Physical Review A* 78 (2008), p. 043812 (cited on pages 31, 57).

[111] A. Kalachev. "Writing and reading quantum states of light with tunable cavity: Application to single-photon sources." In: *Optics and Spectroscopy* 109 (2010), pp. 32–39 (cited on pages 31, 57).

[112] L.-M. Duan and C. Monroe. "Colloquium: Quantum networks with trapped ions." In: *Reviews of Modern Physics* 82 (2010), p. 1209 (cited on pages 31, 57).

[113] C. Kurz, M. Schug, P. Eich, J. Huwer, P. Müller, and J. Eschner. "Experimental protocol for high-fidelity heralded photon-to-atom quantum state transfer." In: *Nature communications* 5 (2014), p. 5527 (cited on pages 31, 57).

[114] S. Ritter, C. Nölleke, C. Hahn, A. Reiserer, A. Neuzner, M. Uphoff, M. Mücke, E. Figueroa, J. Bochmann, and G. Rempe. "An elementary quantum network of single atoms in optical cavities." In: *Nature* 484 (2012), p. 195 (cited on page 31).

[115] N. Kalb, A. Reiserer, S. Ritter, and G. Rempe. "Heralded storage of a photonic quantum bit in a single atom." In: *Physical review letters* 114 (2015), p. 220501 (cited on page 31).

[116] C. Kurz, P. Eich, M. Schug, P. Müller, and J. Eschner. "Programmable atom-photon quantum interface." In: *Physical Review A* 93 (2016), p. 062348 (cited on page 31).

[117] J. Brito, S. Kucera, P. Eich, P. Müller, and J. Eschner. "Doubly heralded single-photon absorption by a single atom." In: *Applied Physics B* 122 (2016), p. 36 (cited on page 31).

[118] S. Rosenblum, A. Borne, and B. Dayan. "Analysis of deterministic swapping of photonic and atomic states through single-photon Raman interaction." In: *Physical Review A* 95 (2017), p. 033814 (cited on page 31).

[119] O. Bechler, A. Borne, S. Rosenblum, G. Guendelman, O. E. Mor, M. Netser, T. Ohana, Z. Aqua, N. Drucker, R. Finkelstein, et al. "A passive photon–atom qubit swap operation." In: *Nature Physics* 14 (2018), p. 996 (cited on page 31).

[120] M. Körber, O. Morin, S. Langenfeld, A. Neuzner, S. Ritter, and G. Rempe. "Decoherence-protected memory for a single-photon qubit." In: *Nature Photonics* 12 (2018), p. 18 (cited on pages 31, 38, 45, 52, 61, 64, 145, 146).

[121] A. V. Gorshkov, A. André, M. Fleischhauer, A. S. Sørensen, and M. D. Lukin. "Universal approach to optimal photon storage in atomic media." In: *Physical review letters* 98 (2007), p. 123601 (cited on pages 31, 57).

[122] M. Fleischhauer, S. Yelin, and M. Lukin. "How to trap photons? Storing single-photon quantum states in collective atomic excitations." In: *Optics communications* 179 (2000), pp. 395–410 (cited on pages 31, 32, 35, 38, 39, 41, 45, 53, 57, 58, 60, 66, 145).

[123] J. Dilley, P. Nisbet-Jones, B. W. Shore, and A. Kuhn. "Single-photon absorption in coupled atom-cavity systems." In: *Physical Review A* 85 (2012), p. 023834 (cited on pages 31, 32, 35, 38, 39, 41, 45, 57, 58, 60, 66, 145).

[124] A. V. Gorshkov, A. André, M. D. Lukin, and A. S. Sørensen. "Photon storage in Λ-type optically dense atomic media. I. Cavity model." In: *Physical Review A* 76 (2007), p. 033804 (cited on pages 32, 35–39, 41, 45, 47, 53, 57, 58, 60, 61, 64, 66, 69, 145).

[125] H. Carmichael. *An open systems approach to quantum optics: lectures presented at the Université Libre de Bruxelles, October 28 to November 4, 1991*. Vol. 18. Springer Science & Business Media, 2009 (cited on pages 34, 65).

[126] S. Blum, G. A. Olivares-Rentería, C. Ottaviani, C. Becher, and G. Morigi. "Single-photon frequency conversion in nonlinear crystals." In: *Physical Review A* 88 (2013), p. 053807 (cited on page 35).

[127] P. Müller, T. Tentrup, M. Bienert, G. Morigi, and J. Eschner. "Spectral properties of single photons from quantum emitters." In: *Physical Review A* 96 (2017), p. 023861 (cited on page 36).

[128] A. V. Gorshkov, A. André, M. D. Lukin, and A. S. Sørensen. "Photon storage in Λ-type optically dense atomic media. II. Free-space model." In: *Physical Review A* 76 (2007), p. 033805 (cited on pages 45, 47, 57).

[129] J. Dalibard, Y. Castin, and K. Mølmer. "Wave-function approach to dissipative processes in quantum optics." In: *Physical review letters* 68 (1992), p. 580 (cited on pages 45, 64).

[130] G. S. Vasilev, D. Ljunggren, and A. Kuhn. "Single photons made-to-measure." In: *New Journal of Physics* 12 (2010), p. 063024 (cited on page 47).

[131] M. Keller, B. Lange, K. Hayasaka, W. Lange, and H. Walther. "A calcium ion in a cavity as a controlled single-photon source." In: *New Journal of Physics* 6 (2004), p. 95 (cited on pages 47, 57).

[132] P. B. Nisbet-Jones, J. Dilley, D. Ljunggren, and A. Kuhn. "Highly efficient source for indistinguishable single photons of controlled shape." In: *New Journal of Physics* 13 (2011), p. 103036 (cited on page 47).

[133] I. Novikova, A. V. Gorshkov, D. F. Phillips, A. S. Sørensen, M. D. Lukin, and R. L. Walsworth. "Optimal control of light pulse storage and retrieval." In: *Physical Review Letters* 98 (2007), p. 243602 (cited on page 48).

[134] A. V. Gorshkov, T. Calarco, M. D. Lukin, and A. S. Sørensen. "Photon storage in λ-type optically dense atomic media. IV. Optimal control using gradient ascent." In: *Physical Review A* 77 (2008), p. 043806 (cited on page 48).

[135] N. Khaneja, T. Reiss, C. Kehlet, T. Schulte-Herbrüggen, and S. J. Glaser. "Optimal control of coupled spin dynamics: design of NMR pulse sequences by gradient ascent algorithms." In: *Journal of magnetic resonance* 172 (2005), pp. 296–305 (cited on page 48).

[136] J. R. Johansson, P. D. Nation, and F. Nori. "QuTiP 2: A Python framework for the dynamics of open quantum systems." In: *Computer Physics Communications* 184 (2013), pp. 1234–1240 (cited on page 48).

[137] R. Johansson et al. *qutip/qutip: QuTiP 4.2.0*. 2017 (cited on page 48).

[138] C. P. Koch. "Controlling open quantum systems: tools, achievements, and limitations." In: *Journal of Physics: Condensed Matter* 28 (2016), p. 213001 (cited on pages 48, 67).

[139] O. Morin, M. Körber, S. Langenfeld, and G. Rempe. "Deterministic Shaping and Reshaping of Single-Photon Temporal Wave Functions." In: *Physical Review Letters* 123 (2019), p. 133602 (cited on pages 52, 145).

[140] T. Macha, E. Uruñuela, W. Alt, M. Ammenwerth, D. Pandey, H. Pfeifer, and D. Meschede. "Non-adiabatic Storage of Short Light Pulses in an Atom-Cavity System." In: *arXiv preprint arXiv:1903.10922* (2019) (cited on page 52).

[141] M. V. Berry. "Transitionless quantum driving." In: *Journal of Physics A: Mathematical and Theoretical* 42 (2009), p. 365303 (cited on page 52).

[142] L. Giannelli and E. Arimondo. "Three-level superadiabatic quantum driving." In: *Physical Review A* 89 (2014), p. 033419 (cited on page 52).

[143] A. I. Konnov and V. F. Krotov. "On global methods for the successive improvement of control processes." In: *Automation and Remote Control* 60 (1999), pp. 1427–1436 (cited on page 56).

[144] T. Caneva, T. Calarco, and S. Montangero. "Chopped random-basis quantum optimization." In: *Physical Review A* 84 (2011), p. 022326 (cited on page 56).

[145] H. Mack and W. P. Schleich. "A Photon Viewed from Wigner Phase Space." In: *Optics & Photonics News Trends* 3 (2003), pp. 29–35 (cited on page 57).

[146] R. J. Glauber. "The quantum theory of optical coherence." In: *Physical Review* 130 (1963), p. 2529 (cited on page 57).

[147] H. P. Specht, C. Nölleke, A. Reiserer, M. Uphoff, E. Figueroa, S. Ritter, and G. Rempe. "A single-atom quantum memory." In: *Nature* 473 (2011), p. 190 (cited on page 57).

[148] M. Khudaverdyan, W. Alt, I. Dotsenko, T. Kampschulte, K. Lenhard, A. Rauschenbeutel, S. Reick, K. Schörner, A. Widera, and D. Meschede. "Controlled insertion and retrieval of atoms coupled to a high-finesse optical resonator." In: *New Journal of Physics* 10 (2008), p. 073023 (cited on page 57).

[149] H. J. Kimble. "Strong interactions of single atoms and photons in cavity QED." In: *Physica Scripta* 1998 (1998), p. 127 (cited on page 57).

[150] L. Giannelli, T. Schmit, T. Calarco, C. P. Koch, S. Ritter, and G. Morigi. "Optimal storage of a single photon by a single intracavity atom." In: *New Journal of Physics* 20 (2018), p. 105009 (cited on pages 58, 60, 61, 69).

[151] N. V. Vitanov, A. A. Rangelov, B. W. Shore, and K. Bergmann. "Stimulated Raman adiabatic passage in physics, chemistry, and beyond." In: *Reviews of Modern Physics* 89 (2017), p. 015006 (cited on page 64).

[152] R. Dum, P. Zoller, and H. Ritsch. "Monte Carlo simulation of the atomic master equation for spontaneous emission." In: *Physical Review A* 45 (1992), p. 4879 (cited on pages 64, 65).

[153] K. Rojan, D. M. Reich, I. Dotsenko, J.-M. Raimond, C. P. Koch, and G. Morigi. "Arbitrary-quantum-state preparation of a harmonic oscillator via optimal control." In: *Physical Review A* 90 (2014), p. 023824 (cited on page 67).

[154] M. H. Goerz, E. J. Halperin, J. M. Aytac, C. P. Koch, and K. B. Whaley. "Robustness of high-fidelity Rydberg gates with single-site addressability." In: *Physical Review A* 90 (2014), p. 032329 (cited on page 67).

[155] K. Kobzar, T. E. Skinner, N. Khaneja, S. J. Glaser, and B. Luy. "Exploring the limits of broadband excitation and inversion pulses." In: *Journal of Magnetic Resonance* 170 (2004), pp. 236–243 (cited on page 67).

[156] K. Kobzar, T. E. Skinner, N. Khaneja, S. J. Glaser, and B. Luy. "Exploring the limits of broadband excitation and inversion: II. Rf-power optimized pulses." In: *Journal of Magnetic Resonance* 194 (2008), pp. 58–66 (cited on page 67).

[157] T. Chaneliere, D. Matsukevich, S. Jenkins, S.-Y. Lan, T. Kennedy, and A. Kuzmich. "Storage and retrieval of single photons transmitted between remote quantum memories." In: *Nature* 438 (2005), p. 833 (cited on page 67).

[158] M. W. Doherty, N. B. Manson, P. Delaney, F. Jelezko, J. Wrachtrup, and L. C. Hollenberg. "The nitrogen-vacancy colour centre in diamond." In: *Physics Reports* 528 (2013), pp. 1–45 (cited on pages 75, 83).

[159] T. Schröder, S. L. Mouradian, J. Zheng, M. E. Trusheim, M. Walsh, E. H. Chen, L. Li, I. Bayn, and D. Englund. "Quantum nanophotonics in diamond." In: *JOSA B* 33 (2016), B65–B83 (cited on page 75).

[160] R. Albrecht, A. Bommer, C. Deutsch, J. Reichel, and C. Becher. "Coupling of a single nitrogen-vacancy center in diamond to a fiber-based microcavity." In: *Physical review letters* 110 (2013), p. 243602 (cited on pages 75, 83, 146).

[161] R. Brouri, A. Beveratos, J.-P. Poizat, and P. Grangier. "Photon antibunching in the fluorescence of individual color centers in diamond." In: *Optics letters* 25 (2000), pp. 1294–1296 (cited on page 75).

[162] C. Kurtsiefer, S. Mayer, P. Zarda, and H. Weinfurter. "Stable solid-state source of single photons." In: *Physical review letters* 85 (2000), p. 290 (cited on page 75).

[163] J. Teissier, A. Barfuss, P. Appel, E. Neu, and P. Maletinsky. "Strain coupling of a nitrogen-vacancy center spin to a diamond mechanical oscillator." In: *Physical review letters* 113 (2014), p. 020503 (cited on page 75).

[164] P. Ovartchaiyapong, K. W. Lee, B. A. Myers, and A. C. B. Jayich. "Dynamic strain-mediated coupling of a single diamond spin to a mechanical resonator." In: *Nature communications* 5 (2014), p. 4429 (cited on page 75).

[165] L. Kipfstuhl, F. Guldner, J. Riedrich-Möller, and C. Becher. "Modeling of optomechanical coupling in a phoxonic crystal cavity in diamond." In: *Optics express* 22 (2014), pp. 12410–12423 (cited on pages 75, 82, 83, 145, 146).

[166] L. Li, T. Schröder, E. H. Chen, M. Walsh, I. Bayn, J. Goldstein, O. Gaathon, M. E. Trusheim, M. Lu, J. Mower, et al. "Coherent spin control of a nanocavity-enhanced qubit in diamond." In: *Nature communications* 6 (2015), p. 6173 (cited on pages 75, 83).

[167] K. W. Lee, D. Lee, P. Ovartchaiyapong, J. Minguzzi, J. R. Maze, and A. C. B. Jayich. "Strain coupling of a mechanical resonator to a single quantum emitter in diamond." In: *Physical Review Applied* 6 (2016), p. 034005 (cited on page 75).

[168] E. MacQuarrie, T. Gosavi, N. Jungwirth, S. Bhave, and G. Fuchs. "Mechanical spin control of nitrogen-vacancy centers in diamond." In: *Physical review letters* 111 (2013), p. 227602 (cited on page 75).

[169] E. MacQuarrie, T. Gosavi, A. Moehle, N. Jungwirth, S. Bhave, and G. Fuchs. "Coherent control of a nitrogen-vacancy center spin ensemble with a diamond mechanical resonator." In: *Optica* 2 (2015), pp. 233–238 (cited on page 75).

[170] J. Wrachtrup and F. Jelezko. "Processing quantum information in diamond." In: *Journal of Physics: Condensed Matter* 18 (2006), S807 (cited on page 75).

[171] L. Childress and R. Hanson. "Diamond NV centers for quantum computing and quantum networks." In: *MRS bulletin* 38 (2013), pp. 134–138 (cited on page 75).

[172] K. Nemoto, M. Trupke, S. J. Devitt, A. M. Stephens, B. Scharfenberger, K. Buczak, T. Nöbauer, M. S. Everitt, J. Schmiedmayer, and W. J. Munro. "Photonic architecture for scalable quantum information processing in diamond." In: *Physical Review X* 4 (2014), p. 031022 (cited on page 75).

[173] J. Wrachtrup, F. Jelezko, B. Grotz, and L. McGuinness. "Nitrogen-vacancy centers close to surfaces." In: *MRS bulletin* 38 (2013), pp. 149–154 (cited on page 75).

[174] S. Hong, M. S. Grinolds, L. M. Pham, D. Le Sage, L. Luan, R. L. Walsworth, and A. Yacoby. "Nanoscale magnetometry with NV centers in diamond." In: *MRS bulletin* 38 (2013), pp. 155–161 (cited on page 75).

[175] R. Schirhagl, K. Chang, M. Loretz, and C. L. Degen. "Nitrogen-vacancy centers in diamond: nanoscale sensors for physics and biology." In: *Annual review of physical chemistry* 65 (2014), pp. 83–105 (cited on page 75).

[176] L. Rondin, J.-P. Tetienne, T. Hingant, J.-F. Roch, P. Maletinsky, and V. Jacques. "Magnetometry with nitrogen-vacancy defects in diamond." In: *Reports on progress in physics* 77 (2014), p. 056503 (cited on page 75).

[177] K. Kepesidis, S. Bennett, S. Portolan, M. D. Lukin, and P. Rabl. "Phonon cooling and lasing with nitrogen-vacancy centers in diamond." In: *Physical Review B* 88 (2013), p. 064105 (cited on pages 76, 77, 83, 86, 87).

[178] J. Cirac, M. Lewenstein, and P. Zoller. "Laser cooling a trapped atom in a cavity: Bad-cavity limit." In: *Physical Review A* 51 (1995), p. 1650 (cited on page 77).

[179] V. Vuletić, H. W. Chan, and A. T. Black. "Three-dimensional cavity Doppler cooling and cavity sideband cooling by coherent scattering." In: *Physical Review A* 64 (2001), p. 033405 (cited on page 77).

[180] S. Zippilli and G. Morigi. "Mechanical effects of optical resonators on driven trapped atoms: Ground-state cooling in a high-finesse cavity." In: *Physical Review A* 72 (2005), p. 053408 (cited on pages 77, 84, 85, 91).

[181] S. Zippilli and G. Morigi. "Cooling trapped atoms in optical resonators." In: *Physical review letters* 95 (2005), p. 143001 (cited on pages 77, 84, 85, 91).

[182] S. Zippilli, G. Morigi, and W. P. Schleich. "Ground state cooling in a bad cavity." In: *Journal of Modern Optics* 54 (2007), pp. 1595–1606 (cited on page 77).

[183] S. Stenholm. "The semiclassical theory of laser cooling." In: *Reviews of modern physics* 58 (1986), p. 699 (cited on pages 77, 78, 114).

[184] K.-M. C. Fu, C. Santori, P. E. Barclay, L. J. Rogers, N. B. Manson, and R. G. Beausoleil. "Observation of the dynamic Jahn-Teller effect in the excited states of nitrogen-vacancy centers in diamond." In: *Physical Review Letters* 103 (2009), p. 256404 (cited on pages 80, 83).

[185] C. Law. "Effective Hamiltonian for the radiation in a cavity with a moving mirror and a time-varying dielectric medium." In: *Physical Review A* 49 (1994), p. 433 (cited on page 81).

[186] R. J. Glauber. *Quantum theory of optical coherence: selected papers and lectures*. John Wiley & Sons, 2007 (cited on page 82).

[187] B. J. M. Hausmann, B. J. Shields, Q. Quan, Y. Chu, N. P. de Leon, R. Evans, M. J. Burek, A. S. Zibrov, M. Markham, D. Twitchen, et al. "Coupling of NV centers to photonic crystal nanobeams in diamond." In: *Nano letters* 13 (2013), pp. 5791–5796 (cited on page 83).

[188] M. J. Burek, Y. Chu, M. S. Liddy, P. Patel, J. Rochman, S. Meesala, W. Hong, Q. Quan, M. D. Lukin, and M. Lončar. "High quality-factor optical nanocavities in bulk single-crystal diamond." In: *Nature communications* 5 (2014), p. 5718 (cited on page 83).

[189] M. J. Burek et al. "Diamond optomechanical crystals." In: *Optica* 3 (2016), pp. 1404–1411 (cited on page 83).

[190] P. Tamarat, T. Gaebel, J. Rabeau, M. Khan, A. Greentree, H. Wilson, L. Hollenberg, S. Prawer, P. Hemmer, F. Jelezko, et al. "Stark shift control of single optical centers in diamond." In: *Physical review letters* 97 (2006), p. 083002 (cited on page 83).

[191] M. W. Doherty, N. B. Manson, P. Delaney, and L. C. Hollenberg. "The negatively charged nitrogen-vacancy centre in diamond: the electronic solution." In: *New Journal of Physics* 13 (2011), p. 025019 (cited on page 83).

[192] J. R. Maze, A. Gali, E. Togan, Y. Chu, A. Trifonov, E. Kaxiras, and M. D. Lukin. "Properties of nitrogen-vacancy centers in diamond: the group theoretic approach." In: *New Journal of Physics* 13 (2011), p. 025025 (cited on page 83).

[193] A. Sipahigil, M. L. Goldman, E. Togan, Y. Chu, M. Markham, D. J. Twitchen, A. S. Zibrov, A. Kubanek, and M. D. Lukin. "Quantum interference of single photons from remote nitrogen-vacancy centers in diamond." In: *Physical review letters* 108 (2012), p. 143601 (cited on page 83).

[194] H. Bernien, L. Childress, L. Robledo, M. Markham, D. Twitchen, and R. Hanson. "Two-photon quantum interference from separate nitrogen vacancy centers in diamond." In: *Physical Review Letters* 108 (2012), p. 043604 (cited on page 83).

[195] A. Gali, T. Simon, and J. Lowther. "An ab initio study of local vibration modes of the nitrogen-vacancy center in diamond." In: *New Journal of Physics* 13 (2011), p. 025016 (cited on pages 83, 146).

[196] R. Betzholz, J. M. Torres, and M. Bienert. "Quantum optical master equation for solid-state quantum emitters." In: *Physical Review A* 90 (2014), p. 063818 (cited on page 83).

[197] T. A. Abtew, Y. Sun, B.-C. Shih, P. Dev, S. Zhang, and P. Zhang. "Dynamic Jahn-Teller effect in the NV- center in diamond." In: *Physical review letters* 107 (2011), p. 146403 (cited on page 83).

[198] J. Eschner, G. Morigi, F. Schmidt-Kaler, and R. Blatt. "Laser cooling of trapped ions." In: *JOSA B* 20 (2003), pp. 1003–1015 (cited on page 84).

[199] G. Morigi, J. Eschner, and C. H. Keitel. "Ground state laser cooling using electromagnetically induced transparency." In: *Physical review letters* 85 (2000), p. 4458 (cited on page 84).

[200] M. Bienert and G. Morigi. "Cavity cooling of a trapped atom using electromagnetically induced transparency." In: *New Journal of Physics* 14 (2012), p. 023002 (cited on pages 84, 91).

[201] J. I. Cirac, R. Blatt, P. Zoller, and W. Phillips. "Laser cooling of trapped ions in a standing wave." In: *Physical Review A* 46 (1992), p. 2668 (cited on pages 85, 114).

[202] G. Morigi. "Cooling atomic motion with quantum interference." In: *Physical Review A* 67 (2003), p. 033402 (cited on page 85).

[203] B. Mollow. "Power spectrum of light scattered by two-level systems." In: *Physical Review* 188 (1969) (cited on page 89).

[204] I. Wilson-Rae, N. Nooshi, J. Dobrindt, T. J. Kippenberg, and W. Zwerger. "Cavity-assisted backaction cooling of mechanical resonators." In: *New Journal of Physics* 10 (2008), p. 095007 (cited on page 95).

[205] F. Marquardt, J. P. Chen, A. A. Clerk, and S. Girvin. "Quantum theory of cavity-assisted sideband cooling of mechanical motion." In: *Physical review letters* 99 (2007), p. 093902 (cited on page 95).

[206] G. Fuchs, G. Burkard, P. Klimov, and D. Awschalom. "A quantum memory intrinsic to single nitrogen–vacancy centres in diamond." In: *Nature Physics* 7 (2011), p. 789 (cited on pages 95, 146).

[207] M. G. Dutt, L. Childress, L. Jiang, E. Togan, J. Maze, F. Jelezko, A. Zibrov, P. Hemmer, and M. Lukin. "Quantum register based on individual electronic and nuclear spin qubits in diamond." In: *Science* 316 (2007), pp. 1312–1316 (cited on pages 95, 146).

[208] H. Y. Chen, E. MacQuarrie, and G. D. Fuchs. "Orbital state manipulation of a diamond nitrogen-vacancy center using a mechanical resonator." In: *Physical review letters* 120 (2018), p. 167401 (cited on pages 95, 146).

[209] M. Bienert. "Manifestations of Mechanical Effects of Light in Atom Optics." PhD thesis. Universität Ulm, 2004 (cited on page 97).

[210] P. Münstermann, T. Fischer, P. Maunz, P. Pinkse, and G. Rempe. "Observation of cavity-mediated long-range light forces between strongly coupled atoms." In: *Physical review letters* 84 (2000), p. 4068 (cited on page 111).

[211] C. Von Cube, S. Slama, D. Kruse, C. Zimmermann, P. W. Courteille, G. Robb, N. Piovella, and R. Bonifacio. "Self-synchronization and dissipation-induced threshold in collective atomic recoil lasing." In: *Physical review letters* 93 (2004), p. 083601 (cited on page 111).

[212] B. Zhu, J. Schachenmayer, M. Xu, F. Herrera, J. G. Restrepo, M. J. Holland, and A. M. Rey. "Synchronization of interacting quantum dipoles." In: *New Journal of Physics* 17 (2015), p. 083063 (cited on page 111).

[213] S. B. Jäger, M. Xu, S. Schütz, M. J. Holland, and G. Morigi. "Semiclassical theory of synchronization-assisted cooling." In: *Physical Review A* 95 (2017), p. 063852 (cited on pages 111, 117).

[214] P. Domokos and H. Ritsch. "Collective cooling and self-organization of atoms in a cavity." In: *Physical review letters* 89 (2002), p. 253003 (cited on page 111).

[215] A. T. Black, H. W. Chan, and V. Vuletić. "Observation of collective friction forces due to spatial self-organization of atoms: from Rayleigh to Bragg scattering." In: *Physical review letters* 91 (2003), p. 203001 (cited on page 111).

[216] J. Asbóth, P. Domokos, H. Ritsch, and A. Vukics. "Self-organization of atoms in a cavity field: Threshold, bistability, and scaling laws." In: *Physical Review A* 72 (2005), p. 053417 (cited on page 111).

[217] K. Arnold, M. Baden, and M. Barrett. "Self-organization threshold scaling for thermal atoms coupled to a cavity." In: *Physical review letters* 109 (2012), p. 153002 (cited on page 111).

[218] S. Schütz, H. Habibian, and G. Morigi. "Cooling of atomic ensembles in optical cavities: Semiclassical limit." In: *Physical Review A* 88 (2013), p. 033427 (cited on pages 111, 114, 134).

[219] H. Ritsch, P. Domokos, F. Brennecke, and T. Esslinger. "Cold atoms in cavity-generated dynamical optical potentials." In: *Reviews of Modern Physics* 85 (2013), p. 553 (cited on page 111).

[220] S. Schütz and G. Morigi. "Prethermalization of atoms due to photon-mediated long-range interactions." In: *Physical review letters* 113 (2014), p. 203002 (cited on page 111).

[221] S. Schütz, S. B. Jäger, and G. Morigi. "Thermodynamics and dynamics of atomic self-organization in an optical cavity." In: *Physical Review A* 92 (2015), p. 063808 (cited on page 111).

[222] S. B. Jäger, S. Schütz, and G. Morigi. "Mean-field theory of atomic self-organization in optical cavities." In: *Physical Review A* 94 (2016), p. 023807 (cited on page 111).

[223] S. Gopalakrishnan, B. L. Lev, and P. M. Goldbart. "Frustration and glassiness in spin models with cavity-mediated interactions." In: *Physical review letters* 107 (2011), p. 277201 (cited on pages 111, 127).

[224] P. Strack and S. Sachdev. "Dicke quantum spin glass of atoms and photons." In: *Physical review letters* 107 (2011), p. 277202 (cited on pages 111, 127).

[225] M. Landini, N. Dogra, K. Kroeger, L. Hruby, T. Donner, and T. Esslinger. "Formation of a spin texture in a quantum gas coupled to a cavity." In: *Physical review letters* 120 (2018), p. 223602 (cited on pages 111, 146).

[226] F. Mivehvar, F. Piazza, and H. Ritsch. "Disorder-driven density and spin self-ordering of a Bose-Einstein condensate in a cavity." In: *Physical review letters* 119 (2017), p. 063602 (cited on pages 111, 113).

[227] R. M. Kroeze, Y. Guo, V. D. Vaidya, J. Keeling, and B. L. Lev. "Spinor self-ordering of a quantum gas in a cavity." In: *Physical review letters* 121 (2018), p. 163601 (cited on pages 111, 113, 146).

[228] Z. Zhang, C. H. Lee, R. Kumar, K. Arnold, S. J. Masson, A. Grimsmo, A. Parkins, and M. Barrett. "Dicke-model simulation via cavity-assisted Raman transitions." In: *Physical Review A* 97 (2018), p. 043858 (cited on pages 111, 113).

[229] R. M. Kroeze, Y. Guo, and B. L. Lev. "Dynamical spin-orbit coupling of a quantum gas." In: *arXiv preprint arXiv:1904.08388* (2019) (cited on pages 111, 113).

[230] H. Habibian, S. Zippilli, and G. Morigi. "Quantum light by atomic arrays in optical resonators." In: *Physical Review A* 84 (2011), p. 033829 (cited on pages 114, 133).

[231] Y. Castin, H. Wallis, and J. Dalibard. "Limit of Doppler cooling." In: *JOSA B* 6 (1989), pp. 2046–2057 (cited on page 114).

[232] C. Gardiner and M. Collett. "Input and output in damped quantum systems: Quantum stochastic differential equations and the master equation." In: *Physical Review A* 31 (1985), p. 3761 (cited on page 116).

[233] P. Domokos, P. Horak, and H. Ritsch. "Semiclassical theory of cavity-assisted atom cooling." In: *Journal of Physics B: Atomic, Molecular and Optical Physics* 34 (2001), p. 187 (cited on pages 117, 134, 135).

[234] C. W. Gardiner et al. *Handbook of stochastic methods*. Vol. 3. springer Berlin, 1985 (cited on page 117).

[235] M. Xu, S. B. Jäger, S. Schütz, J. Cooper, G. Morigi, and M. Holland. "Supercooling of atoms in an optical resonator." In: *Physical review letters* 116 (2016), p. 153002 (cited on page 117).

[236] C. Cohen-Tannoudji, B. Diu, and F. Laloë. "Quantum mechanics vol. 1." In: (1977) (cited on page 117).

[237] R. H. Dicke. "Coherence in spontaneous radiation processes." In: *Physical review* 93 (1954), p. 99 (cited on page 117).

[238] K. Hepp and E. H. Lieb. "On the superradiant phase transition for molecules in a quantized radiation field: the Dicke maser model." In: *Annals of Physics* 76 (1973), pp. 360–404 (cited on page 117).

[239] Y. K. Wang and F. Hioe. "Phase transition in the Dicke model of superradiance." In: *Physical Review A* 7 (1973), p. 831 (cited on page 117).

[240] M. Gross and S. Haroche. "Superradiance: An essay on the theory of collective spontaneous emission." In: *Physics reports* 93 (1982), pp. 301–396 (cited on page 117).

[241] C. Rackauckas and Q. Nie. "Adaptive methods for stochastic differential equations via natural embeddings and rejection sampling with memory." In: *Discrete and continuous dynamical systems. Series B* 22 (2017), p. 2731 (cited on page 121).

[242] S. Schreppler, N. Spethmann, N. Brahms, T. Botter, M. Barrios, and D. M. Stamper-Kurn. "Optically measuring force near the standard quantum limit." In: *Science* 344 (2014), pp. 1486–1489 (cited on pages 127, 146).

[243] F. Haas, J. Volz, R. Gehr, J. Reichel, and J. Estève. "Entangled states of more than 40 atoms in an optical fiber cavity." In: *Science* 344 (2014), pp. 180–183 (cited on pages 127, 146).

[244] K. Baumann, C. Guerlin, F. Brennecke, and T. Esslinger. "Dicke quantum phase transition with a superfluid gas in an optical cavity." In: *Nature* 464 (2010), p. 1301 (cited on pages 127, 146).

[245] D. Nagy, G. Kónya, G. Szirmai, and P. Domokos. "Dicke-model phase transition in the quantum motion of a Bose-Einstein condensate in an optical cavity." In: *Physical review letters* 104 (2010), p. 130401 (cited on pages 127, 146).

[246] S. Sachdev. "Quantum magnetism and criticality." In: *Nature Physics* 4 (2008), p. 173 (cited on page 127).

[247] J. Gallego, W. Alt, T. Macha, M. Martinez-Dorantes, D. Pandey, and D. Meschede. "Strong Purcell effect on a neutral atom trapped in an open fiber cavity." In: *Physical review letters* 121 (2018), p. 173603 (cited on page 146).

COLOPHON

This document was typeset using the typographical look-and-feel `classicthesis` developed by André Miede and Ivo Pletikosić. The style was inspired by Robert Bringhurst's seminal book on typography "*The Elements of Typographic Style*". `classicthesis` is available for both LaTeX and LyX:

`https://bitbucket.org/amiede/classicthesis/`

Happy users of `classicthesis` usually send a real postcard to the author, a collection of postcards received so far is featured here:

`http://postcards.miede.de/`

Thank you very much for your feedback and contribution.

Final Version as of June 26, 2020 (version 1.01).